Dissertation zur Erlangung des Doktorgrades der Fakultät für Chemie und Pharmazie der Ludwig-Maximilians-Universität München

Nanocarriers based on sequence-defined oligomers for tumor-targeted siRNA and miRNA delivery

Katharina Sophie Müller

aus

Stuttgart, Deutschland

2016

Erklärung

Diese Dissertation wurde im Sinne von § 7 der Promotionsordnung vom 28. November 2011 von Herrn Prof. Dr. Ernst Wagner betreut.

Eidesstattliche Versicherung

Diese Dissertation wurde eigenständig und ohne unerlaubte Hilfe erarbeitet.

München, 15.09.2016

.....

Katharina Müller

Dissertation eingereicht am 15.09.2016

1. Gutachter: Prof. Dr. Ernst Wagner

2. Gutachter: Prof. Dr. Stefan Zahler

Mündliche Prüfung am 27.10.2016

Table of contents

1 Introduction

Chapter 1.1, 1.2, 1.3, 1.4 (partly) have been adapted from:

Katharina Müller, Ernst Wagner, "RNAi-based Nano-Oncologicals – Delivery and Clinical Applications." In Nano-Oncologicals: New Targeting and Delivery Approaches, Alonso, M. J.; Garcia-Fuentes, M., Eds. Controlled Release Society and Springer 2014, 245-268.

1.1 RNA interference (RNAi)

Sequence-specific, post-transcriptional gene silencing in animals (miRNA) and plants (siRNA) proceeds in significantly different fashion. In animals, endogenous miRNAs regulate gene expression during embryonic development and cellular differentiation. miRNA genes derive from independent transcription units or from introns of protein-coding genes [1]. They are mainly clustered in the human genome and miRNAs within a cluster are often related to each other [2]. miRNA genes are transcribed by RNA polymerase II (Pol II) into long primary transcripts (pri-miRNAs) in the nucleus [3] (Figure 1A). Here, they are processed firstly by a RNase-III-type endonuclease termed Drosha, along with the double-stranded (ds) RNA-binding protein of DiGeorge syndrome critical region gene 8 (DGCR8) into so called miRNA precursor (pre-miRNA), a ~70 nucleotide (nt) stem-loop structure [4]. Afterwards pre-miRNA is transported into the cytoplasm by exportin 5, a dsRNA-binding protein. Once in the cytoplasm, pre-miRNA is recognized by another RNase III, called Dicer. Dicer and its ds-RNA-binding protein partners, HIV-1 TAR RNA-binding protein (TRBP) and protein activator of protein kinase PKR (PACT), process pre-miRNA into ~22 nt mature miRNA [5]. This RNA duplex possessing a 5´phosphate and ~2 nt 3`overhang, which is characteristic of a RNAase III product [6], is then loaded into the RNA-induced silencing complex (RISC). RISC contains one member of the Argonaute protein family (Ago 1 to Ago 4). Only one of the Argonaute proteins (Ago2) provides the RISC with endonuclease activity under special conditions (see below). The so called antisense or guide strand of miRNA which enters the RISC is the one whose 5´end is less firmly paired [7]. If the guide strand shows imperfect sequence homology, the passenger strand is unwinded and discarded by a bypass mechanism that necessitates helicase activity. If the guide strand has perfect sequence complementary to its passenger strand and Ago2 is part of the RISC, the passenger strand is cleaved. The extent of sequence complementary also influences the further procedure of RISC. In

the rare case of perfect or near perfect Watson-Crick base pairing between the miRNA and the 3`untranslated region (3`UTR) of its target mRNA, this leads to direct sequence specific cleavage of the mRNA, comparable to the siRNA pathway (Figure 1B). However, the more common mechanism of miRNA induced gene silencing occurs with miRNA binding with imperfect base pairing. The first 2-7 or 2-8 nucleotides from the 5´end of the miRNA, the seed sequence, must have perfect complementarity. Mismatches at the 3´end of the miRNA are tolerated. In this case miRNA induces mRNA degradation and therefore translational repression [5]. Because of their gene silencing capability without perfect match, one miRNA can regulate up to hundreds of different mRNAs [1]. In 2005 Lim et al. already observed this effect using microarray analysis [8]. Moreover, Dicer can process pre-miRNA into miRNAs altering their length in 1-2 nt. This length difference influences the miRNA seed sequences as well as guide strand loading into the RISC, thus increasing the target mRNAs for a single miRNA [9]. In contrast, different miRNAs can silence a common single mRNA [10]. Therefore, reestablishment or overexpression of a single miRNA or silencing of miRNAs using antagomirs in cancer could lead to off-target effects that must be considered carefully.

The siRNA mechanism is also based on endogenous double–stranded RNAs, which often derive from mRNAs, transposons, viruses or heterochromatic DNA [11]. These RNAs are processed by Dicer (Figure 1B) but, in contrast to miRNA, request a perfect match with the target mRNA along about 20 nucleotides and therefore, at least in theory, each siRNA has only one specific mRNA target. siRNA triggered gene silencing mainly serves as an innate immune defense protecting nematodes, insects and plants against invasive nucleic acids from pathogens [12]. The siRNA guide strand always has to have perfect complementary to its target mRNA and therefore leads to mRNA cleavage. The guide strand interacts with the catalytic, RNase H-like PIWI domain of Ago2 at the 5`end and with a PIWI-Argonaute-Zwille (PAZ) domain at the 3`end [3]. The targeting mRNA is cleaved between bases 10 and 11 relative to the 5`end of the siRNA guide strand [5]. In contrast to miRNA, targeted cleavage sites can be both translated and untranslated regions of the target mRNA.

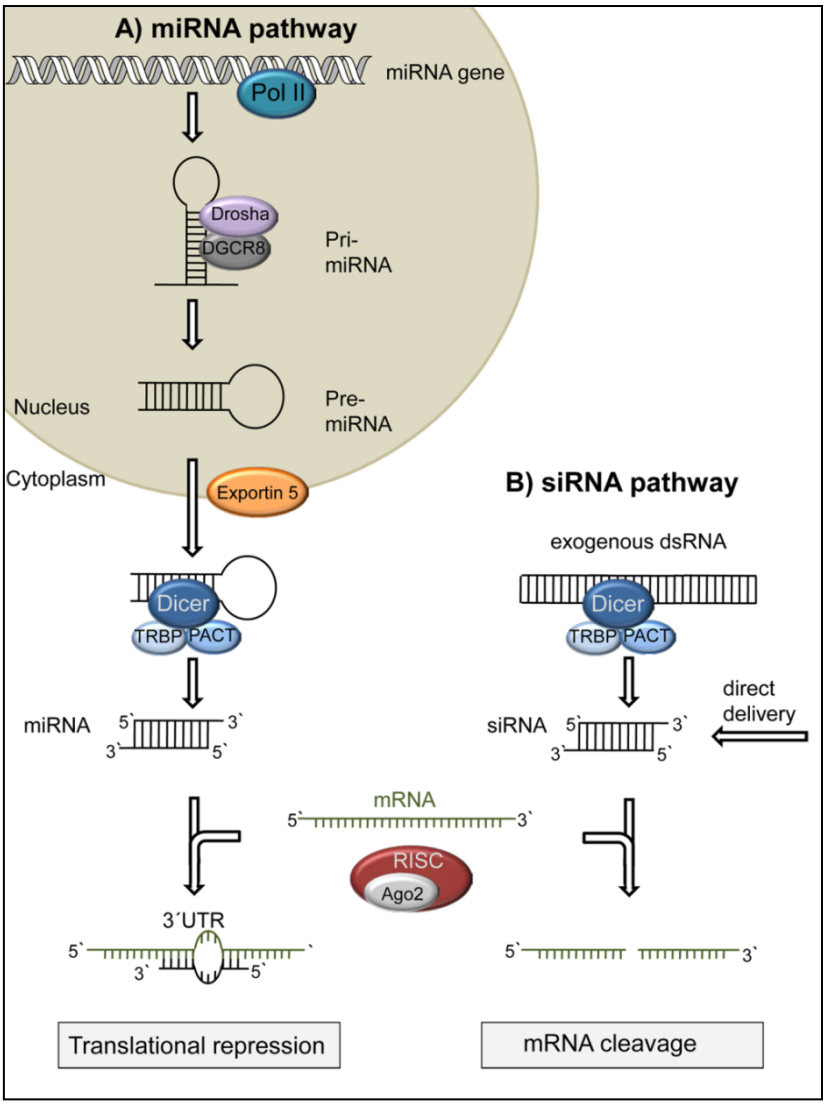

Figure 1. **Mechanism of RNAi in mammalian cells.** A) miRNA pathway. Endogenous miRNA genes are transcribed by RNA polymerase II into primary miRNA (pri-miRNA). The endonuclease Drosha and ds-RNA binding protein DGCR8 then process pri-miRNA into precursor miRNA (pre-miRNA), which is exported into cytoplasm by Exportin 5. In the cytoplasm pre-miRNA is cut by the RNAse III, Dicer, together with TRBP (HIV-1 TAR RNA-binding protein) and PACT (protein activator of protein kinase PKR) into a dsRNA consisting of ~22 nt and a 5´phosphate and ~2 nt 3`overhang. The miRNA guide strand is then loaded into the RISC (RNA-induced silencing complex) - Argonaute (Ago 1 or Ago 2) complex and recognizes its targeting mRNA. In mammalian cells, the guide strand has imperfect complementarity to the target mRNA, which leads to translational repression and therefore less protein. B) siRNA pathway. Analogous to pre-miRNA exogenous dsRNA is processed in the cytoplasm by Dicer, TRBP and PACT into siRNA. Alternatively exogenous siRNA can be directly delivered. siRNA/Ago2 RISCs require perfect complementary for target mRNA cleavage. Adapted from [13].

Mammalian cells do not express siRNAs or miRNAs with perfect match to mRNA targets. However, artificially delivered or transfected, perfectly matched exogenous dsRNA can be processed in the cytoplasm similar to pre-miRNA by Dicer into siRNA of 21-25

nucleotides in length [14]. The siRNA duplex is then incorporated into the RISC and the passenger strand is cleaved and expelled. Sequence –specific gene silencing by such artificial RISCs is found. Short siRNAs can directly intervene with the RNAi pathway without need for cleavage by Dicer, when introduced into the cytoplasm. Therefore synthetic 21 bp siRNA are widely used for research and therapeutic applications of RNAi [12, 15-17]. The gene knockdown caused by a siRNA is often temporary. Edinger et al. found a maximum downregulation at mRNA level after 24 h and at protein level after 48 h in *in vitro* studies [18]. In other studies a silencing of 3-4 weeks in nondividing liver cells was observed *in vivo* indicating that the transient gene knockdown is due to dilution effects of siRNA concentration in the cytosol through cell division [19]. Zimmermann et al. observed silencing of apolipoprotein B for 11 days, when they applied a liposomal siRNA formulation systemically into cynomolgus monkeys [20]. Considering these different findings, the dose regime for RNAi based nanodrugs should be calculated carefully, when transferred to clinical application [19].

1.2 Nucleic acid therapy

Several human clinical trials using RNAi or related RNA-modulating nano-oncological drugs for cancer therapy are currently carried out. Major investments in the development of these therapeutics have been made in the last years with the prospect of commercial drugs in the next 5-10 years [21, 22].

1.2.1 siRNA therapeutics

Davis and colleagues firstly reported systemic siRNA delivery in humans for cancer treatment *via* targeted nanoparticles. Their formulation consisted of a cyclodextrin-containing polymer, adamantane conjugated to polyethylene glycol (PEG) for steric stabilization, adamantane-PEG (AD-PEG) with the targeting ligand transferrin binding to transferrin receptors, which are frequently upregulated in cancer cells, and siRNA targeting the M2 subunit of ribonucleotide reductase (RRM2), a crucial factor of tumor malignancy. These nanoparticles, named CALAA-01, were systemically administered to patients with solid cancers. The phase I study implied a phase Ia open-labelled, multi-center, dose escalation study (3-30 mg m^{-2}) and a phase Ib extension study (18-27 mg m^{-2}) of patients suffering from solid tumors. Biopsies from tumor tissues were analyzed and a reduction of mRNA and protein levels of RRM2 was observed. The RNAi was

confirmed by 5´-RNA-ligand-mediated RACE PCR technique detecting a RRM2 mRNA fragment in tumor tissue of the patient receiving the highest dose [23-25].

Atu027 is a lipid-based siRNA nanoparticle approach which has recently been tested in a phase I clinical trial. Atu027 contains siRNA targeting protein kinase N3 (PKN3). PKN3 mediates malignant cell growth [26]. Atu027 has been shown to silence PKN3 when it was systemically delivered in mice, rats and nonhuman primates without stimulation of the innate immune system. In pancreatic and prostate cancer mouse models Atu027 decreased tumor growth and lymph node metastasis formation [27]. In a phase I clinical trial 34 patients suffering from advanced solid tumors were treated with Atu027. Atu027 was well tolerated, 41 % of patients showed disease stabilization and some patients showed reduction of metastases demonstrating the potential of this siRNA delivery system [28]. Furthermore, Atu027 was examined in combination with gemcitabine in a phase Ib/IIa study to examine safety, pharmacokinetics and efficacy in advanced pancreatic carcinoma. The combinatorial treatment was safe and well tolerated and tendency towards twice-weekly dosing regimen could be observed [29].

ALN-VSP consists of a lipid nanoparticle with two siRNAs, one targeting vascular endothelial growth factor A (VEGF), the other one targeting kinesin spindle protein (KSP). RNAi specific effectiveness of ALN-VSP as well as antitumor activity has been proven in preclinical animal studies. In a phase I dose- escalation study 41 patients with advanced tumors and hepatic and extrahepatic metastases were intravenously treated with ALN-VSP with doses of 0.01-1.5 mg/kg every two weeks. ALN-VSP was generally well tolerated and occurring adverse events were comparable to other targeted chemotherapies. Furthermore, both siRNAs and cleavage products of VEGF mRNA could be detected in hepatic and extrahepatic tumor biopsies indicating that the antitumoral effects of ALN-VSP underlie an RNAi mechanism. Fifty percent of patients treated with doses greater than 0.7 mg/kg achieved stable disease including one patient with endometrial cancer and multiple liver metastases, who attained a major response meaning disappearance of all target and non-target lesions [25, 30].

1.2.2 miRNA replacement therapy

MRX34 was developed to deliver miR-34 mimic, a synthetic double stranded miRNA of 20-25 nucleotides, which was the first microRNA assessed in a clinical phase I study. MRX34 is a delivery system based on a mixture of different lipids. miR-34 is frequently

downregulated in many human cancer types leading to metastasis, anti-apoptosis, chemoresistance and tumor proliferation [31]. Anti-tumor activity of miR-34 has been shown in non-small cell lung cancer in mice. miR-34 was systemically delivered using a neutral lipid emulsion, which led to a decrease of proliferation markers, increased apoptosis of tumors and therefore to reduced tumor burden [32]. The efficiency of MRX34 has been proven in preclinical studies. In a survival study MRX34 was intravenously delivered in mice with hepatocellular carcinoma. All treated animals stayed alive and appeared healthy in comparison to control groups. In a phase I trial MRX34 has shown partial responses in patients with renal cell carcinoma, acral melanoma and hepatocellular carcinoma. Furthermore, MRX34 revealed a manageable safety profile and led to long-term stable disease in some patients [33, 34]. Currently, participants are recruited for an open-label, multicenter, dose-escalation phase I study to examine safety, pharmacokinetics and pharmacodynamics of MRX34 in patients with primary liver cancer, advanced or metastatic cancer (see www.clinicaltrials.gov for details, ClinicalTrials.gov Identifier: NCT01829971).

1.3 siRNA and miRNA design

There are several barriers that restrict the direct use of miRNA or siRNA for therapeutic application. First of all, naked RNA is rapidly cleaved by ribonucleases (RNAses), which are commonly occurring in a wide variety of organisms. RNAse interacts with the RNA backbone catalyzing its hydrolysis [35]. Therefore, the poor RNAse resistance limits the application of non-modified RNA *in vitro* and *in vivo*. Moreover, synthetic miRNAs or siRNAs are eliminated from the blood-stream by excretion in urine or bile. Due to their small size RNA molecules are able to pass the capillaries of the kidney glomerulus easily [36]. The biological half-life of siRNA has been reported to be 2-6 minutes, whereas chemically stabilized siRNA circulated for 30-50 minutes [37].

Another limiting factor concerning direct use of siRNA and miRNA is toxicity. Naked dsRNAs are able to cause off-target effects (OTEs). For example, one siRNA can regulate numerous unintended transcripts. This emerges when siRNA acts in a miRNA-related manner with partial sequence complementary. It has been reported, that many off-targets silenced by siRNA showed 3´UTR perfect complementary to the seed region of the siRNA, but not throughout the entire guide strand [38, 39].

In addition, siRNA can induce an innate immune response. This immunogenicity is divided into two groups: activation of toll-like receptors (TLR) or non-TLR-mediated

immune response [40] and derives from the stimulation of pattern recognition receptors (PRRs). PRRs recognize invariant molecular structures of pathogens [36, 41]. Relating to siRNA, two classes of PPRs are affected: TLRs and cytoplasmic receptors. TLR3, TLR7 and TLR8 recognize synthetic siRNA [42]. TLR3 located in endosomes and cell surfaces is only activated by dsRNA, which is typically for viruses [43]. After siRNA detection TLR3 activates interferon-γ (INFγ) and interleukin-12 (IL-12) causing anti-angiogenic effects [40]. TLR7 and TLR8 are stimulated by either single-stranded RNA (ssRNA) or RNA duplexes. They are expressed in endosomes and lysosomes and in the endoplasmic reticulum of plasmacytoid dendritic cells, B cells and myeloid cells [36]. TLR7 and TLR8 cause nuclear translocation of nuclear factor κ-light-chain-enhancer of activated B cells (NF-κB) and downstream activation of interferon-α (INFα) and inflammatory cytokines [40, 44]. siRNAs can also provoke a non-TLR-mediated immune response by activating cytoplasmic receptors. dsRNA-binding protein kinase leads to inhibition of protein translation and interferon response after recognizing siRNA. In addition, retinoic acid-inducible gene 1, another cytoplasmic PRR, causes interferon response and upregulation of other inflammatory mediators [36]. Chemical modification and variations in siRNA design reduce the risk of OTEs and immune responses [42]. In correlation to siRNA, the risk of miRNAs causing toxicity is likely to be lower since physiologic gene expression networks have managed to adapt to regulatory effects of endogenous miRNAs [45]. Nevertheless, side effects of miRNA-based therapies have to be examined before usage in clinical application. Chemical changes in the backbone of siRNA and miRNA were introduced to improve stability and reduce immunogenicity of these molecules. A common strategy comprises the modification of the ribose 2´-OH group of siRNA (Figure 2), which is involved in the hydrolysis mechanism of many serum RNAses. The substitution of this functional group with 2´-O-methyl (2´OMe), 2´-deoxy (2´H), 2´-fluoro (2´F) or 2´-methoxyethyl (2´-MOE) ribonucleotides (Figure 2A) have proven to increase RNAse resistance without losing the ability to enter the RISC and to interact with Ago2 [46-48]. Furthermore, 2´-OMe uridine or guanosine modifications have been shown to prevent stimulation of the innate immune system by avoiding activation of TLRs [49]. Other established procedures are the incorporation of phosphorothioate backbone linkages at the 3´-end of the siRNA strand to improve the stability against endonucleases or the replacement of a nonbridging phosphodiester oxygen by an isoelectronic borane (BH3-) moiety to increase activity and RNAse resistance (Figure 2B) [50]. Locked nucleic acid (LNA) (Figure 2C) includes a methylene bridge linking the 2´-oxygen to the 4´-carbon of the ribose ring. This modification ensures that the ribose ring is locked in the 3´-endo conformation and therefore increases nuclease resistance to

RNA oligonucleotides. Moreover, LNAs are processed by the siRNA machinery, because they maintain an A-form helix geometry typical for RNA-RNA duplexes, in a normal way and reduce unintended OTEs [51]. LNAs are widely used as antagomirs because of their thermodynamic stability and therefore efficient binding to miRNA seeds. Antagomirs are single-stranded oligonucleotides with perfect complementary to a miRNA. If hybridized with its corresponding miRNA, target mRNA recognition and therefore gene regulation is hampered [52].

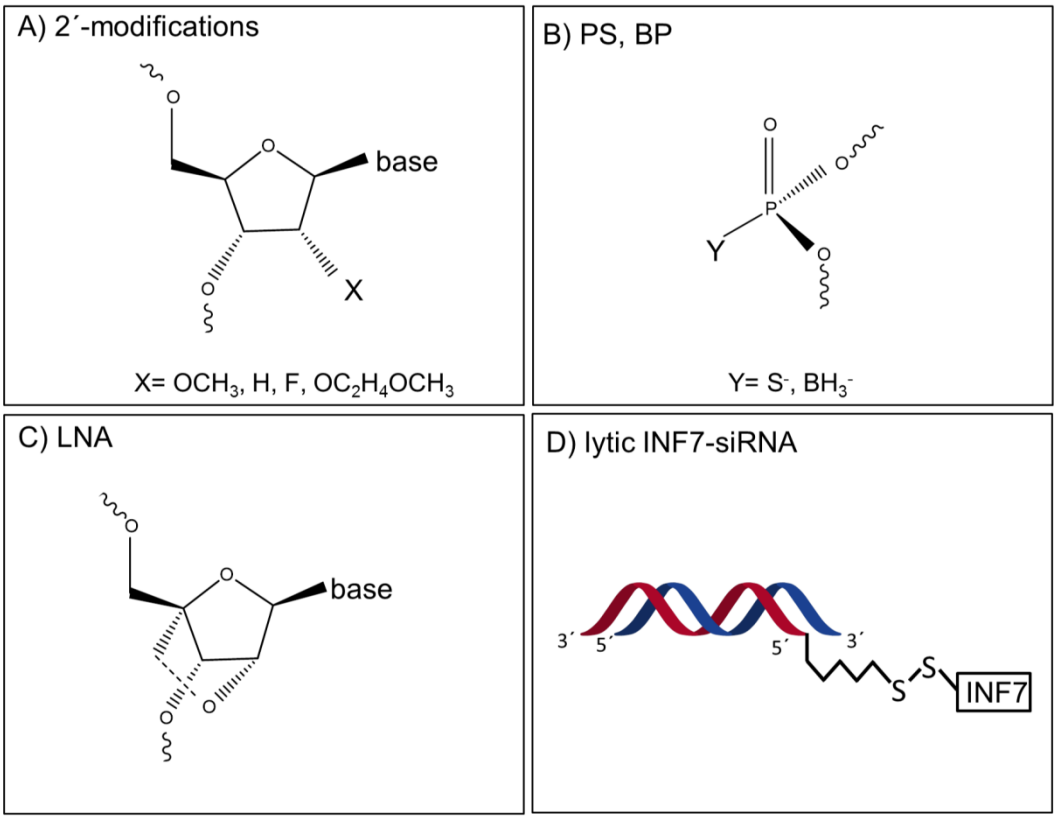

Figure 2. Chemical modifications of RNA. A) Stabilizing 2´-OH modifications. 2´OMe: X = OCH_3; 2´deoxy: X = H; 2´fluoro: X = F; 2´methoxyethyl (2´-MOE): X = $OCH_2H_4OCH_3$ B) Stabilizing backbone modifications. phosphorothioate linkage (PS): Y = S-; boranophosphate (BP): Y = BH_3- C) Locked nucleic acid (LNA); methylene bridge between 2´-oxygen and 4`-carbon of the ribose ring D) endosomolytic INF7-siRNA; the pH-triggered fusogenic peptide INF7 (sequence: GLFE AIEG FIEN GWEG MIDG WYGC) is covalently linked to the 5´-end of the siRNA sense strand. Adapted from [13].

Strategies to increase the delivery of RNA molecules comprise their conjugation to small molecules or peptides. A prominent example is the attachment of lipophilic moieties to siRNA. Cholesterol was linked to the 3´-end of the siRNA sense strand resulting in silencing of its target apolipoprotein B (apoB) *in vitro* and *in vivo* in liver and jejunum [37]. This is accomplished by interactions of siRNA with lipoproteins in the circulation and

uptake into cells by low-density-lipoprotein-receptor (LDL-receptor). Long-chain fatty acids and bile acids conjugated to apoB-siRNA also mediate silencing of apoB in mice and hamsters [53]. Furthermore, improved delivery due to cholesterol conjugation has been reported for antisense oligonucleotides [54]. Krützfeldt et al. successfully silenced miR-122, frequently expressed in hepatocytes, by treating mice with a chemically modified cholesterol antagomir. In liver, levels of miR-122 and 3-hydroxy-3-methylglutaryl-CoA-reductase (Hmgcr), a miR-122 target, were decreased after tail-vain injection of miR-122 antagomir. Furthermore, due to the fact that Hmgcr is involved in endogenous cholesterol biosynthesis, cholesterol levels in plasma were significantly reduced [55]. To improve the endosomal escape Dohmen et al. conjugated INF7 [56], an acidic peptide analogue of the amino terminus of the influenza virus hemagglutinin HA2 subunit, to the 5´-end of the siRNA sense strand (Figure 2D). This INF7-siRNA showed pH-dependent lytic activity and therefore an increased gene silencing efficiency when delivered with sequence defined oligomers *in vitro* [57].

1.4 RNA delivery *via* sequence defined oligomers

Naked siRNA or miRNA in the circulation have to find their site of action, such as a specific tissue or cancer cells. Since these molecules do not possess any targeting domain and because of their polyanionic nature do not passively enter cells across cell membranes, they have to be delivered by conjugation or formulations with targeting ligands and shielding domains [58]. Mammalian cells are surrounded by the complex extracellular matrix (ECM), a dense mesh of fibrous proteins and glycosaminoglycans, which has to be overcome by the RNA molecules, as well [59]. After siRNA and miRNA entered their target cell *via* endocytosis, they must escape from endosomes, avoiding entrapment and degradation in lysosomes [60]. These extracellular and intracellular barriers have to be addressed during the development of potent delivery systems [61, 62]. Using classical polymers it is impossible to incorporate various functional domains in precise manner. As a solution, sequence defined oligomers have been designed, which combine multifunctionality with chemical precision. These potent nucleic acid delivery vehicles are obtained via solid phase-supported synthesis (SPS). This method has been adapted by Hartmann et al. for the synthesis of defined polyamides starting from a fixed resin and alternate assembly of diacids and diamines [63]. Schaffert et al. extended the strategy to the synthesis of larger cationic oligomers using Fmoc-protected artificial polyamino acids [64]. With this method our group has established a library of over 1000

oligomers with different shapes, arms, stability motifs, motifs to enhance the endosomal escape, with or without shielding or targeting ligands [65-70]. The positively charged oligomers are able to complex nucleic acids *via* electrostatic interactions forming so called polyplexes (see chapter 1.4.1). For stable polyplex formation using different nucleic acid cargos (such as siRNA versus pDNA), in general different polymer requirements have been observed [71, 72]. Also with sequence-defined oligomers, additional stabilization was required for siRNA (as opposed to pDNA) to form stable polyplexes. Oligomers modified with two fatty acids (oleic acid or linolic acid) at central (T-shape) or terminal (i-shape, U-shape) positions showed enhanced stability due to hydrophobic interactions (Figure 3). In addition, terminal cysteines (two-arms, three-arms) which are able to form disulfide bridges after siRNA complexation stabilize polyplexes in a covalent manner. High stability is a very important feature for sufficient polyplex application. Incorporation of tyrosine trimers increased stability *in vitro*, in full serum (as evaluated by FCS) and *in vivo* (as evaluated by NIR fluorescence bioimaging in mice) [73-75].

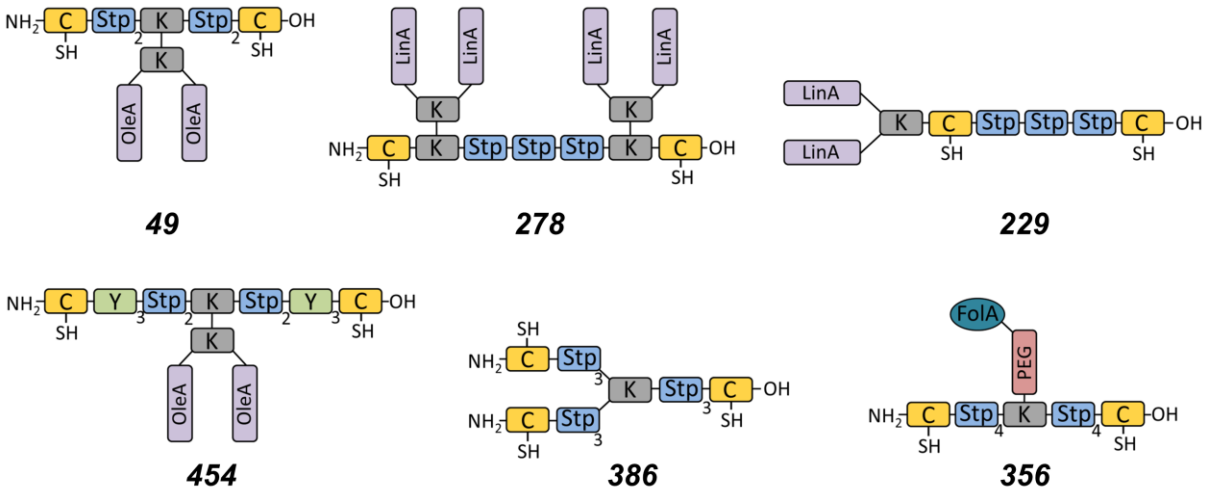

Figure 3. Schematic illustration of oligomers. ***49*** (T-shape), ***278*** (U-shape), ***229*** (i-shape), ***454*** (T-shape with tyrosines), ***386*** (three-arm), ***356*** (two-arm with PEG and folate targeting). C, cysteine; K, lysine; Y_3, tyrosine trimer; Stp, succinoyl tetraethylene pentamine; FolA, folic acid; OleA, oleic acid; LinA, linolic acid. Adapted from [13].

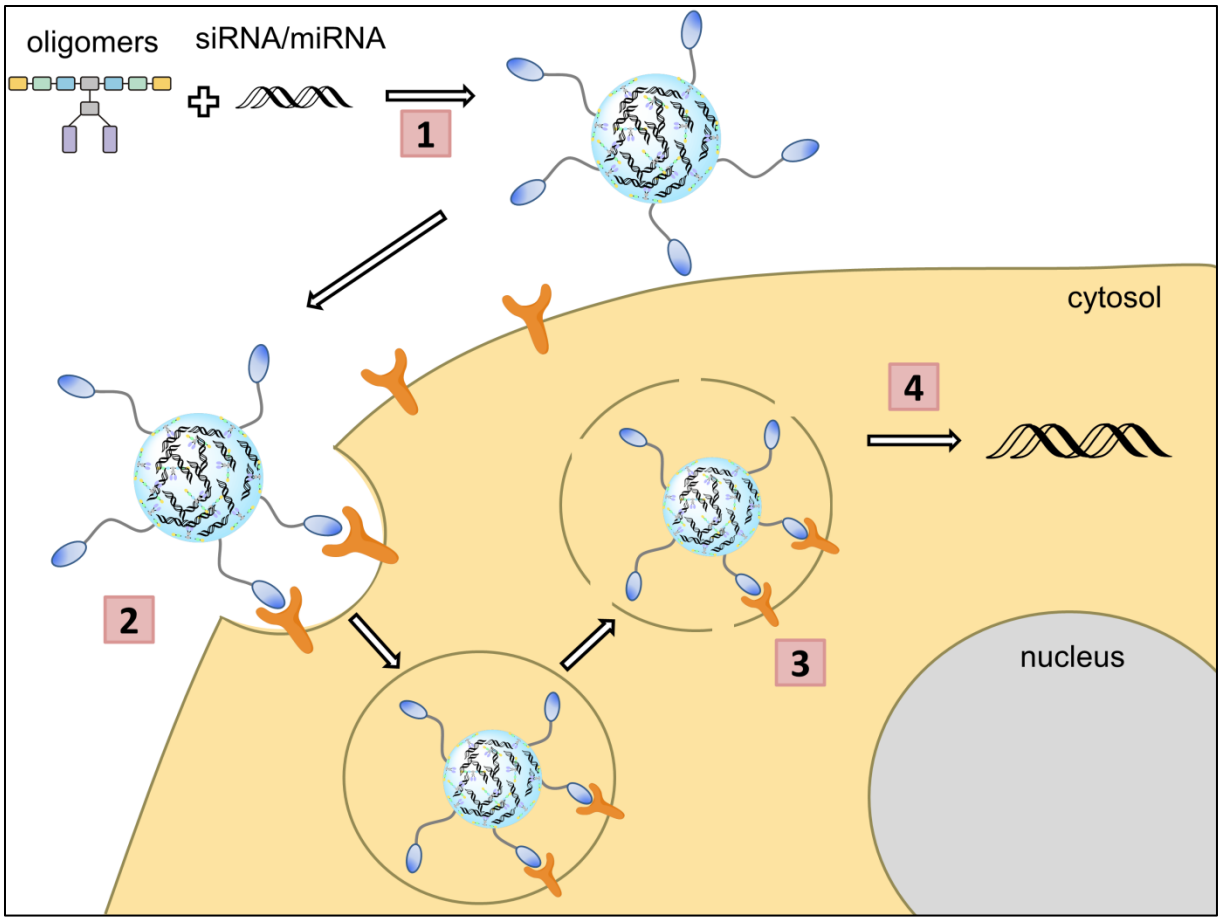

Figure 4. siRNA and miRNA delivery using sequence defined oligomers. Polyplex formation through RNA complexation via electrostatic interactions with oligomers (1). Polyplexes that are equipped with targeting ligands (blue ellipse) bind to receptors on the target cell surface and are internalized via endocytosis (2). Polyplexes escape the endosome via proton sponge (3) and the cargo RNA is set free in the cytosol (4) where RNAi takes place.

1.4.1 RNA complexation

Negatively charged RNA can be complexed by positively charged oligomers via electrostatic interactions (Figure 4 (1)) [76]. Different artificial oligoamino acids were generated (Figure 5) based on the idea to lend an effective microdomain from the gold standard for gene delivery polyethylenimine (PEI) [77]: the protonatable diaminoethane motif (Figure 5, bottom left). The artificial building blocks differ in the type of acid (glutaric acid, phthalic acid, succinic acid) and in the number of protonable amine repeats: triethylene tetramine (tt), tetraethylene pentamine (tp), and pentaethylene hexamine (ph).

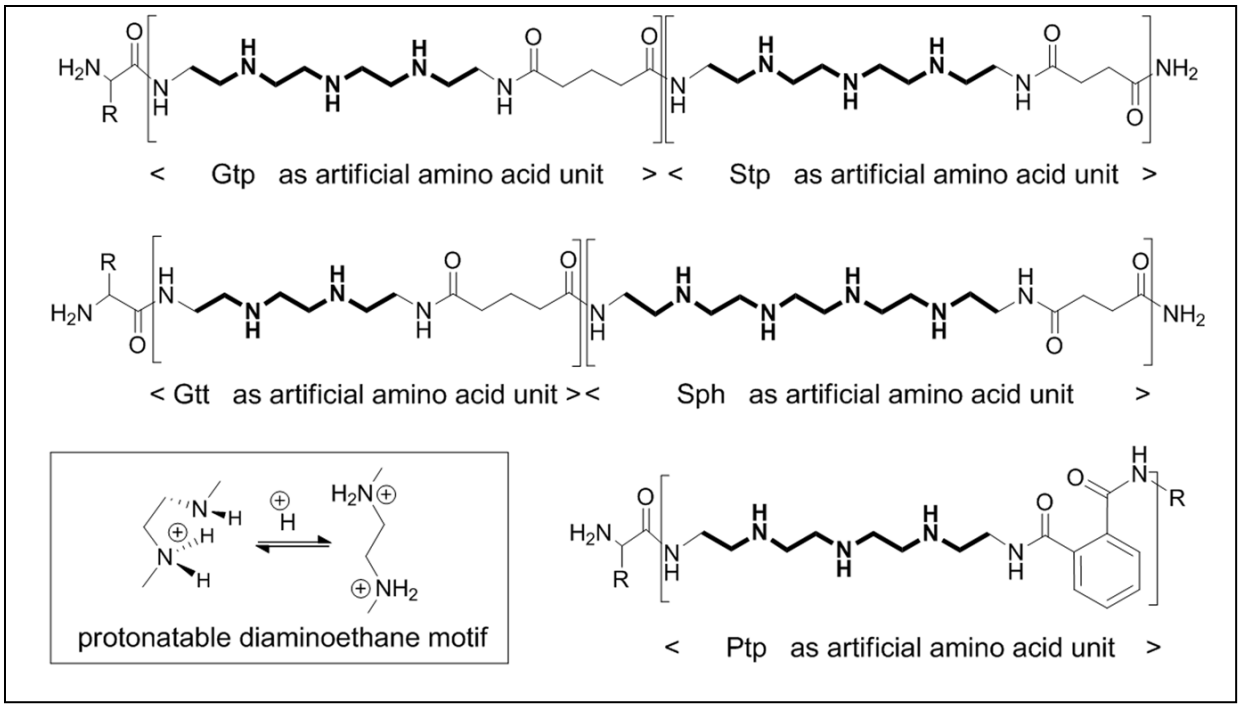

Figure 5. Sequence-defined oligomers as RNA carriers. Artificial amino acids: glutaroyl tetraethylene pentamine (Gtp), succinoyl tetraethylene pentamine (Stp), glutaroyl triethylene tetramine (Gtt), succinoyl pentaethylene hexamine (Sph), and phthaloyl tetraethylene pentamine (Ptp). Endosomal protonation of the diaminethane motif is presented in the box (bottom left). Adapted from [13].

Artificial cationic building blocks such as Gtp, Stp, Ptp, or Sph could be easily merged with natural peptide sequences or lipidic domains, resulting in precise and pure carriers for nucleic acid delivery. The oligoamine components are only partly cationic at physiological pH, but sufficiently charged for binding nucleic acids via electrostatic interactions. Upon endosomal acidification, they gain additional cationic charges required for destabilizing lipid membranes and escape from endolysosomes to the cytoplasm [78] (see chapter 1.4.3)

1.4.2 Targeting ligands and shielding domains

Nanoparticles <1 µm in size are uptaken by cells *via* unspecific endocytosis [79, 80]. *In vivo* particles up to 400 nm can accumulate in solid tumors due to the enhanced permeability and retention (EPR) effect as they often have high vascular density and gaps in blood vessels [81, 82]. However, a more elegant way to direct particles specific to cells is the use of targeting ligands *in vitro* and *in vivo* [61, 83] (Figure 4 (2)). Cancer cells often overexpress receptors on their surface, which can be used for targeted delivery [23, 84-86].

The folate receptor (FR) is a prominent example. It is overexpressed in various cancer types including ovarian, breast, colon and kidney cancer [87-89]. FR is a membrane glycoprotein, which binds folic acid, an essential vitamin, with high affinity ($K_d \approx 10^{-9}$ M). Two isoforms of FR have been found in humans: α and β [90, 91]. As most normal mammalian cells do not express FR, but maintain their folate level via a low affinity reduced folate carrier or proton-coupled folate transporter, FR is favourable to target [92, 93]. Once folic acid containing polyplexes or other folic acid containing drugs have bound to FR, the membrane around this receptor complex invaginates by forming an endosome. With increasing acidification of the endosome receptor conformation changes and the conjugate is released [94, 95]. Folate mediated delivery has been widely used for different therapeutic anticancer agents [96], for example for protein toxins [97], liposomes [98], micelles [99] or polymer-based formulations [100-103]. To elaborate the folate targeting concept for siRNA delivery *via* sequence defined oligomers, Dohmen et al. developed folic acid modified oligomers containing Stp (Figure 3, ***356***). The polyplexes consisting of these oligomers and INF7-siRNA showed efficient and ligand specific gene silencing *in vitro* and an increased retention in KB tumor tissue due to targeting effects *in vivo* [57].

Targeting the epidermal growth factor receptor (EGFR) is another strategy for the specific delivery of nanoparticles [104-106]. EGFR is a transmembrane receptor tyrosin kinase involved in cell proliferation, survival, adhesion, migration and differentiation [107]. EGFR is overexpressed in bladder, cervix, oesophagus, head and neck, ovary, breast, endometrium, colon, lung and brain [108, 109]. Specific drugs have been developed to target the EGFR in cancer therapy [110]. Erlotinib and gefitinib for example reversibly inhibit the tyrosine kinase domain of the EGFR. The monoclonal antibodies cetuximab and panitumumab inhibit ligand binding to the EGFR, enhance receptor internalization and promote cytotoxicity [111]. This shows that the EGFR is an interesting receptor for targeted delivery of polyplexes. Li et al. used phage display to identify a peptide ligand (GE11) that bound specifically and efficiently to the EGFR [112]. GE11 consists of the amino acid sequence YHWYGYTPQNVI and revealed less mitogenic activity than epidermal growth factor (EGF), the natural ligand of EGFR. Coupling GE11 to pDNA/LPEI polyplexes led to efficient gene delivery without receptor activation [113] and polyinosine/cytosine (polyIC)/PEI polyplexes had similar antitumor effects when linked to GE11 compared to EGF *in vitro* and *in vivo* [114]. Mickler et al. demonstrated a slower uptake mechanism via clathrin-mediated endocytosis for GE11-pDNA/PEI polyplexes

compared to EGF-pDNA/PEI polyplexes. The delayed uptake of GE11 polyplexes turned out to be as efficient as for EGF polyplexes with less receptor activation [104].

A drawback to specific targeted delivery of polyplexes is their positive charge. Usually a surplus of cationic oligomer at the surface is used, which can lead to aggregation and unspecific interaction with blood compounds and non-target cells [115]. Flexible water-soluble polymers such as PEG are widely used for nanoparticle shielding to overcome this drawback. Furthermore, the incorporation of PEG protects polyplexes from recognition by the innate immune system, decreases cytotoxicity and increases solubility, stability and circulation time [116-118]. PEG can also serve as spacer between a targeting ligand and the cationic oligomers increasing the binding of ligand and receptor [57, 119]. Despite of the advantages offered by PEG, a high degree of PEGylation may reduce polyplex compaction and stability, cellular uptake and endosomal escape of nanoparticles [120-122].

1.4.3 Endosomal escape

After uptake into cells *via* unspecific or specific endocytosis polyplexes have to be released from the endosome to find their site of action in the cytosol (Figure 4 (3),(4)). Naturally endosomes become late endosomes and lysosomes or return to the membrane to recycle its contents for example receptors [123]. Over time an acidification of endosomes from 5.5 - 6.3 to less than 5.5 (late endosomes) and 4.6 for lysosomes takes place [124]. This acidification driven by V-ATPases is important for vesicular trafficking [125]. In case of cationic polymers containing diaminoethane motifs (see chapter 1.4.1) acidification leads to protonation of oligomer amines, enhanced endosomal Cl^- accumulation, osmotic swelling and rupture of the endosome, the so called “proton sponge effect” [126, 127]. To enhance the endosomal escape, sequence-defined oligomers were modified with lipid moieties or histidines. Lipids did not only improve the stability of polyplexes, but also the endosomal escape by lysing membranes in a favorable pH-specific manner due to their amphiphilic character and cationization at endosomal pH of 5 to 6 [65]. Oleic or linolic acid emerged as most potent fatty acids in gene silencing without significant cytotoxicity [75]. Furthermore, Lächelt et al. integrated histidines into targeted and shielded oligomers for pDNA delivery. These polyplexes demonstrated an enhanced total buffer capacity and therefore a more continuous cationization pH profile resulting in increased endosomal escape [78]. Alternatively, lytic

peptides can be introduced to enhance endosomal escape due to their ability to directly disrupt endosomal membranes [128]. The influenza peptide INF7 electrostatically bound to polyplexes [56] or influenza peptide-siRNA conjugates delivered with oligomers (as mentioned before) [57] have proven to enhance the endosomal escape successfully. Furthermore, a pH-responsive endosomolytic form of the peptide melittin has been shown to improve transfection efficiency when incorporated into polymers. The amines of melittin had to be modified with dimethylic anhydride (DMMAn) to reduce extracellular toxicity. In the acidic endosome these protecting groups are cleaved and the lytic activity of melittin is restored [116, 129].

1.5 Mesoporous silica nanoparticles

Mesoporous silica with ordered pores in the size range between 2 µm and 10 µm was first reported in the early 1990 [130] Several attempts were later made to reduce the particle size of these new materials down to only about a hundred nanometers; however, it took about another decade that individual porous silica particles were synthesized in this size-range. At some point these mesoporous silica nanoparticles became known as MSN. Their colloidal stability and their good biocompatibility opened the way for their use in biomedical applications [131]. MSNs consist of a non-crystalline, amorphous silicon dioxide body interwoven by numerous pores imparting them with large surface areas and huge void volumes. These empty channels (mesopores) can absorb and encapsulate large amounts of bioactive materials with similar dimensions. Typical MSNs are about 100-200 nm in size, have surface areas around 1000 m^2/g, pore sizes around 2-3 nm and pore volumes of about 1 cm^3/g [132]. Due to progress and development in MSN synthesis their particle size, morphology, pore size, and pore structure can be freely designed, and the surface chemistry can be widely controlled [133]. In 2001 micrometer-sized silica particles were first explored for drug delivery purposes by Vallet-Regi et al., who studied particles with different pore sizes for the loading and release of ibuprofen [134]. Since the development of their nanometer-sized counterparts, MSNs have been studied for the delivery of various therapeutic agents to cells in order to control different diseases like diabetes, inflammation and cancer [135-137]. In the area of cancer research MSNs are recently used for the delivery of siRNA. In this regard MSNs are often coated with PEI to bind siRNA via electrostatic interactions, enhance cellular uptake and facilitate endosomal escape [138]. Tamanoi and coworkers demonstrated sufficient siRNA delivery and knockdown of eGFP and the cancer targets Akt and K-ras

using PEI-modified MSNs [139]. Instead of binding siRNA on the surface of MSNs Li et al. loaded siRNA in the pores of magnetic mesoporous silica nanoparticles and capped them with PEI. These particles showed effective eGFP silencing as well. Additionally they knocked down the endogenous B-cell lymphoma 2 (*Bcl-2*) gene [140]. Another approach for siRNA delivery with MSNs is the encapsulation of these particles into liposomes. Brinker and coworkers encapsulated MSNs loaded with siRNA into a lipid bilayer consisting of DOPC, DOPE and cholesterol. This particle formulation led to higher siRNA encapsulation capacity and was more stable when incubated under physiological conditions. In addition to PEG for shielding, a peptide targeting ligand (SP94) and an endosomolytic peptide (H5WYG) were added to the lipid bilayer. Loaded with different siRNA these MSNs were able to silence 90% of cyclin A2, B1, D1, and E and killed >90% of HCC within 48 h of hepatocellular carcinomas [141]. Furthermore, MSNs can be used for dual delivery of anticancer therapeutics as they offer two surfaces (exterior and interior) that can be functionalized individually. He et al. loaded doxorubicin into the 2.9 nm small pore MSNs and attached siRNA targeting Bcl-2 *via* polyamidoamine (PAMAM) dendrimers to the outside of the MSNs. They demonstrated efficient Bcl-2 silencing leading to a significant suppression of nonpump resistance and an enhanced anticancer action of doxorubicin in multidrug resistant A2780/AD human ovarian cancer cells [142]. A similar approach was achieved by Meng et al. by loading doxorubicin into phosphate-coated small pores of MSN and attaching siRNA targeting the P-glycoprotein drug exporter to PEI onto the outer surface both *via* electrostatic interactions. With this formulation a synergistic inhibition of tumor growth and a significant Pgp knockdown was shown in multidrug resistant MCF-7 cells tumor-bearing mice [143]. Additionally, MSNs displayed high biocompatibility, elimination through the renal route and accumulation in tumor xenografts [137].

In summary, mesoporous silica nanoparticles offer several attractive features for siRNA delivery such as their dual-functional surfaces, high loading capacity, large surface areas, biocompatibility, biodegradability and stable framework.

1.6 Aim of the thesis

The use of RNAi in cancer treatment is an excellent opportunity for new highly sophisticated therapies. But, even though the discovery of RNAi dates back nearly 20 years already, only a few siRNA or miRNA delivery systems are in clinical studies. Several barriers have to be overcome in the biological environment for sufficient delivery.

The formulations have to withstand the forces in the blood stream thus an adequate stability is required. Furthermore, they have to be in a suitable size range, so that they are not eliminated immediately by the urinary tract, and possess shielding domains to avoid unspecific interactions with blood components or cell membranes, and targeting ligands for receptor specific delivery. Once the delivery systems have reached their target tissue, they have to be uptaken into cells, normally *via* endocytosis, subsequently they have to escape from the endosome again and finally they should set their cargo free in the cytosol. To meet all these requirements, sequence-defined oligomers offer an outstanding platform as they can be designed precisely, flexibly and with multiple functionalities. Thus, the focus of the thesis was the development of efficient tumor-targeted siRNA and miRNA delivery systems using sequence-defined oligomers with suitable sizes, stability, targeting ligands and biocompatibility.

The first aim of the thesis was the evaluation of a new stability motif, the CRC motif, for its suitability in polyplex stabilization and influence on transfection efficiency. Therefore, non-targeted and shielded and targeted oligomers with and without CRC motif should be examined and compared. Here, the highly efficient targeting ligand folic acid (FolA) had to be used.

The second aim was the evaluation and screening of a small oligomer library, which combined different oligomer topologies, stability motifs and endosomal escape domains. All oligomers contained the shielding reagent polyethylene glycol (PEG) and the targeting ligand FolA for efficient and receptor specific gene silencing. This study aimed at the investigation of structure-activity relationships and at the determination of the optimal candidate for folate receptor (FR) - targeted siRNA delivery.

The third aim of the thesis was the examination of oligomers with shielding and FR-targeting obtained *via* native chemical ligation (NCL). The feasibility of this method to identify candidates for successful targeted delivery from our existing library without completely new synthesis should be shown.

The fourth aim was the application of post-PEGylation to optimize polyplexes towards highly efficient and targeted siRNA and miRNA delivery vehicles. Defined T-shaped lipo-oligomers containing several stability motifs had to be used as core polyplexes and modified with different targeting ligands *via* maleimide reaction. Resulted particles should be of suitable size and stability for FR-targeted siRNA delivery *in vitro* and *in vivo.* Therefore different PEGylation ratios were to be examined biophysically and biologically and a modification of the FolA ligand was to be established. Moreover, this concept had

to be transferred to other targeting ligands for the delivery of therapeutic nucleic acids. For this purpose, post-PEGylated EGFR targeted lipo-oligocation polyplexes had to be developed for antitumoral treatment with miR-200c and EG5 siRNA.

The fifth aim of the thesis was the evaluation of a siRNA delivery system based on mesoporous silica nanoparticles (MSNs). MSNs with different compositions, surfaces and pore sizes should be examined for their siRNA loading capacity, transfection efficiency and biocompatibility.

2 Materials and Methods

2.1 Materials

2.1.1 Chemicals and reagents

Chemicals and reagents	Source
Agarose NEEO ultra-quality	Carl Roth (Karlsruhe, Germany)
Alexa fluor 488-labelled secondary antibody	Invitrogen (Carlsbad, USA)
Allophycocyanin (APC)-conjugated anti folic acid receptor 1 IgG1 antibody	R&D Systems (Minneapolis, USA)
ATP	Roche (Penzberg, Germany)
Boric acid	Sigma-Aldrich (Munich, Germany)
Bromophenol blue	Sigma-Aldrich (Munich, Germany)
Cell culture consumables	NUNC (Langenselbold, Germany)
CellTiter-Glo®	Promega, (Wisconsin, USA)
Coenzyme A	Sigma-Aldrich (Munich, Germany)
Collagen	Biochrom (Berlin, Germany)
DAPI (4′,6-diamidino-2-phenylindole)	Sigma-Aldrich (Munich, Germany)
Dimethyl sulfoxide (DMSO)	Sigma-Aldrich (Munich, Germany)
D-luciferin sodium	Promega (Mannheim, Germany)
DOTAP(1,2-dioleoyl-3-trimethylammonium-propane (chloride salt, 18:1 TAP)	Avanti Polar Lipids (Alabaster, USA)
Doxorubicin	Sigma-Aldrich (Munich, Germany)
DTNB	Sigma-Aldrich (Munich, Germany)
DTT	Sigma-Aldrich (Munich, Germany)
Dulbecco`s modified Eagle`s medium (DMEM)	Sigma-Aldrich (Munich, Germany)
DMEM/Ham`s F12 medium	Sigma-Aldrich (Munich, Germany)
Dimethylsulfoxid (DMSO)	Bernd Kraft (Duisburg, Germany)
EDTA disodium salt dihydrate	Sigma-Aldrich (Munich, Germany)
EGFR antibody	Dako (Glostrup, Denmark)
Ethidium bromide (EtBr)	Sigma-Aldrich (Munich, Germany)
Fetal bovine serum (FBS)	Life Technologies (Carlsbad, USA)

GelRed™	Biotum (Hayward, USA)
L-Glutathion	Sigma-Aldrich (Munich, Germany)
Glycylglycine	Sigma-Aldrich (Munich, Germany)
Heparin-sodium-25000 (source: pig)	Ratiopharm (Ulm, Germany)
HEPES (N-(2-hydroxyethyl)piperazine-N´-(2-ethanesulfonic acid)	Biomol GmbH (Hamburg, Germany)
INF7 peptide	Biosyntan (Berlin, Germany)
Lipofectamine® 2000	Thermo Fisher (Waltham, USA)
Lysis buffer	Promega (Mannheim, Germany)
Magnesium chloride hexahydrate	AppliChem (Darmstadt, Germany)
MTT (3-(4,5-dimethylthiazol-2-yl)-2,5-diphenyltetrazolium bromide)	Sigma-Aldrich (Munich, Germany)
Paraformaldehyde	Sigma-Aldrich (Munich, Germany)
Penicilline	Biochrom (Berlin, Germany)
Propidium iodide	Sigma-Aldrich (Munich, Germany)
Puromycin	Sigma-Aldrich (Munich, Germany)
Restriction enzymes (BamHI, NotI, SpeI)	New England Biolabs (Ipswich, USA)
RPMI-1640 (folate free)	Life Technologies (Carlsbad, USA)
Sodium citrate	Sigma-Aldrich (Munich, Germany)
Streptomycin	Biochrom (Berlin, Germany)
Triton X-100	Sigma-Aldrich (Munich, Germany)
Trizma® base	Sigma-Aldrich (Munich, Germany)
Trypsin/EDTA	Biochrom (Berlin, Germany)

2.1.2 RNA duplexes

All RNA duplexes were purchased from Axolabs GmbH (Kulmbach, Germany):

eGFP siRNA

- sense: 5´-AuAucAuGGccGAcAAGcAdTsdT-3´,
- antisense: 5´-UGCUUGUCGGCcAUGAuAUdTsdT-3´;

control siRNA (ctrl siRNA)/ control RNA (ctrl RNA)

- sense: 5´-AuGuAuuGGccuGuAuuAGdTsdT-3′
- antisense: 5´-CuAAuAcAGGCcAAuAcAUdTsdT-3′

AHA1 siRNA

- sense: 5´-GGAuGAAGuGGAGAuuAGudTsdT-3′
- antisense: 5´-ACuAAUCUCcACUUcAUCCdTsdT-3′
- Cy5 and Cy7 labelled AHA1-siRNA was labelled at the sense strand: (Cy5/Cy7) (NHC6)-GGAuGAAGuGGAGAuuAGudTsdT

EG5 siRNA

- sense: 5´-ucGAGAAucuAAAcuAAcudTsdT-3´
- antisense: 5´-AGUuAGUUuAGAUUCUCGAdTsdT-3´

miRNA-200c

- sense: 5´-UCCAUCAUUACCCGGCAGUAUUA-3`
- antisense: 5`- UAAUACUGCCGGGUAAUGAUGGA-3’

Peptide modified INF7-siRNAs were synthesized as published in [57]. INF7 in free mercapto form was obtained from Biosyntan (Berlin, Germany):

INF7-eGFP siRNA

- sense: INF7-ss-C6–5´-AuAucAuGGccGAcAAGcAdTsdT-3´
- antisense: 5´-UGCUUGUCGGCcAUGAuAUdTsdT-3´

control INF7-ctrl siRNA

- sense: INF7-ss-C6–5´-AuGuAuuGGccuGuAuuAGdTsdT-3´
- antisense: 5´-CuAAuAcAGGCcAAuAcAUdTsdT-3´

small letters: 2´-methoxy; s: phosphorothioate

2.1.3 Sequence defined oligomers and MSNs

Sequence defined oligomers were synthesized by:

- chapter 3.1: Philipp Klein as described in [144].
- chapter 3.2: Dr. Dongsheng He as described in [67].
- chapter 3.3: Dr. Can Yang Zhang as described in [145].
- chapter 3.4: Resynthesis of ***454*** [73] and ***595*** [144] by Philipp Klein.
  post-PEGylation reagents by Philipp Klein as described in [146] and [147].

Chapter 3.5: Mesoporous silica nanoparticles (MSNs) were synthesized by Dr. Karin Möller as described in [148].

2.2 Methods

2.2.1 Polyplex formation

For polyplex formation 500 ng siRNA or miRNA were used for non-targeted CRC polyplexes (chapter 3.1) and for polyplexes before post-PEGylation (chapter 3.4). For targeted polyplexes (chapter 3.1, 3.2, 3.3) and unmodified polyplexes before NCL (chapter 3.3) 200 ng siRNA were used. The calculated amount of oligomer at indicated N/P ratios were diluted in separate tubes (10 µL each) in HBG (pH 7.4, 20 mM HEPES, 5 % glucose). The polymer solution was added to the RNA solution, mixed by pipetting and incubated for 45 min at RT. In case of post-PEGylation, the PEGylation reagent calculated at indicated molar equivalents of the amount of oligomer was added in 5 µL HBG and incubated for 15 min at RT.

2.2.2 Mesoporous silica nanoparticles (MSN) with oligomer capping

Oligomer ***454*** was attached to MSN samples after loading with siRNA. The oligomer was added directly to the loading solution after the complete siRNA uptake had been confirmed by Nanodrop 2000c spectrometer (Thermo Scientific) analysis and after redispersion of the sample. Usually, 50 µg of oligomer ***454*** were added to 100 µg MSN and shaken for 1 h at 37 °C. This was followed by a 7 minute centrifugation at 14000 rpm. The supernatant was taken off (and measured as a reference in the cell transfection experiments) and was replaced with PBS buffer at pH = 7.4. Cell transfections were performed shortly thereafter. Experiments were carried out by Dr. Karin Möller (Department of Chemistry, LMU Munich).

2.2.3 MSNs with DOTAP capping

DOTAP layer was attached to MP-MSN samples after loading with siRNA. Here, the supernatant loading solution was removed, and to 100 µg of MSN sample 25 µL of a 30 wt% DOTAP solution (2.5 mg/mL in 60:40 H_2O:EtOH) was added by micropipette. The solution was carefully redispersed with the pipette tip, followed by short sonification for 2 seconds. Afterwards, 225 µL cold water (4°C) was subsequently added and again mixed with the pipette for 30 seconds. A 2-fold washing in 100 µl sterile PBS at pH = 7.4 (centrifugation for 3.5 minutes at 14000 rpm) was performed to remove excess lipid. The

final sample was kept in PBS buffer for cell transfection. Experiments were carried out by Dr. Karin Möller (Department of Chemistry, LMU Munich).

2.2.4 Particle size and zeta potential

Particles were measured in a folded capillary cell (DTS 1070) using a Zetasizer Nano ZS with backscatter detection (Malvern Instruments, Worcestershire, UK). For the measurement of CRC-oligomers (chapter 3.1) and NCL-oligomers (chapter 3.3) 10µg of nucleic acid and the calculated amount of oligomer at the indicated N/P ratio were incubated in a total volume of 50 µL HEPES buffer (20 mM, pH 7.4). After polyplex formation the solution was diluted 1:20 with HEPES buffer. For the measurement of post-PEGylated polyplexes (chapter 3.4) particles were prepared as described above with a threefold approach in order to have enough material for measurements. For size measurements, the equilibration time was 0 min, the temperature was 25 °C and an automatic attenuator was used. The refractive index of the solvent was 1.330 and the viscosity was 0.8872 mPa·s. Each sample was measured three times. In case of post-PEGylated polyplexes the sample was diluted 1:16 with HEPES buffer for zeta potential measurements. Zeta potentials were calculated by the Smoluchowski equation. Ten to fifteen subruns lasting 10 s each at 25 °C (n = 3) were measured.

2.2.5 Agarose gel shift assays

A 2.5% agarose gel was prepared by dissolving agarose in TBE buffer (Trizma® base 10.8 g, boric acid 5.5 g, disodium EDTA 0.75 g, and 1 L of water) and boiling it up to 100 °C. GelRed® was added and the agarose gel was casted in the electrophoresis unit. Polyplexes were prepared as described above. MSN samples containing 500 ng siRNA were used. For the gel shift with reducing agents 5 µL of a L-glutathione (GSH) solution was added to 20 µL of the polyplex solution to indicated concentrations. The GSH stock solution had a concentration of 50 M and was adjusted to pH 7.4. HEPES buffer (20mM, pH 7.4) was used as negative control (0 M GSH). For serum gel shifts CRC polyplexes were formed with 2.5 µg control siRNA and oligomers were diluted in separate tubes to a total volume of 12.5 µL HEPES. For serum gel shifts with post-PEGylated polyplexes particles were formed as described above with a final siRNA concentration of 250 µg/mL and final siRNA concentration of 200 µg/mL after PEGylation. Afterwards FBS was added to the samples to a final concentration of 90% FBS. The samples were incubated either at room temperature or 37 °C for the indicated time points. In all cases, 20 µL of

polyplex solution were placed into the sample pockets after 4 µL of loading buffer (6 mL of glycerine, 1.2 mL of 0.5 M EDTA, 2.8 mL of H_2O, 0.02 g of bromophenol blue) was added. Electrophoresis was run at 120 V for 40 min, if not stated otherwise.

2.2.6 Ellman´s assay

The polyplex solution (containing 500 ng siRNA, N/P 10) without or with post-PEGylation was diluted to 30 µL with HBG, and 170 µL working solution (2.44 mL Ellman´s buffer and 60 µL DTNB solution (c= 4 mg/mL)) were added. After 15 min incubation at 37 °C absorption at 412 nm was measured using a GENESYS^{TM} UV-VIS spectrophotometer (Thermo Fisher, Waltham, USA). The percentage of free mercapto groups is based on the theoretical amount (100%) of cysteines (i.e. 2 or 4 molar equivalents in oligomers ***454*** or ***595***, respectively) applied in the polyplex formation.

2.2.7 Ethidium bromide compaction assay

A Cary Eclipse spectrophotometer (Varian, Germany) was used for the quantification of ethidium bromide (EtBr) fluorescence at the excitation wavelength λex = 510 nm and emission wavelength λem = 590 nm. FolA-targeted polyplexes (chapter 3.2) were formed with 5 µg siRNA in 200 µL HBG. LPEI (synthesized by Wolfgang Rödl, Pharmaceutical Biotechnology, LMU Munich, as described in [149]) polyplexes at N/P 6 were chosen as positive control. After polyplex formation 800 µL EtBr solution (c=0.4 µg/mL) was added. Post-PEGylated polyplexes (chapter 3.4) were prepared as described above containing 500 ng siRNA at N/P 10. A threefold approach was prepared in order to have enough material for measurements. The polyplex solution was filled up to 1 mL with EtBr solution (c = 0.5 µg/mL) before measurements. A HBG and EtBr solution in the defined volumes was used as blank. Free siRNA (corresponding amount in HBG and EtBr solution) was assigned to 100 %. The fluorescence intensity of EtBr measured after 3 min of incubation was determined in relation to the 100 % value. Triplicates were measured.

2.2.8 Transmission electron microscopy (TEM)

TEM measurements of MSNs were performed on a Jeol JEM-2011 microscope operating at 200 kV with a CCD detection unit. Samples were dispersed in ethanol and one drop of the resulting solution was then dried on a carbon-coated copper grid. TEM was carried out by Steffen Schmidt (Department of Chemistry, LMU).

2.2.9 siRNA loading and desorption of MSN

siRNA concentrations were determined by UV measurements performed with the Nanodrop 2000c spectrometer (Thermo Fisher, Waltham, USA), with the nucleic acid module (sample volume 1.5 µL). siRNA adsorption was performed with aliquots of MSN samples. Usually amounts of 100 µg that were exposed to 100 µL siRNA solutions (either in water or MES buffer solution at pH = 5) of predetermined concentration. Samples were vortexed and shaken at 37 °C for defined adsorption times between 15 minutes to several hours. Subsequently, samples were centrifuged (14000 rpm, 7 min) and the supernatant was measured again with the Nanodrop to determine the adsorbed amount by difference calculations. To study the desorption process, the supernatant from the loading process was taken off by micropipette and was replaced with 100 µL PBS buffer desorption solution at pH = 7.4. The cumulative desorption was measured in the supernatant solution after centrifugation at preset time intervals. Samples were vortexed and again shaken after each measurement without change of the buffer solution. Experiments were carried out by Dr. Karin Möller (Department of Chemistry, LMU Munich).

2.2.10 Cell culture

Nuro2A/eGFPLuc cells (mouse neuroblastoma), T24, T24/eGFPLuc-200cT (human bladder cancer) cells and MDA-MB 231 (human breast cancer) cells were cultivated in Dulbecco`s modified Eagle`s medium (DMEM). In case of T24/eGFPLuc-200cT cells media was supplemented with 0.4 µg/mL puromycin. KB/eGFPLuc (human cervix carcinoma) cells were grown in folate-free RPMI-1640 and Huh7 or Huh7/eGFPLuc (human hepatocellular carcinoma) in a 1:1 mixture of DMEM and Ham`s F12 medium. All cell lines were cultivated at 37 °C in humidified atmosphere containing 5 % CO_2. All media were supplemented with 10 % fetal bovine serum (FBS), 100 U/mL penicillin and 100 µg/mL streptomycin.

2.2.11 Generation of T24/eGFPLuc-200cT cells

The sequence coding for the eGFP-luciferase fusion protein was PCR-amplified from peGFPluc (Clontech, Saint-Germain-en-Laye, France) using the oligonucleotides eGFPluc_fw (AGTCGGATCCACCATGGTGAGCAAGGGCGAGG) and eGFPluc_rv (GACTACTAGTGCGCAGCTTTCATTACACGGCGATCTTTCCG) (Sigma-Aldrich,

Munich, Germany). BamHI and SpeI were included as restriction sites. The fragment was inserted into the open reading frame of miR-200c Reporter Vector (LR-0073, Biocat, Heidelberg, Deutschland) with the miR-200c binding site TCCATCATTACCCGGCAGTATTA *via* the restriction sites. The completed new plasmid (eGFPLuc-200cT) was transformed into *E.Coli DH5α* and purified using Endo Free Plasmid Maxi Kit (Qiagen, Hilden, Germany). Correctness of the sequence was confirmed by sequencing (GATC Biotech, Konstanz, Germany). Foresaid experiments were carried out by Philipp Heissig (PhD student, Pharmaceutical Biotechnology, LMU Munich). Afterwards, eGFPLuc-200cT was linearized with NotI and purified using High Pure PCR Product Purification Kit (Roche, Penzberg, Germany). Linearized eGFPLuc-200cT was transfected into T24 WT cells using Lipofectamine® 2000 according to the manusfacturer´s protocol and seeded in low density into plates with Dulbecco`s modified Eagle`s medium (DMEM) containing 0.4 µg/mL puromycin. Clones that successfully grew under puromycin selection were picket and analyzed for their luciferase expression using a Centro LB 960 plate reader luminometer (Berthold Technologies, Bad Wildbad, Germany). Clones that successfully integrated the eGFPLuc-200cT plasmid were sorted by Dr. Joachim Ellwart (Helmholtz Zentrum München) with flow cytometry. T24/eGFPLuc-200cT cells were authentificated by DSMZ (Braunschweig, Germany).

2.2.12 Gene silencing

2.2.12.1 Gene silencing of polyplexes

Gene silencing experiments were performed with the indicated cell line and with the indicated RNAs. Silencing experiments were performed in triplicates in 96-well plates. One day prior to transfection 5000 Neuro2A/eGFPLuc, 4000 KB/eGFPLuc (on collagen coated plates), 3500 T24/eGFPLuc-200cT or 5000 Huh7/eGFPLuc cells/well were seeded. Used RNAs were either siRNA against eGFP for silencing the eGFPLuc fusion protein (optional with INF7 modification), miRNA-200c mimic or control RNA with scrambled sequences (optional with INF7 modification). Before transfection the medium was replaced by 80 µL fresh medium for CRC/FolA-PEG containing polyplexes (chapter 3.1/3.2), NCL polyplexes (chapter 3.3) or core polyplexes without PEGylation (chapter 3.4) or 75 µL for post-PEGylated polyplexes (chapter 3.4). Polyplexes were prepared as described above, 20 µL (CRC, FolA-PEG, NCL polyplexes, core polyplexes without PEGylation) or 25 µL (post-PEGylated polyplexes) polyplex solution were added to each well and incubated at 37 °C. Medium was replaced at the indicated time. At 48 h after

initial transfection, cells were treated with 100 µL cell lysis buffer. Luciferase activity in 35 µL cell lysate was measured using a Centro LB 960 plate reader luminometer (Berthold Technologies, Bad Wildbad, Germany) and a luciferin-LAR (1M glycylglycine, 100mM $MgCl_2$, 500mM EDTA, DTT, ATP, coenzyme A) buffer solution. The relative light units (RLU) were presented as percentage of the luciferase gene expression obtained with buffer treated control cells.

2.2.12.2 Gene silencing of MSNs

Gene silencing experiments were performed in KB/eGFPLuc cells. siRNA against eGFP for silencing the eGFPLuc fusion protein or its negative control sequence ctrl siRNA were used. Silencing experiments were performed in triplicates in 96-well plates. 24 h prior to transfection plates were coated with collagen and 4000 cells/well were seeded. Before transfection, the medium was replaced with 80 µL fresh growth medium. 20 µl of MSN suspension (containing usually 10 µg MSN, but also as low as 0.06 µg MSN in PBS buffer at pH = 7.4) were added to each well and incubated at 37°C. The medium was replaced after the indicated incubation time. 48 h after initial transfection, cells were treated with 100 µL cell lysis buffer per well and luciferase activity was measured as described above.

2.2.13 Flow cytometry

2.2.13.1 Cellular internalization of CRC containing oligomers, FolA-PEG oligomers and NCL-oligomers

KB/eGFPLuc cells were seeded into 24-well plates coated with collagen at a density of $5*10^4$ cells/well. After 24 h, culture medium was replaced with 400 µL fresh growth medium. Polyplexes (N/P 20) in 100 µL HBG, containing 1.35 µg siRNA (20% of the nucleic acid was Cy5-labelled) were added to each well and incubated at 37 °C for the indicated time. All experiments were performed in triplicates. Subsequently, cells were washed with 500 µL PBS containing 500 I.U./mL of heparin (source pig) for 15 min to remove any polyplexes sticking to the cell surface. After an additional PBS washing step, cells were detached with trypsin/EDTA and taken up in growth medium, centrifuged and taken up in PBS with 10% FBS. Cellular internalization was assayed by excitation of Cy5 at 635 nm and detection of emission at 665 nm. Cells were gated by forward/sideward scatter and pulse width for exclusion of doublets. DAPI (4′,6-diamidino-2-phenylindole) was used to discriminate between viable and dead cells. Data were recorded by Cyan™

ADP flow Cytometer (Dako, Hamburg, Germany) using Summit™ acquisition software (Summit, Jamesville, NY, USA) and analyzed by FlowJo® 7.6.5 flow cytometric analysis software.

2.2.13.2 Cellular internalization of post-PEGylated polyplexes

KB/eGFPLuc (collagen coated plates), T24/eGFPLuc-200cT, MDA-MB 231, Huh7/eGFPLuc cells were seeded 24 h before transfection in 24-well plates with a density of $5x10^4$ cells/ well in 1000 µL growth media. After 24 h, media was replaced by 400 µL fresh media for polyplexes without PEGylation or 375 µL for post-PEGylated polyplexes. For receptor blocking experiments, the cells were incubated with the same volume of folic acid saturated media 30 min before transfection at 37 °C. Polyplex solution containing 2.5 µg siRNA (10% Cy5 labelled) in 100 µL (non-PEGylated polyplexes) or 125 µL (PEGylated polyplexes) was added and incubated for 45 min at 37 °C. After incubation, cells were washed twice with 500 µL PBS and incubated with 500 I.U./mL of heparin in PBS for 15 min on ice, to remove non-internalized polyplexes from the cell surfaces. After an additional PBS washing step, cells were detached with trypsin/EDTA and taken up in growth medium, centrifuged and taken up in PBS with 10 % FBS. Cellular internalization was assayed by flow cytometry at a Cy5 excitation wavelength of 635 nm and detection of emission at 665 nm. Cells were gated by forward/sideward scatter and pulse width for exclusion of doublets. DAPI (4′, 6-diamidino-2-phenylindole) was used to discriminate between viable and dead cells. Data were recorded by Cyan™ ADP flow Cytometer (Dako, Hamburg, Germany) using Summit™ acquisition software (Summit, Jamesville, NY, USA) and analyzed by FlowJo® 7.6.5 flow cytometric analysis software. All experiments were performed in triplicates.

2.2.13.3 Receptor level studies

To examine the expression of different receptors 1 x 10^6 cells of the indicated cell line were collected in 150 µL FACS buffer (10% FCS in PBS). For the detection of the folate receptor 10 µL allophycocyanin (APC)-conjugated anti folic acid receptor 1 IgG1 antibody was added and incubated on ice for 1 h. For the detection of the EGFR antibody (IgG1 mouse anti-human) was added (1 µL) and incubated on ice for 1 h. In case of EGFR detection cells were resuspended in 100 µL flow cytometry buffer, an Alexa Fluor 488-labelled secondary antibody (IgG goat anti-mouse) was added and incubated again for 1 h on ice. After the incubation on ice cells were washed twice with FACS buffer, resuspended in 500 µL FACS buffer and analyzed using a Cyan® ADP flow cytometer

(Dako, Hamburg, Germany) in both cases. Doublets were discriminated by gating forward/sideward scatter and forward scatter/pulse width, while counterstaining with DAPI allowed distinguishing between dead and living cells. The amount of folic acid receptor positive cells was analyzed through excitation of the dye at 635 nm and detection of emission at 665/20 nm. The amount of EGFR positive cells was analyzed at alexa 488 excitation wavelength of 517 nm and detection of emission at 492 nm. Data were recorded by Cyan™ ADP flow Cytometer (Dako, Hamburg, Germany) using Summit™ acquisition software (Summit, Jamesville, NY, USA) and analyzed by FlowJo® 7.6.5 flow cytometric analysis software.

2.2.13.4 FolA-PEG-CF cell binding studies

KB/eGFPLuc cells were seeded 24 h before transfection in 24-well plates coated with collagen with a density of $5x10^4$ cells/ well in 1 mL of growth medium. After 24 h, medium was replaced by 500 µL fresh growth medium. L1210 cells ($2x10^5$) were collected in 500µL growth media. An aqueous solution containing 0.2 nmol carboxyfluorescein (CF) tagged FolA (FolA-PEG_{24}-K-CF) or PEG (H_6-PEG_{12}-CF) (synthesized by Dr. Ulrich Lächelt, Pharmaceutical Biotechnology, LMU Munich) as a negative control was added and incubated for 45 min on ice. After incubation, cells were washed with 500 µL PBS. KB cells were detached with trypsin/EDTA and taken up in growth medium, centrifuged and taken up in PBS with 10 % FBS. L1210 cells were centrifuged and taken up in PBS with 10 % FBS. Cellular internalization was assayed by flow cytometry at a FITC excitation wavelength of 494 nm and detection of emission at 518 nm. Cells were gated by forward/sideward scatter and pulse width for exclusion of doublets. DAPI was used to discriminate between viable and dead cells. Data were recorded by Cyan™ ADP flow Cytometer (Dako, Hamburg, Germany) using Summit™ acquisition software (Summit, Jamesville, NY, USA) and analyzed by FlowJo® 7.6.5 flow cytometric analysis software. All experiments were performed in triplicates.

2.2.14 Laser scanning microscopy

2.2.14.1 Cellular internalization of CRC-containing oligomers

KB cells or Neuro2A cells were seeded into an 8-well Labtek chamber slide coated with collagen at a density of 3×10^4 cells/well in 300 µL of growth medium 24 h prior to treatment. Polyplexes were formed as described using a mixture of 80% unlabelled and 20% Cy5 labelled nucleic acid (in total 1.2 µg siRNA for PEGylated polyplexes and 1.5

µg siRNA for non-PEGylated polyplexes) and oligomer at N/P 20 in 60 µL of HBG. Medium was replaced with 240 µL of fresh growth medium, and the polyplex solution was added. For PEGylated polyplexes the chamber slide was incubated at 37°C for 45min. Afterwards medium was changed and cells were incubated again for 4h. Then cells were washed twice with 500 µL PBS and fixed with 4% paraformaldehyde (PFA) solution for 30 min at room temperature. For non-PEGylated polyplexes cells were incubated for 24 h and washed and fixed as described before. Cell nuclei were stained with DAPI and actine was stained with rhodium phalloidin (Life technologies). A Leica TCS SP8 confocal microscope was used for image acquisition.

2.2.14.2 Cellular internalization of post-PEGylated polyplexes

KB/eGFPLuc cells were seeded 24 h before transfection in an 8-well Labtek chamber slide coated with collagen with a density of $2x10^4$ cells/ well in 300 µL media 24 h before treatment. After 24 h, medium was replaced by 280 µL for polyplexes without PEGylation or 275 µL for post-PEGylated polyplexes. Afterwards, polyplexes containing 500 ng siRNA were formed as described above, added to the cells and incubated for 45 min at 37 °C. Twenty percent of siRNA were used in Cy5-labelled form, and the post-PEGylation reagent was spiked with 0.2 molar equivalents of a maleimide-PEG_{28}-Alexa488 (synthesized by Philipp Klein, PhD student, Pharmaceutical Biotechnology, LMU Munich). Afterwards cells were washed twice with 500 µL PBS and fixed with a 4% PFA solution for 30 min at RT. After two washing steps, cells were incubated with DAPI in PBS (1:500). A Leica TCS SP8 confocal microscope was used for image acquisition.

2.2.15 Cell viability

2.2.15.1 MTT assay of polyplexes

MTT assay was performed in triplicates in 96-well plates. One day prior to transfection, T24/eGFPLuc-200cT cells with a density of 3500 cells/well and Huh7/eGFPLuc cells with a density of 5000 cells/well were seeded. Before transfection the medium was replaced by 80 µL fresh medium for polyplexes without PEGylation or 75 µL for PEGylated polyplexes. Polyplexes (20 µL) containing 500 ng eGFP siRNA, miR-200c mimic or ctrl RNA, or 25 µL of PEGylated polyplexes were added to each well (final RNA concentration/well: 370 nM) and incubated at 37°C. Medium was replaced after 45 min incubation time. At 48 h after initial transfection, 10 µL of MTT solution (5 mg/mL) were added to each well. After 2 h incubation time at 37 °C, the supernatant was removed and

cells were lysed by freezing at -80 °C. 100 µL of DMSO were added and plates were incubated at 37 °C for 30 min under shaking. Adsorption at 590 nm against a reference wavelength of 630 nm was measured using SpectraFluorTM Plus microplate reader (Tecan, Groeding, Austria). Cell viability was calculated as percentage of absorption compared to wells treated with HBG buffer.

2.2.15.2 Cell viability after EG5 siRNA transfection

Huh7/eGFPLuc cells were seeded one day prior to transfection with a density of 5000 cells/well. Before transfection the medium was replaced by 75 µL, 25 µL of PEGylated polyplexes containing 500 ng siRNA were added to each well (final siRNA concentration/well: 370 nM) and incubated at 37°C. Medium was replaced after 4 h incubation time. At 72 h after initial transfection cell viability was measured using CellTiter-Glo®.

2.2.15.3 Cell viability of MSNs

One day prior to transfection plates were coated with collagen and 4000 KB/eGFP Luc cells/well were seeded. Before transfection, medium was replaced with 80 µL fresh growth medium. 20 µl of MSN solution (with either eGFP-siRNA or control siRNA) were added to each well and incubated at 37 °C. Medium was replaced after the indicated incubation time. After 48 h CellTiter-Glo® assay was performed according to the manufacturer's protocol. All experiments were performed in triplicates.

2.2.16 RT-qPCR

Cells were seeded 24 h before transfection in 6-well plates with a density $1.5x10^5$ cells/ well (T24) and $2x10^5$ cells/ well (MDA-MB 231, Huh7) in 2000 µL growth media. After 24 h, media was replaced by 750 µL fresh media, polyplex solution containing 5 µg EG5 siRNA, miR-200c mimic or ctrl RNA (in 250 µL) was added to each well (final RNA concentration/well: 370 nM) and incubated at 37 °C. Medium was replaced after 45 min incubation time. In case of L1210 suspension cells $1.5x10^5$ cells/well were seeded in 975 µL growth media and transfected with 25 µL of post-PEGylated polyplexes containing 5 µg siRNA after 2 h. At 24 h after initial transfection adherent and suspension cells were lysed and RNA was purified using miRCURY™ RNA Isolation Kit (Exiqon, Vedbæk, Dänemark). RNA was transcribed with the Transcriptor First Strand cDNA Synthesis Kit® (Roche, Penzberg, Germany) according to the manufacturer´s protocol. Quantitative

real-time PCR was performed using UPL Probes Master and Probes (Roche, Penzberg, Germany) on a LightCycler 480TM system with GAPDH as a housekeeper. Following primers were used: EG5 (probe #100): forward: TTCCCCTGCATCTTTCAATC, reverse: TTCAGGCTTATTCATTATGTTCTTTG (Sigma Aldrich, Munich, Germany); ZEB1 (probe #52): forward: GCCAACAGACCAGACAGTGTT, reverse: TCTTGCCCTTCCTTTCCTG; GAPDH (probe #45): forward: TCCACTGGCGTCTTCACC, reverse: GGCAGAGATGATGACCCTTT (Sigma Aldrich, Munich, Germany). Results were analyzed using the ΔCT method.

2.2.17 Proliferation assay

Cells were seeded 24 h before transfection in 6-well plates with a density of $1.5x10^5$ cells/well for T24 cells and $2x10^5$ cells/well for MDA-MB 231 cells in 2000 µL growth media. After 24 h, media was replaced by 750 µL fresh media, polyplex solution containing 5 µg miR-200c mimic or ctrl RNA (in 250 µL) was added to each well (final siRNA concentration/well: 370 nM) and incubated at 37 °C. Medium was replaced after 4 h incubation time. At 24 h after transfection cells were detached with trypsin/EDTA, taken up in growth medium, centrifuged and 2000 MDA-MB 231 cells and 750 T24 cells were seeded in 96-well plates. Proliferation was measured at the indicated time points using CellTiter-Glo®.

2.2.18 Doxorubicin resistance assay

One day prior to transfection 3500 cells/well (T24) or 5000 cells/well (MDA-MB 231) were seeded. Before transfection the medium was replaced by 75 µL and 25 µL of post-PEGylated polyplexes containing 500 ng miR-200c mimic or ctrl RNA (prepared as described above) were added to each well and incubated at 37 °C (final RNA concentration/well : 370 nM). Medium was replaced after 4 h incubation time. At 24 h after transfection cells were treated with 10 µM (T24) or 15 µM (MDA-MB 231) doxorubicin and incubated for 72 h. After this incubation time a MTT assay was performed.

2.2.19 Cell cycle analysis

Cells were seeded 24 h before transfection in 24-well plates with a density of $1.75x10^4$ cells/well (T24) or $2.5x10^4$ cells/well (Huh7) in 1000 µL growth media. After 24 h, media

was replaced by 375 µL and polyplex solution containing 2.5 µg EG5-siRNA, miR-200c mimic or ctrl RNA in 125 µL was added and incubated at 37°C (final siRNA concentration/well: 370 nM). Medium was replaced after 45 min (Huh7) or 4 h (T24) incubation time and cells were incubated for the indicated time. Afterwards, cells were detached with trypsin/EDTA, taken up in growth medium, centrifuged and incubated on ice for 3 h in propidium iodide staining solution (0.1 % sodium citrate, 0.1 % Triton X-100 and 50 µg/mL propidium iodide). Thereafter, cells were washed, taken up in PBS and cell cycle was analyzed by flow cytometry at an excitation wavelength of 488 nm and detection of emission with a 613/20 bandpass filter. Cells were gated by forward/sideward scatter and pulse width for exclusion of doublets. Data were recorded by Cyan™ ADP flow cytometer (Dako, Hamburg, Germany) using Summit™ acquisition software (Summit, Jamesville, NY, USA) and analyzed by FlowJo® 7.6.5 flow cytometric analysis software.

2.2.20 Scratch assay

MDA-MB 231 cells were seeded 24 h before transfection in 6-well plates with a density of $2x10^5$ cells/ well in 2000 µL growth media. After 24 h, media was replaced by 750 µL fresh media, polyplex solution containing 5 µg miR-200c mimic or ctrl siRNA (in 250 µL) was added to each well (final RNA concentration/well: 370 nM) and incubated at 37 °C. Medium was replaced after 4h incubation time. After 24 h, cell layer was broken through a scratch using a 200 µL pipette tip. Cells were washed with PBS and microscope (Axiovert 200, Zeiss, Oberkochen, Germany) pictures were taken at different time points. Image J was used for statistical analysis.

2.2.21 Mitotic aster formation

Huh7/eGFPLuc cells were seeded 24 h before transfection in an 8-well Labtek chamber slide with a density of $2x10^4$ cells/ well in 300 µL media. After 24 h, media was replaced by 225 µL, 75 µL of PEGylated polyplexes containing 1.5 µg siRNA were added to each well (final siRNA concentration/well: 370 nM) and incubated for 45 min at 37 °C. Afterwards, media was replaced and cells were incubated for 48 h. Thereafter, cells were washed twice with 500 µL PBS and fixed with a 4% paraformaldehyde solution for 30 min at RT. After two washing steps, cells were incubated with DAPI in PBS (1:500) for 15 min at RT. An Axiovert 200 fluorescence microscope (Zeiss, Oberkochen, Germany) was used for image acquisition.

2.2.22 *In vivo* experiments

All in vivo experiments were performed in female NMRI nu/nu mice (Janvier, Le Genest-St-Isle) housed in isolated ventilated cages with a 12 h day/night interval and food and water ad libitum. For biodistribution in tumor bearing mice 1×10^6 L1210 cells were injected subcutaneously into the left flank of animals. Animals were treated after tumors reached an appropriate volume of 500−700 mm^3. Animal experiments were performed by Eva Kessel (vet MD student, Pharmaceutical Biotechnology, LMU Munich) according to guidelines of the German law of protection of animal life and were approved by the local animal experiments ethical committee.

2.2.23 Biodistribution of polyplexes

Polyplexes containing 50 µg of AHA1-siRNA, 50% Cy7-labelled and 50% nonlabelled, were mixed in a total volume of 200 µL for non-PEGylated polyplexes and 250 µL for PEGylated polyplexes. Mice were anesthetized with 3% isoflurane in oxygen, and polyplexes were injected into the tail vein. Distribution of polyplexes was measured after 0 min, 15 min, 30 min, 1 h, 4 h, and 8 h using a CCD camera and analyzed via Living Image software. Experiments were performed in triplicates.

2.2.24 RT-qPCR of AHA1-siRNA in organs

RNA was extracted from organs using peqGOLD TriFastTM (PEQLAB Biotechnology GmBH, Germany) according to the manufacturer's protocol. RNA (1 µg) was transcribed with qScript microRNA cDNA synthesis kit (Quanta BioScience, USA) into cDNA. RT-qPCR was performed using PerfecTa SYBR Green SuperMix (Quanta BioScience, USA) on a LightCycler 480 system (Roche, Germany) with miR-191 as a housekeeper. Following primers were used: miR-191 forward, GCGCAACGGAATCCCAAAAG, and AHA1 forward, GAGACTAATCTCCACTTC (Sigma-Aldrich, Munich, Germany). Results were analyzed using the ΔC_T method.

2.2.25 Statistical analysis

Unless otherwise stated, results are presented as arithmetic mean ± standard deviation (SD) and the number of replicates. Statistical significance was determined in two-tailed t-tests or 2-way ANOVA. Significance levels were used as indicated.

3 Results

3.1 Integration of twin disulfides into sequence-defined oligomers for stabilization of siRNA polyplexes

This chapter has been partly adapted from:

Philipp M. Klein, Katharina Müller, Christina Gutmann, Petra Kos, Ana Krhac Levacic, Daniel Edinger, Miriam Höhn, Jean-Christophe Leroux, Marc A. Gauthier, Ernst Wagner, "Twin disulfides as opportunity for improving stability and transfection efficiency of oligoaminoethane polyplexes", Journal of Controlled Release, 2015, 205:109-19.

Efficient siRNA delivery with cationic oligomers is strongly dependent on polyplex stability. Therefore several stabilizing domains, such as hydrophobic and aromatic motifs and cysteines forming disulfide bridges have been integrated into oligomers [65, 73, 150]. Wu et al. found a new bioreducible motif with orthogonal disulfide pairing forming stable dimers and multicyclic structures when integrated into peptides [151]. This so called twin disulfide motif consists of two cysteines with another amino acid in-between: CXC. Arginine as central amino acid (CRC) has been proven advantageous for stable peptide dimerization. As will be described in detail in the PhD thesis of Philipp Klein (Pharmaceutical Biotechnology, LMU Munich), the CRC motif was integrated into sequence defined oligomers to enhance the stability and transfection efficiency of siRNA polyplexes compared to carriers with a single cysteine residue [144]. Structure-activity relations of oligomers with and without PEG chains or targeting ligands were examined.

3.1.1 Previous design and biophysical characterization of CRC containing oligomers

The oligomer ***386*** (*3arm*) served as lead structure for the design of CRC containing oligomers (Figure 6). It consists of three arms, each containing three Stps for siRNA binding and endosomal buffering. ***386*** has proven high siRNA binding and gene silencing in previous studies [65, 150]. The CRC motif was incorporated into each arm replacing the cysteine residue of ***386*** in ascending numbers. Additionally, the influence on targeted delivery of CRC was examined using 2-arm oligomers, each arm with four Stps and a

terminal cysteine or CRC motif. FolA was used as targeting ligand and PEG_{24} as shielding reagent. FolA targeted polyplexes have been shown efficient siRNA delivery before in combination with the influenza hemagglutinin H2A derived peptide INF7 [56] coupled to siRNA for endosomal release [57]. To examine receptor specificity of targeted polyplexes FolA was additionally replaced by succinic acid (SucA), which has the same negative charge, but does not bind to the folate receptor. The library of CRC containing oligomers (synthesized by Philipp Klein, PhD student, Pharmaceutical Biotechnology, LMU Munich) is presented in Figure 6.

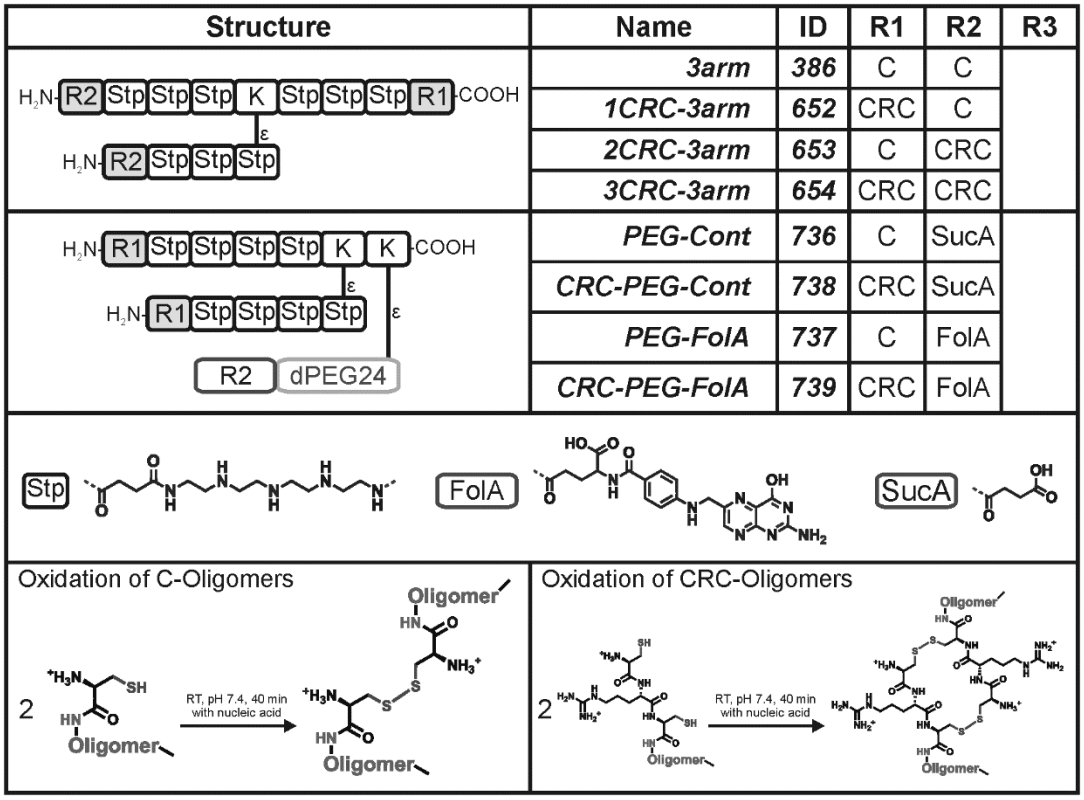

Figure 6. Topology of sequence-defined 3-arm and PEGylated 2-arm oligomers. Schematic overview of the structures with different modifications (C: cysteine, CRC: cysteine-arginine-cysteine, FolA: folic acid, SucA: succinic acid Stp: succinoyl-tetraethylene-pentamine, K: lysine). Each structure has a short name and an internal database identification number. The formation of disulfide bonds, respectively twin disulfide bonds, occurs during the incubation with nucleic acid (bottom of figure). Adapted from [144].

Next, Philipp Klein examined particle sizes and zeta potentials of polyplexes via dynamic light scattering (DLS) and via the application of an electric field using a Zetasizer Nano ZS (Figure 7).

A)

	N/P	Z-average [nm]	Mean PDI	Mean Zeta potential [mV]
3arm	12	951 ± 26	0.34 ± 0.03	17.7 ± 0.4
3arm	20	806 ± 21	0.36 ± 0.04	20.0 ± 0.6
1CRC-3arm	16	450 ± 8	0.26 ± 0.01	22.8 ± 0.4
2CRC-3arm	16	358 ± 1	0.19 ± 0.01	23.4 ± 0.4
3CRC-3arm	16	191 ± 2	0.09 ± 0.01	28.3 ± 0.3

PDI: polydispersity index

B)

	N/P	Z-average [nm]	Mean PDI	Mean Zeta potential [mV]
PEG-Cont	12	65 ± 23	0.42 ± 0.12	0.17 ± 0.27
PEG-FolA	12	105 ± 7	0.08 ± 0.02	0.06 ± 0.07
CRC-PEG-Cont	12	95 ± 9	0.18 ± 0.02	-0.11 ± 0.34
CRC-PEG-FolA	12	171 ± 24	0.12 ± 0.03	-0.10 ± 0.06

PDI: polydispersity index

Figure 7. Particle size (Z-average) and zeta potential of siRNA polyplexes of A) three arm oligomers and B) PEGylated oligomers formed in HEPES buffer. Polyplexes were diluted 1:20 with HEPES before measurement. Variations refer to the median of three measurements of the sample. The study was performed by Philipp Klein (PhD student, Pharmaceutical Biotechnology, LMU Munich). Adapted from [65] and [144].

3arm formed large particles almost in the micrometer range at N/P (ratio between protonatable amines of oligomers and phosphates of siRNA) 12 and 20 [65]. With the introduction of CRC the size successively decreased from about 800 nm for *3arm* to less than 200 nm for *3CRC-3arm* (Figure 7A) displaying a better siRNA compaction of oligomers containing the CRC motif. Additionally, the polydispersity index (PDI) decreased with increasing number of twin disulfides, which indicated uniform shaped particles. In contrast, the zeta potential increased from about 18 mV (*3arm*) to about 30 mV (*3CRC-3arm*). For PEGylated oligomers suitable sizes were obtained for all formulations (Figure 7B). Oligomers containing the CRC motif (*CRC-PEG-Cont*, *CRC-PEG-FolA*) displayed larger sizes compared to oligomers with only one terminal cysteine (*PEG-Cont, PEG-FolA*). Additionally, the influence of folic acid as hydrophobic ligand was very noticeably as FolA-particles were significantly larger (105 nm without CRC and 171 nm with CRC) compared to untargeted controls (65 nm without CRC and 95 nm with CRC). The zeta potential was around 0 mV for all PEGylated particles showing a perfect shielding.

The siRNA binding ability of oligomers was examined in gel shift assays (Figure 8). In this assay free siRNA migrates in the gel due to its negative charge, whereas in polyplexes siRNA is retained in the pockets of the gel.

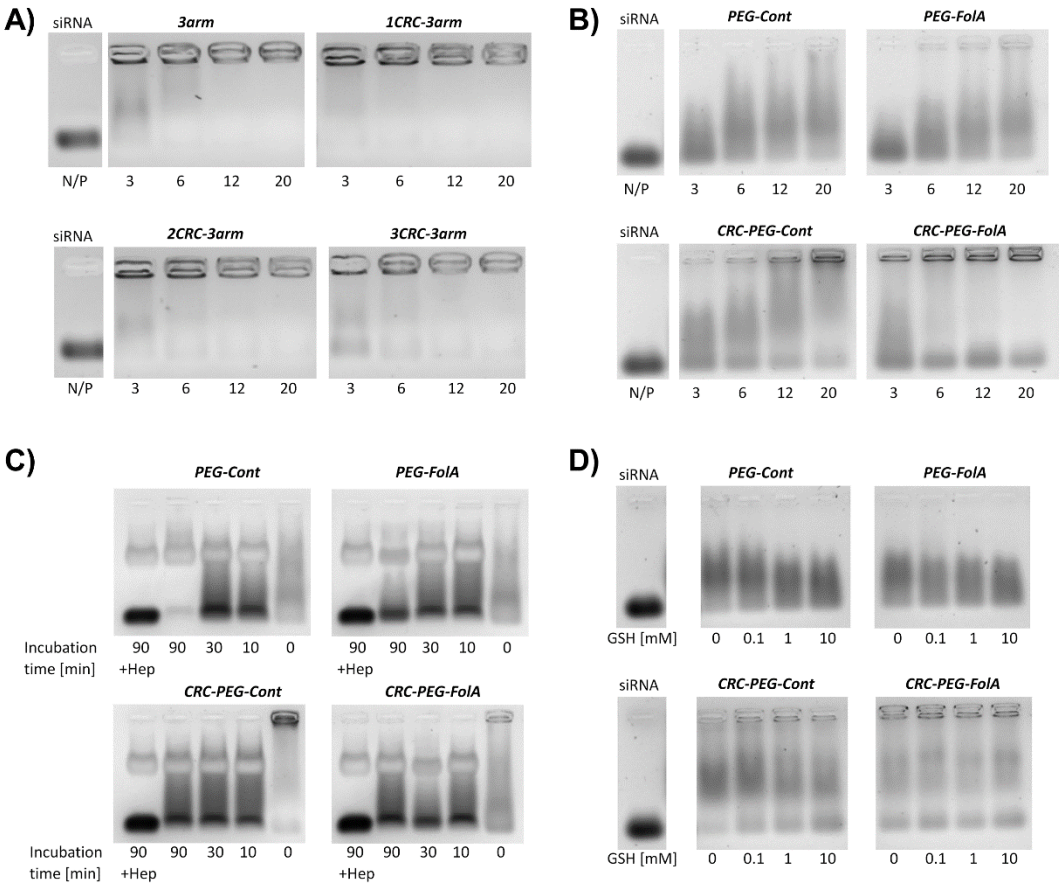

Figure 8. Stability and siRNA binding of polyplexes of A) three-arm oligomers at indicated N/P ratios, B) PEGylated oligomers at indicated N/P ratios, C) PEGylated oligomers at N/P 20 incubated in serum at 37°C for indicated time points and D) PEGylated oligomers at N/P 20 after GSH incubation in different concentrations. Left lanes: free siRNA. Gel shifts were performed by Philipp Klein (PhD student, Pharmaceutical Biotechnology, LMU). Adapted from [144].

The siRNA binding of *3arm* in comparison to *1CRC-3arm*, *2CRC-3arm* and *3CRC-3arm* was studied at N/P ratios from 3 to 20 (Figure 8A). All oligomers released siRNA at N/P 3. With higher N/P ratios sufficient binding of siRNA could be observed in all cases. For PEGylated structures a clear effect of the CRC motif on siRNA binding could be demonstrated (Figure 8B). CRC containing oligomers revealed a higher siRNA binding at all N/P ratios in comparison to oligomers with only one terminal cysteine. The stability of PEG containing CRC oligomers was further investigated in the presence of serum at 37°C (Figure 8C). These conditions should resemble *in vivo* conditions. Polyplexes were

incubated for 0 min, 10 min, 30 min and 90 min. After 90 min negatively charged heparin destroying the polyplexes via electrostatic disturbance was additionally added. Again, an enhanced stability could be observed with CRC containing oligomers at 0 min incubation time. With longer serum incubation siRNA was released in all cases regardless of the modification. Nevertheless, all oligomers bound the majority of siRNA after 90 min, which can be seen in comparison to released siRNA after heparin addition (90 min plus/minus heparin treatment). To obtain information about the behaviour of PEGylated polyplexes towards physiological reducing agents a gel shift in the presence of glutathione (GSH) was performed (Figure 8D). In nature, the GHS concentrations are 0.02 mM outside cells and 1-11 mM inside cells. Polyplexes should be stable outside cells and should disintegrate inside the cell to release their cargo. Therefore GSH concentrations from 0 to 10 mM were tested. For oligomers having only one terminal cysteine the siRNA binding was weak at all GSH concentrations with a tendency towards less binding with increasing GSH. The incorporation of the CRC motif increased the stability of polyplexes significantly with no difference between GSH concentrations.

3.1.2 Cellular internalization of CRC containing oligomers

Within the current thesis, the intracellular distribution of polyplexes was examined by confocal laser scanning microscopy in mouse neuroblastoma Neuro2A/eGFPLuc cells or human cervix carcinoma KB/eGFPLuc cells (Figure 9). KB cells overexpress the folate receptor (FR) and are therefore used for the investigation of FolA targeted delivery. siRNA was spiked with Cy-5 labelled siRNA (red) and polyplexes were incubated on cells for 24 h (3-arm oligomers, Figure 9A) and 45 min (PEGylated oligomers, Figure 9B) at 37°C. The short time incubation of 45 min should avoid unspecific uptake of particles.

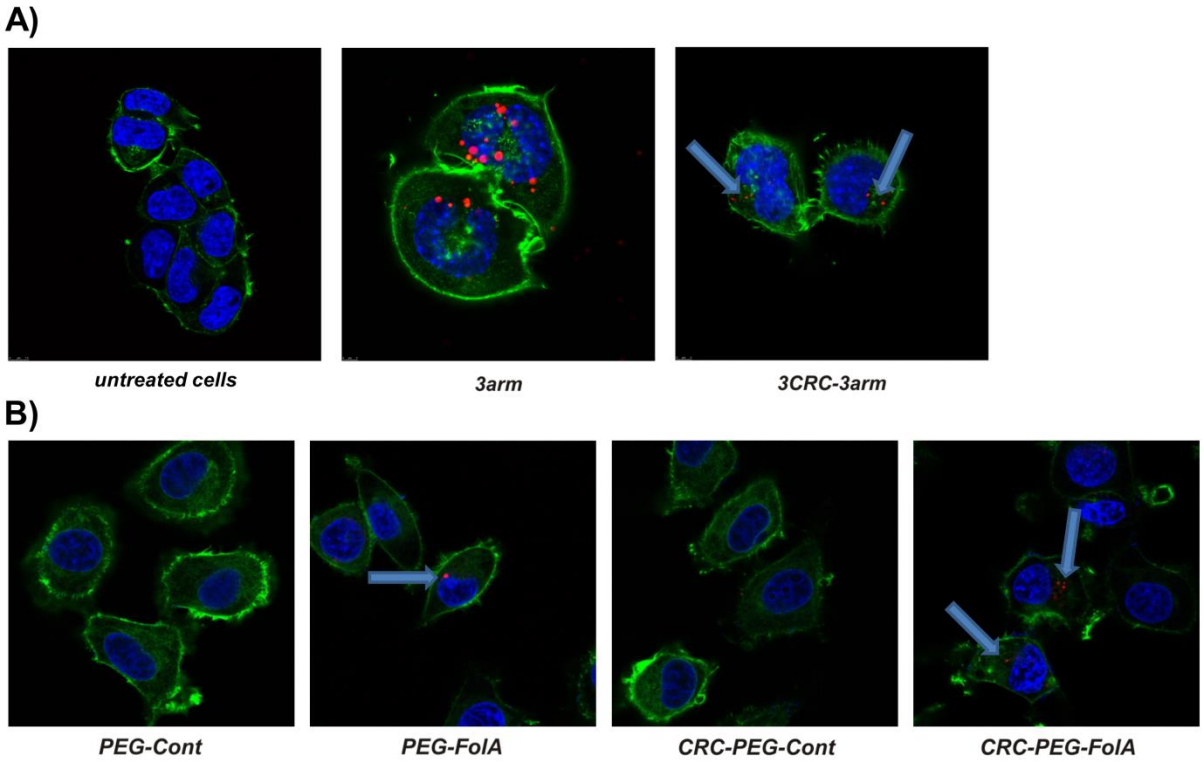

Figure 9. Intracellular distribution of A) 3-arm siRNA polyplexes in Neuro2A/eGFPLuc cells and B) PEGylated siRNA polyplexes in KB/eGFPLuc acquired by confocal laser scanning microscopy. Polyplexes were formed at N/P 20. Nuclei were stained with Hoechst 33342 (blue), actin was stained with rhodamine phalloidin (green) and siRNA was spiked with 20% Cy5 labelled siRNA (red). The images show the overlay of the different channels. Blue arrows point at polyplexes inside cells. *In vitro* preparation was carried out by Katharina Müller; microscopy pictures were taken by Miriam Höhn (Pharmaceutical Biotechnology, LMU). Adapted from [144].

An equal distribution of particles could be observed for all 3-arm oligomers (Figure 9A). *3arm* without twin disulfides revealed large aggregated polyplexes in cellular vehicles in comparison to *3CRC-3arm*, which formed very small particles, consistent with DLS measurements. PEGylated polyplexes without targeting ligand were almost not visible in cells indicating a minor uptake. On the other hand, FolA containing polyplexes could be observed inside cells for both, *PEG-FolA* and *CRC-PEG-FolA* showing a clear targeting effect. For *CRC-PEG-FolA* a denser distribution in cells was found. The receptor specific uptake of PEGylated polyplexes was further investigated *via* flow cytometry (Figure 10). Once again, a superior uptake of PEGylated oligomers could be demonstrated with FolA containing oligomers in comparison to oligomers without targeting ligand with and without CRC motif.

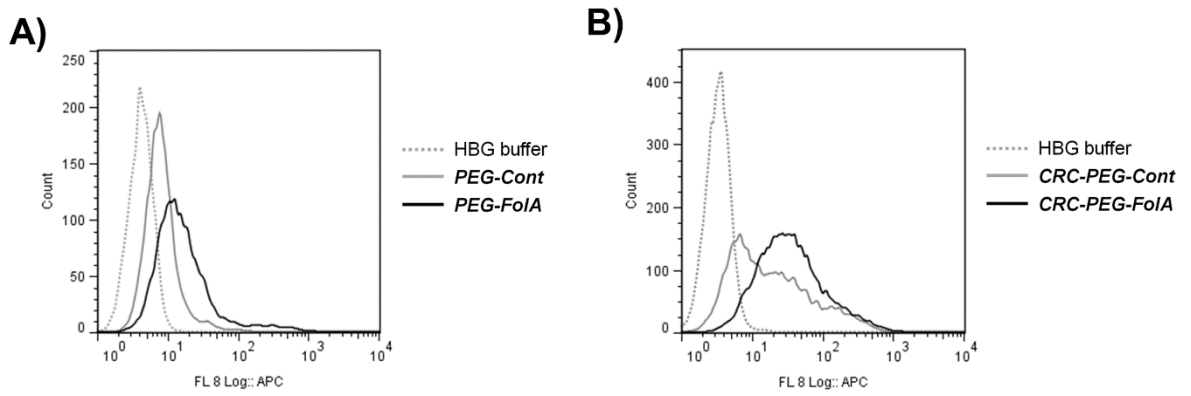

Figure 10. Cellular internalization of Cy5-labelled siRNA (N/P 20) polyplexes after 45 min incubation time on cells determined by flow cytometry. The intensity of the Cy5 signal indicates the amount of polyplexes being internalized by KB/eGFPLuc cells. A) PEG-Cont (gMFI = 8.07) in solid gray, PEG-FolA (gMFI= 15.9) in solid black and HBG buffer only treated cells in dotted gray. B) CRC-PEG-Cont (gMFI= 18.3) in solid gray, CRC-PEG-FolA (gMFI = 31.4) in solid black and HBG buffer (gMFI= 4.54) only treated cells in dotted gray. gMFI indicates the geometric mean fluorescence intensity. Adapted from [144].

3.1.3 Gene silencing of CRC containing oligomers

Gene silencing experiments were performed in N2A/eGFPLuc cells or KB/eGFPLuc cells, both stably expressing an eGFP-luciferase fusion protein (Figure 11). Polyplexes were transfected with siRNA against eGFP (eGFP siRNA) or control siRNA (ctrl siRNA) with no silencing capacity (Figure 11 A,B). Additionally, INF7 was attached to eGFP siRNA or ctrl siRNA in order to enhance the endosomal escape (see chapter 1.3 and 1.4.3) of PEGylated oligomers (Figure 11 C). Polyplexes were incubated on cells at 37 °C for 48 h (Figure 11A) or, in case of targeted PEGylated oligomers, for 45 min to avoid unspecific uptake (Figure 11B,C).

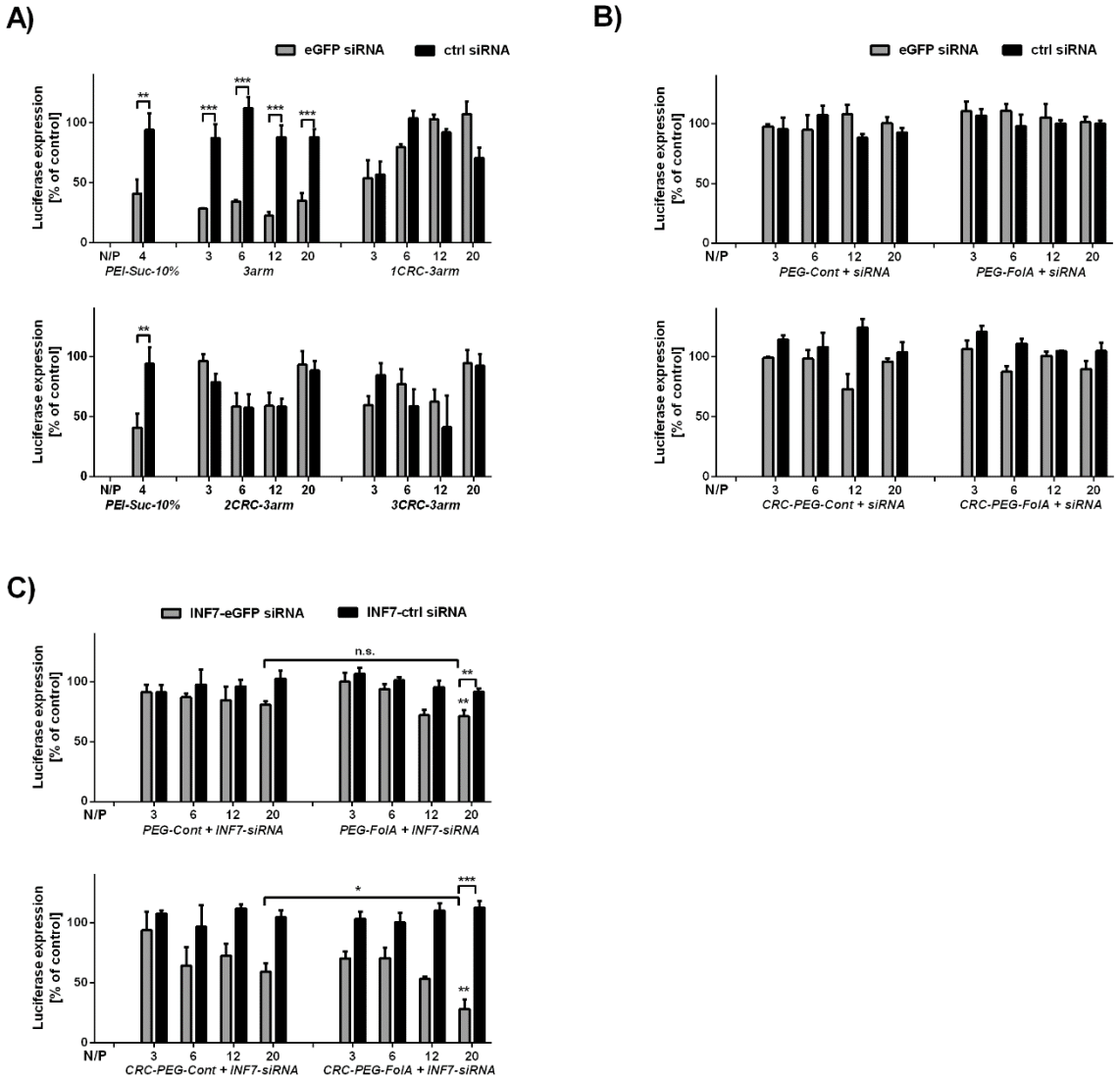

Figure 11. Gene silencing of A) 3-arm structures and B, C) PEGylated structures. Polyplexes containing eGFP-targeted siRNA (eGFP siRNA) or control siRNA (ctrl siRNA) were tested in (A) Neuro2A/eGFPLuc or (B) KB/eGFPLuc cells. C) Polyplexes containing eGFP-targeted INF7-siRNA (INF7-eGFP siRNA) or control INF7-siRNA (INF7-ctrl siRNA) were tested in KB/eGFPLuc cells. Polyplexes at the indicated N/P ratios were incubated on cells for 45 min (B,C) or 48 h (A). Top: polyplexes with single cysteine oligomers. Bottom: polyplexes with twin disulfide-forming oligomers. PEI-Suc-10% serves as positive control. Data are presented as mean value (±SD) out of triplicates; notes on top of transfection bars without arrow indicate if there is statistical significance between single cysteine structure and its corresponding CRC analogous for same N/P (n. s.= $p > 0.05$; *$p < 0.05$; **$p < 0.01$; ***$p < 0.001$, Student's t-test, two-tailed). Adapted from [144].

The oligomer *3arm* showed very good gene knockdown at N/P ratios from 3 to 20. Interestingly, the insertion of the CRC motif abolished gene silencing in all cases (Figure 11A). PEGylated oligomers revealed no gene silencing efficiency, when transfected without INF7-eGFP siRNA (Figure 11B). When INF7 was coupled to siRNA, gene silencing could be observed (Figure 11C). *CRC-PEG-FolA* showed gene silencing

efficiency up to 70 % at N/P 20 whereas only 20 % knockdown could be achieved with *PEG-FolA*. Here, the insertion of the twin-disulfide motif was beneficial in comparison to single terminal cysteines. For control structures without FolA (*PEG-Cont* and *CRC-PEG-Cont*) only moderate gene knockdown could be observed confirming the FolA ligand-dependent uptake.

3.2 Folate-PEG-oligomer conjugates for targeted siRNA delivery

This chapter has been partly adapted from:

Dongsheng He, Katharina Müller, Ana Krhac Levacic, Petra Kos, Ulrich Lächelt and Ernst Wagner, "Combinatorial Optimization of Sequence-Defined Oligo(ethanamino)amides for Folate Receptor-Targeted pDNA and siRNA Delivery", Bioconjugate Chemistry*, 2016, 27 (3), 647–659.*

FolA, which led to potent and receptor specific siRNA delivery when coupled to CRC-oligomers, was furthermore attached to different oligomer topologies to figure out structure-activity relationships of targeted sequence-defined oligomers. Targeting the FR is a widely used strategy as it is overexpressed in many cancer types and binds folic acid with high affinity (see chapter 1.4.2). By using SPS various oligomer combinations can be synthesized fast, precise and pure. With this method 42 sequence-defined oligomers containing FolA or control amino acids without targeting effect were synthesized by Dr. Dongsheng He (PhD thesis 2016, Pharmaceutical Biotechnology, LMU Munich) and analyzed for their targeted pDNA or siRNA delivery efficiency. The current thesis focussed on the biological evaluation of siRNA polyplexes.

3.2.1 Previous design and biophysical characterization of FolA-PEG- oligomer conjugates

Based on the previously published and highly efficient oligomer ***356*** [57] different topologies and building block combinations were established. ***356*** formed only monomolecular particles, as the high PEG content prevented intermolecular nucleic acid compaction. Thus, the two-arm structure was only partially retained in this study. For some oligomers it was extended to four arms to enhance the amount of positive charges. The arms were branched through lysines and contained the cationic siRNA binding regions Stp (five nitrogens) or Sph (six nitrogens). As ***356*** transfected only with INF7 modified siRNA, alternating histidines were added to some oligomers for endosomal buffering [78]. To enhance the stability of polyplexes tyrosine trimers for hydrophobic interactions [73] and terminal cysteines for disulfide bridge formation [57, 150] were additionally integrated.

Topology	Sequence	No.
2-arm 	C-Stp$_4$-K-(PEG$_{24}$-FolA)-Stp$_4$-C	356
	K-(PEG$_{24}$-Acetate)-K-(Sph$_3$-C)$_2$	#1
	K-(PEG$_{24}$-FolA)-K-(Sph$_3$-C)$_2$	#2
	K-(PEG$_{24}$-Acetate)-K-(Sph$_4$-C)$_2$	#3
	K-(PEG$_{24}$-FolA)-K-(Sph$_4$-C)$_2$	#4
2-arm-H 	K-(PEG$_{24}$-E)-K-[(H-Stp)$_3$-H-C]$_2$	#5
	K-(PEG$_{24}$-FolA)-K-[(H-Stp)$_3$-H-C]$_2$	#6
	K-(PEG$_{24}$-E)-K-[(H-Stp)$_4$-H-C]$_2$	#7
	K-(PEG$_{24}$-FolA)-K-[(H-Stp)$_4$-H-C]$_2$	#8
2-arm-Y$_3$ 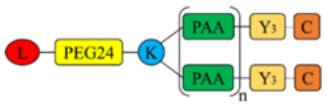	K-(PEG$_{24}$-E)-K-(Stp$_3$-Y$_3$-C)$_2$	#9
	K-(PEG$_{24}$-FolA)-K-(Stp$_3$-Y$_3$-C)$_2$	#10
	K-(PEG$_{24}$-E)-K-(Stp$_4$-Y$_3$-C)$_2$	#11
	K-(PEG$_{24}$-FolA)-K-(Stp$_4$-Y$_3$-C)$_2$	#12
	K-(PEG$_{24}$-E)-K-(Sph$_3$-Y$_3$-C)$_2$	#13
	K-(PEG$_{24}$-FolA)-K-(Sph$_3$-Y$_3$-C)$_2$	#14
	K-(PEG$_{24}$-E)-K-(Sph$_4$-Y$_3$-C)$_2$	#15
	K-(PEG$_{24}$-FolA)-K-(Sph$_4$-Y$_3$-C)$_2$	#16
2-arm-H-Y$_3$ 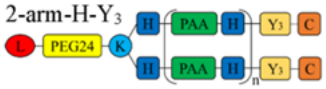	K-(PEG$_{24}$-E)-K-[(H-Stp)$_3$-H-Y$_3$-C]$_2$	#17
	K-(PEG$_{24}$-FolA)-K-[(H-Stp)$_3$-H-Y$_3$-C]$_2$	#18
	K-(PEG$_{24}$-E)-K-[(H-Stp)$_4$-H-Y$_3$-C]$_2$	#19
	K-(PEG$_{24}$-FolA)-K-[(H-Stp)$_4$-H-Y$_3$-C]$_2$	#20
4-arm 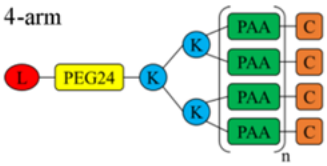	K-(PEG$_{24}$-E)-K-[K-(Stp$_3$-C)$_2$]$_2$	#21
	K-(PEG$_{24}$-FolA)-K-[K-(Stp$_3$-C)$_2$]$_2$	#22
	K-(PEG$_{24}$-E)-K-[K-(Stp$_4$-C)$_2$]$_2$	#23
	K-(PEG$_{24}$-FolA)-K-[K-(Stp$_4$-C)$_2$]$_2$	#24
	K-(PEG$_{24}$-A)-K-[K-(Sph$_3$-C)$_2$]$_2$	#25
	K-(PEG$_{24}$-FolA)-K-[K-(Sph$_3$-C)$_2$]$_2$	#26
	K-(PEG$_{24}$-A)-K-[K-(Sph$_4$-C)$_2$]$_2$	#27
	K-(PEG$_{24}$-FolA)-K-[K-(Sph$_4$-C)$_2$]$_2$	#28
4-arm-H 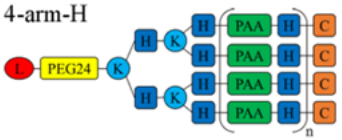	K-(PEG$_{24}$-E)-K-[H-K-((H-Stp)$_3$-H-C)$_2$]$_2$	#29
	K-(PEG$_{24}$-FolA)-K-[H-K-((H-Stp)$_3$-H-C)$_2$]$_2$	#30
	K-(PEG$_{24}$-E)-K-[H-K-((H-Stp)$_4$-H-C)$_2$]$_2$	#31
	K-(PEG$_{24}$-FolA)-K-[H-K-((H-Stp)$_4$-H-C)$_2$]$_2$	#32
	K-(PEG$_{24}$-E)-K-[H-K-((H-Sph)$_3$-H-C)$_2$]$_2$	#33
	K-(PEG$_{24}$-FolA)-K-[H-K-((H-Sph)$_3$-H-C)$_2$]$_2$	#34
4-arm-Y$_3$ 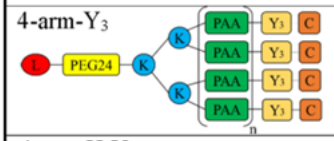	K-(PEG$_{24}$-E)-K-[K-(Stp$_3$-Y$_3$-C)$_2$]$_2$	#35
	K-(PEG$_{24}$-FolA)-K-[K-(Stp$_3$-Y$_3$-C)$_2$]$_2$	#36
	K-(PEG$_{24}$-E)-K-[K-(Stp$_4$-Y$_3$-C)$_2$]$_2$	#37
	K-(PEG$_{24}$-FolA)-K-[K-(Stp$_4$-Y$_3$-C)$_2$]$_2$	#38
4-arm-H-Y$_3$ 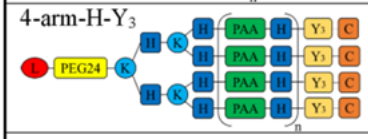	K-(PEG$_{24}$-E)-K-[H-K-((H-Stp)$_3$-H-Y$_3$-C)$_2$]$_2$	#39
	K-(PEG$_{24}$-FolA)-K-[H-K-((H-Stp)$_3$-H-Y$_3$-C)$_2$]$_2$	#40
	K-(PEG$_{24}$-E)-K-[H-K-((H-Stp)$_4$-H-Y$_3$-C)$_2$]$_2$	#41
	K-(PEG$_{24}$-FolA)-K-[H-K-((H-Stp)$_4$-H-Y$_3$-C)$_2$]$_2$	#42
Stp 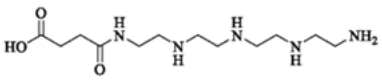	PEG 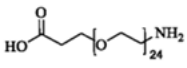	
Sph 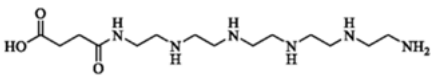	FolA 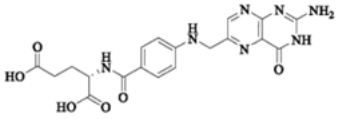	

Figure 12. Overview of oligomer topologies and compositions. L: FolA (folic acid) ligand or corresponding negative control (A, alanine; E, glutamate); PAA, poly(amino acid) (Stp, succinoyl-tetraethylene-pentamine; Sph, succinoyl-pentaethylene-hexamine); PEG, polyethylene glycol; K, lysine; H, histidine; Y, tyrosine; C, cysteine. K-(and K-[refer to branchings by α- and ε-amino modification of lysines. Adapted from [67].

Twenty-four PEG units served as shielding domains [118] and FolA as targeting ligand. In order to examine the targeting effect of these oligomers, FolA was replaced by alanine, glutamate or acetate. These combinations resulted in 42 oligomer structures (synthesized by Dr. Dongsheng He, PhD thesis 2016, Pharmaceutical Biotechnology, LMU Munich), which are presented in Figure 12.

The siRNA binding ability of selected oligomers was examined in gel shift assays (Figure 13). As already observed for ***356*** [57] only weak siRNA retention could be found for two-arm oligomers, which slightly improved with high N/P ratios. In comparison, the siRNA binding was enhanced with four-arm structures, e.g. #6 vs. #30 or #18 vs. #40. Unexpectedly, the insertion of tyrosine trimers did not enhance the stability, but weaken it (#2 vs. #14 or #22 vs. #36). In contrary, more siRNA could be found in the pockets when histidines were included (#10 vs. #18 or #36 vs. #40).

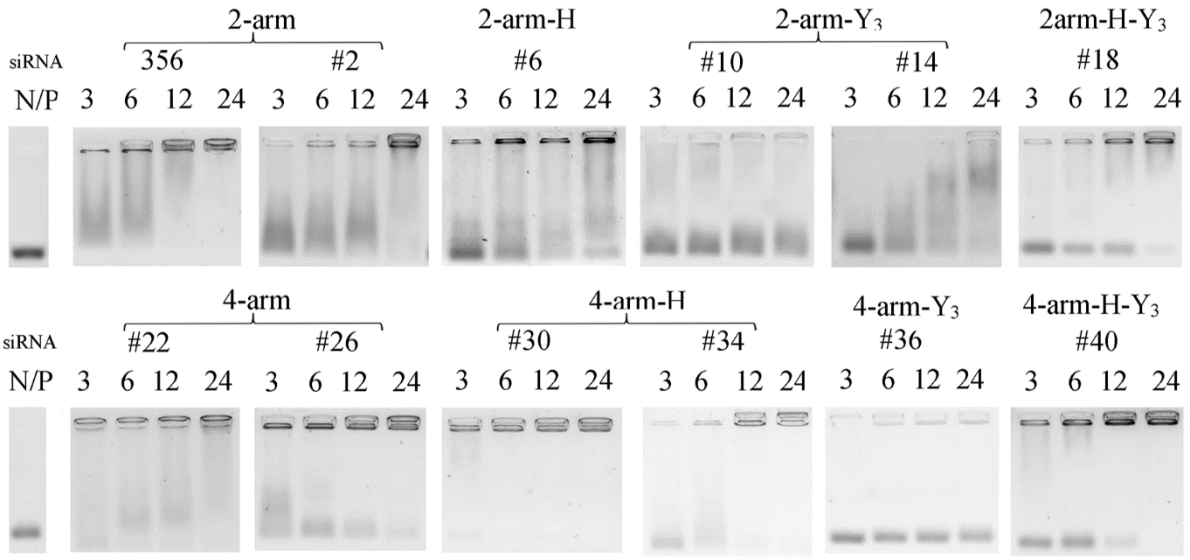

Figure 13. Gel retardation assays of siRNA polyplexes formed in HBG at the indicated N/P ratios. Left lanes: free siRNA. Gel shifts were performed by Dr. Dongsheng He (PhD thesis 2016, Pharmaceutical Biotechnology, LMU Munich). Adapted from [67].

The siRNA compaction was further examined in an ethidium bromide exclusion assay (Figure 14). In this assay the compaction can be monitored by the fluorescence intensity of intercalating ethidium bromide. In most cases, a higher siRNA compaction could be found for four arm oligomers in comparison to two arm oligomers. The best siRNA compaction ability could be observed for the basic two-arm (#1-4) and four-arm (#21-28) oligomers without additional tyrosines and histidines. Again, oligomers containing tyrosine trimers revealed the worst siRNA compaction ability.

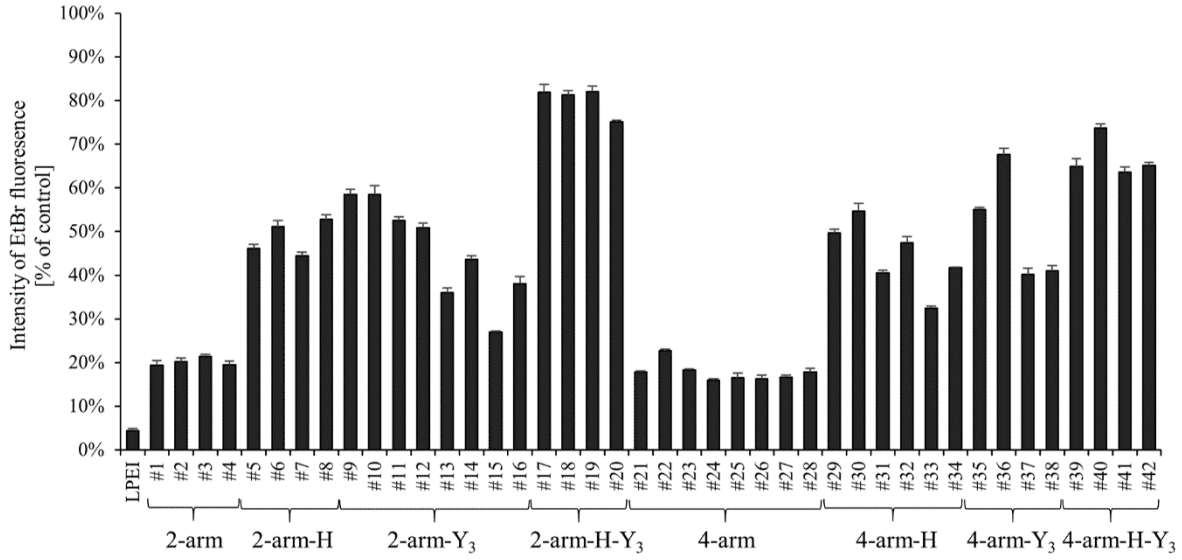

Figure 14. siRNA compaction of oligomers determined by ethidium bromide exclusion assay at N/P 12 with LPEI N/P 6 as control. Measurements were performed by Dr. Dongsheng He (PhD thesis 2016, Pharmaceutical Biotechnology, LMU Munich). Adapted from [67].

3.2.2 Gene silencing and cellular internalization of FolA-PEG-oligomer conjugates

In the current thesis, gene silencing of the oligomer library was tested in KB/eGFPLuc cells because of their high FR expression (Figure 15, 2-arm oligomers, and Figure 16, 4-arm oligomers). Polyplexes were transfected with eGFP siRNA in comparison to ctrl siRNA. Additionally, siRNA modified with INF7 peptide was used to enhance the endosomal escape. Here again, a short incubation time of 45 min at 37 °C was chosen to examine the targeting effect. Consistent with previous studies [57] ***356*** showed high gene silencing with INF7-eGFP siRNA and only moderate gene silencing with eGFP siRNA. In comparison, the same structure without FolA (***188***) did not transfect KB/eGFPLuc cells demonstrating a targeting effect. When Stp was replaced by three Sph (#1-2) (Figure 15) only moderate gene silencing could be observed with INF7-eGFP siRNA. On the other hand, oligomers containing four Sph (#3-4) showed superior gene silencing, but without receptor specificity. The insertion of histidines into two-arm oligomers (#5-8) did not lead to higher transfection efficiency compared to ***356***.

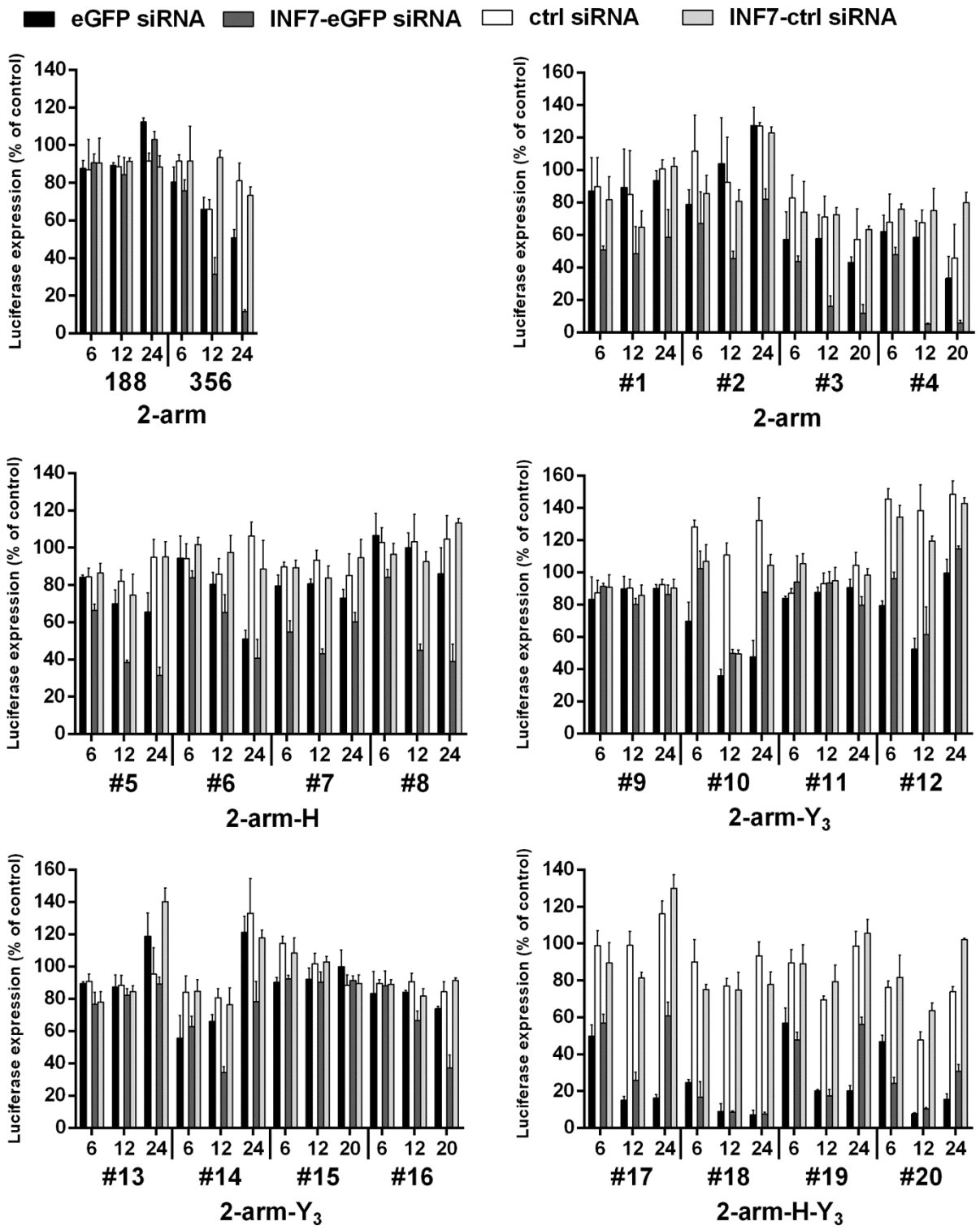

Figure 15. Gene silencing in folate receptor-expressing KB/eGFPLuc cells of 2-arm oligomers. Polyplexes formed with eGFP targeted siRNA (eGFP siRNA), control siRNA (ctrl siRNA), and corresponding INF7 peptide modified siRNA (INF7-eGFP siRNA and INF7-ctrl siRNA) at N/P 6, 12 and 20 or 24 were tested for eGFPLuc gene silencing. Cells were incubated with polyplexes for 45 min at 37°C. Luciferase activities at 48 h after transfection are presented as a percentage of relative light units (RLU) obtained with buffer treated control cells. Data are shown as mean ± SD (n = 3). Adapted from [67].

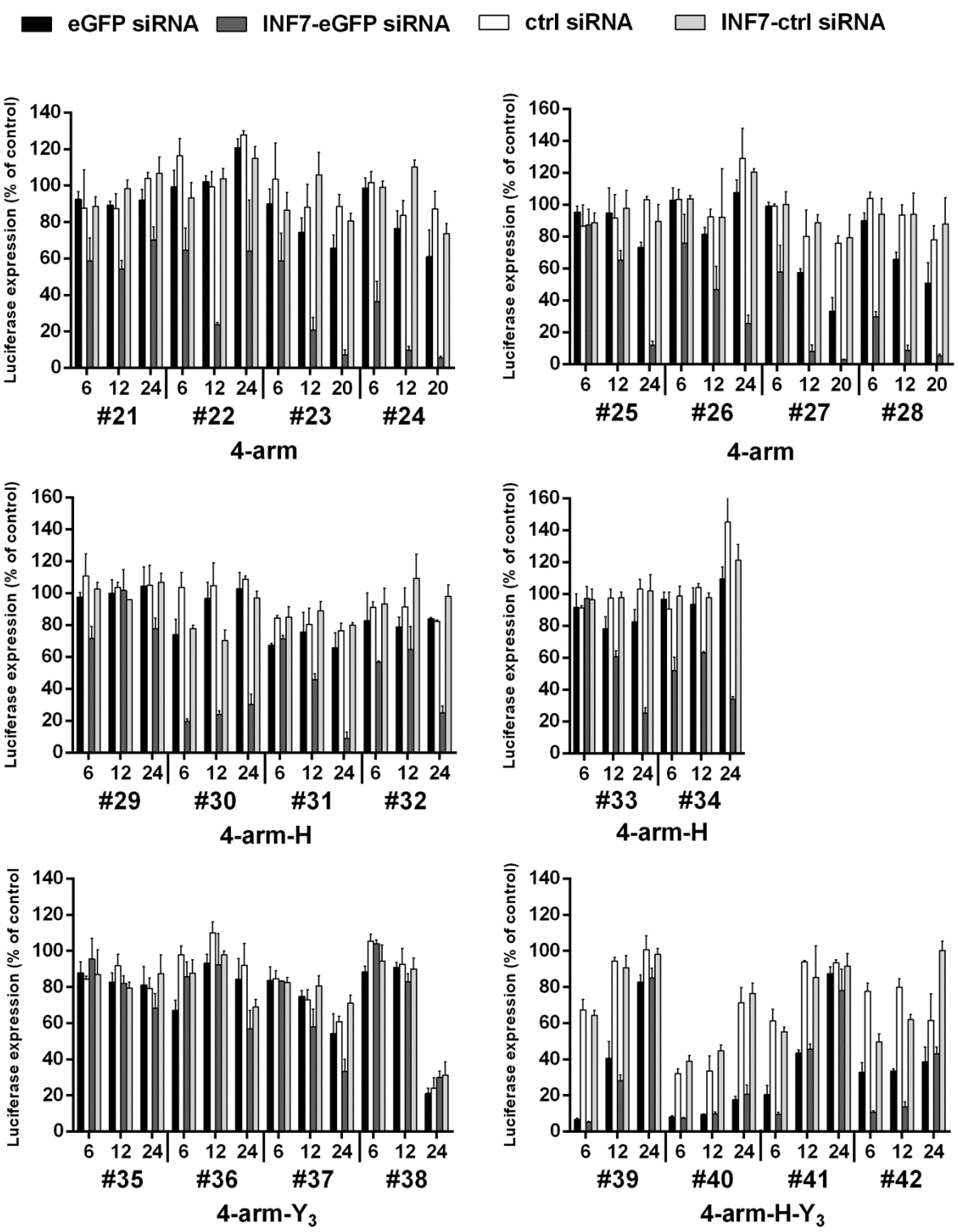

Figure 16. Gene silencing in folate receptor-expressing KB/eGFPLuc cells of 4-arm oligomers. Polyplexes formed with eGFP targeted siRNA (eGFP siRNA), control siRNA (ctrl siRNA), and corresponding INF7 peptide modified siRNA (INF7-eGFP siRNA and INF7-ctrl siRNA) at N/P 6, 12 and 20 or 24 were tested for eGFPLuc gene silencing. Cells were incubated with polyplexes for 45 min at 37 °C Luciferase activities at 48 h after transfection are presented as a percentage of relative light units (RLU) obtained with buffer treated control cells. Data are shown as mean ± SD (n = 3). Adapted from [67].

Two-arm oligomers with tyrosine trimers (#9-16) displayed receptor specific, but still lower gene silencing. Very high knockdown efficiency (up to 93 %) could be obtained with the integration of both, histidines and tyrosine trimers (#17-20). These oligomers even transfected without INF7 modified siRNA, but not in a receptor specific manner. Basic four-arm oligomers (#21-28) showed effective gene silencing with INF7-eGFP siRNA, regardless of the cationic backbone, but again without targeting effect (Figure 16). With the insertion of histidines (#29-34) the transfection efficiency was slightly reduced. Remarkably, oligomer #30 transfected receptor specifically as its negative control #29 showed worse gene silencing. Four-arm oligomers modified with tyrosine trimers completely lost their gene silencing ability (#35-38). Again, 4-arm oligomers modified with histidines and tyrosine trimers revealed very high, but unspecific, knockdown even without INF7-eGFP siRNA and at low N/P ratios (#39-42). These oligomers also reduced the luciferase activity with ctrl siRNA indicating an unspecific cytotoxicity. All other oligomers revealed sufficient biocompatibility as they did not show that high unspecific luciferase reduction. Figure 17 shows the cellular internalization in KB/eGFPLuc cells of oligomers determined by flow cytometry. Here, only oligomers that revealed receptor specific gene silencing and the highly efficient 2-arm-H-Y_3 formulation were chosen. FolA containing oligomers #14, #18 and #30 were examined in comparison to their negative controls #13, #17 and #29. All FolA-oligomers showed a slightly higher cellular uptake than their corresponding oligomers without FolA with the clearest result for #30. The high cellular internalization of #17 and #18 confirmed the high transfection efficiency.

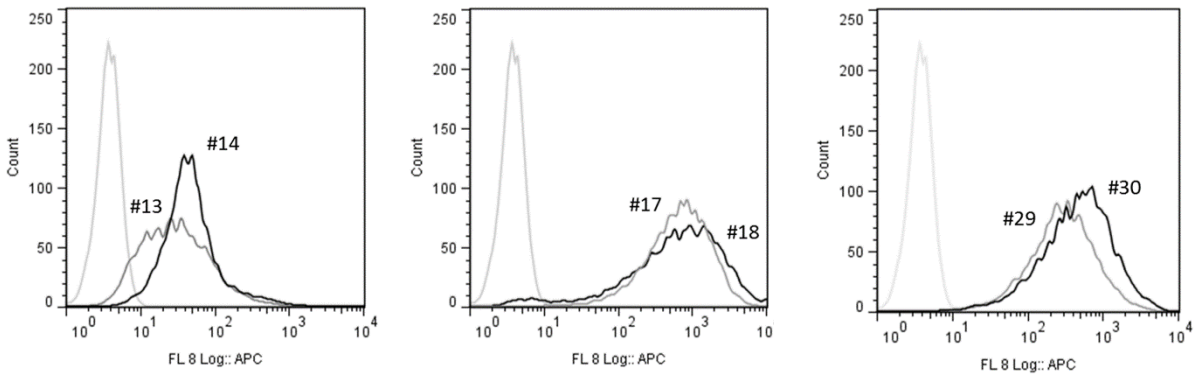

Figure 17. Cellular internalization of Cy5-labelled siRNA (N/P 12) polyplexes after 45 min incubation time on KB/eGFPLuc cells determined by flow cytometry. The intensity of the Cy5 signal indicates the amount of polyplexes being internalized by KB/eGFPLuc cells. Light gray curve: HBG buffer treated cells; dark gray curve: ligand free control oligomers treated cells; and black curve, folate containing oligomers treated cells. All experiments were performed in triplicates. One representative histogram is shown. Adapted from [67].

3.3 Native chemical ligation for the equipment of siRNA polyplexes with shielding and folic acid targeting

This chapter has been partly adapted from:

Can Yang Zhang, Petra Kos, Katharina Müller ,Waldemar Schrimpf, Christina Troiber, Ulrich Lächelt, Claudia Scholz , Don C. Lamb and Ernst Wagner, "Native chemical ligation for conversion of sequence-defined oligomers into targeted pDNA and siRNA carriers", Journal of Controlled Release, 2014, 180:42-50.

In this chapter, native chemical ligation (NCL) [152-154] was applied to facilitate the screening process of sequence defined oligomers for their ability to deliver siRNA receptor specifically. Here, in contrary to the previous chapters PEG and FolA were not attached to oligomers in the SPS process, but to already synthesized ones. With the NCL method, which was adapted for SPS by Blanco-Canosa et al. [155], oligomers without targeting ligand containing N-terminal cysteines could be selected from our existing library and easily equipped with PEG and FolA under mild conditions in almost quantitative yields. In the NCL reaction (performed by Dr. Can Yang Zhang (visiting PhD student at LMU Munich in 2013)) an amide bond is formed by transthioesterification followed by intramolecular nucleophilic rearrangement between the thioester and cysteine (Figure 18). For the successful reaction an oligomer with an N-terminal cysteine and a ligation partner with a C-terminal, aromatic N-acylurea moiety (such as N-acyl-benzimidazolinone, Nbz) are necessary.

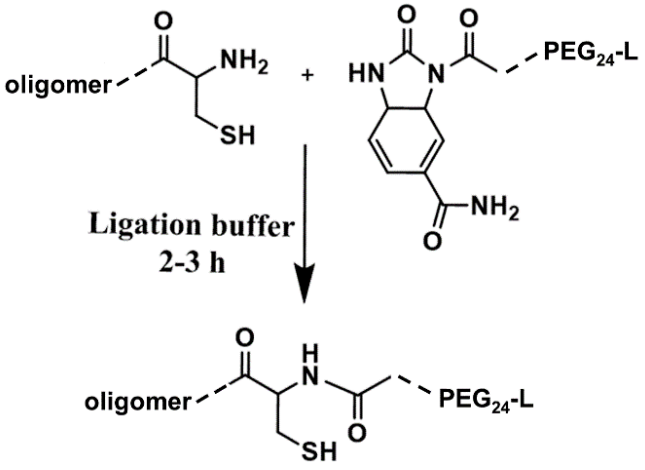

Figure 18. Native chemical ligation (NCL) of Nbz-PEG_{24}-L oligomer and an oligomer with N-terminal cysteines resulting in a new PEGylated oligomer. L: FolA or alanine; ligation buffer: 6 M guanidinium hydrochloride, 200 mM disodium hydrogen phosphate, 20 mM tris(2-carboxyethyl)phosphine hydrochloride (TCEP*HCl) and 200 mM 4-mercapto-phenylacetic acid. Adapted from [145].

3.3.1 Design of shielded and FolA-targeted oligomers obtained *via* NCL

Six non-targeted oligomers of different topologies were selected for the modification *via* NCL (Figure 19). Two 2-arm structures (***468***, ***465***), three 3-arm structures (***386***, ***512***, ***589***) and one 4-arm structure (***606***) were chosen as they have proven efficient pDNA and/or siRNA delivery in previous studies [65, 73, 78]. Oligomers contained the siRNA binding domains Stp (***468***, ***465***, ***386***, ***589***) or Sph (***512***, ***606***), stabilizing tyrosine trimers (***468***, ***465***, ***589***) and histidines (***606***) enhancing the endosomal escape. The most important prerequisites for the NCL reaction were N-terminal cysteines, which all oligomers offered.

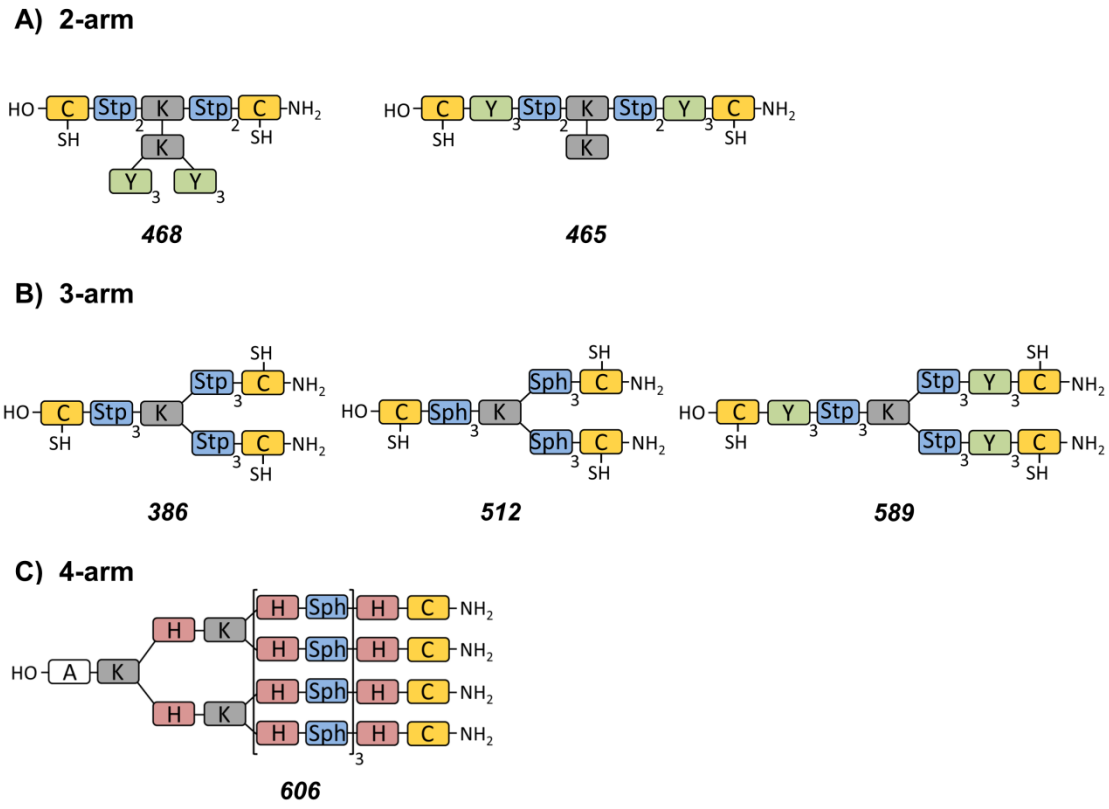

Figure 19. Oligomers of different topologies used for NCL reaction. Adapted from [145].

The NCL ligation substrates ***500*** and ***501*** were synthesized by Dr. Can Yang Zhang (visiting PhD student at LMU Munich in 2013) and Dr. Christina Gutmann (former Troiber, PhD thesis 2013, LMU Munich) *via* SPS (Table 1). Both oligomers contain 24 PEG units for shielding and N-acyl-benzimidazolinone (Nbz) for the reaction with the oligomer cysteines. The targeting ligand FolA was integrated into ***500***; ***501*** served as control with alanine instead of FolA. For NCL a molar ratio of 1:1 (ligation substrate:

oligomer), in order to couple only one oligomer arm, was used resulting in twelve PEG-shielded oligomers (***659***–***670***) with or without FolA-targeting (Table 1).

Table 1. Activated NCL substrates and oligomers synthesized *via* NCL. All oligomers were synthesized by Dr. Can Yang Zhang (visiting PhD student at LMU Munich in 2013) and Dr. Christina Gutmann (former Troiber, PhD thesis 2013, LMU Munich). FolA: folic acid, targeting ligand; A: alanine, corresponding negative control. Adapted from [145].

	topology	No.	sequence
NCL substrates		***500***	Nbz-G-PEG24-FolA
		501	Nbz-G-PEG24-A
oligomers synthesized *via* NCL	2-arm	***659***	C-Y3-Stp2-K(K)-Stp2-Y3-C-G-PEG24-A
		660	C-Y3-Stp2-K(K)-Stp2-Y3-C-G-PEG24-FolA
		661	C-Stp2-K(K-(Y3)2)-Stp2-C-G-PEG24-A
		662	C-Stp2-K(K-(Y3)2)-Stp2-C-G-PEG24-FolA
	3-arm	***663***	C-Sph3-K(Sph3-C)-Sph3-C-G-PEG24-A
		664	C-Sph3-K(Sph3-C)-Sph3-C-G-PEG24-FolA
		665	C-Stp3-K(Stp3-C)-Stp3-C-G-PEG24-A
		666	C-Stp3-K(Stp3-C)-Stp3-C-G-PEG24-FolA
		667	C-Y3-Stp3-K(Stp3-Y3-C)-Stp3-Y3-C-G-PEG24-A
		668	C-Y3-Stp3-K(Stp3-Y3-C)-Stp3-Y3-C-G-PEG24-FolA
	4-arm	***669***	A-K-(H-K-(H-Sph-H-Sph-H-Sph-H-C)2)-H-K-(H-Sph-H-Sph-H-Sph-H-C)-H-Sph-H-Sph-H-Sph-H-C-G-PEG24-A
		670	A-K-(H-K-(H-Sph-H-Sph-H-Sph-H-C)2)-H-K-(H-Sph-H-Sph-H-Sph-H-C)-H-Sph-H-Sph-H-Sph-H-C-G-PEG24-FolA

3.3.2 Biophysical characterization of shielded and FolA-targeted oligomers obtained *via* NCL

Gel shift assays (Figure 20) revealed less siRNA binding ability of PEGylated oligomers compared to unmodified oligomers in all cases. The 2-arm topologies demonstrated almost no siRNA retention (***659***-***662***). 3-arm structures, especially with tyrosine trimers (***667***, ***668***), led to better siRNA binding at high N/P ratios. Significant, but moderate, siRNA retention was observed for the 4-arm structures (***669***-***670***).

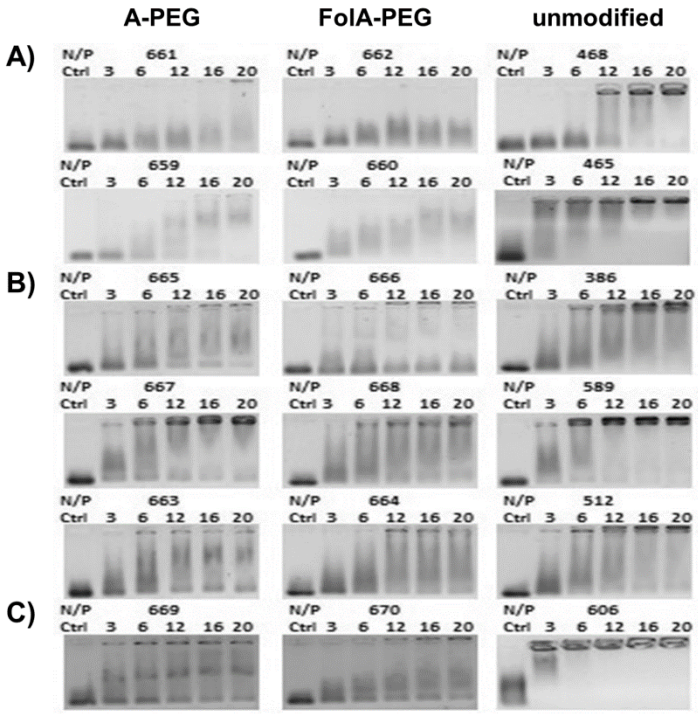

Figure 20. siRNA binding of 2-arm (A), 3-arm (B) and 4-arm structures (C) at indicated N/P ratios. FolA-PEG: folic acid receptor targeted oligomer (FolA, folic acid); A-PEG: corresponding negative control for the evaluation of targeting effects (A, alanine); unmodified: oligomer before NCL reaction. Assays were performed by Dr. Can Yang Zhang (visiting PhD student at LMU Munich in 2013). Adapted from [145].

Polyplex sizes of unmodified and PEGylated oligomers were determined *via* DLS measurements (Table 2). Almost all oligomers formed big aggregates (>1800 nm) with siRNA. Only the 3-arm structures ***589***, ***667*** and ***668*** with tyrosine trimer modification revealed smaller particles (<600 nm). The zeta potential of polyplexes (Table 2) was significantly lowered through the modification with PEG. Unmodified oligomers revealed zeta potentials of +21 mV to +33 mV, which could be reduced to +1 mV to +10 mV for FolA-PEG polyplexes and to +7 mV to +17 mV for A-PEG polyplexes. Alanine controls demonstrated slightly higher zeta potentials than corresponding FolA-PEG oligomers presumably due to the terminal protonatable amine of alanine.

Table 2. Z-average [nm] and zeta potentials [mV] of siRNA polyplexes (N/P 16) formed in HEPES buffer determined with DLS. Variations refer to the median of three measurements of the same sample. Measurements were carried out by Dr. Can Yang Zhang (visiting PhD student in 2013). Adapted from [145].

topology	No.	modification	Z-average [nm]	Zeta potential [mV]
2-arm	468	unmodified	5423 ± 357	22.7 ± 0.7
	661	A-PEG	2978 ± 123	7.1 ± 0.3
	662	FolA-PEG	4215 ± 225	4.4 ± 0.1
	465	unmodified	4294 ± 205	23.1 ± 0.5
	659	A-PEG	1952 ± 173	9.2 ± 0.4
	660	FolA-PEG	3836 ± 214	1.3 ± 0.2
3-arm	512	unmodified	2000 ± 119	28.6 ± 0.8
	663	A-PEG	2108 ± 217	16.9 ± 0.5
	664	FolA-PEG	2530 ± 175	6.4 ± 0.15
	386	unmodified	2256 ± 126	23.3 ± 0.6
	665	A-PEG	2202 ± 12	15.3 ± 0.4
	666	FolA-PEG	2838 ± 39	4.3 ± 0.4
	589	unmodified	368 ± 27	21.3 ± 0.7
	667	A-PEG	276 ± 15	7.3 ± 0.8
	668	FolA-PEG	563 ± 44	2.5 ± 0.5
4-arm	606	unmodified	740 ± 31	33.5 ± 0.4
	669	A-PEG	833 ± 38	12.3 ± 0.6
	670	FolA-PEG	1725 ± 217	10.3 ± 0.5

3.3.3 Gene silencing and cellular internalization of shielded and FolA-targeted oligomers obtained *via* NCL

In the current thesis, the transfection efficiency was examined on FR-rich KB/eGFPLuc cells with 45 min incubation time at 37 °C in order to determine a targeting effect (Figure 21). Polyplexes were tested with siRNA against eGFP, optionally with INF7 modification for enhanced endosomal escape and in comparison to ctrl siRNA. PEGylated polyplexes without targeting ligand (A-PEG), with FolA (FolA-PEG) and unmodified polyplexes were examined. No gene silencing was obtained with 2-arm polyplexes with central tyrosines (***661***, ***662***) in line with the insufficient siRNA binding ability as seen in gel shifts (Figure 21A). PEGylated 2-arm polyplexes with peripheral tyrosine modification showed moderate transfection efficiency with INF7 for the untargeted structure (***659***) and no gene silencing with FolA ligand (***660***), whereas the unmodified corresponding structure (***465***) did transfect KB/eGFPLuc cells with and without INF7 (Figure 21B). FolA-PEGylated 3-arm with Stp (***666***) showed high gene knockdown with INF7 modified siRNA and moderate gene knockdown without INF7 at high N/P ratios (Figure 21C). Corresponding A-PEG (***665***) and unmodified oligomer (***386***) demonstrated moderate gene silencing with INF7-siRNA, as well, but not as high as with FolA ligand. When Sph was inserted into 3-arm oligomers high gene silencing with INF7-siRNA could be found for all modifications

without targeting effect (Figure 21D). In contrary, a clear targeting effect was demonstrated with 3-arm oligomers containing tyrosine trimers, when transfected with INF7-siRNA (***667***, ***668***) (Figure 21E). The negative control ***667*** did not transfect at all, whereas FolA targeted ***668*** showed gene silencing up to 70 %. Histidine modified 4-arm structures (Figure 21F) demonstrated minor transfection efficiency with FolA-PEG (***670***), that was nevertheless better than with the A-PEG control (***669***).

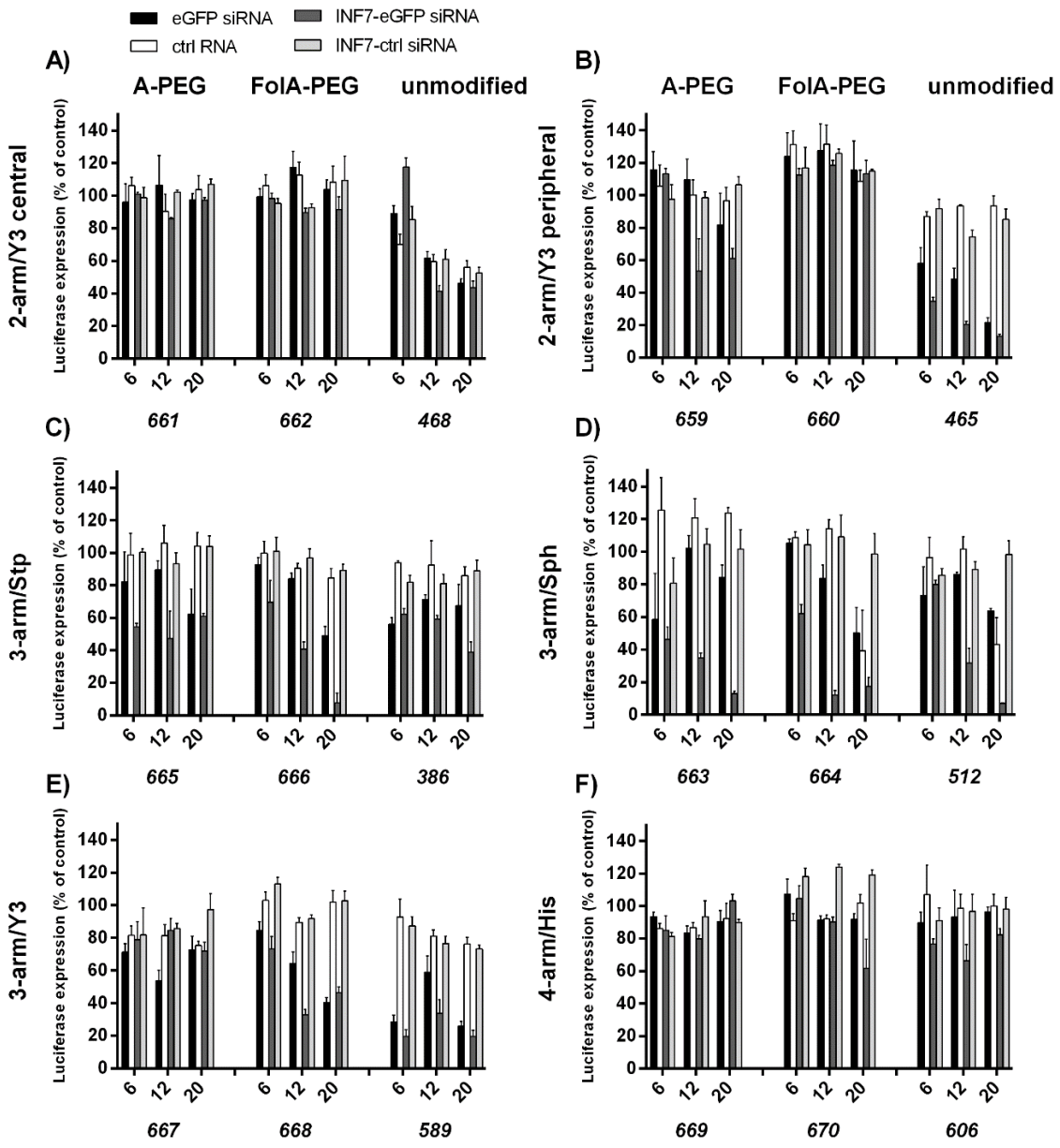

Figure 21. Gene silencing (n=3, mean ± SD) of 2-arm oligomers with central (A) or peripheral (B) oligotyrosines; 3-arms without (C (Stp), D (Sph)) or with oligotyrosines (E); and 4-arm oligomer with histidines (F) at indicated N/P ratios. Polyplexes were transfected on KB/eGFPLuc cells with 45 min incubation time. Each row compares A-PEG, FolA-PEG or unmodified oligomers. For siRNA, different shadings from left to right indicate eGFP siRNA, ctrl siRNA, INF7-eGFP siRNA and INF7-ctrl RNA. Adapted from [145].

The cellular internalization of oligomers showing targeting effects in transfections was further examined by flow cytometry (Figure 22). Here, 3-arm, 3-arm/Y3 or 4-arm/His polyplexes were incubated on KB/eGFPLuc cells for 45 min and 4 h. In all cases, FolA-PEG (blue) polyplexes displayed higher cellular uptake in comparison to A-PEG (red) polyplexes confirming the enhanced FR mediated uptake. Unmodified polyplexes (green) displayed significant cellular internalization, as well, probably due to their positive charge and large sizes enhancing interactions with cell membranes.

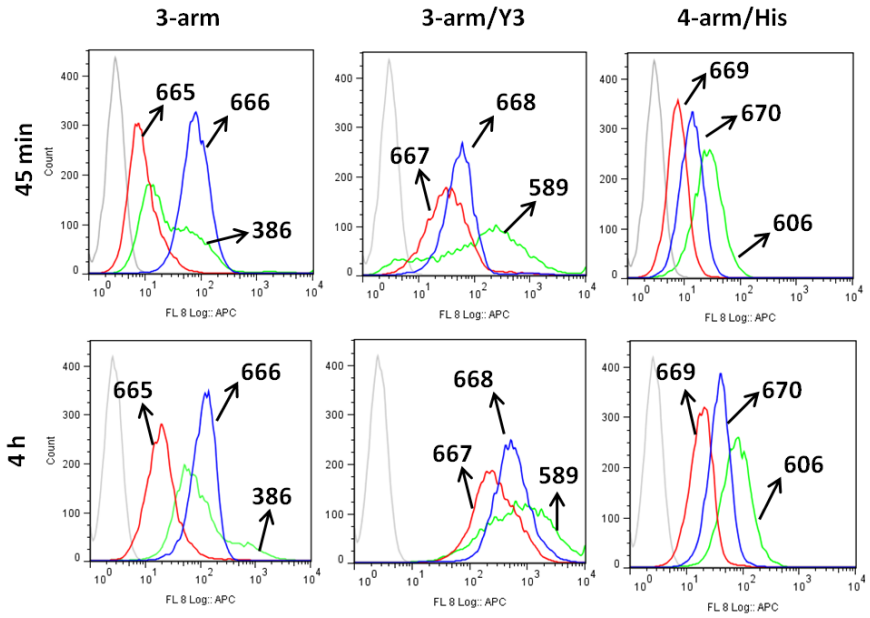

Figure 22. Cellular internalization of Cy5-labelled siRNA (N/P 12) polyplexes after 45 min and 4 h determined by flow cytometry. Dead cells (DAPI positive, less than 2%) were excluded from analysis. The intensity of the Cy5 signal indicates the amount of polyplexes being internalized by KB/eGFPLuc. Unmodified oligomers are presented in green, FolA-PEG oligomers in blue, alanine-PEG controls in red and HBG buffer only treated cells in grey. All experiments were performed in triplicates. One representative histogram is shown. Adapted from [145].

3.4 Post-PEGylation of siRNA lipo-oligoamino amide polyplexes for receptor specific siRNA and miRNA delivery

3.4.1 Post-PEGylation principle

Post-PEGylation has been applied to convert untargeted and non-shielded pDNA/PEI polyplexes into carriers having these functional domains [156-158]. In contrary to NCL, already formed polyplexes, not oligomers, were modified in order to avoid problems with siRNA packaging into the polyplex core. In this thesis, the established post-PEGylation concept was transferred to sequence-defined oligomers for siRNA delivery. For polyplex formation two precise T-shaped cationic lipo-oligomers, ***454*** (chapter 3.4.2 and 3.4.3) and ***595*** (chapter 3.4.2), were selected (Figure 23A). These structures were generated by SPS and contain four units Stp, two lysines for branching and linkage with the two central oleic acids, two hydrophobic tyrosine trimers, and two terminal cysteines (***454***) or CRC units (***595***). The incorporation of tyrosine trimers and the CRC motif has been shown to be beneficial for the stability of siRNA polyplexes in previous chapters. Oleic acids improved the stability of polyplexes via hydrophobic interactions and enhanced endosomal escape due to endosomolytic activity in previous studies [78, 150]. Terminal cysteines or twin disulfides are beneficial for siRNA polyplex stability due to their strong disulfide bridge formation [144, 151]. The two chosen oligomers combine foresaid moieties and were used as efficient and stable carriers for non-targeted siRNA delivery before [73, 144]. For polyplex formation an N/P ratio of 10 was used. After 45 min of polyplex formation, the particles were incubated for another 15 min with the post-PEGylation reagents consisting of maleimide linked with PEG_{28} and a ligand (Figure 23B). Maleimide reacts with free cysteine thiols of polyplexes that are not engaged in internal disulfide bridge formation.

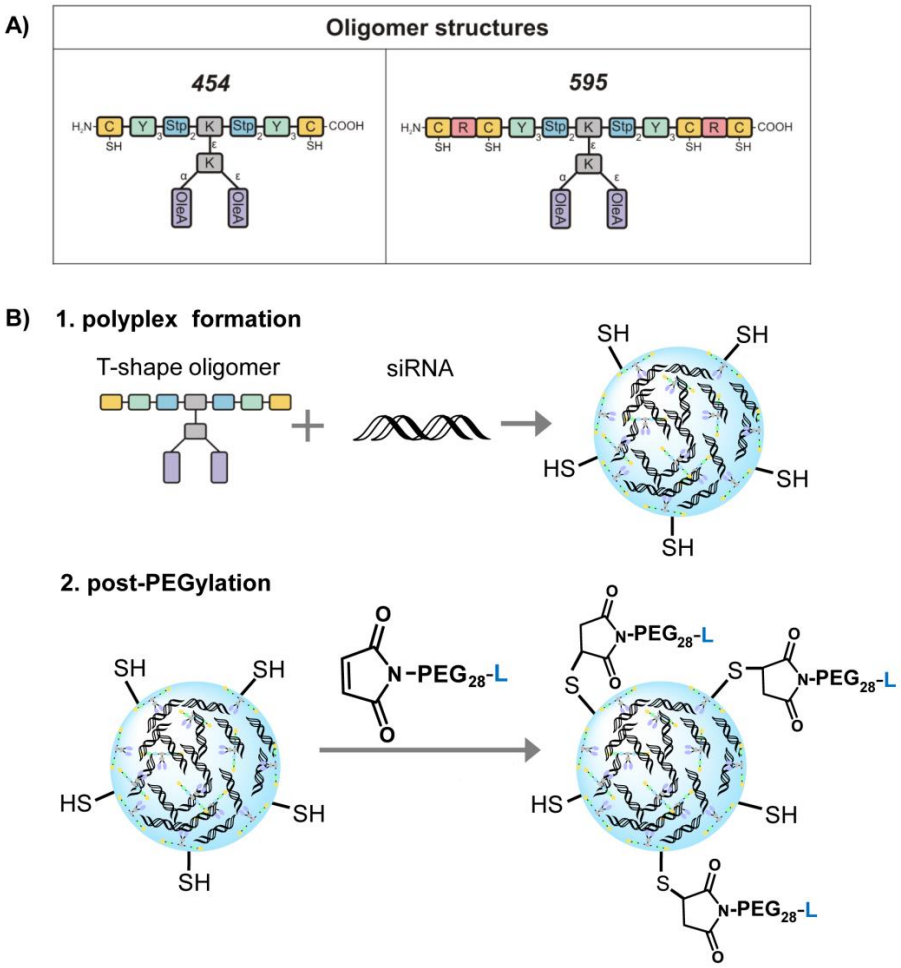

Figure 23. Schematic overview (A) of oligomers ***454*** and ***595***. (B) Polyplex formation and post-PEGylation of polyplexes. L: targeting ligand. ***454*** and ***595*** were synthesized by Philipp Klein (PhD student, Pharmaceutical Biotechnology, LMU Munich). Adapted from [146].

3.4.2 Post-PEGylation using tetra-glutamylated folic acid as ligand for receptor-targeted delivery

This chapter has been adapted from:

Katharina Müller, Eva Kessel, Philipp M. Klein, Miriam Höhn and Ernst Wagner, "Post-PEGylation of siRNA lipo-oligoamino amide polyplexes using tetra-glutamylated folic acid as ligand for receptor-targeted delivery", Molecular Pharmaceutics, 2016, 13(7):2332-45.

For the post-PEGylation of T-shaped lipo-oligomer siRNA polyplexes FolA was used as targeting ligand as it has shown its potency before. In addition to standard hydrophobic FolA, an alternative tetra-γ-glutamyl folic acid ligand (gE4-FolA) with four additional negative charges was applied (Figure 24). This biomimetic modification resembles the

natural cellular polyglutamylation of FolA [159, 160]. Studies with methotrexate-containing polymers have confirmed the beneficial effect of such an oligoglutamylation in FR-targeted delivery [68, 161]. Twenty-eight PEG units were used as shielding domains.

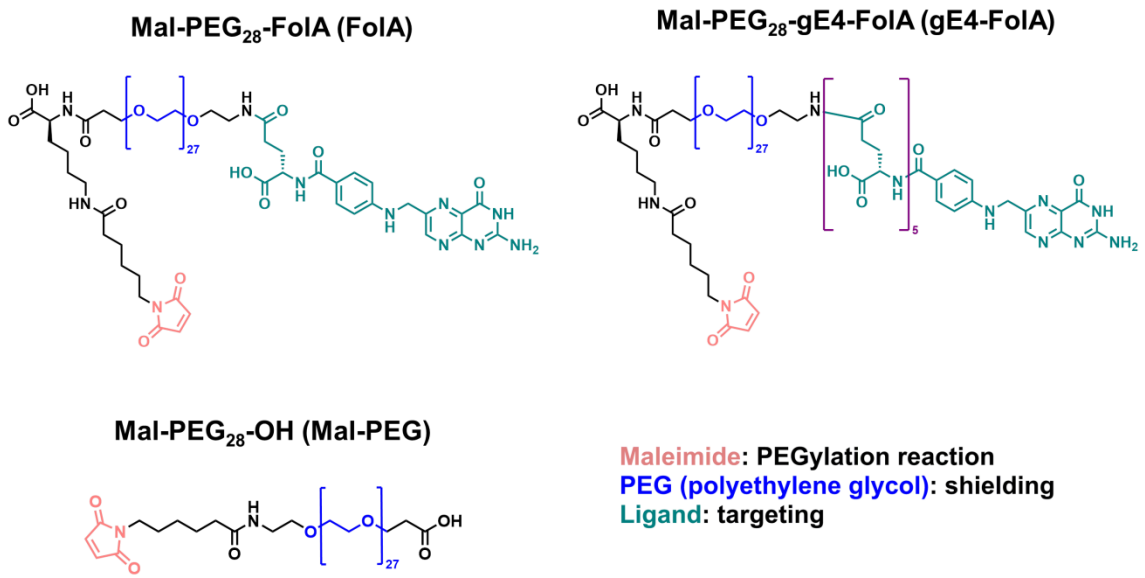

Figure 24. Amino acid sequence of the post-PEGylation reagents Mal-PEG$_{28}$-FolA (FolA), Mal-PEG$_{28}$-gE4-FolA (gE4-FolA) and ligand free Mal-PEG$_{28}$-OH (Mal-PEG). Post-PEGylation reagents were synthesized by Philipp Klein (PhD student, Pharmaceutical Biotechnology, LMU Munich). Adapted from [146].

3.4.2.1 Biophysical characterization of post-PEGylated polyplexes

The equivalents of added post-PEGylation reagents were defined as relative molar ratios to the oligomer molecules ***454*** or ***595*** applied in the polyplex formation. As each oligomer contains two (***454***) or four (***595***) cysteines, in theory maximum 2 or 4 eq of PEG-reagent for ***454*** or ***595***, respectively, might be coupled to bind all cysteines. However, the number of mercapto groups available after siRNA polyplex formation is reduced because of the intended, stabilizing oxidative disulfide cross-linkage of oligomers. The coupling reaction between oligomer cysteines and ligand-free maleimide-PEG (Figure 24) was verified by an Ellman's assay (Figure 25).

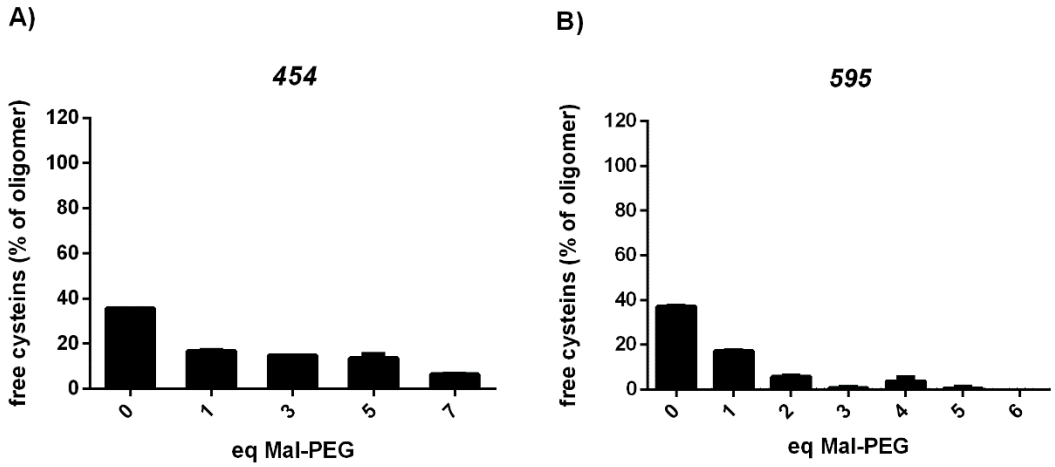

Figure 25. Percentage of residual cysteine mercapto (SH) groups as determined with Ellman´s assay (n=3, mean ±SD) for A) ***454*** and B) ***595*** polyplexes (formed by incubation for 45 min at RT with 500 ng siRNA at N/P 10) after modification with increasing molar equivalents of Mal-PEG for further 15 min at RT. The percentage of free mercapto groups is based on the theoretical amount (100%) of cysteines (i.e. 2 or 4 molar equivalents in oligomers ***454*** or ***595***, respectively) applied in the polyplex formation. Adapted from [146].

The percentage of residual free cysteine mercapto groups after polyplex formation, but before PEGylation (Figure 25, “0 eq Mal-PEG”) was 36 % (0.72 mol eq of mercapto groups) in the case of ***454*** and 37 % (1.48 mol eq of mercapto groups) in the case of ***595***, demonstrating that the majority of mercapto groups had already reacted during the 45 min polyplex formation. After reaction with PEGylation reagent for further 15 min a PEG equivalents-dependent decrease of free cysteines could be observed, demonstrating successful post-PEGylation of polyplexes. A difference in ***454*** and ***595*** polyplex reactivity toward PEG within this short 15 min time period was observed. For ***454*** polyplexes, one molar equivalents (1 eq) of Mal-PEG resulted in a consumption of mercapto groups to residual 17 % (0.34 molar eq of mercapto groups) and did not further reduce unless an excess of more than 5 eq of PEG was applied. Most likely, mercapto groups hidden within the polyplex but not engaged in disulfide bridges are sterically hindered and not available for PEGylation. Zeta potential measurements (see below) indicate further PEGylation beyond 1 eq, most probably by maleimide reaction with the oligomer amines [162]. In contrast ***595*** polyplexes reacted more avidly, reducing the mercapto equivalents from 1.48 (non-PEGylated) to 17 %/0.68 molar mercapto equivalents (by 1 eq of Mal-PEG) and to 0.7 %/0.03 molar mercapto equivalents by 3 eq of Mal-PEG. Particle sizes and zeta potentials of post-PEGylated polyplexes modified with Mal-PEG-FolA reagents were examined via dynamic light scattering (DLS) and via the application of an electric field using a Zetasizer Nano ZS (Figure 26). At low molar

equivalents the size of FolA ligand-PEG modified ***454*** and ***595*** particles ranged around 100−150 nm in all cases (Figure 26C,D). With increasing amount of PEGylation reagent, the particles started to agglomerate. These findings are consistent with earlier reports describing the tendency of polymer-conjugated hydrophobic FolA to agglomerate [163]. PEGylation with ligand-free Mal-PEG did not display such an agglomeration phenomenon over a broad range of PEG equivalents, unless a very high excess of >5 eq was applied (Figure 26E,F). In case of the tetra-glutamylated folic acid ligand (gE4-FolA) and ***454***, the agglomeration started at 0.1 eq (Figure 26A), and in the case of ***595***, gE4-FolA at 0.5 eq (Figure 26B). The same situation was found with maleimide-PEG_{28}-folic acid (FolA), where particles agglomerated at 0.5 eq with ***454*** (Figure 26C) and at 1 eq with ***595*** (Figure 26D). Beyond one equivalent of gE4-FolA, the size of particles decreased again to an appropriate size of around 150 nm for both oligomers (Figure 26A,B). This result demonstrated an improved repulsion of polyplexes modified with the tetraglutamylated PEGylation reagent due to the highly negative surface charge. Particles with suitable sizes also showed a PDI ≤ 0.2. In the case of standard FolA ligand, the agglomeration (sizes between 2000 nm and 8000 nm) was observed also at higher degrees of PEGylation equivalents, resulting into heterogeneous particles (Figure 26C,D). The heterogeneity of FolA-particles could be seen in number size distributions as well (Figure 27).

A) ***454*, gE4-FolA**

gE4-FolA [mol eq]	Z-average [nm]	PDI	Zeta potential [mV]
0	117.67 ± 1.32	0.145 ± 0.016	26.9 ± 4.86
0.01	117.43 ± 1.23	0.163 ± 0.005	17.3 ± 0.92
0.05	130.1 ± 1.7	0.147 ± 0.027	18.3 ± 0.82
0.1	4118 ± 427.75	0.356 ± 0.09	1.43 ± 0.18
0.5	3165 ± 429.26	0.683 ± 0.128	-11.16 ± 0.38
1	1824 ± 115.86	0.490 ± 0.06	-13.97 ± 0.70
3	194.23 ± 1.1	0.136 ± 0.02	-16.36 ± 0.99
5	140.73 ± 0.96	0.155 ± 0.01	-19.1 ± 0.75
7	143.13 ± 1.33	0.162 ± 0.012	-19.3 ± 0.7

B) ***595*, gE4-FolA**

gE4-FolA [mol eq]	Z-average [nm]	PDI	Zeta potential [mV]
0	158.03 ± 6.42	0.217 ± 0.018	31.9 ± 1.71
0.01	134.2 ± 1.51	0.230 ± 0,006	18.93 ± 2.58
0.05	136.67 ± 0.74	0.138 ± 0.014	18.83 ± 1.10
0.1	126.23 ± 2.19	0.260 ± 0.021	21.37 ± 1.53
0.5	4248 ± 468	0.450 ± 0.057	-3.07 ± 0.1
1	3973 ± 465	0.371 ± 0.039	-12.67 ± 0.47
2	120.2 ± 0.7	0.143 ± 0.01	-19.6 ± 0.83
3	148.8 ± 1.23	0.151 ± 0.014	-20.8 ± 0.06
4	149.23 ± 2.94	0.19 ± 0.014	-22.17 ± 0.45
5	152.97 ± 2.7	0.21 ± 0.004	-24.9 ± 1.57
6	142.13 ± 1.2	0.17 ± 0.005	-22.2 ± 1.04

Figure 26 ***(first part).*** Z-average [nm], PDI determined in DLS and zeta potential [mV] (n=3, mean ± SD) of ***454*** polyplexes (A, C, E) and ***595*** polyplexes (B, D, F) post-PEGylated with increasing molar equivalents of gE4-FolA (A, B), FolA (C, D) or Mal-PEG (E, F). Adapted from [146].

C) ***454*, FolA**

FolA [mol eq]	Z-average [nm]	PDI	Zeta potential [mV]
0	117.67 ± 1.32	0.145 ± 0.016	26.9 ± 4.86
0.01	124.4 ± 2.55	0.147 ± 0.007	27.27 ± 1.46
0.05	120.8 ± 2.91	0.152 ± 0.016	28.27 ± 0.76
0.1	140.47 ± 2.21	0.158 ± 0.016	18.37 ± 0.35
0.5	2954 ± 555	0.348 ± 0.02	11.43 ± 0.32
1	3585 ± 361.11	0.277 ± 0.14	3.13 ± 0.72
3	4369 ± 409	0.374 ± 0.11	-0.44 ± 0.26
5	5073 ± 266	0.325 ± 0.02	-5.43 ± 0.62
7	1706 ± 32	0.32 ± 0.07	-12.03 ± 0.8

D) ***595*, FolA**

FolA [mol eq]	Z-average [nm]	PDI	Zeta potential [mV]
0	158.03 ± 6.42	0.217 ± 0.018	31.9 ± 1.71
0.01	116.77 ± 1.76	0.179 ± 0,019	34.6 ± 0.98
0.05	106.13 ± 1.60	0.201 ± 0.018	32.97 ± 0.87
0.1	113.73 ± 2.78	0.173 ± 0.015	32.47 ± 0.75
0.5	102 ± 1.75	0.145 ± 0.002	22.8 ± 0.53
1	3191 ± 172	0.354 ± 0.058	5.88 ± 0.35
2	3016 ± 114	0.395 ± 0.05	4.64 ± 0.172
3	6276 ± 732	0.449 ± 0.062	-2.18 ± 0.30
4	6644 ± 419	0.698 ± 0.058	-6.19 ± 0.80
5	6785 ± 322	0.938 ± 0.107	-7.28 ± 0.47
6	4625 ± 462	0.429 ± 0.040	-10.67 ± 0.70

E) ***454*, Mal-PEG**

Mal-PEG [mol eq]	Z-average [nm]	PDI	Zeta potential [mV]
0	135.07 ± 3.78	0.150 ± 0.01	32.57 ± 0.67
0.01	141.27 ± 2.67	0.133 ± 0.01	32.33 ± 1.19
0.05	141.07 ± 1.12	0.102 ± 0.01	27.83 ± 0.23
0.1	225.83 ± 1.05	0.221 ± 0.01	11.47 ± 0.21
0.5	151.2 ± 1.65	0.161 ± 0.02	9.45 ± 0.31
1	206.43 ± 1.25	0.232 ± 0.01	5.31 ± 0.51
3	217.2 ± 3.53	0.257 ± 0.02	7.26 ± 0.44
5	396.73 ± 30.78	0.433 ± 0.09	5.14 ± 0.19
7	1414 ± 128.8	0.330 ± 0.08	5.29 ± 0.51

F) ***595*, Mal-PEG**

Mal-PEG [mol eq]	Z-average [nm]	PDI	Zeta potential [mV]
0	157.23 ± 2.81	0.209 ± 0.01	38.97 ± 1.16
0.01	129.67 ± 1.88	0.165 ± 0.01	35.93 ± 0.55
0.05	119.60 ± 1.05	0.145 ± 0.003	31.73 ± 0.98
0.1	156.67 ± 2.70	0.140 ± 0.01	20.17 ± 0.70
0.5	184.77 ± 1.42	0.140 ± 0.02	13.73 ± 1.00
1	221.13 ± 2.14	0.287 ± 0.01	7.46 ± 0.43
2	169.03 ± 6.17	0.223 ± 0.01	0.52 ± 0.10
3	204.30 ± 9.22	0.295 ± 0.02	-1.26 ± 0.33
4	176.20 ± 11.22	0.271 ± 0.01	0.46 ± 0.15
5	137.20 ± 10.52	0.356 ± 0.06	0.03 ± 0.15
6	166.00 ± 4.4	0.281 ± 0.003	-0.24 ± 0.19

Figure 26 ***(continued)*** Z-average [nm], PDI determined in DLS and zeta potential [mV] (n=3, mean ± SD) of ***454*** polyplexes (A, C, E) and ***595*** polyplexes (B, D, F) post-PEGylated with increasing molar equivalents of gE4-FolA (A, B), FolA (C, D) or Mal-PEG (E, F). Z-average (harmonic intensity averaged particle diameter) is given by cumulants analysis. Core polyplexes were formed at N/P 10 with a siRNA concentration of 25 µg/mL and a final siRNA concentration of 20 µg/mL after PEGylation. Adapted from [146].

The effect of post-PEGylation on the surface charge of polyplexes is shown by zeta potential measurements in Figure 26. With no or low equivalents of PEGylation reagents (≤0.05 eq for ***454***; ≤0.1 eq for ***595***) the zeta potential was around +20 to +30 mV. In the

case of gE4-FolA the zeta potential was neutral at 0.1 eq for ***454*** (+1.43 mV) and 0.5 eq for ***595*** (−3.07 mV). At these equivalents polyplexes formed agglomerates (Figure 26A,B). With higher molar equivalents of gE4-FolA the zeta potential decreased to around −20 mV for both oligomers.

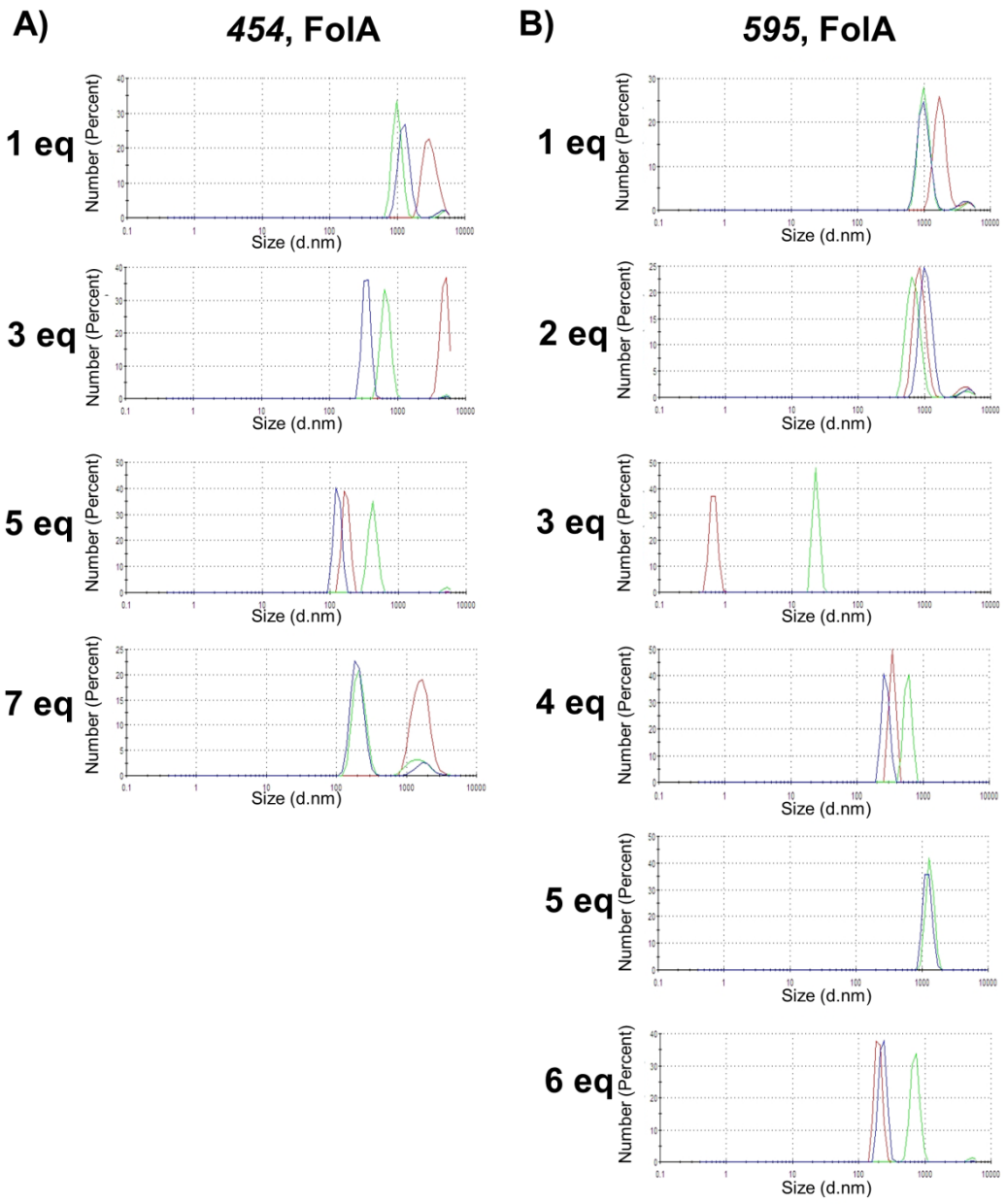

Figure 27. Number size distribution determined with DLS of ***454*** polyplexes (A) and ***595*** polyplexes (B) post-PEGylated with increasing molar equivalents FolA. Three measurements are presented in different colours. Core polyplexes were formed at N/P 10 with a siRNA concentration of 25 µg/mL and a final siRNA concentration of 20 µg/mL after PEGylation. Number averages were calculated from intensity distribution using Mie theory [164]. Adapted from [146].

Zeta potentials for particles post-PEGylated with FolA (Figure 26C,D) did not decrease as fast as with gE4-FolA and could not fall below −12 mV, as FolA only contains one negative charge, while gE4-FolA has five negative charges due to the tetra-glutamylation. Considering these findings particles with suitable sizes and zeta potentials were obtained with molar equivalents of gE4-FolA of ≥2 eq. The number size distribution of polyplexes post-PEGylated with FolA is shown in Figure 27. A heterogeneous particle formation can be assumed as the measurements demonstrated different sizes for one formulation. Figure 28 shows the siRNA compaction within the PEGylated polyplexes determined with an EtBr assay. Polyplexes formed with oligomers without PEGylation showed 80% reduction of EtBr fluorescence, demonstrating good compaction of siRNA. For FolA-PEGylation, the siRNA compaction did not change (Figure 28C,D). PEGylation with gE4-FolA led to a higher EtBr fluorescence (only 60% reduction), indicating a reduction of siRNA compaction.

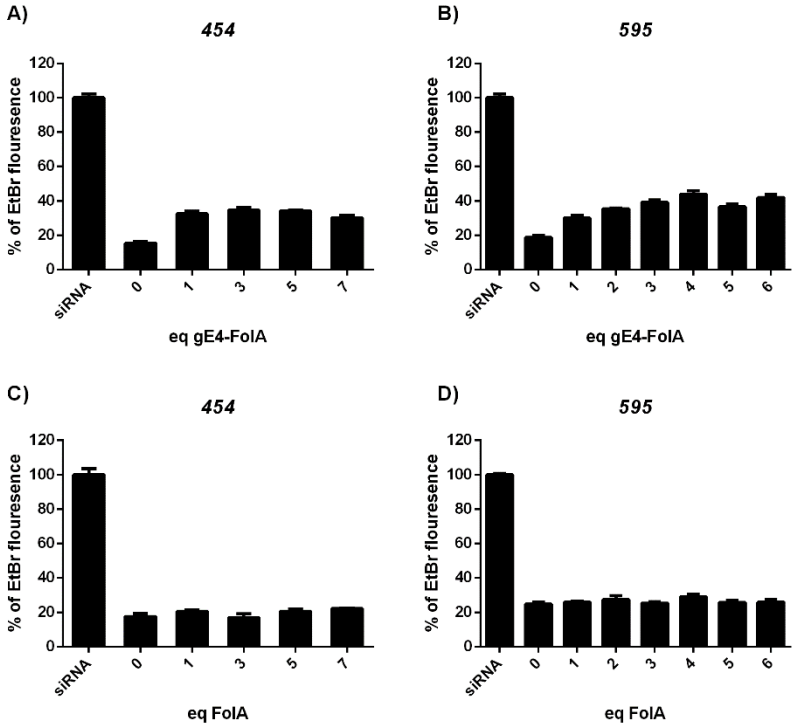

Figure 28. siRNA compaction of post-PEGylated polyplexes determined with ethidium bromide. Lower intensity of EtBr fluorescence indicates better compaction of the nucleic acid within the polyplex. 100 % presents siRNA without oligomers (n=3, mean ± SD). ***454*** polyplexes (A, C) and ***595*** polyplexes (B, D) post-PEGylated with increasing molar equivalents of gE4-FolA (A, B) or FolA (C, D). Core polyplexes were formed at N/P 10 with a siRNA concentration of 25 µg/mL and a final siRNA concentration of 20 µg/mL after PEGylation. Adapted from [146].

3.4.2.2 Gene silencing of post-PEGylated polyplexes

The transfection efficiency was determined in human cervix carcinoma KB/eGFPLuc cells overexpressing the folic acid receptor (Figure 29). Cells were incubated with formulations for a short period of only 45 min at 37 °C to avoid unspecific uptake of particles. Polyplexes were transfected with eGFP siRNA targeting the eGFP-luciferase and control siRNA (ctrl siRNA) with no gene silencing capacity. At low ratios of molar equivalents (0.01−0.05 eq) of both gE4-FolA and FolA PEG reagents, a moderate gene silencing comparable with non-PEGylated polyplexes (0 eq) was observed. PEGylated ***454*** polyplexes with gE4-FolA ligand (Figure 29A) showed potent gene silencing of about 90% for ≥1 eq PEG reagent. The knockdown remained high until 7 eq of applied PEG reagent. The transfections with control siRNA indicated some nonspecific effects for 1 eq (40%), which however resolved with a higher PEGylation. The transfection efficiency of PEGylated ***595*** polyplexes with gE4-FolA was highest for 1 eq (Figure 29B), but decreased with increasing equivalents of >1. At 4 eq gene silencing was not observed anymore. The reasons remained unclear; possibly free ligand-PEG reagent or ligand-PEG reacted with free polymer could block the FR, making it inaccessible for targeted polyplexes; alternatively endosomal escape of polyplexes might have been hampered by abundant PEGylation. Toxic effects were not observed for ***595*** at any ratio of gE4-FolA. Encouragingly, extended incubation of cells for 1 and 2 days (instead of 45 min only) with ***595*** PEGylated with 1.5 eq of gE4-FolA demonstrated a still retained receptor specificity of silencing (Figure 30A,B) and lack of cytotoxicity (Figure 30C,D). Polyplexes post-PEGylated with standard FolA ligand (Figure 29C,D) led to efficient gene silencing with higher molar equivalents (≥1 eq) both for ***454*** and ***595***. In the case of ***595*** a heterogeneous gene silencing for 1 to 3 eq (50%, 83%, 50%) and a robust knockdown for 4−6 eq (about 86%) was observed. This heterogeneity in transfection efficiency might be explained with the tendency of these FolA-PEGylated particles to agglomerate (Figure 26) leading to heterogeneous structures (Figure 27).

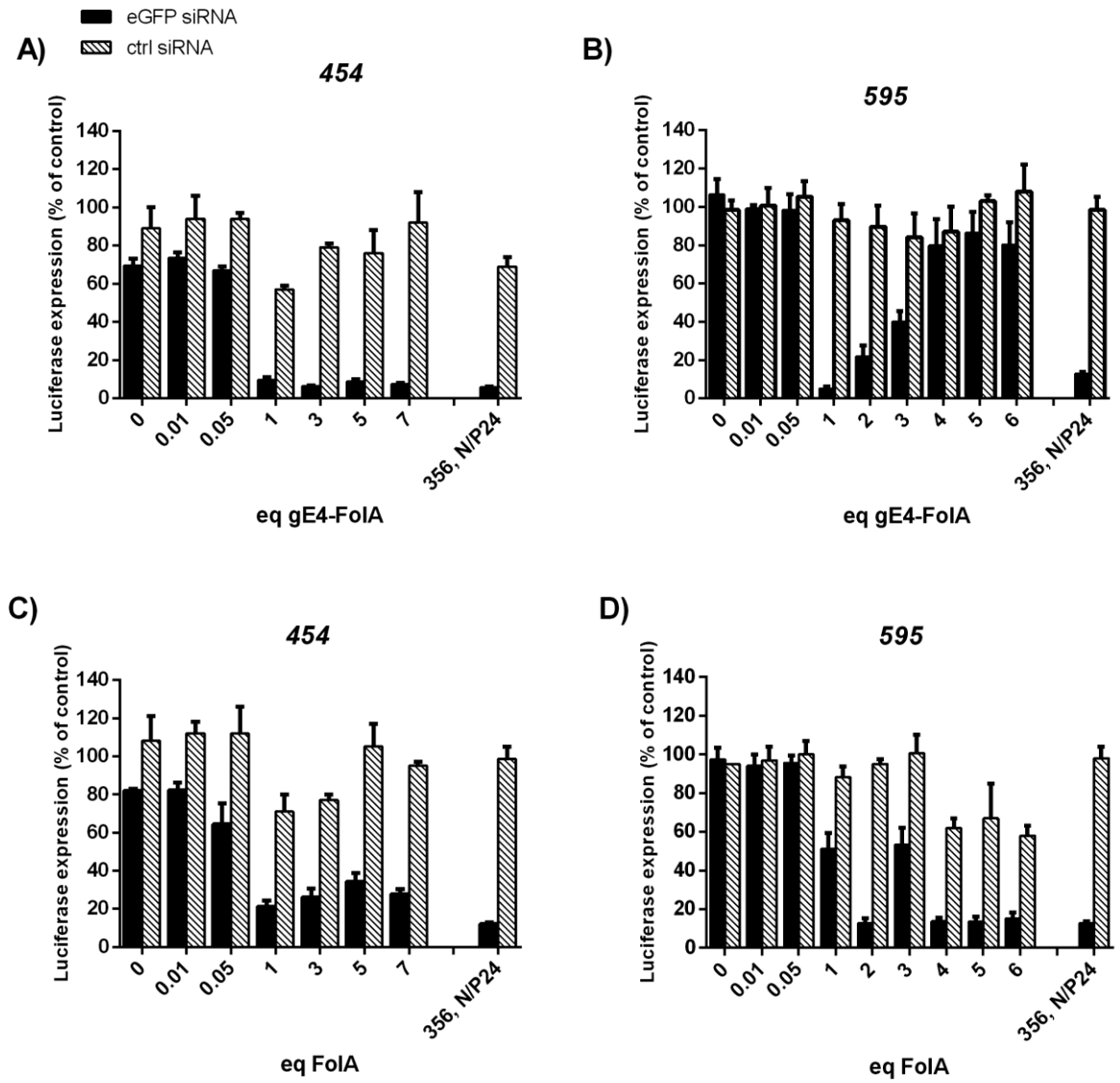

Figure 29. Gene silencing (n = 3, mean ± SD) of ***454*** polyplexes (A,C) and ***595*** polyplexes (B,D) post-PEGylated with increasing molar equivalents of gE4-FolA (A,B) or FolA (C,D). Polyplexes were incubated on KB-eGFP/Luc cells with 500 ng of siRNA targeting eGFP (eGFP siRNA) and 500 ng of control siRNA (ctrl siRNA) for 45 min. Oligomer ***356***, applied with 200 ng of Inf7 peptide-conjugated (eGFP or ctrl) siRNAs, served as positive control [57]. Core polyplexes were formed at N/P 10 with a siRNA concentration of 25 µg/mL and a final siRNA concentration of 20 µg/mL after PEGylation. Adapted from [146].

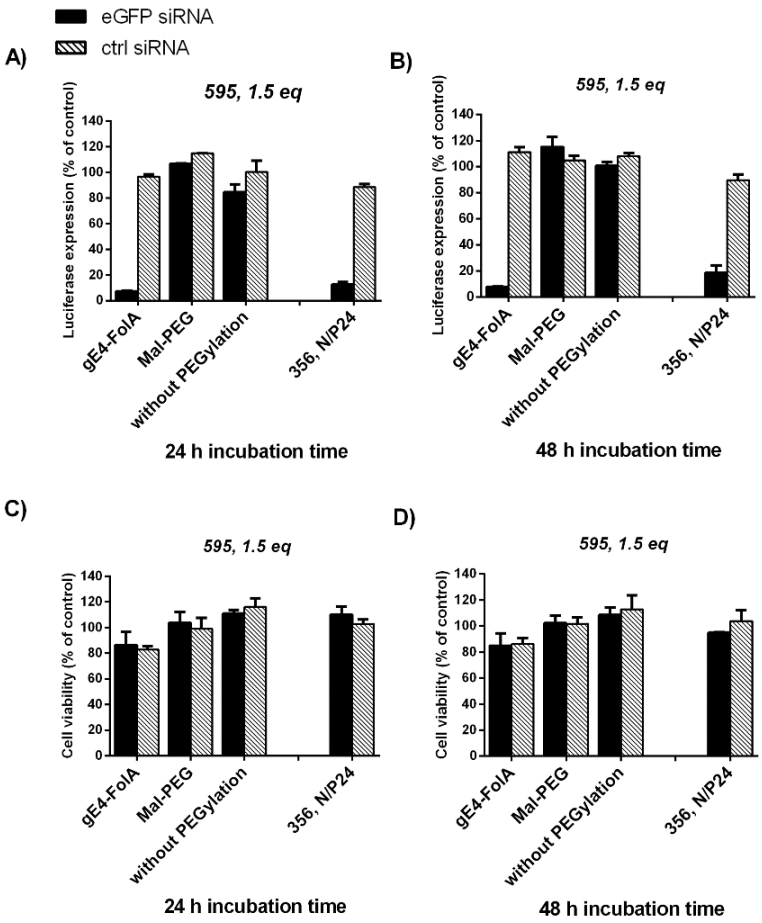

Figure 30. Gene silencing (A, B) and cell viability (C, D) of KB/eGFPLuc cells at extended incubation times with ***595*** polyplexes PEGylated with 1.5 eq of gE4-FolA, 1.5 eq Mal-PEG or without PEGylation (n=3, mean ± SD). Polyplexes were incubated on cells for 24 h (A, C) or 48 h (B, D). Polyplexes were tested in KB-eGFP/Luc cells with siRNA targeting eGFP (eGFP siRNA) and ctrl siRNA. Core polyplexes were formed at N/P 10 with a siRNA concentration of 25 µg/mL and a final siRNA concentration of 20 µg/mL after PEGylation. Oligomer ***356*** is a folate-PEG containing oligomer serving as positive control. For endosomal escape, ***356*** polyplexes depend on INF7 peptide-conjugated (GFP or ctrl) siRNAs. Adapted from [146].

To evaluate the receptor specificity of transfections, folate receptors were blocked by incubating cells with folic acid-saturated medium at 30 min before transfection (Figure 31). Gene silencing of gE4-FolA-PEGylated ***454*** and ***595*** polyplexes was completely lost at PEGylation >1 eq (Figure 31A,B). This, together with the data presented in Figure 29 verifies a folic acid receptor-dependent gene silencing process, similar as for the ***356*** positive control polyplexes. Figure 31 also revealed for both polymers a receptor-independent transfection of ***454*** and ***595*** polyplexes when PEGylated with only 1 eq of gE4-FolA or when PEGylated with FolA at any equivalent (Figure 31C,D). The known agglomeration of these polyplexes (Figure 26) obviously reduces the folate receptor specificity.

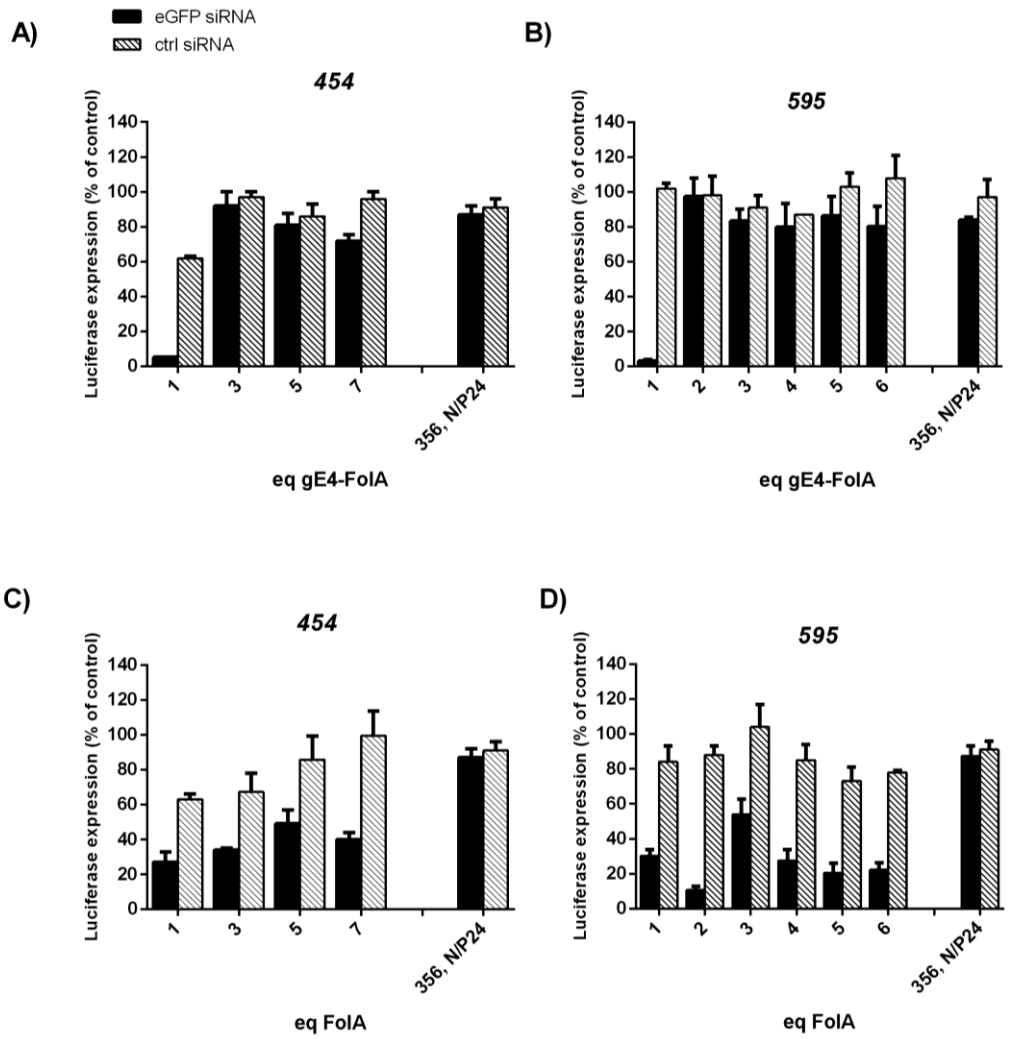

Figure 31. Gene silencing (n = 3, mean ± SD) of ***454*** polyplexes (A,C) and ***595*** polyplexes (B,D) post-PEGylated with increasing molar equivalents of gE4-FolA (A,B) or FolA (C,D). Polyplexes were incubated on KB-eGFP/Luc cells with 500 ng of siRNA targeting eGFP (GFP siRNA) and 500 ng of control siRNA for 45 min. Cells were incubated 30 min before transfection with saturated folic acid media to block the folate receptor. Oligomer ***356***, applied with 200 ng of INF7 peptide-conjugated (GFP or control) siRNAs, serves as positive control [57]. Adapted from [146].

3.4.2.3 Cellular internalization of post-PEGylated polyplexes

The cellular internalization of post-PEGylated particles into KB cells was investigated by flow cytometry (Figure 32). The uptake experiments were performed without or with blockade of the folic acid receptor, to examine receptor specificity. Cellular uptake of non-PEGylated polyplexes was high for both oligomers. For 100−200 nm small ***454*** or ***595*** polyplexes, which were PEGylated with >1 eq of gE4-FolA, the uptake could be completely blocked with free folic acid (Figure 32A,B). For agglomerated particles formed with 1 eq of gE4-FolA or with PEG-FolA at any PEGylation ratio, cellular uptake was

extremely high, saturating the Cy5 fluorescence channel. Folic acid competition could only partly block internalization of these polyplexes (Figure 32C,D). This finding is consistent with the presence of particle agglomerates (Figure 27), resulting partly in receptor-independent uptake and gene silencing (Figure 31).

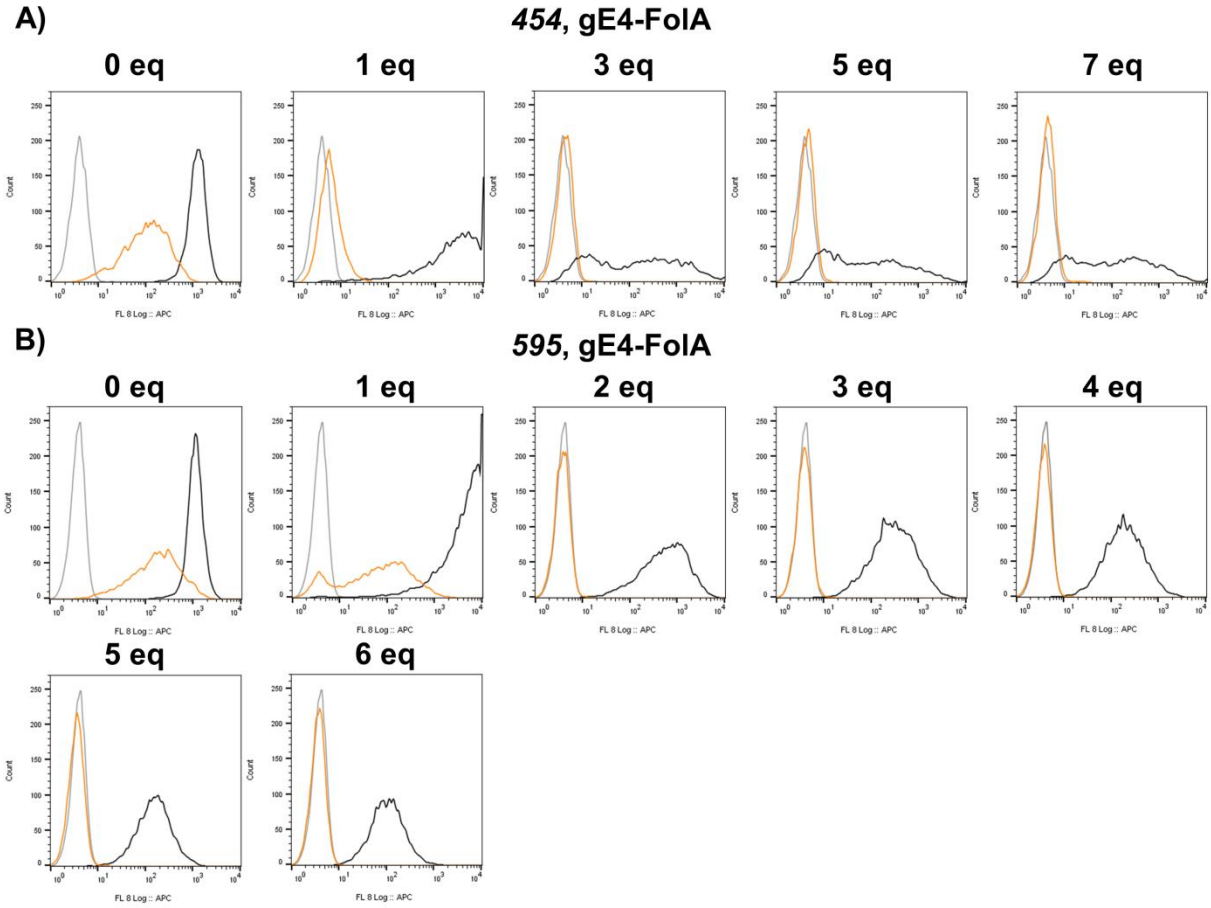

Figure 32 ***(first part).*** Cellular internalization of Cy5-labelled siRNA determined by flow cytometry of ***454*** polyplexes (A, C) and ***595*** polyplexes (B, D) post-PEGylated with increasing molar equivalents of gE4-FolA (A, B) or FolA (C, D). Internalization of polyplexes was examined in KB-eGFP/Luc cells after 45 min incubation at 37 °C. The intensity of the Cy5 signal resembles the amount of internalized polyplexes. “Count” represents cumulative counts of cells with indicated Cy5 fluorescence after gating by forward/sideward scatter and pulse width. Dead cells (DAPI positive, less than 2 %) were excluded from analysis. Post-PEGylated polyplexes are presented in black, blockade of post-PEGylated polyplexes (0.5 h incubation of cells with a saturated folic acid solution at 37 °C) in orange and HBG buffer in grey. Core polyplexes were formed at N/P 10 with a siRNA concentration of 25 µg/mL and a final siRNA concentration of 20 µg/mL after PEGylation. Experiments were performed in triplicates. One representative blot is shown. Adapted from [146].

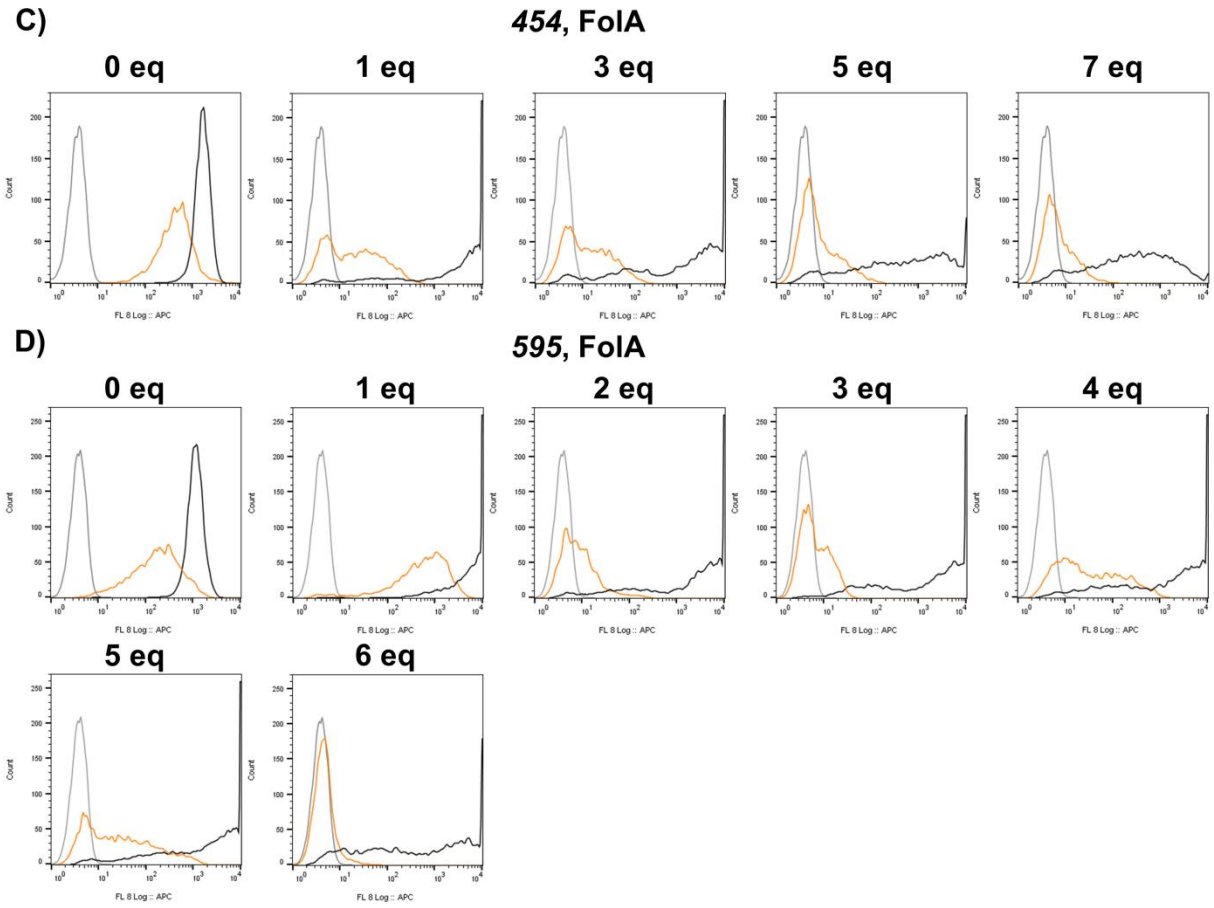

Figure 32 ***(continued).*** Cellular internalization of Cy5-labelled siRNA determined by flow cytometry of ***454*** polyplexes (A, C) and ***595*** polyplexes (B, D) post-PEGylated with increasing molar equivalents of gE4-FolA (A, B) or FolA (C, D). Post-PEGylated polyplexes are presented in black, blockade of post-PEGylated polyplexes (0.5 h incubation of cells with a saturated folic acid solution at 37 °C) in orange and HBG buffer in grey. Core polyplexes were formed at N/P 10 with a siRNA concentration of 25 µg/mL and a final siRNA concentration of 20 µg/mL after PEGylation. Experiments were performed in triplicates. One representative blot is shown. Adapted from [146].

Confocal laser scanning microscopy provided information on the intracellular distribution of PEGylated polyplexes (Figure 33). Fluorescently labelled siRNA (red) and Mal-PEG (green) were used for spiking the siRNA and the PEGylation reagent, respectively. Without PEGylation (0 eq) considerable unspecific uptake was observed for both ***454*** and ***595*** lipo-oligomers. For ***454*** polyplexes with 1 eq of gE4-FolA, big yellow punctuated structures were detectable (Figure 33A), based on polyplex agglomeration. The yellow colour, resulting from the overlay of siRNA and PEGylation agent, confirmed a successful PEGylation. With higher molar equivalents of gE4-FolA (avoiding aggregate formation) instead of the big punctuate structures a more even cell binding with smaller yellow structures (Figure 33A, 3 to 7 eq and Figure 33B, 4 eq) and uptake into cells (Figure 33A, 3 and 7 eq and Figure 33B, 3 and 4 eq) was observed, consistent with

transfections and flow cytometry data. The red dots in the cytoplasm indicate free siRNA after separation from the polyplex or polyplex without PEGylation reagent. For ***595*** polyplexes (Figure 33B,D) with 1 eq of gE4-FolA, the yellow structures were not as big as for ***454***. For 4 eq, free ligand (green) was located at the cell membrane, and for equivalents ≥5 eq, only a few particles were observed in cells (Figure 33B), both findings explain the insufficient transfection efficiency of ***595*** polyplexes at higher PEGylation degrees. For particles post-PEGylated with FolA a similar result was found for ***454*** and ***595*** for all ratios (Figure 33C,D). Small particles, but no agglomerates, that were sufficiently post-PEGylated (yellow) could be found again supporting the hypothesis of a heterogeneous size distribution. As agglomerates are washed away in the process, only small particles could be found in cells.

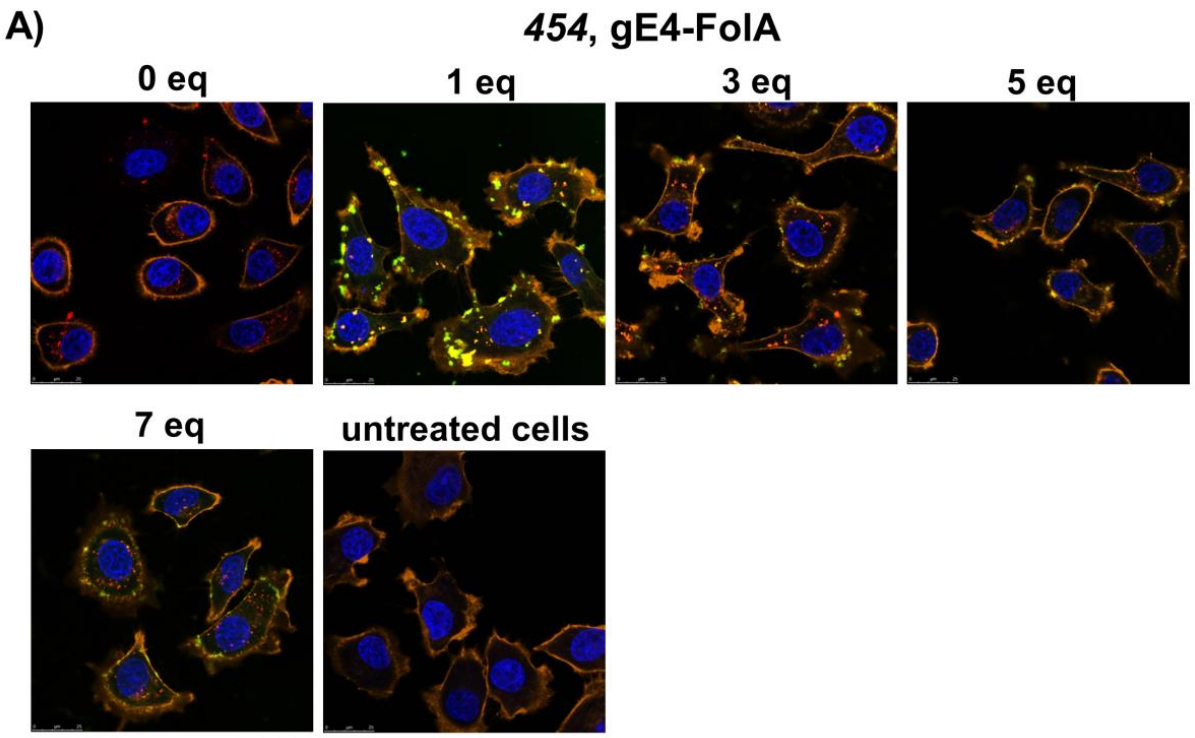

Figure 33 ***(first part).*** Intracelluar distribution of ***454*** polyplexes (A, C) and ***595*** polyplexes (B, D) post-PEGylated with increasing molar equivalents of gE4-FolA (A, B) or FolA (C, D) acquired by confocal laser scanning microscopy. Polyplexes were tested in KB/eGFPLuc cells with 500 ng control siRNA. Nuclei were stained with DAPI (blue), actin cytoskeleton was stained with rhodamine phalloidin (orange), siRNA was spiked with 10 % Cy5 labelled siRNA (red) and the incorporated PEGylation agent was spiked with a defined amount (0.2 eq) Alexa 488-PEG-Mal (green). Yellow presents the overlay of siRNA and PEG. Core polyplexes were formed at N/P 10 with a siRNA concentration of 25 µg/mL and a final siRNA concentration of 20 µg/mL after PEGylation. The images show the overlay of the different channels. *In vitro* preparation was carried out by Katharina Müller; microscopy pictures were taken by Miriam Höhn (Pharmaceutical Biotechnology, LMU Munich). Adapted from [146].

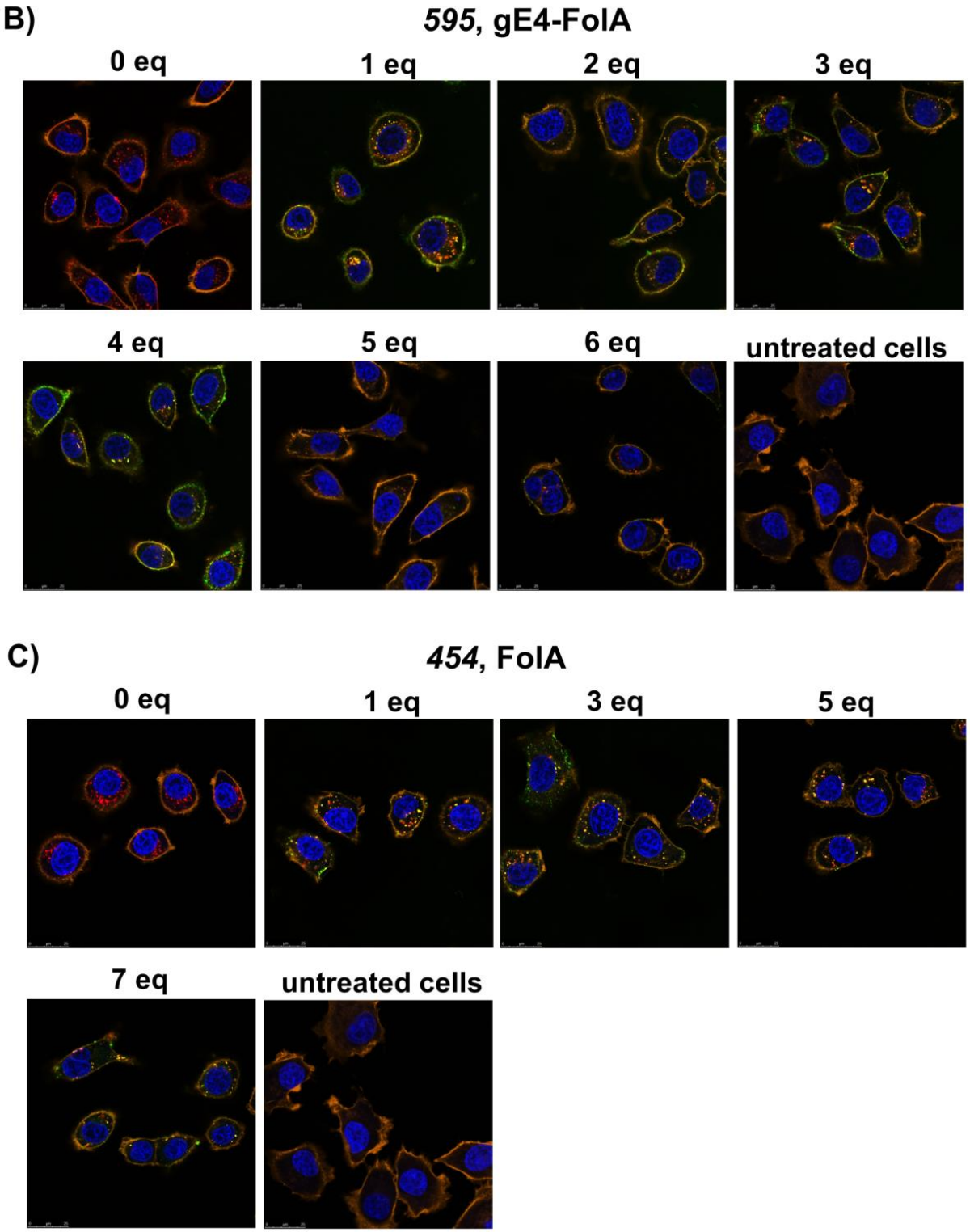

Figure 33 ***(second part).*** Intracelluar distribution of ***454*** polyplexes (A, C) and ***595*** polyplexes (B, D) post-PEGylated with increasing molar equivalents of gE4-FolA (A, B) or FolA (C, D) acquired by confocal laser scanning microscopy. Nuclei were stained with DAPI (blue), actin cytoskeleton was stained with rhodamine phalloidin (orange), siRNA was spiked with 10 % Cy5 labelled siRNA (red) and the incorporated PEGylation agent was spiked with a defined amount (0.2 eq) Alexa 488-PEG-Mal (green). Yellow presents the overlay of siRNA and PEG. In vitro preparation was carried out by Katharina Müller; microscopy pictures were taken by Miriam Höhn (Pharmaceutical Biotechnology, LMU Munich). Adapted from [146].

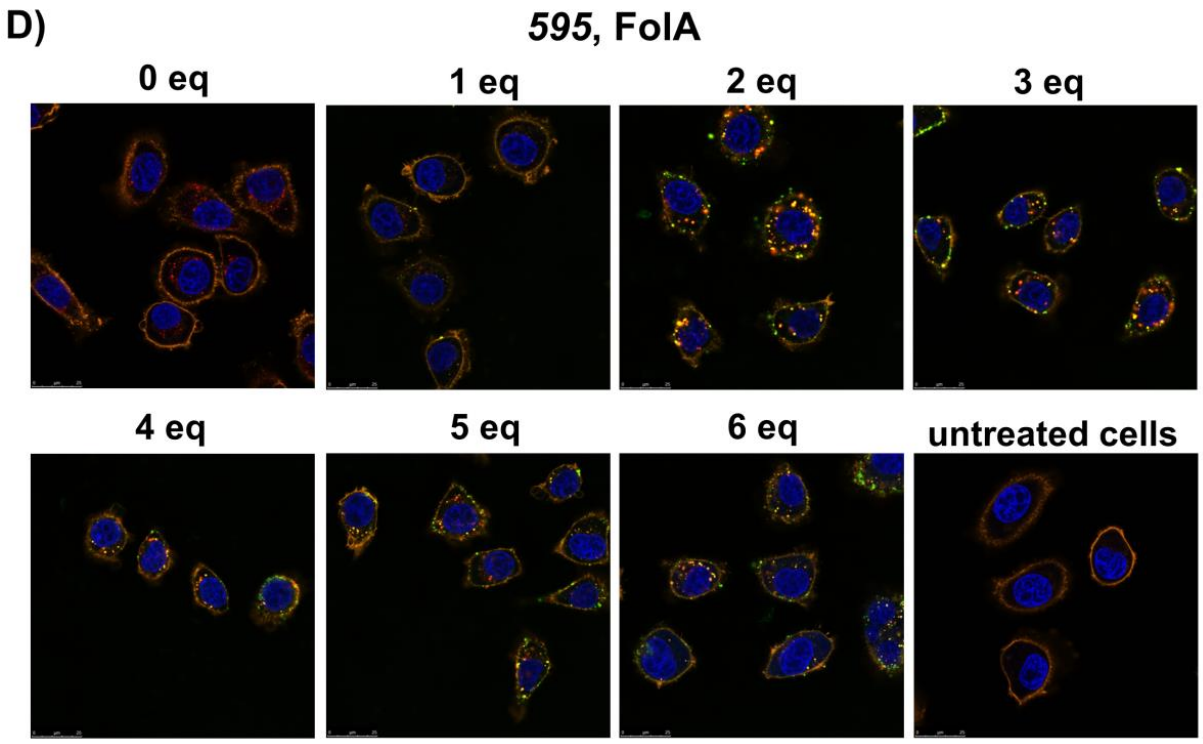

Figure 33 ***(continued).*** Intracelluar distribution of ***454*** polyplexes (A, C) and ***595*** polyplexes (B, D) post-PEGylated with increasing molar equivalents of gE4-FolA (A, B) or FolA (C, D) acquired by confocal laser scanning microscopy. Nuclei were stained with DAPI (blue), actin cytoskeleton was stained with rhodamine phalloidin (orange), siRNA was spiked with 10 % Cy5 labelled siRNA (red) and the incorporated PEGylation agent was spiked with a defined amount (0.2 eq) Alexa 488-PEG-Mal (green). Yellow presents the overlay of siRNA and PEG. In vitro preparation was carried out by Katharina Müller; microscopy pictures were taken by Miriam Höhn (Pharmaceutical Biotechnology, LMU Munich). Adapted from [146].

3.4.2.4 In vivo biodistribution of post-PEGylated polyplexes

Biodistribution of PEGylated ***454*** and ***595*** polyplexes was examined in NMRI nu/nu mice after intravenous tail vein administration. Cy7 labelled siRNA against human AHA1 (without gene target in mice) was detected via near-infrared (NIR) fluorescence imaging. First experiments were carried out with rather high degree of 3 eq of gE4-FolA-PEGylation for both oligomers, as these formulations showed convincing sizes, zeta potentials, and targeting effects *in vitro*. *In vivo* experiments were not performed with standard PEG-FolA, as post-PEGylated polyplexes with this reagent formed agglomerates. It quickly became apparent that the selected gE4-FolA PEGylated ***454*** and ***595*** siRNA polyplexes were highly labile *in vivo*, showing a high bladder signal of siRNA already after 15 min, similar as for free siRNA, and no detectable signal after 4 h (Figure 34). Therefore, in further studies a lower degree of PEGylation (2 and 1.5 eq)

was tested for both oligomers. DLS measurements showed suitable sizes between 130 and 300 nm for all polyplexes prepared at the 10-fold higher concentration that has to be used for *in vivo* studies (Figure 35). PEGylation with 1.5 eq led to a longer persistence of siRNA in livers of mice for both oligomers, which still could be detected after 8 h when livers were examined *ex vivo* (Figure 34). A lower PEGylation degree could not be tested *in vivo* because of the tendency of this polyplexes to agglomerate.

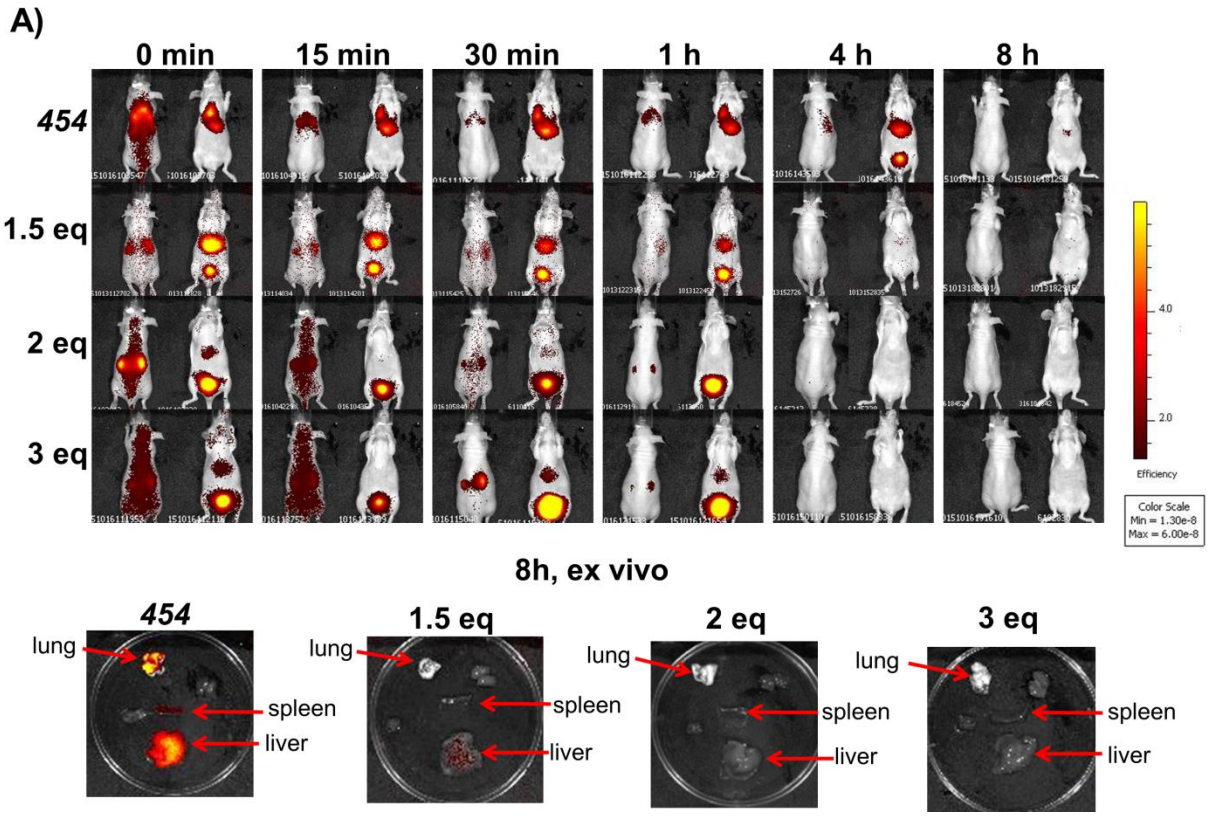

Figure 34 ***(first part).*** Time-dependent biodistribution of siRNA polyplexes after intravenous administration (n=3) in mice and *ex vivo* analysis of organs. A) ***454*** without PEGylation, 1.5 eq, 2 eq and 3eq gE4-FolA and B) ***595*** without PEGylation, 3 eq, 2 eq and 1.5 eq gE4-FolA. Core polyplexes were formed at N/P 10 with a siRNA concentration of 250 µg/mL and a final siRNA concentration of 200 µg/mL after PEGylation. Ventral and dorsal position of one representative mouse of each group is shown. Animal experiments were carried out by Eva Kessel (vetMD student, Pharmaceutical Biotechnology, LMU Munich). Adapted from [146].

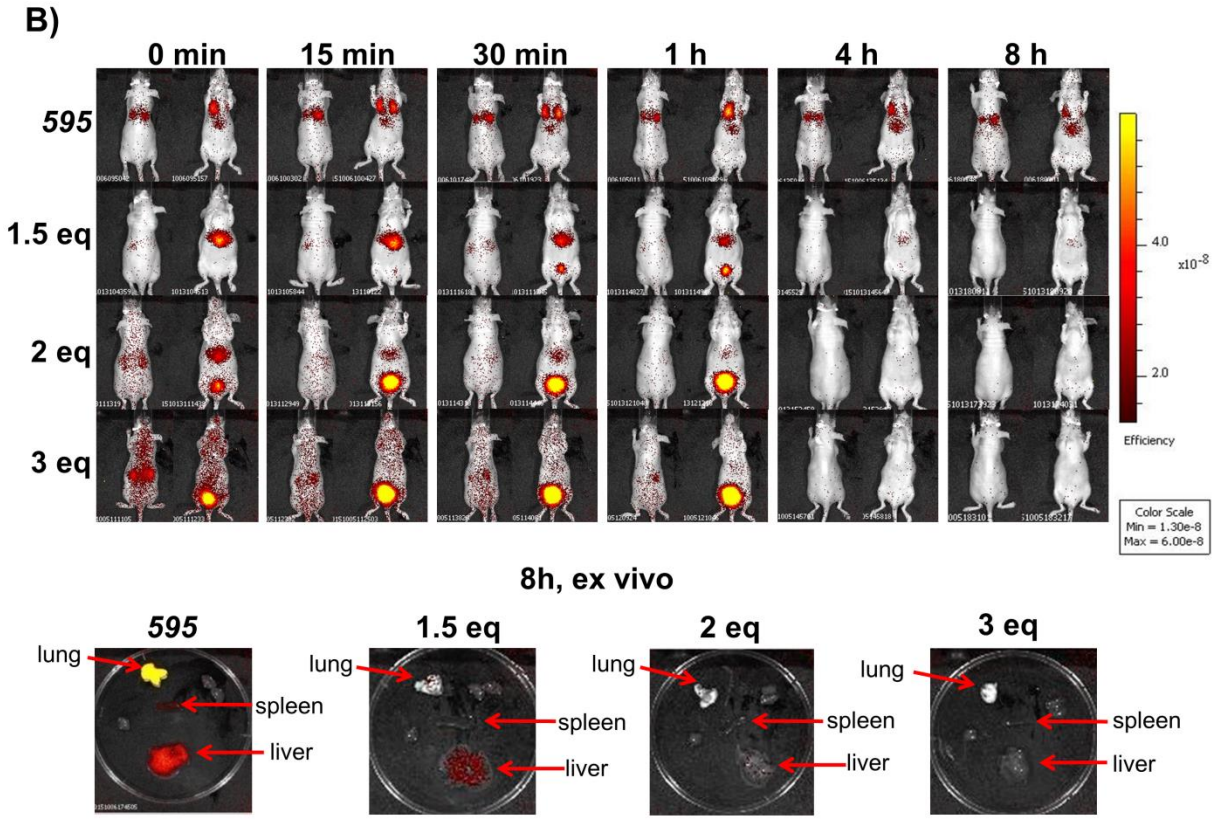

Figure 34 *(continued).* Time-dependent biodistribution of siRNA polyplexes after intravenous administration (n=3) in mice and *ex vivo* analysis of organs. A) ***454*** without PEGylation, 1.5 eq, 2 eq and 3eq gE4-FolA and B) ***595*** without PEGylation, 3 eq, 2 eq and 1.5 eq gE4-FolA. Animal experiments were carried out by Eva Kessel (vetMD student, Pharmaceutical Biotechnology, LMU Munich). Adapted from [146].

A) ***454*, gE4-FolA**

gE4-FolA [mol eq]	Z-average [nm]	PDI	Zeta potential [mV]
1.5	220.3 ± 9.44	0.218 ± 0.008	-19.7 ± 1.00
2	143.9 ± 15.53	0.334 ± 0.044	-19.3 ± 1.19
3	150.9 ± 0.73	0.199 ± 0.004	-22.1 ± 1.50

B) ***595*, gE4-FolA**

gE4-FolA [mol eq]	Z-average [nm]	PDI	Zeta potential [mV]
1.5	273.23 ± 1.29	0.279 ± 0.003	-21.3 ± 0.87
2	241.47 ± 3.38	0.239 ± 0.012	-20.7 ± 0.30
3	129.10 ± 1.39	0.251 ± 0.019	-27.0 ± 1.05

Figure 35. Z-average [nm], PDI, zeta potential [mV] of siRNA polyplexes determined by DLS (n=3 ± SD), generated at *in vivo* concentration (250 µg siRNA/mL) by PEGylation of ***454*** and ***595*** polyplexes with 1.5 eq, 2 eq or 3 eq of gE4-FolA. Adapted from [146].

Further biodistribution experiments were performed in mice bearing L1210 tumors. L1210 cells overexpress the FR as well and are able to bind FolA even to a higher degree compared to KB cells (Figure 36).

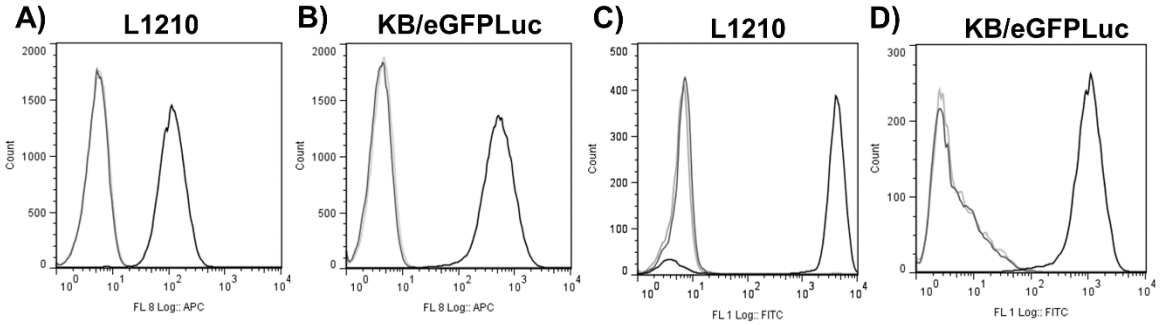

Figure 36. Cellular association of an allophycocyanin labelled folate antibody against the folate receptor (A,B) (black) and of carboxyfluorescein tagged FolA (C,D) (black) determined by flow cytometry of L1210 cells (A,C) and KB/eGFPLuc cells (B,D). As negative controls an allophycocyanin labelled IgG1 isotype control antibody (A,B) and carboxyfluorescein tagged PEG (C,D) were used (dark grey). Control cells (buffer treated cells) are presented in light grey. "Count" represents cumulative counts of cells with indicated Cy5 fluorescence after appropriate gating by forward/sideward scatter and pulse width. Dead cells (DAPI positive, less than 2 %) were excluded from analysis. Experiments were performed in triplicates. One representative blot is shown. Adapted from [146].

For further *in vivo* studies ***595*** polyplexes PEGylated with 1.5 eq of gE4-FolA were selected, as they showed favourable stability and targeted gene silencing in comparison to ***454*** (Figure 37A). Additionally, *in vitro* experiments with L1210 cells using ***595*** polyplexes PEGylated with 1.5 eq of gE4-FolA demonstrated specific silencing of endogenous EG5 gene (as chosen reporter) by RT-qPCR (Figure 37B) and specific uptake compared to ***595*** PEGylated with Mal-PEG or ***595*** without PEGylation (Figure 37C).

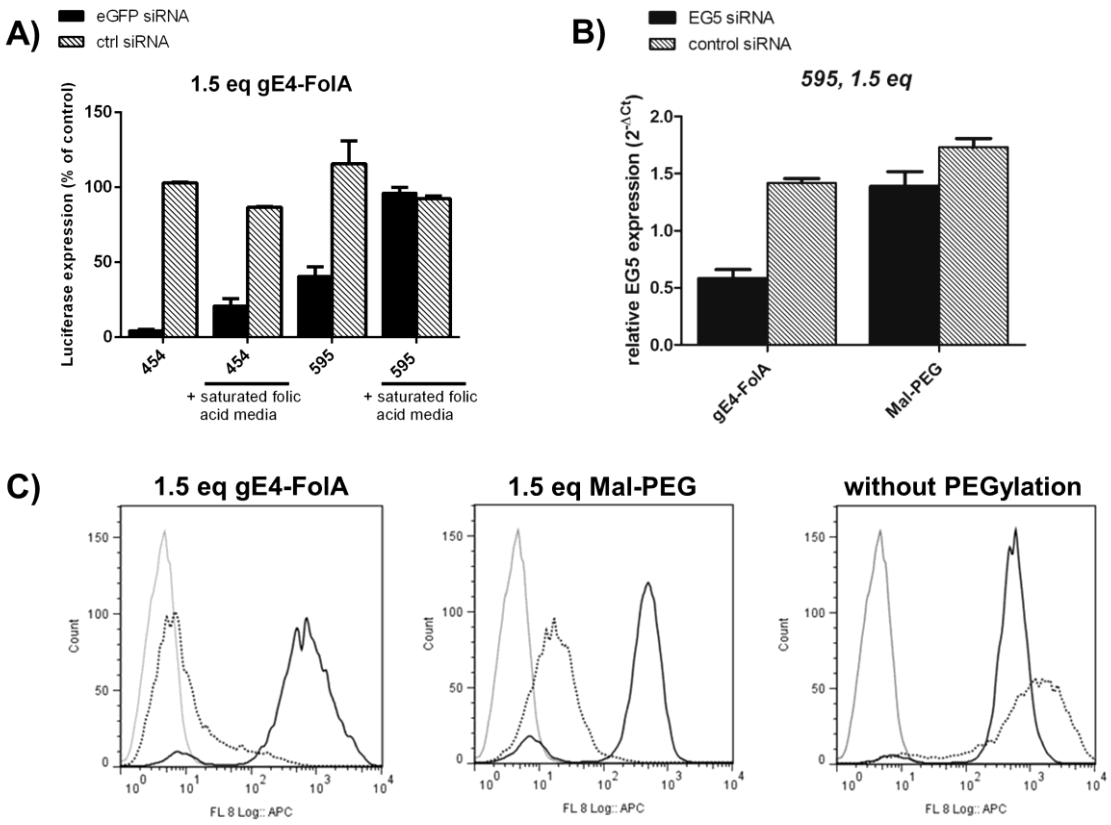

Figure 37. A) Gene silencing (n=3, mean ± SD) of ***454*** and ***595*** polyplexes PEGylated with 1.5 eq of gE4-FolA. Cells were incubated 30 min before standard transfection with a saturated folic acid solution to block the folate receptor, if specified. Polyplexes were tested in KB/eGFPLuc cells with siRNA targeting eGFP (eGFP siRNA) and control siRNA (ctrl siRNA). B) Relative EG5 expression in L1210 cells determined with RT-qPCR (n=3, mean ± SD). Cells were transfected with ***595*** PEGylated with 1.5 eq gE4-FolA or 1.5 eq Mal-PEG using siRNA against EG5 (EG5 siRNA) or control siRNA. C) Cellular internalization of Cy5-labelled siRNA into L1210 cells determined by flow cytometry of ***595*** PEGylated with 1.5 eq gE4-FolA, 1.5 eq Mal-PEG and without PEGylation (n=3) after 45 min incubation at 37 °C. Post-PEGylated polyplexes are presented in black, blockade of post-PEGylated polyplexes (0.5 h incubation of cells with a saturated folic acid solution at 37 °C) in dotted black and HBG buffer in grey. Core polyplexes were formed at N/P 10 with a siRNA concentration of 25 µg/mL (A,C) or 250 µg/mL (B) and a final siRNA concentration of 20 µg/mL (A,C) or 200 µg/mL (B) after PEGylation. Adapted from [146].

Figure 38 shows the biodistribution of ***595*** PEGylated with 1.5 eq gE4FolA and the control groups ***595*** polyplexes without PEGylation or with PEGylation but without targeting ligand (Mal-PEG), and free siRNA in mice bearing L1210 tumors. Figure 38A clearly shows the rapid clearance of free siRNA by the kidney. After 4 h no signal could be detected anymore, meaning a total removal of siRNA. In contrary, all ***595*** groups revealed persistence of NIR-labelled siRNA up to 8 h in mice, when animals had to be sacrificed to analyze their organs. PEGylated ***595*** polyplexes with gE4-FolA largely accumulated in the liver after initial distribution. Similar results were obtained for PEGylated polyplexes without ligand and non-PEGylated polyplexes.

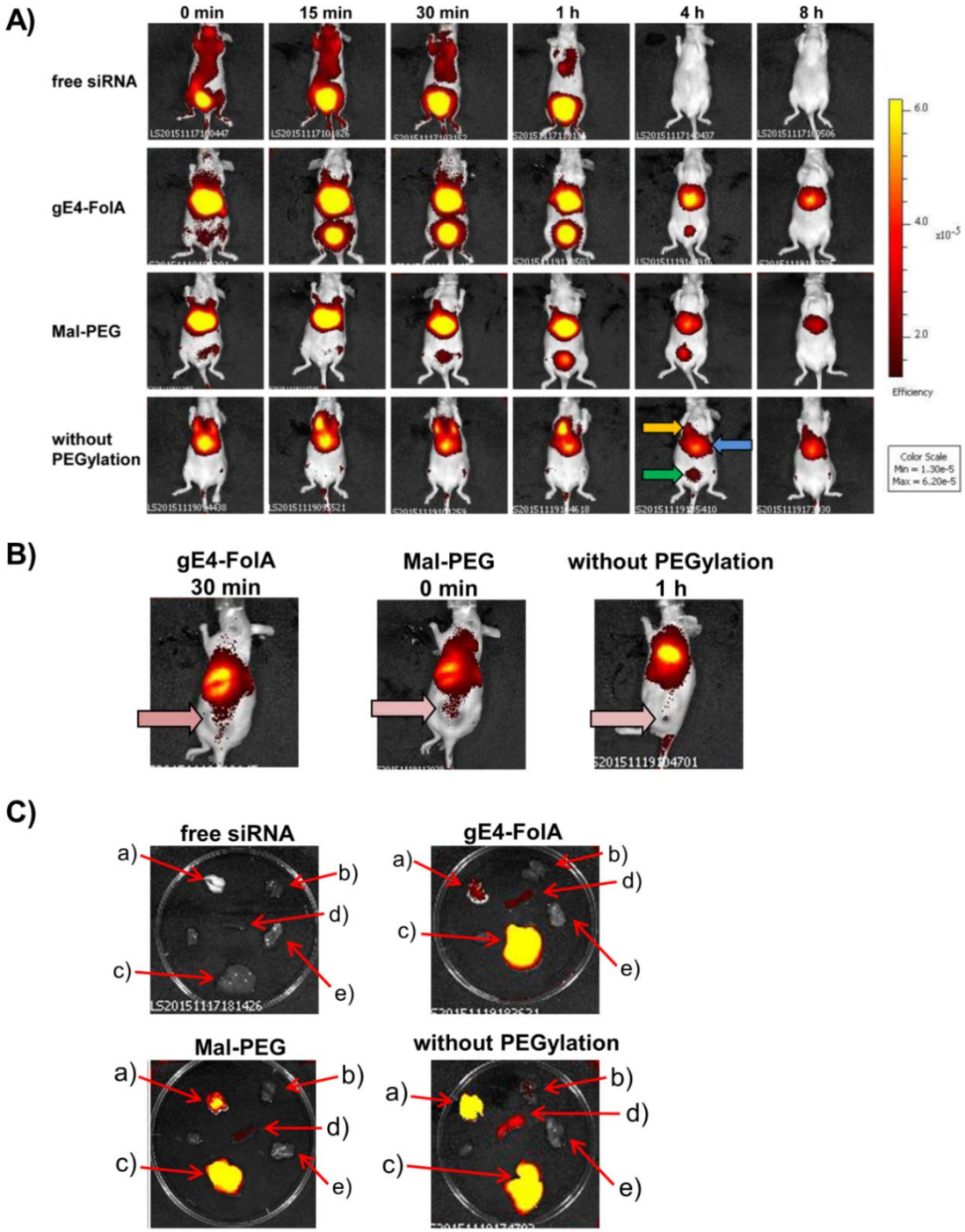

Figure 38. Biodistribution of siRNA polyplexes after intravenous administration into NMRI nu/nu mice bearing subcutaneous L1210 tumors (n = 3 mice). Mice were treated with 50 µg of free siRNA, ***595*** polyplexes PEGylated with 1.5 eq of gE4-FolA, ***595*** polyplexes PEGylated with 1.5 eq of Mal-PEG, and ***595*** polyplexes without PEGylation. Core polyplexes were formed at N/P 10 with a siRNA concentration of 250 µg/mL and a final siRNA concentration of 200 µg/mL after PEGylation. A) Time-dependent distribution. Dorsal position of one representative mouse of each group is shown. The orange arrow represents a lung signal, the blue one a liver signal, and the green one a bladder signal. B) Lateral position of one representative mouse at indicated time points. The rose arrow points to tumors with measurable fluorescence signal. C) *Ex vivo* images of lung, kidney, spleen, liver and tumor at 8 h after administration. a) lung b) kidney c) liver d) spleen e) tumor. Animal experiments were carried out by Eva Kessel (vetMD student, Pharmaceutical Biotechnology, LMU Munich Biotechnology, LMU). Adapted from [146].

A short-term L1210 tumor-associated signal was detected for all ***595*** groups, however disappearing after 30 min for gE4-FolA, after initial application for PEG polyplexes, and after 1 h for non-PEGylated polyplexes (Figure 38B). Interestingly, PEGylation of ***595*** polyplexes led to a reduced lung signal as seen in mice during treatement and in *ex vivo* lungs (Figure 38A,C). To verify this observation, a more quantitative RT-qPCR analysis, detecting intact AHA1-siRNA present in the tissue at the end of the experiment (8 h), was performed (Figure 39). The highest relative siRNA amount in lung was detected for ***595*** polyplexes without PEGylation, followed by PEGylated particles, the lowest abundance in lung was found for the gE4-FolA particles (Figure 39A). No siRNA was found in lungs from animals treated with free siRNA and in untreated animals (control). Additionally, qPCR analysis of AHA1-siRNA was performed in the subcutaneous FR-positive L1210 tumors and livers (Figure 39B,C). As expected from imaging results only a low siRNA amount was found in the tumor as compared to the lungs and livers. Nevertheless, when normalized to lung accumulation, the siRNA quantity in tumors of gE4-FolA particles was higher as for ligand-free PEGylated ***595*** polyplexes and in the same range as for the more stable non-PEGylated particles (Figure 39D).

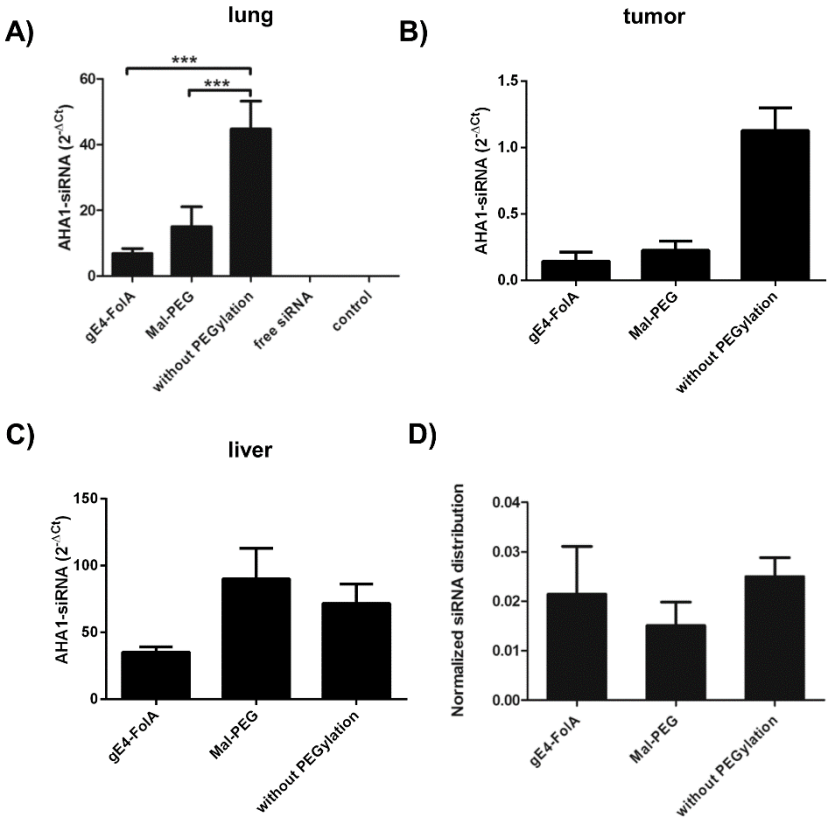

Figure 39. Relative amounts of AHA1-siRNA in A) lung, B) tumor, C) liver (n = 3 ± SD, one-way ANOVA, ***p < 0.05) determined at 8 h after delivery with polyplexes of ***595*** PEGylated with 1.5 eq gE4-FolA, ***595*** PEGylated with 1.5 eq Mal-PEG, and ***595*** without PEGylation. (C) Normalized tumor to lung distribution ratio of AHA1-siRNA. Core polyplexes were formed at N/P 10 with a siRNA concentration of 250 µg/mL and a final siRNA concentration of 200 µg/mL after PEGylation. Adapted from [146].

3.4.3 Post-PEGylation using the peptide ligand GE11 for EGF receptor targeted siRNA and miRNA delivery

This chapter has been adapted from:

Katharina Müller, Philipp M. Klein, Philipp Heissig, Andreas Roidl and Ernst Wagner, "EGF receptor targeted lipo-oligocation polyplexes for antitumoral siRNA and miRNA delivery", Nanotechnology, 2016, 27(46):464001.

The presented post-PEGylation principle can be easily transferred to other ligands. Accordingly, the peptide ligand GE11 (see chapter 1.4.2) was used for epidermal growth factor receptor (EGFR) targeted delivery with the core polyplex ***454***. Here, not only eGFP siRNA was delivered, but also two therapeutic RNAs: miRNA-200c and siRNA targeting EG5. The tumor suppressor miR-200c [165-174] regulates epithelial to mesenchymal transition by targeting ZEB1 and ZEB2. ZEB1 and ZEB2 downregulate the epithelial marker E-cadherin inducing invasion and migration of cancer cells [166, 167, 175, 176]. Besides miRNA-200c suppresses anoikis resistance by targeting TrkB [168] and stemness by targeting Bmi1 [169] [170]. Kopp et al. showed that miRNA-200c additionally targets the proto-oncogene Kras [171]. Kras is a GTPase regulating cell differentiation, proliferation and survival. Mutations mainly in the codon 12, 13 and 61 convert the proto-oncogene into an activated oncogene [177]. By transfecting miRNA-200c targeting KRAS or pre-miRNA 200c Kopp et al. could enhance chemosensitivity towards doxorubicin and reduce cell proliferation and migration in breast cancer cells. As miRNA-200c is frequently downregulated in many human cancers including breast cancer, ovarian cancer, prostate cancer, endometrial cancer and bladder cancer [178-182] and because of its negative effects on tumor progression it can be seen as important tumor suppressor miRNA and interesting therapeutic RNA. Another antitumoral RNA is siRNA against EG5 [183, 184]. EG5 (Eglin-5, also known as Kinesin-5, KSP, or KIF11) is a member of the kinesin superfamily and necessary for the formation of the spindle apparatus during mitosis. Several small molecule inhibitors for EG5 have been found and used for cancer therapy [185-187] as blockade of EG5 leads to prolonged mitotic arrest, formation of mono-astral spindles and apoptosis of tumor cells [188]. Therefore EG5 is a favourable target gene for siRNA knockdown. Delivery of EG5 siRNA into cancer cells resulted in cytotoxicity, antitumoral effects and reduced tumor growth in mice [68, 102, 189, 190].

Post-PEGylated particles were formed as described in chapter 3.4.1 (Figure 23B). Mal-GE11 was used as post-PEGylation reagent. GE11 consists of the amino acid sequence YHWYGYTPQNVI and was synthesized and coupled to maleimide-PEG_{28} using SPS (Figure 40).

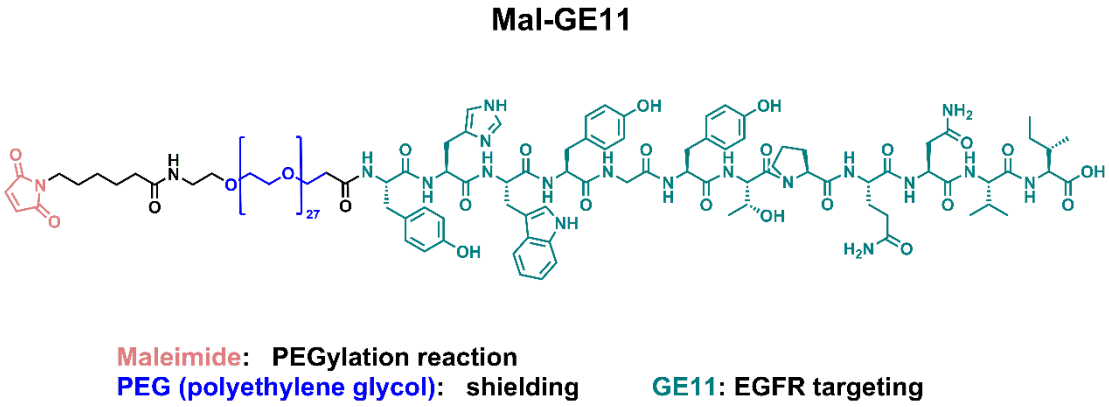

Figure 40. Amino acid sequence of the post-PEGylation reagent Mal-GE11. Mal-GE11 was synthesized by Philipp Klein (PhD student, Pharmaceutical Biotechnology, LMU Munich). Adapted from [147].

3.4.3.1 Biophysical characterization of EGFR targeted post-PEGylated polyplexes

Nanoparticle formation and successful PEGylation was confirmed using dynamic light scattering (DLS) and zeta potential measurements. Increasing molar equivalents from 0.2 eq to 1 eq of Mal-GE11 (Figure 40) or Mal-PEG (Figure 24) calculated on the molar amount of ***454*** were tested (Figure 41A,B). The Z-average values demonstrated suitable siRNA polyplex sizes from 120 nm to 150 nm with uniform particle populations. Only in case of polyplexes with 1 eq Mal-GE11, probably due to agglomeration as seen in chapter 3.4.2, larger particles (~ 400 nm) were detectable. The zeta potential of ***454*** without PEGylation (0 eq) was +40 mV. After reaction with the PEG reagents it decreased to +15 mV with Mal-GE11, and to +8 mV with Mal-PEG, respectively, showing the charge shielding effect of PEGylation.

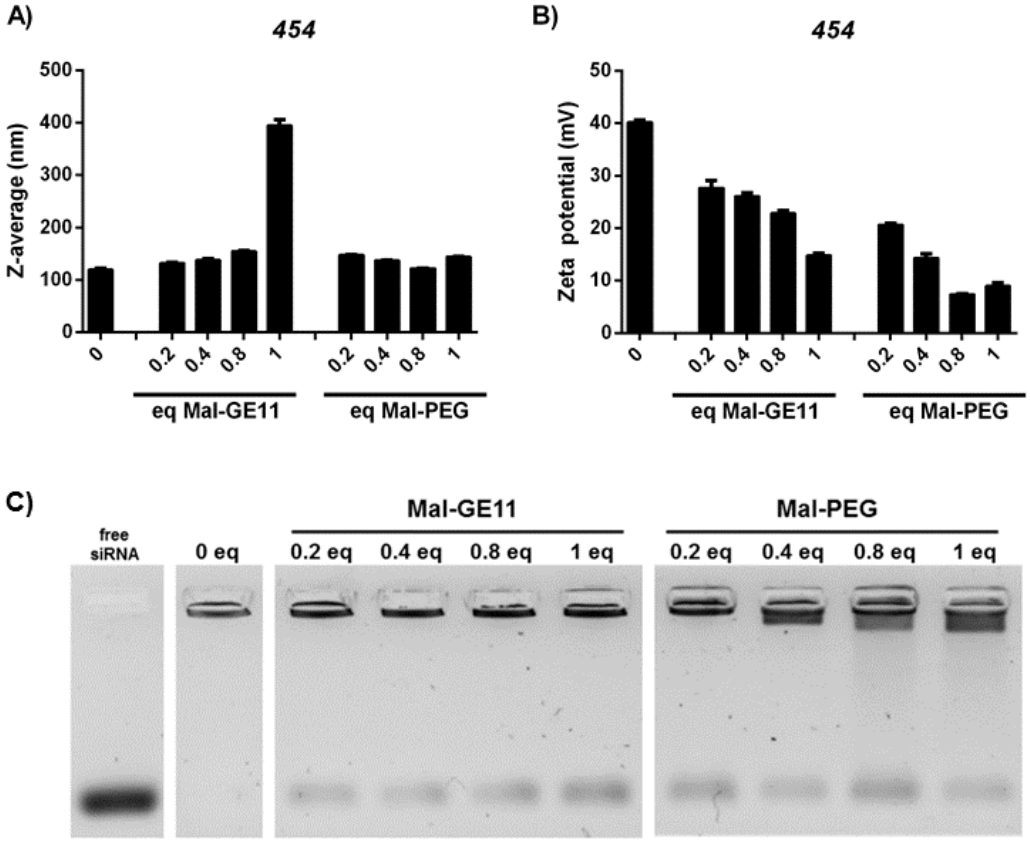

Figure 41. A) Nanoparticle sizes (Z-average, in nm) and B) zeta potentials [mV] of ***454*** polyplexes PEGylated with increasing molar equivalents of Mal-GE11 and Mal-PEG (n=3, mean ± SD). C) Gel retardation of ***454*** polyplexes PEGylated with increasing molar equivalents of Mal-GE11 and Mal-PEG. Core polyplexes were formed at N/P 10 with a siRNA concentration of 25 µg/mL, resulting in a final siRNA concentration of 20 µg/mL after PEGylation. Adapted from [147].

The siRNA binding ability of PEGylated polyplexes was evaluated in a gel retardation assay (Figure 41C). siRNA / ***454*** lipo-polyplexes without PEGylation (0 eq) showed high siRNA binding, as evidenced by the entire siRNA retained in the gel loading pocket. Consistent with gE4-FolA PEGylated polyplexes (Figure 28), PEGylation slightly reduced siRNA polyplex stability. In case of Mal-GE11 the amount of released siRNA correlated with the PEGylation degree, in case of Mal-PEG polyplexes the content of free siRNA remained constant. Nevertheless, most of the siRNA remained polyplex-bound and stayed in the loading pockets. To test the stability of PEGylated formulations in full serum, siRNA nanoparticles were incubated in 90 % FBS for 2 h and 24 h at 37 °C (Figure 42). Only a minor siRNA fraction was released for ***454*** polyplexes without or with Mal-GE11 modification even after 24 h. In contrary, Mal-PEG polyplexes modified at 0.8 - 1 molar equivalents released siRNA significantly. These results indicate a higher stability of ***454*** / Mal-GE11 polyplexes.

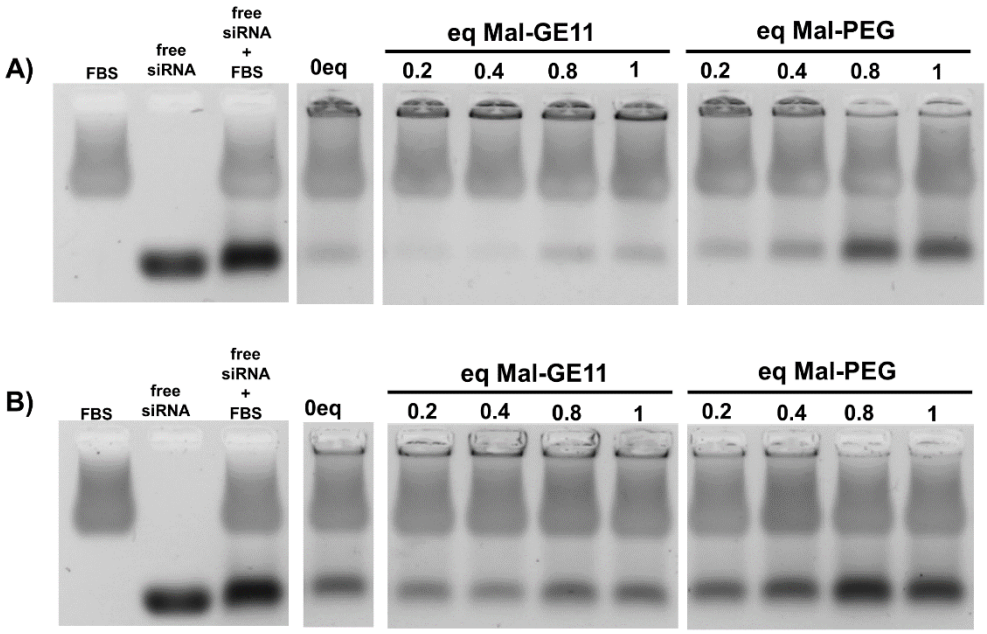

Figure 42. Gel retardation assay of ***454*** polyplexes PEGylated with increasing molar equivalents of Mal-GE11 and Mal-PEG after A) 2 h and B) 24 h incubation in 90 % FBS. Core polyplexes were formed at N/P 10 with a siRNA concentration of 250 µg/mL, resulting in a final siRNA concentration of 200 µg/mL after PEGylation. Adapted from [147].

3.4.3.2 Cellular internalization and gene silencing of EGFR targeted post-PEGylated polyplexes

For the *in vitro* examination of the EGFR targeted polyplexes three cancer cell lines were selected: T24 bladder cancer cells, MDA-MB 231 breast cancer cells and Huh7 hepatocellular carcinoma cells. Chosen cell lines expressed the EGFR to a high degree as shown *via* flow cytometry in Figure 43.

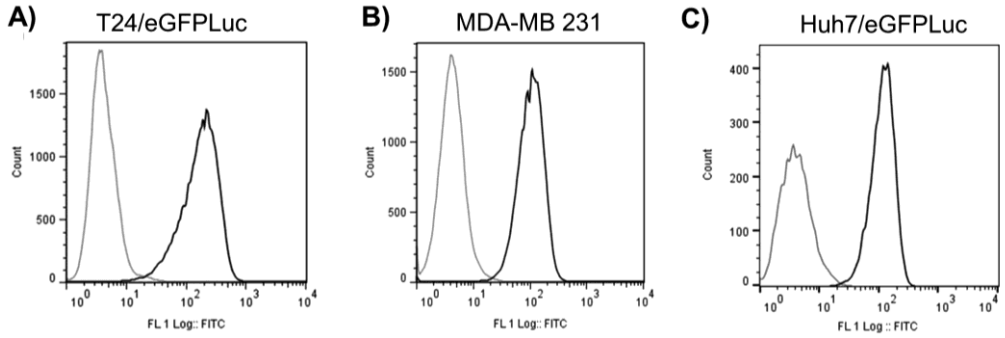

Figure 43. EGFR expression of (A) T24/eGFPLuc-200cT cells, (B) MDA-MB 231 cells and (C) Huh7/eGFPLuc cells. Control cells (buffer treated cells) are presented in grey, EGFR positive cells are presented in black. “Count” represents cumulative counts of cells fluorescence after gating by forward/sideward scatter and pulse width. Dead cells (DAPI positive, less than 2 %) were excluded from analysis. Adapted from [147].

Figure 44 shows the cellular internalization of the post-PEGylated ***454*** polyplexes. Cy5-siRNA polyplexes shielded with 0.2 eq up to 1 eq Mal-GE11 (blue line) were compared with polyplexes without ligand (Mal-PEG, green line) or with polyplexes without PEGylation (black line). At the low PEGylation degree of 0.2 eq, no ligand or shielding effects could be observed. With ≥0.4 eq PEGylation, Mal-GE11 polyplexes showed a clear increase in uptake and significant ligand effect on all three cell lines. The uptake further increased with 0.8 eq Mal-GE11 equivalents. Polyplexes with 1 eq Mal-GE11 displayed extremely high internalization, saturating the Cy5 fluorescence flow cytometry channel; such a high fluorescence, however, is typical for association of aggregated polyplexes (compare Figure 41) which are not considered as useful for further development.

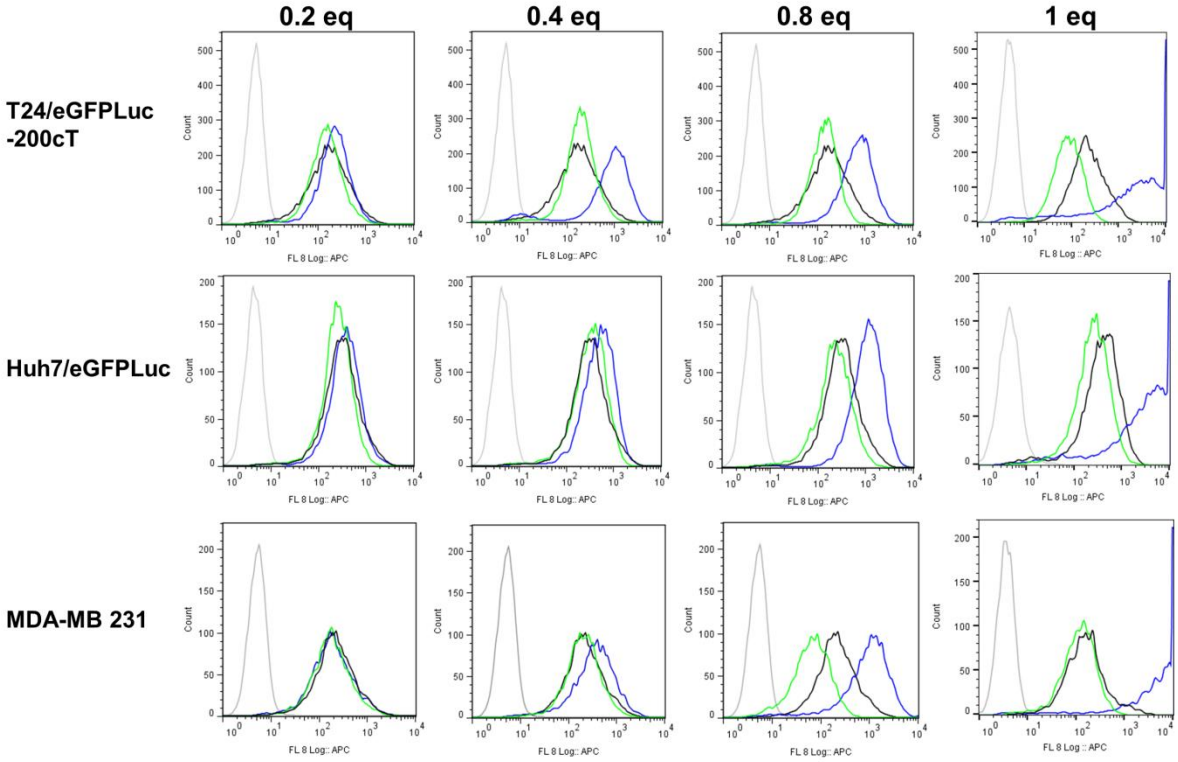

Figure 44. Cellular internalization of Cy5-labelled siRNA determined by flow cytometry of ***454*** polyplexes which were PEGylated with increasing molar equivalents of Mal-GE11 or Mal-PEG. Internalization of polyplexes after 45 min incubation at 37 °C was examined in T24/eGFPLuc-200cT, Huh7/eGFPLuc and MDA-MB 231 cells. The intensity of the Cy5 signal after removal of externally bound polyplexes by a heparin wash resembles the amount of internalized polyplexes. “Count” represents cumulative counts of cells with indicated Cy5 fluorescence after gating by forward/sideward scatter and pulse width. Dead cells (DAPI positive, less than 2 %) were excluded from analysis. Mal-GE11 modified polyplexes are presented in blue, Mal-PEG modified polyplexes are presented in green and non-PEGylated polyplexes are presented in black. Buffer treated cells are presented in grey. Core polyplexes were formed at N/P 10 with a siRNA concentration of 25 µg/mL, resulting in a final siRNA concentration of 20 µg/mL after PEGylation. Experiments were performed in triplicates. One representative blot is shown. Adapted from [147].

The gene silencing efficiency of PEGylated ***454*** polyplexes was examined in T24/eGFPLuc-200cT and Huh7/eGFPLuc cells (Figure 45). Both cell lines stably express the eGFP-luciferase fusion protein. T24/eGFPLuc-200cT cells additionally offer a binding site for miR-200c in the eGFP-luciferase mRNA, which therefore can be blocked by delivered miR-200c. The stable T24/eGFPLuc-200cT cells were specially prepared as test cell line to monitor miR200c delivery in a simple fashion *via* luciferase read-out. Cells were transfected with polyplexes of siRNA against eGFP (eGFP siRNA), a synthetic miR-200c mimic (with a 23 bp siRNA-like structure), or control siRNA without any target gene (ctrl siRNA).

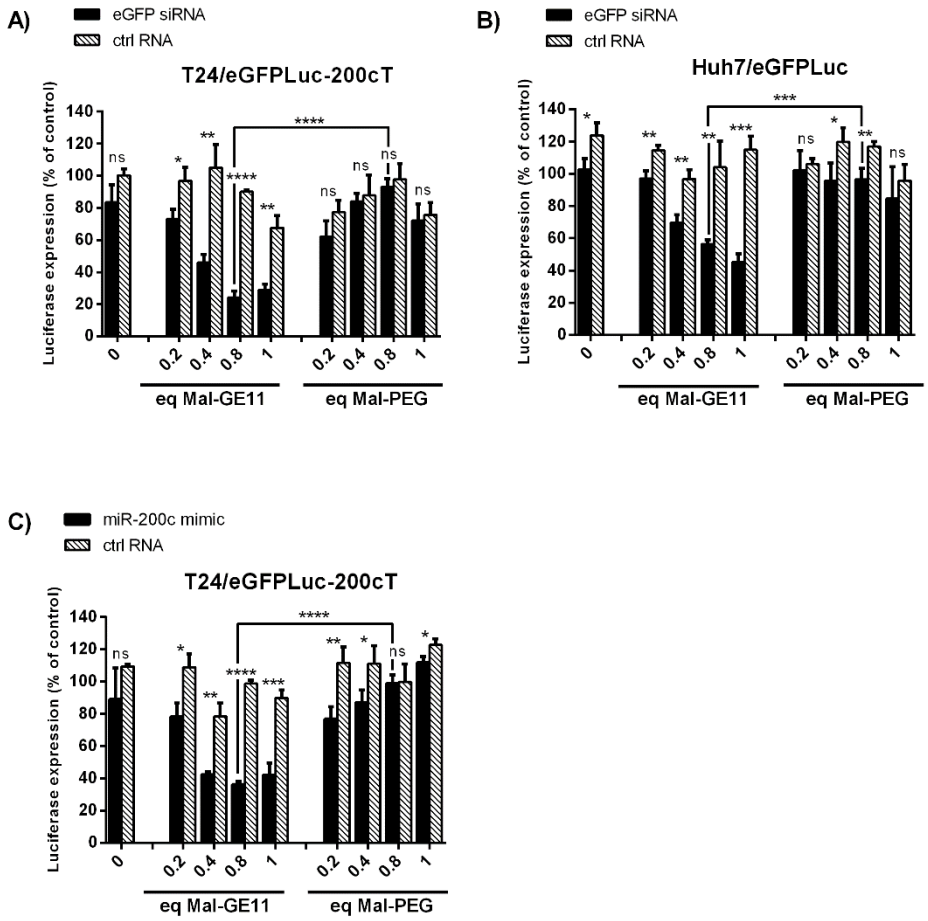

Figure 45. Gene silencing (n=3, mean ± SD) of A) T24/eGFPLuc-200cT cells transfected with eGFP siRNA and ctrl siRNA, B) Huh7/eGFPLuc cells transfected with eGFP siRNA and ctrl siRNA and C) T24/eGFPLuc-200cT cells transfected with miR-200c mimic or ctrl siRNA. Core polyplexes were formed with ***454*** at N/P 10 with a RNA concentration of 25 µg/mL, resulting after PEGylation with increasing molar equivalents of Mal-GE11 or Mal-PEG in a final RNA concentration of 20 µg/mL. Polyplexes were incubated on cells for only 45 min to highlight receptor-specific transfection, gene silencing effects were analyzed at 48 h after transfection. For statistical analysis two-tailed t-test was performed (n=3, mean ± SD, ns (not significant) $p > 0.05$, * $p < 0.05$, ** $p < 0.01$, *** $p < 0.001$, **** $p < 0.0001$). Indicated statistical significance on top of transfection bars without connecting line shows statistical significance between eGFP siRNA/ miR-200c mimic and ctrl siRNA at specified PEGylation equivalents. Indicated statistical significance with connecting line shows statistical significance between 0.8 eq GE11 and 0.8 eq PEG of eGFP siRNA/miR-200c mimic. Adapted from [147].

Neither non-PEGylated nor Mal-PEG modified ***454*** polyplexes showed sufficient gene silencing (Figure 45A-C). In contrast, eGFP siRNA Mal-GE11 polyplexes mediated up to 70 % gene silencing in T24/eGFPLuc-200cT cells (Figure 45A) and up to 55 % in Huh7/eGFPLuc (Figure 45B) cells. Also with miR-200c mimic polyplexes, only for the Mal-GE11 modified nanoparticles a knockdown up to 60 % could be observed (Figure 45 C). Best silencing efficiency was observed for 0.8 to 1 molar equivalents of Mal-GE11. Polyplexes formed with ctrl siRNA did not show significant unspecific knockdown of gene expression, excluding significant toxic effects. This finding could be confirmed by MTT assays (Figure 46), where cell viability was not affected by the transfections. In sum, as polyplexes without targeting ligand or without silencing RNAs did not lead to gene knockdown, the experiments confirm the receptor specificity and potency of the GE11-PEG lipo-polyplexes.

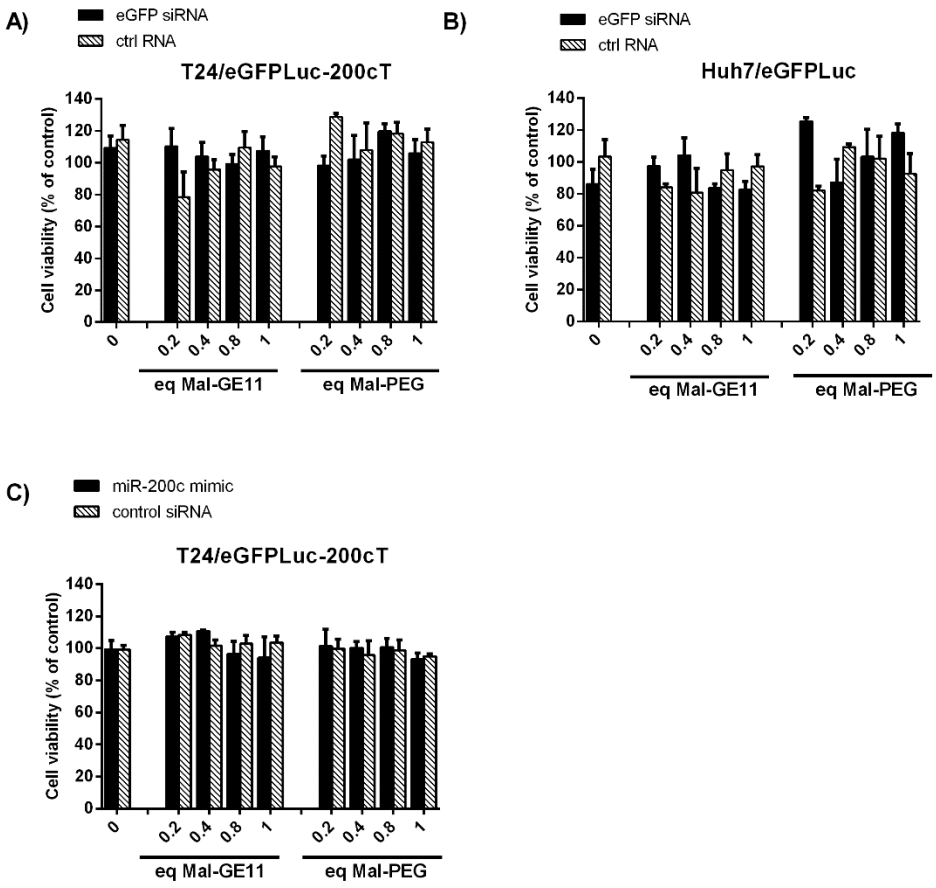

Figure 46. Cell viabilities (n=3, mean ± SD) of A) T24/eGFPLuc-200cT cells transfected with eGFP siRNA and ctrl siRNA, B) Huh7/eGFPLuc cells transfected with eGFP siRNA and ctrl siRNA, and C) T24/eGFPLuc-200cT cells transfected with miR-200c mimic or ctrl siRNA. PEGylated ***454*** polyplexes with increasing molar equivalents of Mal-GE11 and Mal-PEG were tested. Polyplexes were incubated on cells for 45 min. Core polyplexes were formed at N/P 10 with a RNA concentration of 25 µg/mL, resulting in a final RNA concentration of 20 µg/mL after PEGylation. Adapted from [147].

Gene silencing was additionally examined on the mRNA level for the therapeutic miR-200c mimic and therapeutic EG5 siRNA (Figure 47). As the polyplexes modified with 0.8 eq of Mal-GE11 had revealed most suitable particle sizes, zeta potential and gene silencing efficiency they were used for all further experiments.

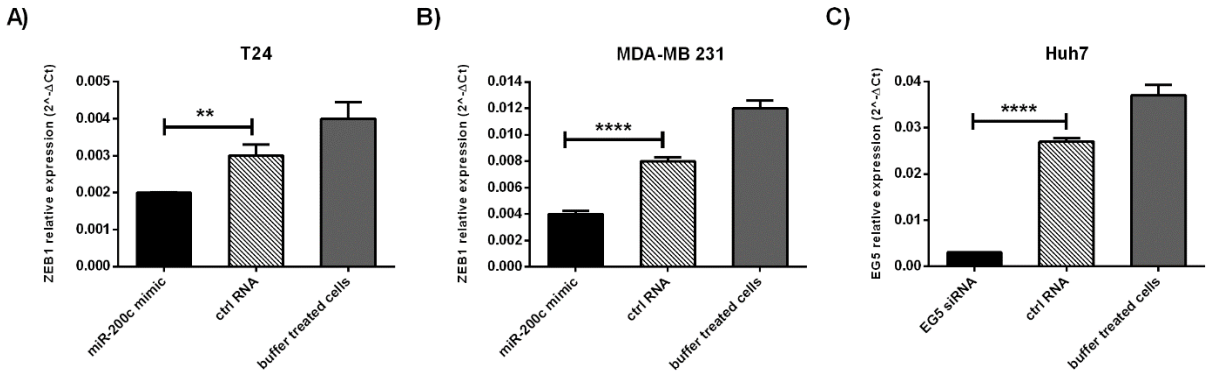

Figure 47. RT-qPCR of ZEB1 expression (A,B) and EG5 expression (C) in A) T24, B) MDA-MB 231 and C) Huh7 cells. Cells were transfected with 0.8 eq Mal-GE11/***454*** polyplexes containing miR-200c mimic (A,B) or EG5 siRNA (C). Core polyplexes were formed at N/P 10 with a siRNA concentration of 25 µg/mL resulting in a final siRNA concentration of 20 µg/mL after PEGylation and were incubated on cells for 45 min. Gene expression levels at 24 hours after transfection were analyzed. For statistical analysis a two-tailed t-test was performed (n=3, mean ± SD, ** $p < 0.01$, **** $p < 0.0001$). Adapted from [147].

In case of silencing with miR-200c, ZEB1 mRNA expression was analyzed, since it is degraded as a direct miR-200c target and involved in mesenchymal to epithelial transition associated with tumor cell migration and invasion. T24 bladder carcinoma and MDA-MB 231 breast cancer cells were used, because these aggressive, advanced mesenchymal cancer types do not express miR-200c [171, 182]. By the delivery of miR-200c, the malignant phenotype of these cell lines should be partly reverted. After transfection with Mal-GE11 ***454*** miR-200c polyplexes, ZEB1 mRNA was significantly downregulated in both cell lines (Figure 47A,B) in comparison with analogous control siRNA polyplexes. Interestingly, particles transfected with ctrl siRNA however also reduced ZEB1 levels in comparison to only buffer-treated cells. Probably GE11 polyplex binding to EGFR (GE11 lipo-poly-fection) followed by intracellular uptake may to some extent affect relative cellular gene expression [191, 192]. As a third additional example of gene silencing, knockdown of the EG5 gene by siRNA was examined on Huh7 cells (Figure 47C). Again a high, significant silencing of EG5 mRNA could be demonstrated by the GE11 polyplexes.

3.4.3.3 Antitumoral effects of miR-200c delivery by GE11 polyplexes

Next, miRNA-200c Mal-GE11 ***454*** polyplexes were used to inhibit tumor cell growth, chemoresistance and migration. To examine the effect on proliferation, T24 and MDA-MB 231 cells were transfected using miR-200c in comparison to ctrl siRNA with and without GE11 ligand, and tumor cell growth was monitored for six days (Figure 48A). On both cell lines a significant reduced proliferation could be observed when transfected with miR-200c polyplexes with GE11 but not without GE11 ligand, indicating the receptor-dependent uptake and biological function of these particles, consistent with preceding transfections and flow cytometry. As advanced mesenchymal tumor cells often display significant resistance against chemotherapeutics [170], the effect of miR-200c mimic on doxorubicin treatment was studied. MDA-MB 231 and T24 cells were treated for 72 h with 15 µM or 10 µM doxorubicin, respectively, after transfection with Mal-GE11 polyplexes (Figure 48B).

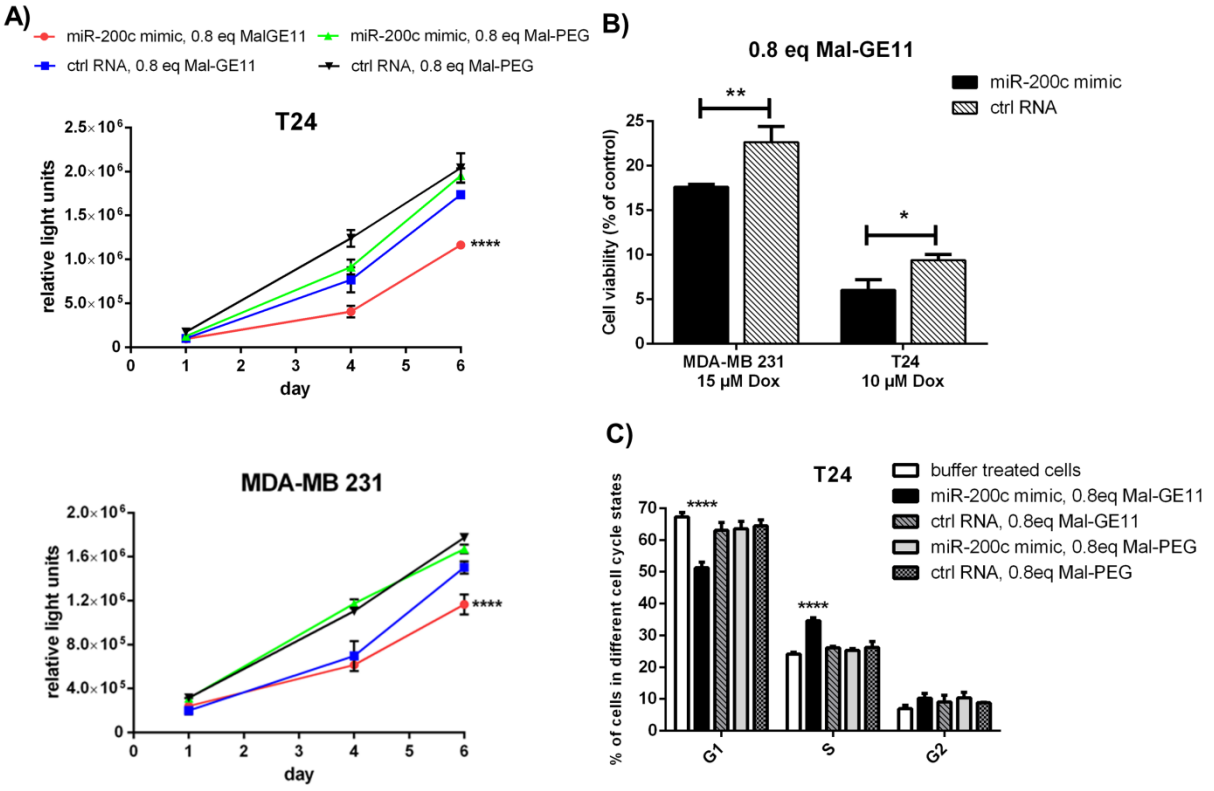

Figure 48. Antitumoral effects of miR-200c mimic transfected with EGFR-targeted polyplexes. A) Proliferation of T24 and MDA-MB 231 cells, B) Sensitivity towards doxorubicin of MDA-MB 231 and T24 cells at 72 hours after treatment with 15 µM or 10 µM doxorubicin, respectively and C) cell cycle analysis of T24 cells at 72 hours after treatment via flow cytometry. Cells were transfected with miR-200c mimic in comparison to ctrl RNA using ***454*** polyplexes PEGylated with 0.8 eq Mal-GE11 or Mal-PEG. Core polyplexes were formed at N/P 10 with a siRNA concentration of 25 µg/mL resulting in a final siRNA concentration of 20 µg/mL after PEGylation and incubated with cells for 4 h. For statistical analysis, 2-way ANOVA (A, C) and two-tailed t-test (B) was performed (n=3, mean ± SD, * $p < 0.05$, ** $p < 0.01$, **** $p < 0.0001$). Adapted from [147].

Cell viability was reduced for both cell lines only with miR-200c mimics and not with control siRNA, demonstrating a higher sensitivity towards doxorubicin. In addition, a miR-200c mediated effect of GE11 polyplexes was demonstrated by cell cycle analysis (Figure 48C). The number of cells in the G1 phase was significantly reduced, and in the S phase significantly enhanced; this was observed only in the miR-200c GE11 group.

To study the effect of miR-200c polyplexes on tumor cell migration, a scratch assay was performed (Figure 49). MDA-MB 231 cells were transfected using nanoparticles post-PEGylated with 0.8 eq Mal-GE11 or Mal-PEG, either containing miR-200c mimics or ctrl RNA. After 24 h a scratch was created, and closure of the scratch, which is an indicator for cell migration, was measured after 24 h and 48 h. For cells treated with miR-200c and Mal-GE11 the scratch size was still 60 % of the initial scratch after 48 h. The effect of GE11 polyplexes became obvious when compared to the almost closed scratch of miR-200c Mal-PEG polyplexes, which after 48 h was only 16 % of the initial scratch size. A slight RNAi-independent effect of GE11 ctrl siRNA nanoparticles could be observed, with a remaining scratch size of 24 % closure (as compared with the 16% of non-targeted miR-200c particle control). This is consistent with a slight anti-tumoral effect of GE11 ligand nanoparticles as also observed in Figure 47.

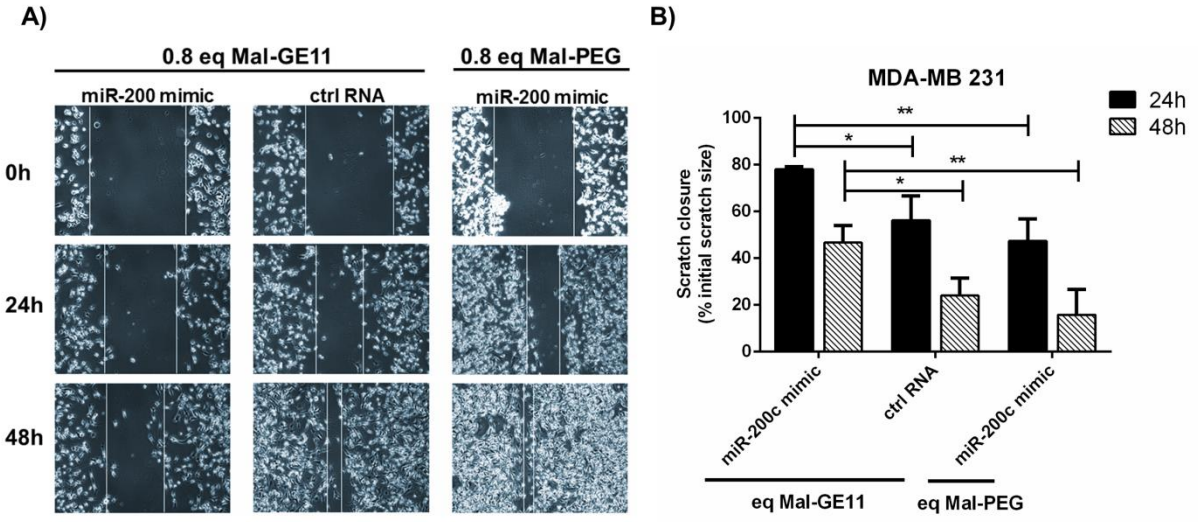

Figure 49. Inhibition of tumor cell migration. MDA-MB 231 cells were treated with ***454*** polyplexes PEGylated with 0.8 eq Mal-GE11 or Mal-PEG for 4 h. Cell layer was broken through a scratch after 24 h and its closure was monitored. A) Images of scratches taken at different time points. B) Scratch closure represented as percentage of initial scratch. For statistical analysis 2-way ANOVA was performed (n=3, mean ± SD, * $p < 0.05$, ** $p < 0.01$). Adapted from [147].

3.4.3.4 Antitumoral effects of EG5 siRNA transferred with GE11 polyplexes

EG5 (Eglin-5, also named Kinesin-5, KSP, or KIF11) is a key player in chromosome separation during mitosis and therefore an interesting target gene in cancer therapy. As displayed in Figure 47C, efficient EG5 gene silencing by GE11 polyplexes was demonstrated in Huh7 hepatocellular carcinoma cells at the mRNA level. The biological antitumoral activity of EG5 siRNA was examined using Huh7/eGFPLuc cells (Figure 50). Only Mal-GE11 ***454*** polyplexes of EG5 siRNA displayed high antitumoral activity (Figure 50A) demonstrating significant ligand specificity again.

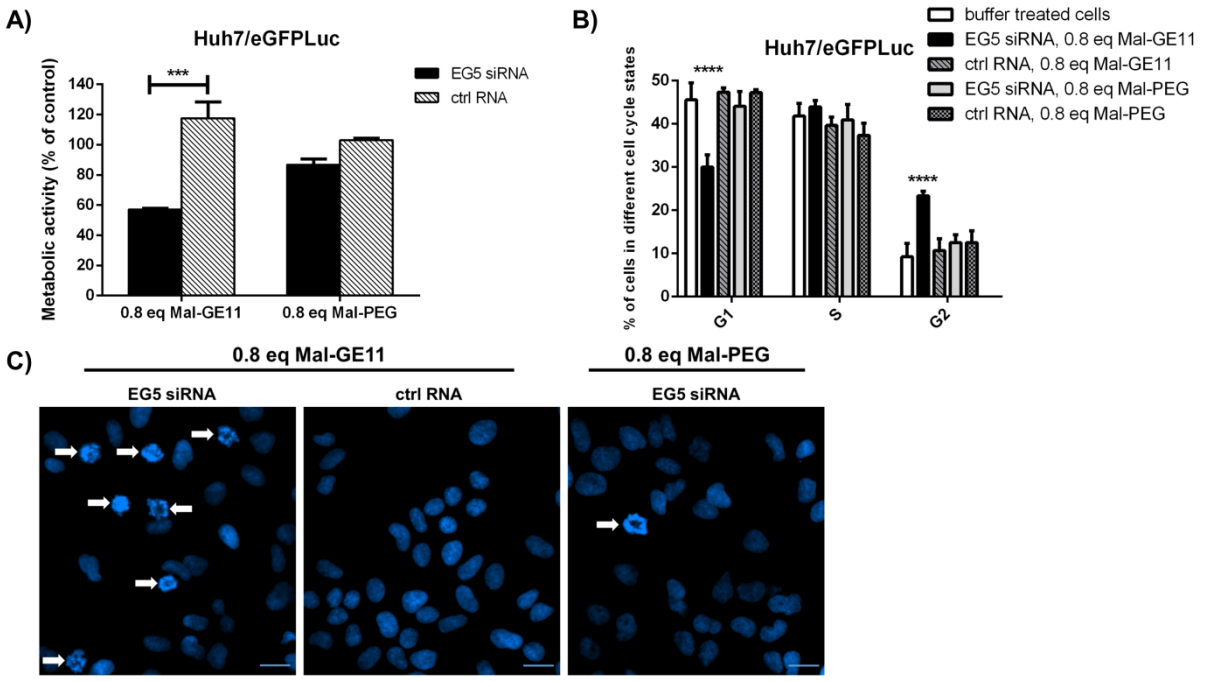

Figure 50. Antitumoral effects of EG5 siRNA transfected with EGFR-targeted polyplexes. A) Metabolic activity of Huh7/eGFPLuc cells at 48 h after 4 h incubation with polyplexes. B) Cell cycle analysis of Huh7/eGFPLuc after 45 min treatment. Cells were analyzed after 48 h *via* flow cytometry. C) Fluorescence microscopy images of DAPI stained nuclei of Huh7/eGFPLuc cells at 48 h after 45 min polyplex treatment. Scale bars represent 20 µm. Cells were transfected with EG5 siRNA and ctrl siRNA using ***454*** polyplexes PEGylated with 0.8 eq Mal-GE11 or Mal-PEG. Core polyplexes were formed at N/P 10 with a RNA concentration of 25 µg/mL, resulting in a final RNA concentration of 20 µg/mL after PEGylation. For statistical analysis a two-tailed t-test (A) and 2-way ANOVA (B) (n=3, mean ± SD , *** $p < 0.001$, **** $p < 0.0001$) was performed. Adapted from [147].

G2/M arrest, another characteristic of EG5 gene blockade, was confirmed *via* flow cytometry (Figure 50B). An enhanced cell fraction in G2/M phase and a decreased

fraction of cells in G1 phase were observed only for cells treated with Mal-GE11 modified nanoparticles containing EG5 siRNA. Furthermore, the formation of mono-astral spindles typical for EG5 knockdown was shown for DAPI stained nuclei of cells (Figure 50C). Asters were predominantly found in cells treated with EG5 siRNA Mal-GE11 polyplexes, occasionally in EG5 siRNA Mal-PEG polyplex-treated cells, but never in control siRNA polyplex-treated cells.

3.5 Mesoporous silica nanoparticles for highly efficient siRNA delivery

This chapter has been adapted from:

Karin Möller, Katharina Müller, Hanna Engelke, Christoph Bräuchle, Ernst Wagner and Thomas Bein, "Highly efficient siRNA delivery from core–shell mesoporous silica nanoparticles with multifunctional polymer caps", Nanoscale, 2016, 8, 4007-4019.

A different approach for effective siRNA delivery is the use of mesoporous silica nanoparticles (MSNs). MSNs consist of solid inorganic materials with a stable matrix and a pore system (see chapter 1.5). MSNs are widely used for siRNA delivery, but as typical MSNs offer pore sizes of about 3 nm, siRNA is generally not loaded into the pores, but bound to the surface via PEI or other positively charged polymers [138, 193-195]. Very few studies are reported where MSNs were developed with larger pores for an internal loading of siRNA [141, 196, 197]. This approach is favorable, because siRNA is more protected from degradation and can be loaded in higher concentrations compared to only being attached to the surface. Accordingly, the development of silica nanoparticles with suitable pores for high siRNA loading and efficient delivery is presented in the following.

3.5.1 Design of MSNs

Large-pore mesoporous silica nanoparticles (LP-MSN) and medium-pore MSNs (MP-MSN) with different chemical compositions and physical properties are shown in Table 3. MSNs were synthesized and characterized by Dr. Karin Möller (Department of Chemistry, LMU Munich) as described in [148]. LP-MSNs consisted of either pure silica (LP-1) or their internal particle surfaces were further modified with different mol% of amino and/or phenyl groups in order to electrostatically interact with siRNA (LP-2 – LP-6). The small surface area of LP-2 to LP-4 (120-220 m^2g^{-1}) resulted from their large pore size and corresponding wall thickness. The pore size of LP-MSNs was around 10 nm.

Table 3. Sample composition and surface properties. Adapted from [148].

	Composition[a] (mol %)	Surface area (m^2g^{-1})	Pore size (cavity/pore) (nm)	Particle size (nm) (TEM)
LP-1	pure silica	220	11/7.4	70-170
LP-2	10.7% NH_2	120	8-12/9.9	
LP-3	3.5% Ph 8% NH_2	186	7-12/9.8	
LP-4	6.6% Ph 3.9% NH_2	123	6-13/9.6	
LP-5	1.1% Ph 1.4% NH_2	294	7-13/10	60-120
LP-6	4.6% Ph 0.5% NH_2	437	10/8	90-200
MP-1	8.5% NH_2 1.3% SH	670	4.7	150
MP-2	5.7% NH_2 1.2% SH	694	3.9	150
MP-3	3.3% NH_2 3.7% SH	937	4.0	150
MP-1-S-S	MP-1 with amino groups coupled to mercapto groups via disulfide bridges			

[a]Determined from elemental analysis

MP-MSNs were synthesized as core-shell particles equipped with a positively charged interior due to amino groups and a negatively charged outer shell coated with mercapto groups. The surface area decreased proportional to the increasing amount of internal amino groups and varied between 700 m^2g^{-1} and 900 m^2g^{-1}. MP-MSNs displayed pore sizes between 4 nm and 5 nm.

3.5.2 Biophysical characterization of MSNs

The size of LP-MSNs and MP-MSNs was determined by transmission electron microscopy (TEM) (Figure 51 and Table 3). LP-MSNs were between 60 nm to 200 nm in size. The size distribution was heterogeneous as different diameters were found for one sample. The images indicate that LP-MSNs displayed a bottleneck-type pore morphology where large cavities are connected via smaller pore-openings. In contrast, evenly-sized MP-MSNs of 150 nm were found in all cases. The pore morphology revealed an ordered stellate arrangement with conically widening pores.

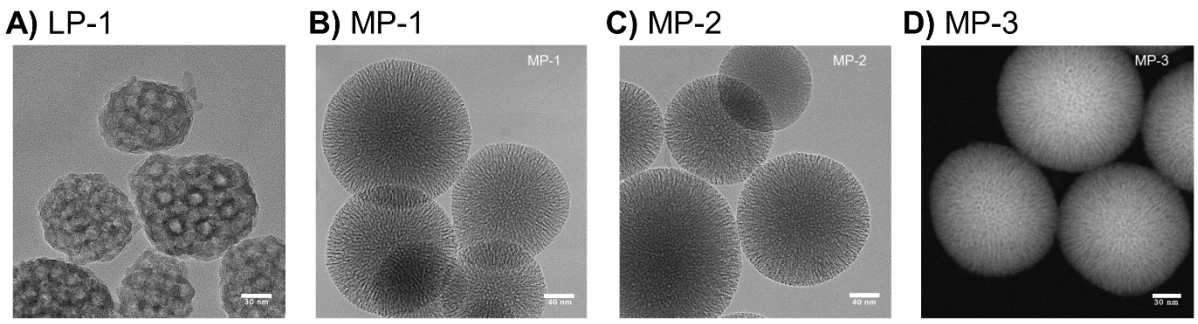

Figure 51. Transmission electron micrograph (TEM) images of A) LP-1, B) MP-1, C) MP-2 and D) MP-3. Scale bars represent 30 nm (A,D) and 40 nm (B,C). TEM was carried out by Steffen Schmidt (Department of Chemistry, LMU Munich). Adpated from [148].

The siRNA binding ability of LP-MSNs was determined in a gel shift assay (Figure 52). Increasing siRNA concentrations (2.5 µg, 6.6 µg or 12µg per mg MSN) were loaded into LP-2, 3 and 4. The gel electrophoresis showed very high siRNA binding for all samples, but also no siRNA release even after 1.5 h.

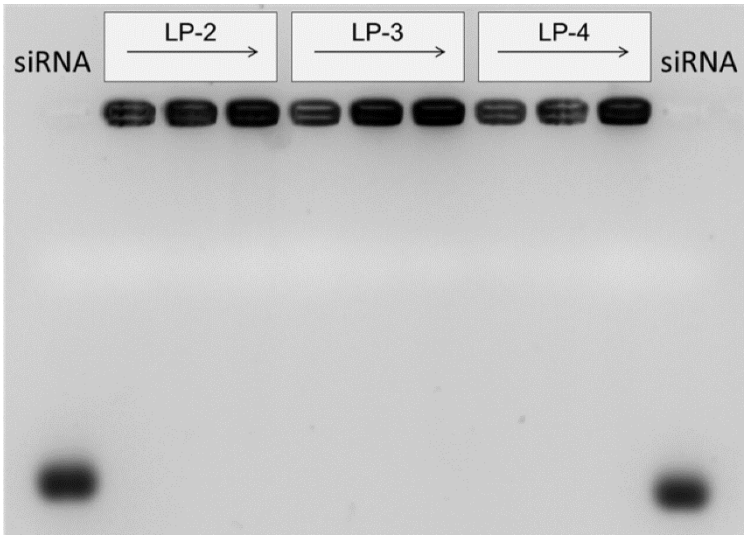

Figure 52. Gel electrophoresis with samples LP-2, LP-3 and LP-4 loaded with either 2.5, 6.6, or 12 µg siRNA per mg MSN (increasing concentration from left to right). Gel electrophoresis was run at 120 V for 1.5 h. Adapted from [148].

Figure 53 shows the siRNA adsorption and release capability of MP-MSNs. Different siRNA concentration were offered (red line) to MP-MSNs and the uptake was measured after 15 min (orange dots) and 1 h (green dots). MP-1 with a pore size of 4.7 nm showed fast uptake of siRNA up to a concentration of 40 µg/mg MSN within 15 min and up to 78

µg/mg MSN after 1h in aqueous solution (Figure 53A). At pH 5 an even higher siRNA uptake of 150 µg/mg MSN after 15 min, of 275 µg/mg MSN after 1 h and of 386 µg/mg MSN after 1 d (blue dot) could be observed (Figure 53B). The elution of siRNA, which is important for further *in vitro* experiments, was measured in PBS buffer (pH 7.4) after 15 min (light green stars) and 2 d (dark green stars). MP-1 released between 16 % and 40 % of the adsorbed siRNA within 15 min and up to 55 % after 2 days. MP-2 with smaller pores of 3.9 nm eluted a higher siRNA amount of 66 % and 75 % after 2 d (Figure 53C). To enhance the siRNA release of MP-1 amino groups were coupled to the mercapto groups *via* disulfide bridges (MP-1-S-S). MP-1-S-S showed a significant slower absorption of siRNA than MP-1 (5 h instead of 1 h for a complete absorption) probably because of a pore size reduction due to the long linker (Figure 53D). Nevertheless, the elution of siRNA was markedly faster with 43-49 % after 15 min and 76 % and 81 % (depending on the loading) after 1 day.

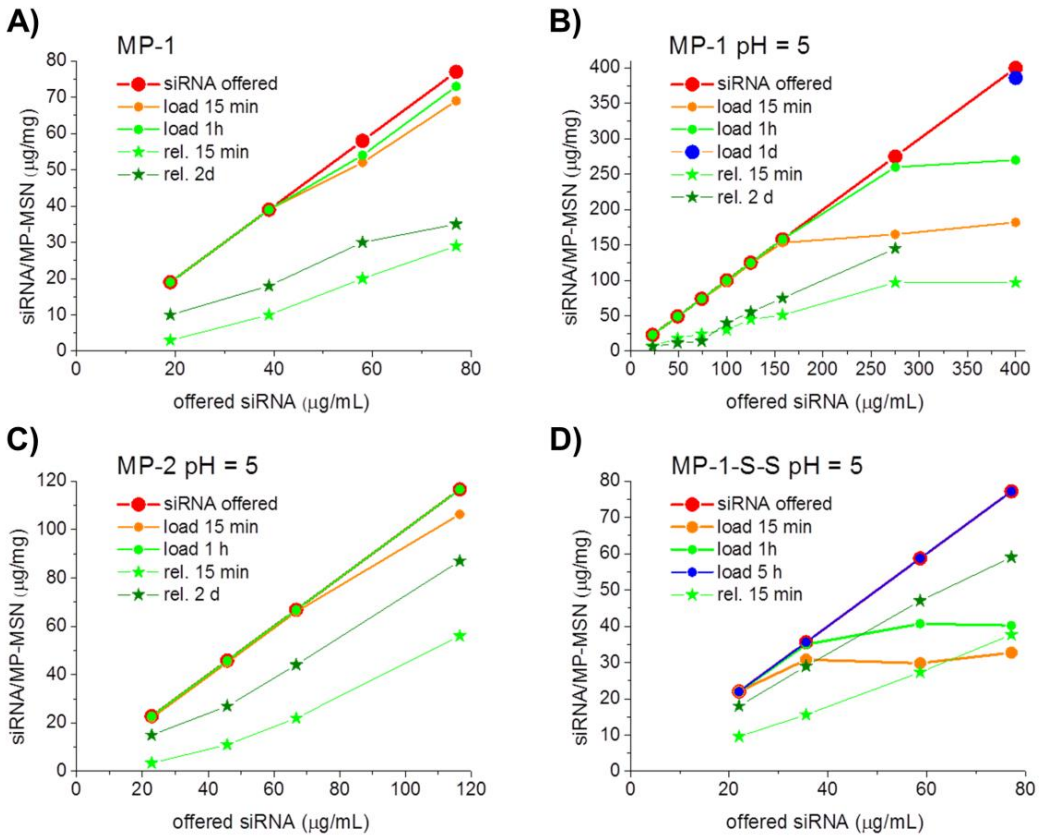

Figure 53. siRNA uptake and release with stellate MP-MSN. Aliquots of 100 µg of MSN were exposed to 100 µL of siRNA solutions with increasing concentrations. A) Uptake in MP-1 from water, and (B-D) uptake from MES buffer at pH = 5 into samples (B) MP-1, (C) MP-2, and (D) MP-1-S-S. Release experiments were performed in 100 µL PBS buffer at pH = 7.4 in all samples. The red curve indicates the offered siRNA amount, and orange and green dots indicate the adsorbed siRNA after 15 minutes and 1 h, respectively. Light green and dark green stars are the cumulatively released amounts of RNA after 15 min and 2 days, respectively. Measurements were carried out by Dr. Karin Möller (Department of Chemistry, LMU Munich). Adapted from [148].

In the following MSNs were combined with the sequence defined oligomer ***454*** (Figure 54), because MSNs alone showed no gene silencing ability in initial experiments (see below). As MSNs are not equipped with any endosomal escape domain, the four Stps and two oleic acids of ***454*** should contribute to endosomal membrane disruption. The interaction between ***454*** and MSNs might either be formed by disulfide-bridges from MSN-mercapto groups and cysteine units in ***454*** or resulted from electrostatic interactions.

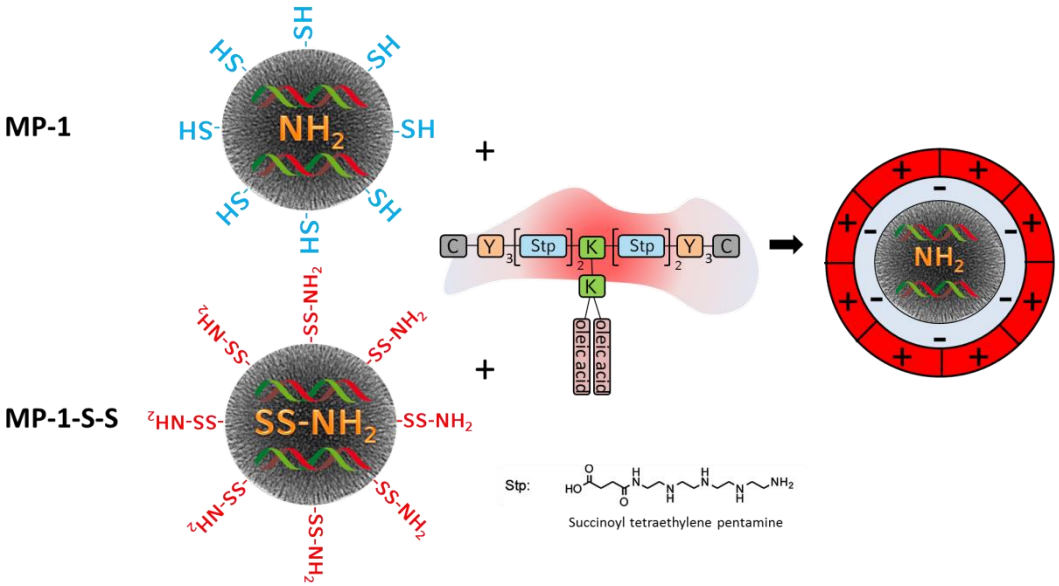

Figure 54. Combination of multifunctional core–shell nanoparticles with ***454***. Medium-pore MSN particles MP-1 are lined internally with amino groups and externally with mercapto groups. In sample MP-1-S-S all functional groups were transformed into disulfide-bridged amino groups. Particles are loaded with siRNA and capped with ***454*** that covers the final particles with a positively charged layer (chemical moieties depicted in this scheme are abbreviated for clarity; C: cysteine, Y: tyrosine, K: lysine). Adapted from [148].

Successful siRNA retention of MP-1-S-S capped with ***454*** is shown in Figure 55. Loaded MSNs (5 wt% siRNA) were combined with different amounts of the oligomer. All samples retained high siRNA contents with some minor siRNA release that decreased with increasing oligomer amount. Importantly, the supernatants of the MES loading solution (MSN-SN) and the first PBS buffer wash solution (PBS-SN) contained only negligible amounts of siRNA showing that ***454*** did not form polyplexes with released siRNA from MSNs.

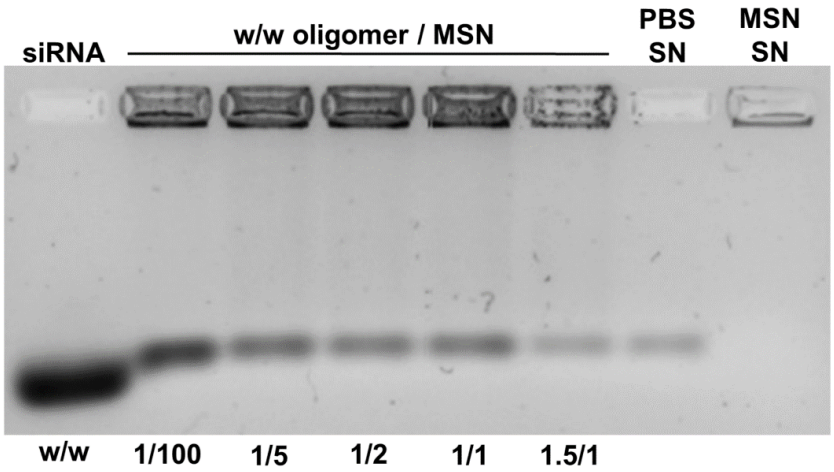

Figure 55. Gel electrophoresis of sample MP-1-S-S (5 wt% siRNA loading in the MSN) with an increasing amount of oligomer ranging from 1/100 up to 1.5/1 w/w polymer to particle. The first and the second supernatant solutions (SN) after sample preparation are included. Adapted from [148].

3.5.3 Gene silencing of MSNs

For gene silencing experiments MSNs were loaded with eGFP siRNA or ctrl siRNA and transfected in KB/eGFPLuc cells. MP-1-S-S without ***454*** capping showed no gene silencing at all, when loaded with 5 wt% eGFP siRNA (Figure 56A, no oligomer). With increasing amounts of oligomer remarkably high transfection efficiency from 60 % up to 90 % could be observed. The supernatants PBS SN and MES SN did not transfect showing that all three components (MSN, ***454*** and siRNA) are needed for a successful delivery system. For further experiments a w/w of 1/2 was chosen as higher oligomer concentrations did not display significant higher gene silencing. MP-MSNs are able to load high siRNA amounts (Figure 53). Therefore, MP-1 coated with ***454*** (w/w 1/2) and increasing siRNA cargos from 5 wt% up to 20 wt% were prepared (Figure 56B). Thus, particle concentration on cells could be reduced while the siRNA amount was kept at 0.5 µg per well. The transfection efficiency was still high in all cases, therefore particle concentration and consequently the siRNA amount per well was further reduced (Figure 56C) from 0.5 µg with the highest load sample (20 wt%) to 0.063 µg siRNA per well. As gene silencing efficiency decreased with decreasing siRNA amounts 0.5 µg siRNA per well turned out to be the optimal concentration for further experiments.

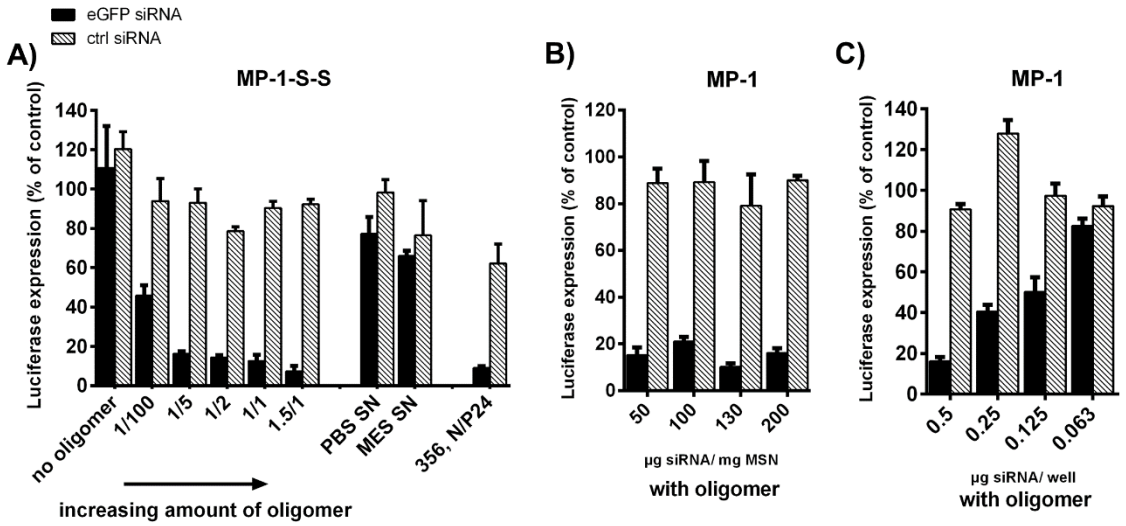

Figure 56. Gene silencing of MSNs. A) MP-1-S-S (5 wt% siRNA loading in the MSN) with an increasing amount of oligomer ranging from 1/100 up to 1.5/1 w/w ***454*** polymer to particle. The first and the second supernatant solutions (SN) after sample preparation are included. B) MP-1 coated with ***454*** (w/w 1/2) with increasing siRNA loadings of 5 wt%, 10 wt%, 13 wt% and 20 wt% siRNA, while keeping the total amount of siRNA at 0.5 µg per well. C) MP-1 coated with ***454*** (w/w 1/2) with decreasing siRNA concentrations/ well. MSNs were loaded with eGFP siRNA or ctrl siRNA and incubated on KB/eGFPLuc cells for 4h (A) or 45 min (B,C) (n=3, mean ± SD). Oligomer ***356***, applied with 200 ng of INF7 peptide-conjugated (eGFP or ctrl) siRNAs serves as positive control [57]. Adapted from [148].

The influence of different pores of MSN on transfection efficiency was examined in Figure 57. The medium-pore MSNs MP-1 with a pore size of 4.7 nm and MP-2 with a pore size of 3.9 nm were compared to the large-pore MSN LP-2 with pore sizes of 10 nm. As seen before, MP-MSNs did not transfect without oligomer ***454*** (Figure 57A,B). MP-1 and MP-2 displayed the same high transfection efficiency with ***454*** (w/w 1/2) regardeless of the siRNA loading. Thus, the minimal pore size difference did not influence the transfection efficiency. On the other hand, knockdown efficiency of LP-2 was only 60 % with 5 wt% siRNA decreasing with a higher siRNA load (8.8 wt%) (Figure 57C). This shows that not only pore size, but also particle morphology and charge density plays a role on transfection efficiency as LP-2 has a smaller surface area and thus high areal amino-group densities.

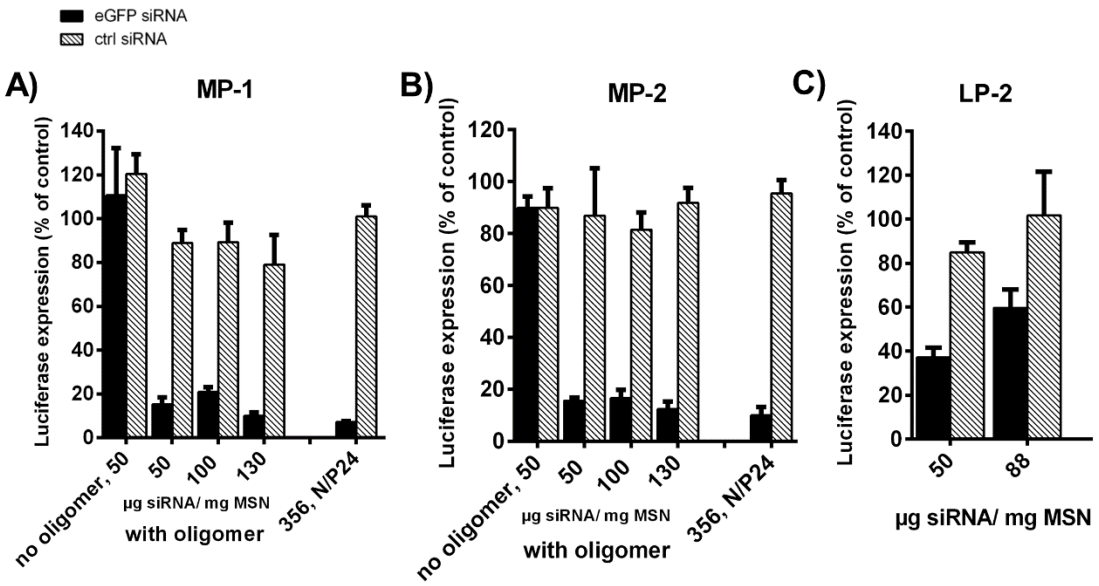

Figure 57. Gene silencing of MSNs. A) MP-1 coated with ***454*** (w/w 1/2) and B) MP-2 coated with ***454*** (w/w 1/2) with increasing siRNA loadings of 5 wt%, 10 wt% and 13 wt% and 20 wt% siRNA. C) LP-2 coated with ***454*** (w/w 1/2) with 5 wt% and 8.8 wt% siRNA load. MSNs were loaded with eGFP siRNA or ctrl siRNA and incubated on KB/eGFPLuc cells for 45 min (n=3, mean ± SD). Oligomer ***356***, applied with 200 ng of INF7 peptide-conjugated (eGFP or ctrl) siRNA, serves as positive control [57]. Adapted from [148].

MP-1-S-S and MP-1 were additionally capped with the standard cationic lipid DOTAP instead of ***454*** to examine the importance of the sequence-defined oligomer (Figure 58)***.***

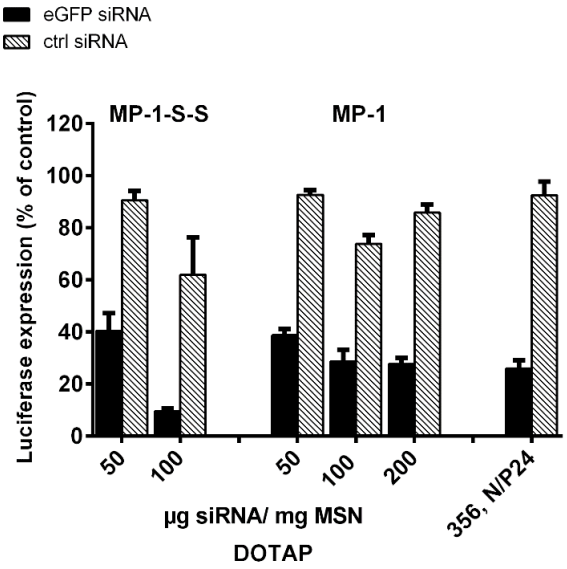

Figure 58. Gene silencing of MSNs. MP-1-S-S and MP-1 capped with DOTAP with increasing siRNA loadings of 5 wt%, 10 wt% and 20 wt% siRNA, while keeping the total amount of siRNA at 0.5 µg per well. MSNs were loaded with eGFP siRNA or ctrl siRNA and incubated on KB/eGFPLuc cells for 4 h (n=3, mean ± SD). Oligomer 356, applied with 200 ng of INF7 peptide-conjugated (eGFP or ctrl) siRNAs, serves as positive control [57]. Adapted from [148].

Figure 58 showes high gene silencing of these particles with different siRNA loadings, that was nevertheless not as high as with ***454*** (Figure 56A,B). The cell viability of MP-1 was examined in Figure 59. MSN concentrations from 0.1 to 0.2 µg per mL for uncapped samples and from 0.025 to 0.2 mg per mL capped with ***454*** were incubated on KB/eGFPLuc cells for 45 min or 4 h. All samples did not influence the cell viability showing the excellent biocompatibility of MSNs.

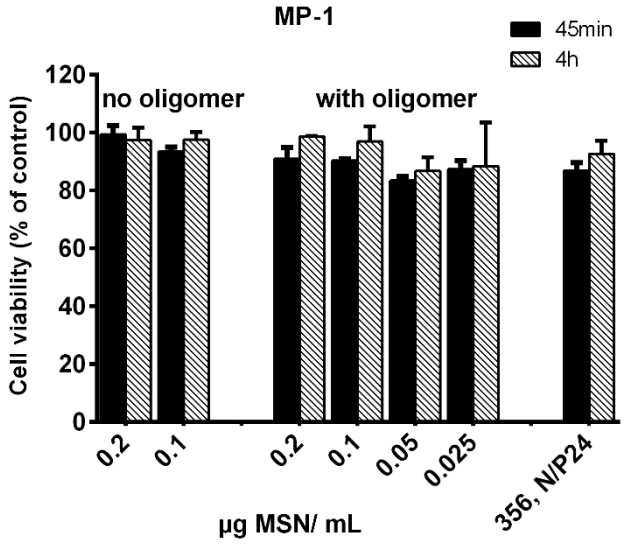

Figure 59. Cell viability of MP-1 with and without ***454*** (w/w 1/2) capping loaded with 5 wt% siRNA. KB/eGFPLuc cells were incubated with different MSN concentrations for 45 min or 4 h (n=3, mean ± SD). Adapted from [148].

4 Discussion

4.1 Integration of twin disulfides into sequence-defined oligomers for stabilization of siRNA polyplexes

For efficient siRNA delivery *in vivo* several obstacles have to be overcome. One critical issue is the stability of polyplexes [146, 198, 199]. As siRNA consists of only 21 bp compared to other nucleic acids, for example pDNA with about 6000 bp, less interelectrolytic interactions with the positive backbone of oligomers take place during polyplex formation [72]. Therefore stability is more critical for siRNA polyplexes than for polyplexes formed with pDNA. Several stability domains like fatty acids and tyrosine trimers for hydrophobic interactions and terminal cysteine residues for disulfide bridge formation have been integrated into oligomers before [57, 73, 150]. A new motif, the CRC motif, was integrated into sequence defined oligomers by Philipp Klein (PhD student, Pharmaceutical Biotechnology, LMU Munich) and examined for its suitability in stabilizing siRNA polyplexes. In the current thesis, these CRC containing siRNA polyplexes were evaluated in uptake and gene silencing experiments. As CRC forms twin disulfides [151] and can be easily inserted into oligomers via SPS it offers good opportunities for an optimal stability motif. The replacement of terminal cysteines of a 3-arm oligomer by one, two or three CRC motifs led to significant smaller particles. At the same time, the PDI decreased indicating a better compaction and homogenous particle formation of CRC-polyplexes. Additionally, the zeta potential increased with the insertion of CRC showing a higher positive surface charge of particles. These results demonstrated the positive effects of the CRC motif on particle formation. For PEGylated structures with and without FolA-ligand the size increased a little bit with the insertion of CRC, but more significant was the tendency towards big particles when FolA was present. Agglomeration effects of FolA due to its hydrophobicity have also been observed in other studies [146, 163]. Additionally, the zeta potential of PEGylated particles was examined. The surface charge of targeted oligomers is very important as unspecific interactions with cell membranes should be avoided [115]. PEGylated oligomers revealed a zeta potential of about 0 mV in all cases showing excellent shielding. Gel shift assays demonstrated that the insertion of CRC did not change the siRNA binding of 3-arm oligomers. In contrary, a better siRNA binding ability could be observed for PEGylated CRC-polyplexes compared to polyplexes formed with oligomers containing only one terminal cysteine. PEG is known to reduce the binding and

compaction ability of ethylenimine motifs in polyplexes [67, 86, 145]. Thus, the insertion of CRC seemed to improve the biophysical properties of PEGylated oligomers as better siRNA retention in gel shift assays indicated a higher stability of polyplexes. This higher stability could also be observed in the presence of serum and under reducing conditions for PEGylated CRC oligomers. The targeting effect of PEGylated polyplexes became obvious in fluorescence microscopy. Here, particles could only be found in FR overexpressing KB/eGFPLuc cells when they were equipped with FolA. This result could be confirmed in flow cytometry. Additionally, the influence of the CRC motif on size of non-PEGylated 3-arm oligomers could be verified in microscopy as big particles were found for 3-arm oligomers, whereas the insertion of three CRC motifs led to small and equal distributed particles. Unfortunately, the gene silencing ability of these 3-arm CRC oligomers was abolished. Here, the size reduction probably had a negative impact as larger particles are more efficient in cell culture transfections due to the promotion of endosomal escape [146, 200]. The lack of endosomal escape could also be observed for PEGylated oligomers as INF7 modified siRNA was needed for efficient gene silencing. Nevertheless, FolA-PEG containing particles with CRC motif showed high and receptor specific gene silencing with INF7 modified siRNA surpassing the transfection efficiency of oligomers with only one terminal cysteine. To sum it up, the insertion of twin disulfides improved the stability of polyplexes, but did not led to more efficient siRNA delivery in general. Non-PEGylated 3-arm oligomers displayed smaller and more defined particles, but lost transfection efficiency with the insertion of the CRC motif. On the other hand, PEGylated CRC-oligomers benefited from the CRC motif. They showed better siRNA binding ability and stability and led to efficient and ligand dependent gene silencing in comparison to PEGylated oligomers with only terminal cysteines.

4.2 Folate-PEG-oligomer conjugates for targeted siRNA delivery

Besides stability, another requirement for sufficient siRNA delivery is the direction of nanoparticles to their site of action without affecting non-target cells. Targeting ligands are widely used for this purpose. The folate receptor (FR) is a favourable tumor target receptor because of its overexpression in many tumor tissues [87, 88, 201]. Folic acid (FolA) has been proven to be a potent ligand for directing drugs to cancer cells [89, 94, 202]. Not surprisingly, targeted siRNA formulations have already been reported by either direct conjugation of FolA with siRNA constructs [203-206] or incorporating FolA as

ligand into lipid [98, 207, 208] or polymer-based formulations [57, 103, 209, 210]. To meet the requirements of a successful targeted delivery system, a library of 42 multifunctional sequence-defined oligomers was created by Dr. Dongsheng He (PhD thesis 2016, LMU Munich) following a combinatorial strategy. To shield the positive charge of the polyplexes leading to unspecific interactions with negatively charged cell membranes 24 PEG units were inserted. Cationic 2- or 4-arm oligomers with Stp or Sph for siRNA binding and endosomal buffering were examined based on the lead structure ***356*** [57]. Additionally, histidines for endosomal buffering, terminal cysteines for stabilization by disulfide crosslinking and tyrosine trimers for hydrophobic stabilization were integrated into oligomers in different combinations. The effect of these functional domains on siRNA binding and complexation was examined in gel shifts and ethidium bromide assays. As expected the larger cationic backbone of 4-arm oligomers led to a better siRNA compaction compared to 2-arm oligomers. Surprisingly, tyrosine trimers reduced siRNA binding and compaction which is contradictory to studies with non-PEGylated siRNA lipoplexes, in which the insertion of tyrosine trimers enhanced the stability of polyplexes [73]. A reason for this result could be the PEGylation of the targeted oligomers. PEG counteracts the hydrophobic interactions of tyrosines as it increases solubility. The best siRNA compaction could be achieved with 2-arm and 4-arm oligomers containing terminal cysteines but no further modification. This result indicated that the right charge density of the cationic backbone is an indispensible requirement. For gene silencing experiments in the current thesis, polyplexes were transfected on FR overexpressing KB/eGFPLuc cells with siRNA against eGFP with and without the endosomolytic INF7 peptide conjugated to siRNA. In general, the use of INF7-siRNA led to better transfection efficiency due to the enhanced endosomal escape. Oligomers containing four arms or an enlarged number of cationic building blocks led to increased transfection efficiency because of their better siRNA binding and complexation. In contrary, the modification of oligomers with either tyrosine trimers or histidines reduced their gene silencing ability for both 2-arm and 4-arm oligomers. This can be explained with the low siRNA compaction of these oligomers. The integration of both tyrosine trimers and histidines into 2-arm oligomers, led to highly efficient gene silencing even without INF7 and at low N/P ratios, identifying this combination as the most effective. Four-arm oligomers with the same modification showed high knockdown as well, but additionally revealed toxic effects. Unfortunately, most oligomers did not transfect in a receptor-specific mode. Significant targeting effects could only be observed for #10, #12, #14 (2-arm-Y3) and #30 (4-arm-H), which could be partly verified in flow cytometry measurements. To provide a clearer overview, siRNA transfection properties of oligomers were summarized in Table 4.

Table 4. Summary of siRNA transfection properties[a]

No.	gene silencing	INF7 dependency	receptor specificity	toxicity
356	++	++	++	-
#2	+	++	-	-
#4	++	++	-	-
#6	+	++	-	-
#8	+	++	-	-
#10	+	-	++	+
#12	+	-	++	-
#14	++	++	++	-
#16	+ (20)	+	+ (20)	-
#18	++	-	+	-
#20	++	-	+	+
#22	++	++	+	-
#24	++	++	+	-
#26	+	++	+	-
#28	++	++	-	-
#30	++	++	++	-
#32	+	++	-	-
#34	+	++	-	-
#36	-	-	-	-
#38	-	-	-	-
#40	++	-	+	+
#42	++	+	+	+

[a]N/P ratio of 12 was used, unless defined differently (in brackets).

Gene silencing (INF7-eGFP siRNA sequence specific reduction of marker gene expression):

-, 0−20%; +, 20−60%; ++, 60−100%.

Dependency on INF7: ++, transfection only with INF7 siRNA; +, more effective with INF7 siRNA; −, as effective with siRNA as with INF7 siRNA.

Receptor specificity: −, no specificity; + moderate specificity (negative ligand control shows lower activity);

++, specific (only FolA ligand shows transfection activity).

Toxicity (metabolic cell activity): +, metabolic activity ≤80%; −, metabolic cell activity >80%.

Adapted from [67].

In contrary to the here presented siRNA polyplexes, experiments with pDNA polyplexes (performed by Dr. Petra Kos and Ana Krhac Levacic, Pharmaceutical Biotechnology, LMU Munich) revealed higher nucleic acid compaction and stability [67]. As mentioned before, an enhanced interaction of the negatively charged pDNA and the positively charged cationic backbone of oligomers takes place as pDNA is around 300 times larger than siRNA [72]. The pDNA transfection efficiency was enhanced with an increased number of oligomer arms and cationic building blocks comparable with siRNA transfections. Furthermore, the insertion of tyrosine trimers and histidines into 2-arm oligomers turned out to be the best combination with the highest transfection efficiency consistent with siRNA transfections. These similarities were unexpected as pDNA and

siRNA carriers have to meet different prerequisites, such as nuclear versus cytosolic site of action. Thus, the common early steps including stability, endocytosis and endosomal release possibly contributed to the same preference of functional domains. Nevertheless, pDNA polyplexes displayed enhanced receptor specificity compared to siRNA polyplexes in general probably due to the higher stability. In conclusion, the screen of 42 FolA-PEG containing oligomers with different additional moieties offered valuable insights into structure-activity relations and revealed oligomers with suitable biophysical properties and high transfection efficiency.

4.3 Native chemical ligation for the equipment of siRNA polyplexes with shielding and folic acid targeting

Native chemical ligation (NCL) has been widely used for the synthesis of large peptides, and even total proteins [152-154]. With this method six sequence-defined oligomers from our library could be easily equipped with shielding domains and the targeting ligand FolA in order to examine structure-activity relationships and to find an optimal carrier without the need of a completely new synthesis. As mentioned before, shielding and targeting is important for sufficient *in vivo* delivery. Oligomers consisting of 2-arms with central or peripheral tyrosine trimers, 3-arms with or without tyrosine trimers and 4-arms with histidines were selected. The oligomers were modified *via* NCL by Dr. Can Yang Zhang (visiting PhD student at LMU Munich in 2013) with an alanine-PEG_{24} or FolA-PEG_{24} reagent to determine the targeting effect. As seen before the siRNA binding ability was strongly improved with the number of cationic arms. PEGylated 2-arm oligomers showed almost no siRNA retention, whereas the siRNA binding increased with 3-arm and 4-arm oligomers. In contrary to chapter 3.2 the insertion of tyrosine trimers into 3-arm oligomers improved the siRNA retention and consequently polyplex stability. The shown benefit of tyrosine trimers is more consistent with previous studies [73]. Probably, the insertion of stability motifs into siRNA polyplexes might lead to different effects depending on the oligomer topology. In chapter 3.2, 2-arm and 4-arm oligomers did not profit from tyrosine trimers, whereas the here presented 3-arm oligomers and T-shaped oligomers in [73] revealed better biophysical properties. Additionally, PEGylated 3-arm oligomers with tyrosine trimers displayed the best particle sizes (<600 nm) whereas all other oligomers formed aggregates with siRNA. The zeta potential was significantly reduced after the NCL reaction showing the successful introduction of shielding reagents. For efficient

gene silencing INF7 modified siRNA had to be used to enhance the endosomal escape for PEGylated oligomers consistent with previous chapters. In case of 2-arm oligomers almost no gene silencing was observed, which can be explained with the insufficient siRNA binding. Interestingly, peripheral tyrosine trimers improved the transfection efficiency in comparison to central tyrosine trimers in 2-arm oligomers. The enhanced transfection efficiency of 3-arm oligomers especially with Sph compared to 2-arm oligomers can be explained with their improved siRNA binding and higher charge density. Surprisingly, 4-arm oligomers only showed moderate gene silencing. Receptor-dependent transfection efficiency of FolA-PEG oligomers compared to their analogous without targeting ligands could be demonstrated with 3-arm/Stp (***666***), 3-arm/Y3 (***668***) and (very slightly) 4-arm/His (***670***). For all other topologies no targeting effect could be found. The transfection efficiency of alanine-PEG oligomers can be attributed to their large sizes, which led to unspecific cellular uptake and gene silencing. In flow cytometry experiments the enhanced uptake of FolA-targeted ***666, 668*** and ***670*** was confirmed. In this study, stability as a prerequisite for a successful siRNA delivery vehicle became obvious again as the insertion of tyrosine trimers and an increased number of positive charges led to more efficient siRNA binding and particle formation. Repeatedly, a higher stability and compaction could be observed with pDNA due to its larger size (experiments performed by Dr. Petra Kos, Pharmaceutical Biotechnology, LMU Munich). All NCL conjugates demonstrated efficient pDNA binding in agarose gel shifts and formed small particles of about 100 nm and 300 nm [145]. In *in vitro* experiments with pDNA, oligomers showed high transfection efficiency and receptor specificity. In contrary to siRNA transfections, the histidinylated 4-arm oligomer was the most effective one. To find out such structure-activity relationships, NCL as a tool to convert untargeted already existing oligomers from our library (>1000 oligomers) into FolA-targeted and PEGylated oligomers turned out to be an easy and effective method making the screen for an ideal *in vivo* delivery vehicle less cost- and time-consuming.

4.4 Post-PEGylation of siRNA lipo-oligoamino amide polyplexes for receptor specific siRNA and miRNA delivery

For tumor-targeted delivery of siRNA *in vivo* the size of nanoparticles plays an important role as well. Nanoparticles with a size below 5.5 nm are rapidly cleared by the urinary tract and eliminated from the body [211], whereas agglomerates block fine capillaries

[212]. In the current thesis, a post-PEGylation strategy was applied to provide well sized siRNA polyplexes with targeting ligands and PEG shielding. This method has been successfully used for pDNA/PEI polyplexes before [156-158]. Here, core nanoparticles were formed with siRNA or miRNA and sequence-defined cationic lipo-oligomers, which were further modified with PEG and targeting ligands. Two t-shaped lipo-oligomers, ***454*** [73] and ***595*** [144], were chosen as they contain stabilizing tyrosine trimers and cysteine residues, formed siRNA polyplexes of 120 nm to 150 nm and have proven their gene silencing ability in previous studies. These core nanoparticles were surface shielded by reaction of cysteines not involved in disulfide cross-linkages with maleimido-PEG reagents, optionally containing the targeting ligands FolA, gE4-FolA or GE11.

4.4.1 Post-PEGylation using tetra-glutamylated folic acid as ligand for receptor-targeted delivery

This chapter has been adapted from:

Katharina Müller, Eva Kessel, Philipp M. Klein, Miriam Höhn and Ernst Wagner "Post-PEGylation of siRNA lipo-oligoamino amide polyplexes using tetra-glutamylated folic acid as ligand for receptor-targeted delivery", Molecular Pharmaceutics, 2016, 13(7):2332-45.

In the first post-PEGylation study, ***454*** and ***595*** polyplexes were modified with reagents consisting of maleimide, 28 PEG units and the targeting ligands FolA or tetra-γ-glutamyl folic acid (gE4-FolA) in increasing molar equivalents. The feasibility of the post-PEGylation concept was shown by an Ellman's assay monitoring the reaction of PEG-maleimide with the cysteines of lipo-oligomers and by a decrease in zeta potential of polyplexes. Unexpectedly, FolA-PEG surface-modified polyplexes agglomerated, probably due to the hydrophobicity of folic acid [163], resulting in ligand-independent gene silencing. This problem was not observed in ligand-free PEGylation and was overcome by the use of gE4-FolA as targeting ligand. This modification can be considered as a biomimetic step, as polyglutamylation of folate by folyl-polyglutamate synthetase takes place in most organisms to increase its cellular retention and binding to DHFR enzyme [159, 213, 214]. Post-PEGylated gE4-FolA siRNA polyplexes displayed biophysical advantages, with sizes between 100 and 200 nm favourable for *in vivo* application, a receptor-specific uptake and effective gene silencing for a broad range of formulations. An additional advantage of the polyglutamylation might be the negative

surface charge of resulting particles (around −20 mV). The negative zeta potential prevents interactions with negatively charged serum proteins like albumin or negatively charged molecules such as HSPG on cell surfaces [215-217], and therefore might reduce adverse effects [218]. Receptor-mediated and effective gene silencing of gE4-FolA PEGylated polyplexes was shown on human cervical carcinoma KB cells overexpressing the FR. A high knockdown efficiency could be obtained demonstrating the potency of the siRNA delivery system. Within an optimal degree of PEGylation, no reduced efficacy was found. Therefore, additional strategies, like the coupling of INF7 to siRNA, to enhance the endosomal escape, as observed for other related polyplex systems and in the chapters before, were not needed [57, 78, 219-221]. The FR specificity of transfections was proven via receptor blockade using folate saturated medium; 100−200 nm small siRNA particles containing the polyglutamylated FolA ligand lost their gene silencing ability upon FR blockade, whereas undefined agglomerates resulting from core polyplex modification with PEG-FolA still transfected KB cells in a receptor-independent manner. Flow cytometry measurements additionally proved the receptor specific uptake of siRNA polyplexes shielded with PEG-gE4-FolA. gE4-FolA PEGylated polyplexes were used to examine the biodistribution in mice after systemic circulation. These studies revealed destabilization of polyplexes by PEGylation as a critical factor limiting their in vivo application. A PEGylation of 3 mol eq led to immediate instability for ***454*** and ***595*** polyplexes *in vivo*, with most siRNA cleared via kidney and bladder already after 15 min. This problem was partially overcome by selecting the ***595*** oligomer (containing two CRC stability motifs) [144] for polyplex core formation and an optimized lower degree of 1.5 eq of gE4-FolA PEGylation reagent. For this formulation persistence in mice up to 8 h as visualized by NIR fluorescence bioimaging could be seen, with a preferential accumulation in liver as typical for nanoparticles [222]. In previous *in vivo* biodistribution studies in mice, FR targeting ***356*** polyplexes circulated for only 15 min and were then cleared rapidly by the kidney due to their small size of only 5.8 nm [57]. Here, ***454*** and ***595*** polyplexes with a size of about 200 nm were far less affected by renal clearance. In contrast to ***356***, a signal could be detected after 8 h in the liver and lung for ***454***, which was even higher for ***595***. Even PEGylated ***454*** polyplexes having a lower stability than ***595*** revealed persistence in mice after 8 h in lung, liver, and spleen. These results demonstrate the importance of sizes of nanoparticles for a successful *in vivo* biodistribution and arrival at their site of action. After 8 h mice were sacrificed to analyze the siRNA distribution of ***595*** formulations in organs. The lung accumulation noticed for the non-PEGylated particles was significantly reduced with PEGylation, especially for gE4-FolA polyplexes. Positively charged and lipid particles are

likely to be taken up by endothelial cells in the lung [223]. This might have been avoided with the negatively charged gE4-FolA particles. With the current formulations, only a moderate transient delivery into the tumor of mice was demonstrated. This is not surprising at all, when considering the low systemic polyplex stability. The destabilization of siRNA polyplexes by PEGylation is consistent with the findings using pre-PEGylated oligomers (chapter 3.2).

4.4.2 Post-PEGylation using the peptide ligand GE11 for EGF receptor targeted siRNA and miRNA delivery

This chapter has been adapted from:

Katharina Müller, Philipp M. Klein, Philipp Heissig, Andreas Roidl and Ernst Wagner, "EGF receptor targeted lipo-oligocation polyplexes for antitumoral siRNA and miRNA delivery", Nanotechnology, 2016, 27(46):464001.

The post-PEGylation principle can be easily transferred to other ligands. The epidermal growth factor receptor (EGFR), a receptor tyrosine kinase, was chosen for the second study, as it is a favourable therapeutic target in cancer therapy [107]. EGFR is upregulated in several solid tumors which is correlated with poor cancer prognosis [108]. The peptidic ligand GE11 has proven acceptable binding ability to the EGFR, efficiency to deliver nanoparticles and, as compared with the natural ligand EGF, no mitotic activity [104, 113, 114, 224, 225]. Thus, GE11 was attached to ***454*** polyplexes with different molar ratios using the post-PEGylation principle. Resulting particles showed characteristics which would be favourable for *in vivo* application, such as polyplex sizes around 120 nm - 155 nm, a reduction in zeta potential from +40 mV without PEGylation, +15 mV with Mal-GE11, to +8 mV with Mal-PEG polyplexes, and a stable siRNA binding with Mal-GE11 particles even upon incubation in full (90%) fetal bovine serum for 24 h.
Receptor-mediated enhanced uptake of GE11-PEGylated siRNA polyplexes could be demonstrated *via* flow cytometry in three different EGFR-positive cancer cell lines: T24 bladder carcinoma, MDA-MB 231 breast cancer, and Huh7 liver cancer. This beneficial cellular uptake of siRNA translated into effective gene silencing by GE11-PEG modified nanoparticles, whereas non-PEGylated or PEGylated particles without targeting ligand had no sufficient gene silencing effect. Mal-GE11 ***454*** polyplexes were not dependent on moieties enhancing the endosomal escape like INF7, which is often diminished for

PEGylated nanoparticles [57, 78, 221, 226]. In the next steps GE11-PEG ***454*** polyplexes were applied for antitumoral delivery of the tumor suppressive microRNA miR-200c or a therapeutic siRNA against EG5. miR-200c [165] is known to revert epithelial to mesenchymal transition by targeting ZEB1 [169] which also leads to less proliferative and migrating cells and to suppress chemoresistance towards doxorubicin by targeting TrkB and Bmi1 [170]. miRNA-200c additionally targets the proto-oncogene KRAS, which regulates cell differentiation, proliferation and survival [171]. Consistently, results with GE11 nanoparticles formulated with miR-200c mimics demonstrated downregulation of ZEB 1 *via* RT-qPCR, both in T24 and MDA-MB 231 cells, less proliferation, enhanced sensitivity of these cells against doxorubicin, and a change in cell cycle. In addition, inhibition of MDA-MB 231 tumor cell migration was observed for the EGFR-targeted miR-200c mimic formulation but not the non-targeted formulation or the control RNA formulation. Additionally, PEGylated formulations with EG5 siRNA were examined. EG5 (Eglin-5, also known as Kinesin-5, KSP, or KIF11) belongs to the kinesin motor proteins; its main role is to separate anti-parallel microtubules from each other [227]. As malfunction in chromosome segregation is strongly related with the development of cancer, EG5 is a favorable gene to target for tumor therapy [228-230]. Efficient EG5 knockdown by GE11-PEG ***454*** siRNA polyplexes could be verified by RT-qPCR. EG5 knockdown resulted in cell cycle arrest in G2/M, also documented by the formation of mono-astral spindles, and tumor cell killing. Interestingly, several assays indicated that GE11 polyplexes may exert antiproliferative effects in an RNAi-independent manner. For example, a slightly decreased growth or migration of cells was observed after treatment with GE11 polyplexes containing ctrl RNA. It is known that GE11 polyplexes do not activate EGFR; in the contrary, natural EGFR signalling is inactivated through rapid endocytosis of polyplex–bound EGFR [104, 106, 107, 113], which may explain the additional antitumoral effects of the GE11 polyplexes. For these reasons, the GE11 peptide ligand appears as very useful to target therapeutic RNAs to cancer cells.

4.5 Mesoporous silica nanoparticles for highly efficient siRNA delivery

Mesoporous silica nanoparticles (MSNs) have proven their efficiency as delivery systems for siRNA in many studies. However, siRNA was mainly attached on the outer surface of MSNs *via* PEI, which enhances its biodegradability and reduces the loading capacity

[138-140, 194, 196, 231, 232]. Constant development of MSN synthesis allows control and design of size (particles and pores), morphology, and pore structure [133]. Here, MSNs with different chemical compositions, inner and outer surfaces, pore sizes (large-pore MSNs (LP-MSN) and medium-pore MSNs (MP-MSN)) and particle sizes were synthesized by Dr. Karin Möller (group of Prof. Thomas Bein, Department of Chemistry, LMU Munich) for efficient siRNA loading and delivery. MP-MSNs consisted of selectively modified inner and outer surfaces, which is important for siRNA loading. TEM images revealed particle sizes of 60 nm to 200 nm and different pore morphologies for LP-MSNs (bottleneck morphology) and MP-MSN (stellate morphology). For sufficient loading of negatively charged siRNA surfaces of MSNs were decorated with amino groups (>1 mol%) that are positively charged at neutral pH. Gel electrophoresis showed high siRNA retention of LP-MSNs, but no siRNA release even after 1.5 h. Similar problems regarding nucleic acid release of LP-MSNs have been reported before [233-235]. Indeed, not only uptake, but also elution of siRNA in cellular environment is an important requirement for a delivery system. Efficient siRNA loading and release could be obtained with MP-MSNs. A minimum pore size of 5 nm had been supposed for efficient siRNA uptake in previous studies [233], but here, MP-2 MSNs with a pore size of only 3.9 nm were able to load very high siRNA amounts of at least 120 µg/mL. In general, the amount of siRNA uptaken into these MP-MSNs was the highest reported so far. Nevertheless, the siRNA uptake of MP-2 was slower compared to MP-1 probably due to a closer contact of siRNA with the pore surfaces because of the smaller pore size (3.9 nm vs. 4.7 nm), which reduces the progressive absorption. This observation is also confirmed when the velocity of siRNA loading of MP-1-S-S is compared to MP-1. Thus, not only pore size, but also pore morphology has to be considered regarding the siRNA release in particular. The bottleneck-like pores with smaller openings than pore diameters of LP-MSN prevented an efficient siRNA release. Additionally, a high concentration of protonated amino groups on the inner surface of MSNs facilitated the siRNA loading process. To sum it up, medium-pore sized MSN with stellate morphology and a high internal surface of amino groups turned out to be optimal for very high siRNA absorption up to 380 µg/mg and efficient siRNA desorption. For gene silencing experiments, MSNs were capped with the sequence-defined oligomer ***454***. ***454*** not only offers endosomal escape domains (Stp and oleic acid) that MSNs lack, but also free cysteines that can be used to couple functionalities such as targeting ligands for further experiments. Gel electrophoresis revealed sufficient siRNA retention of MP-1-S-S after coating with different amounts of ***454***. Gene silencing better than 80 % could be shown with different siRNA and particle concentrations with MP-1, MP-2 and MP-1-S-S. It became very obvious, that sufficient

transfection efficiency could only be obtained when MP-MSNs were capped with ***454***. Efficient gene silencing could be shown with very low particle concentrations (2.5 µg MSN per 100 mL), which could not be achieved in other studies [197, 232]. Compared to MP-MSNs, LP-MSN did not show sufficient gene silencing probably due to the diminished siRNA release resulting from the bottleneck pore morphology. DOTAP capped MP-MSNs showed gene silencing as well. However, sequence-defined oligomers are preferable as capping system as DOTAP does not offer multifunctional domains, robustness and opportunities for future covalent modifications. In summary, MSNs together with sequence-defined oligomers are highly efficient and biocompatible siRNA delivery vehicles.

5 Summary

The delivery of small nucleic acids triggering RNAi for cancer treatment is still a major challenge. Sequence-defined oligomers provide an excellent opportunity to meet all the demands an efficient and multifunctional siRNA or miRNA delivery system has to fulfil. The numerous requirements include stability in the blood stream, a suitable size to avoid rapid elimination or blockage of fine capillaries, shielding to prevent unspecific interactions with blood components or non-target cells and the equipment with receptor specific targeting ligands. After uptake into target cells, the delivery vehicles have to escape the endosome and subsequently release their cargo into the cytosol. Sequence-defined oligomers can be synthesized easily and precise using solid phase-supported synthesis. With this method, building blocks for nucleic acid binding, shielding, targeting, stabilization, or endosomal escape can be stringed together in a precise manner following a modular design. Thus, in this thesis several formulations based on sequence-defined oligomers for efficient and receptor specific siRNA and miRNA delivery have been developed and evaluated.

In the first part, a new stability motif for sequence-defined oligomers was examined. The motif consisted of three amino acids, cysteine-arginine-cysteine (CRC), and has proven its suitability in the stabilization of peptide dimers by forming twin-disulfides in previous studies. In this thesis, siRNA polyplexes were evaluated containing oligomers with CRC integrated in ascending numbers into 3-arm non-targeted oligomers and into PEGylated folate receptor (FR)-targeted 2-arm oligomers. In both cases, the CRC motif had been integrated at the end of the arms instead of a single cysteine. A size reduction had been achieved in 3-arm oligomers with increasing numbers of CRC motifs, whereas it had not influenced the size of PEGylated oligomers. However, remarkably higher stability had been obtained with the insertion of the CRC motif in PEGylated polyplexes, also in the presence of serum and reducing agents. FolA dependent uptake and receptor specific gene silencing was demonstrated with PEGylated CRC-oligomers using endosomolytic peptide INF7 modified siRNA. In contrary, the insertion of the CRC motif abolished the transfection efficiency of non-PEGylated 3-arm oligomers completely.

In the second part, a library of 42 oligomers with different topologies was evaluated in order to figure out structure-activity relationships and the optimal carrier for FR-targeted siRNA delivery. Starting from the lead structure ***356***, 2-arm and 4-arm oligomers had been modified with Stp or Sph for siRNA binding, tyrosine trimers and cysteines to

enhance stability and histidines to improve the endosomal escape. High siRNA binding and compaction had been achieved with 2-arm and 4-arm oligomers without further modification. In gene silencing experiments, oligomers with high charge density due to a large cationic backbone were advantageous. Nevertheless, the best candidates for efficient gene silencing turned out to be 2-arm oligomers with tyrosine trimers and histidine modification. Targeted delivery was obtained with 2-arm oligomers modified with tyrosine trimers and with 4-arm oligomers modified with histidines.

The third part is based on native chemical ligation (NCL) as oligomer synthesis tool to facilitate the screening process for receptor-targeted siRNA delivery. Using NCL, non-targeted 2-arm, 3-arm and 4-arm oligomers with different modifications from our existing library had been easily converted into FR-targeted and shielded oligomers without the need of a new synthesis. In this thesis, structure-activity relationships revealed enhanced siRNA binding with an increased number of cationic arms and a reduced particle size with the insertion of tyrosine trimers into 3-arm oligomers. Additionally, 3-arm oligomers with and without tyrosine trimer modification demonstrated efficient and receptor specific gene silencing.

In the fourth part, the receptor specificity of siRNA and miRNA polyplexes was enhanced using a post-PEGylation strategy. Two t-shaped sequence-defined cationic lipo-oligomers, ***454*** and ***595***, were used as core polyplexes and were further modified with maleimido-PEG reagents containing FolA or tetra-γ-glutamyl folic acid (gE4-FolA) ligands. Formulations with suitable sizes resulting in receptor specific uptake and high gene silencing without the addition of endosomolytic agents were only obtained with gE4-FolA. *In vivo* experiments revealed stability problems of the core polyplexes, which could be partly overcome by lowering the PEGylation degree and by using ***595*** containing the CRC stability motif. Additionally, the post-PEGylation principle was transferred to the peptide ligand GE11 targeting the EGF receptor. Receptor specific uptake and gene silencing not only with eGFP siRNA functioning in a model system, but also with the therapeutic nucleic acids miR-200c and EG5 siRNA were achieved and several antitumoral effects were shown.

In the fifth part, an alternative siRNA delivery system based on mesoporous silica nanoparticles (MSNs) has been evaluated. MSNs with medium-pore (MP) sizes favourable in siRNA absorption and desorption in combination with the t-shaped sequence-defined oligomer ***454*** achieved high gene silencing and excellent biocompatibility.

6 Appendix

6.1 Abbreviations

AD-PEG	adamantane conjugated to PEG
Ago	argonaute protein
apoB	apolipoprotein B
bp	base pairs
DGCR8	DiGeorge syndrome critical region gene 8
DMEM	Dulbecco`s modified Eagle`s medium
DMSO	dimethyl sulfoxide
DOTAP	1,2-dioleoyl-3-trimethylammonium-propane (chloride salt)
dsRNA	double stranded RNA
ECM	extracellular matrix
EGF	epidermal growth factor
EGFR	epidermal growth factor receptor
EPR	enhanced permeability and retention
EtBr	ethidium bromide
2´F	2´-fluoro
FBS	fetal bovine serum
FolA	folic acid
FR	folic acid receptor
gE4-FolA	tetra-γ-glutamyl folic acid
GSH	glutathion
Gtp	glutaroyl tetraethylene pentamine
Gtt	glutaroyl triethylene tetramine
2´-deoxy	2´H
HBG	HEPES buffered glucose
HEPES	N-(2-hydroxyethyl)piperazine-N´-(2-ethanesulfonic acid)
Hmgcr	3-hydroxy-3-methylglutaryl-CoA-reductase

INFα	interferon-α
INF7	synthetic endosomolytic peptide derived from the influenza virus hemagglutinin HA2 N-terminus
LNA	locked nucleic acid
LPEI	linear polyethylenimine
miRNA	micro RNA
mRNA	messenger RNA
2´-MOE	2`-methoxyethyl
MSN	mesoporous silica nanoparticles
MTT	3-(4,5-dimethylthiazol-2-yl)-2,5-diphenyltetrazolium bromide
Nbz	N-acyl-benzimidazolinone
NCL	native chemical ligation
NF-κB	nuclear factor κ-light-chain-enhancer of activated B cells
2´OMe	2´-O-methyl
PAA	poly(amino acid)
PAMAM	polyamidoamine
PEG	polyethylene glycol
Pol II	polymerase II
Pre-miRNA	miRNA precursor
pri-miRNA	primary miRNA
PACT	protein activator of protein kinase PKR
PAZ	PIWI-Argonaute-Zwille
PEI	polyethylenimine
PRR	pattern recognition receptor
Ptp	phthaloyl tetraethylene pentamine
RISC	RNA-induced silencing complex
PKN3	protein kinase N3
RNAi	RNA interference
RRM2	M2 subunit of ribonucleotide reductase
SD	standard deviation
siRNA	small interfering RNA

Sph	succinoyl pentaethylene hexamine
SPS	solid phase-supported synthesis
Stp	succinoyl tetraethylene pentamine
ssRNA	single-stranded RNA
SucA	Succinic acid
TLR	toll-like receptors
TEM	transmission electron microscopy
TRBP	HIV-1 TAR RNA-binding protein
3´UTR	3`untranslated region
VEGF	vascular endothelial growth factor A

6.2 Analytical Data

Mass spectra from compounds synthesized by Philipp Klein were generated by Sören Reinhard and Stephan Morys (PhD students, Pharmaceutical Biotechnology, LMU Munich).

Mass spectrum of Mal-PEG-Folate (FolA):

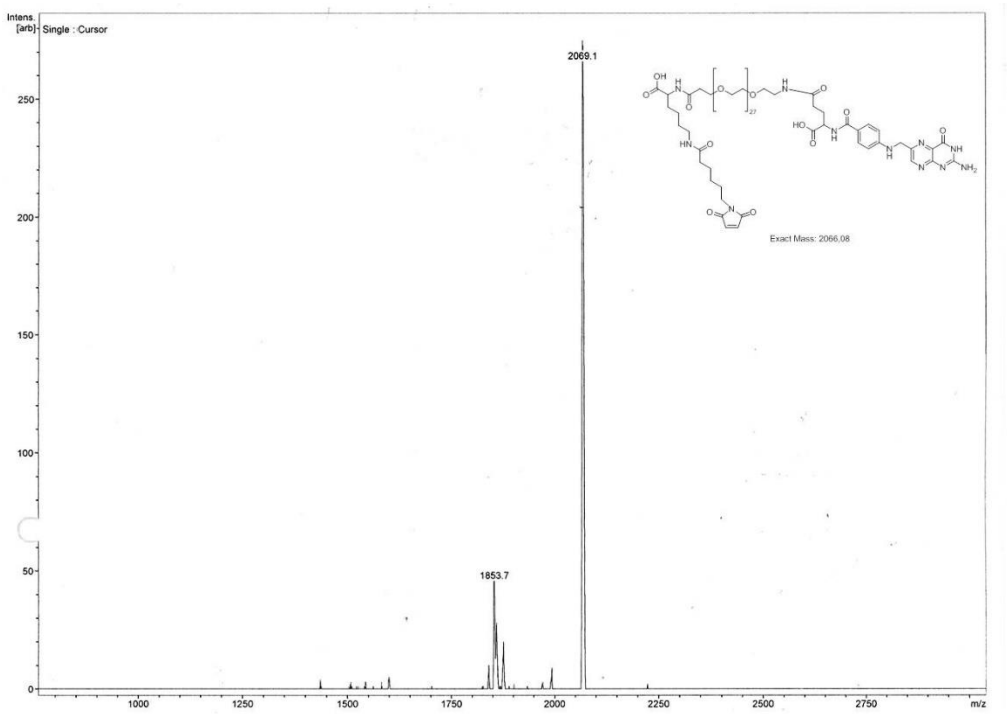

Mass calculated for C94H159N11O39 [M+H]+ 2067.08, mass found 2069.1

Mass spectrum of Mal-PEG-gE4-Folate (gE4-FolA):

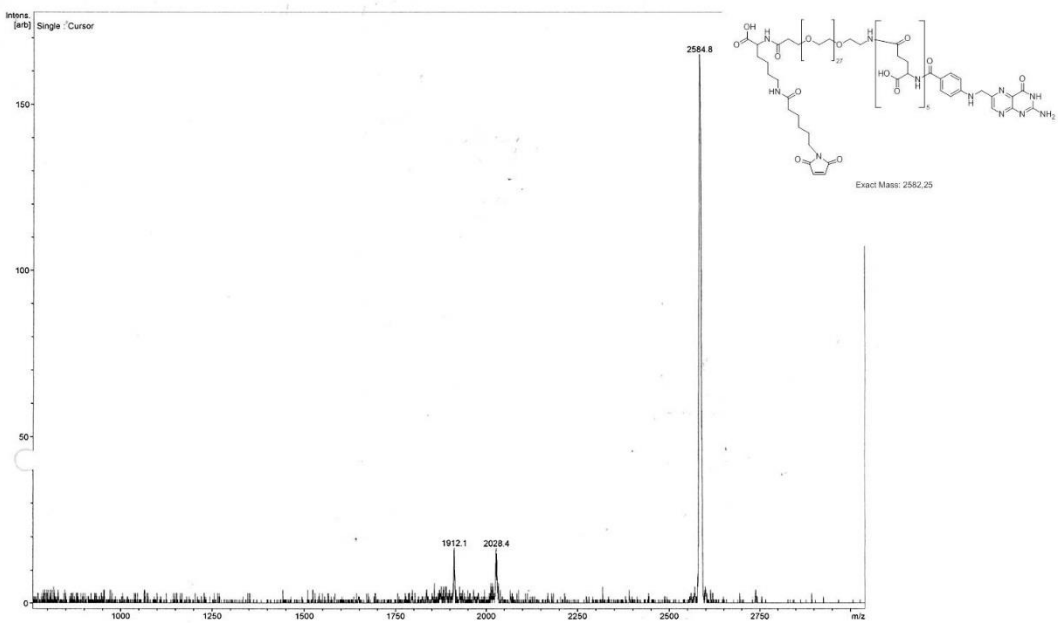

Mass calculated for C114H187N15O51 [M+H]+ 2582.25, mass found 2584.8.

Mass spectrum of Mal-PEG:

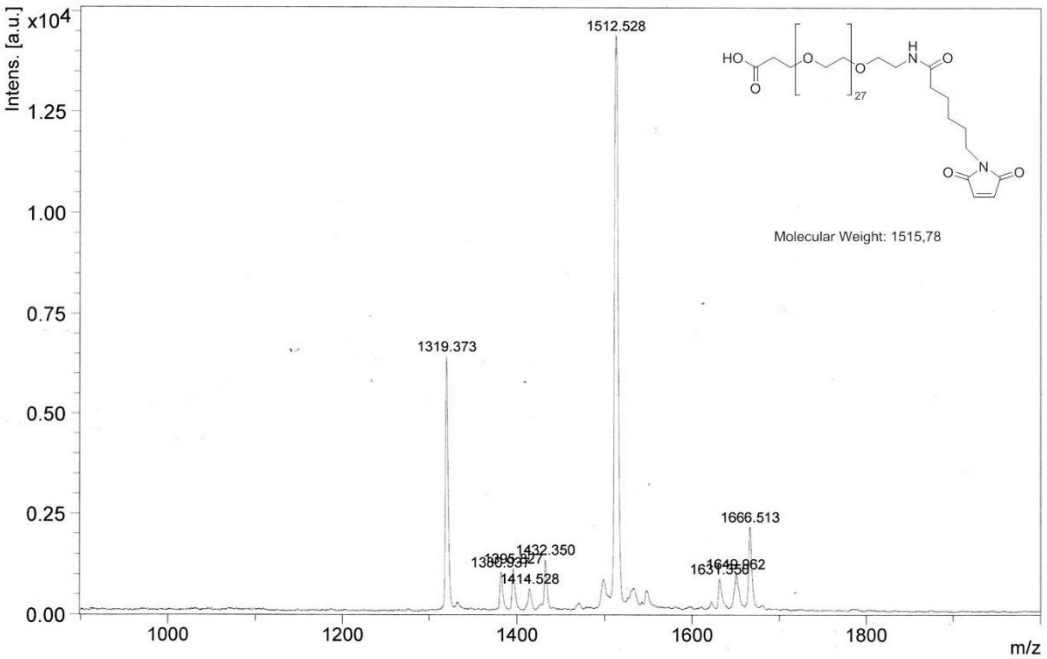

Mass calculated for C69H130N2O33 [M+H]+ 1516.78, mass found 1512.53.

Mass spectrum of Mal-GE11:

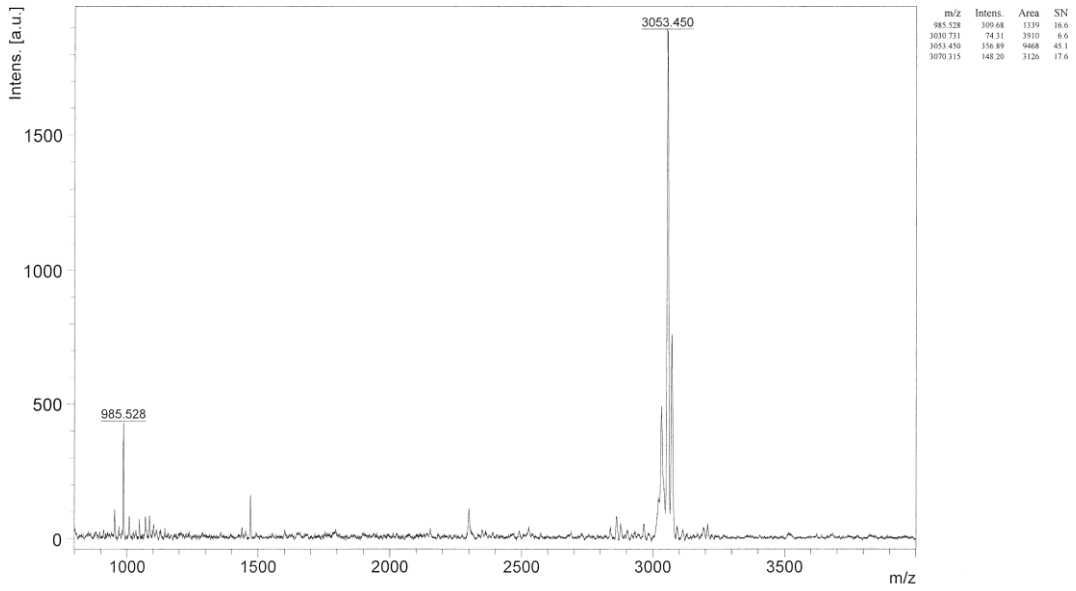

Mass calculated for $C_{144}H_{225}N_{19}O_{51}$: $[M+H]^+$: 3036.6 Da. Masses found: $[M+H]^+$: 3030.7 Da, $[M+Na]^+$: 3053.5 Da, $[M+K]^+$: 3070.

6.3 Publications

6.3.1 Original articles

EGF receptor targeted lipo-oligocation polyplexes for antitumoral siRNA and miRNA delivery; **Müller K**, Klein PM, Heissig P, Roidl A, Wagner E; Nanotechnology. 2016 Nov 18; Epub 2016 Oct 13; 27(46):464001, doi: 10.1088/0957-4484/27/46/464001.

Precise redox-sensitive cleavage sites for improved bioactivity of siRNA lipopolyplexes; Klein PM, Reinhard S, Lee DJ, **Müller K**, Ponader D, Hartmann L, Wagner E; Nanoscale. 2016 Oct 27; 8(42):18098-18104, doi: 10.1039/c6nr05767e.

Post-PEGylation of siRNA lipo-oligoamino amide polyplexes using tetra-glutamylated folic acid as ligand for receptor-targeted delivery; **Müller K,** Kessel E, Klein P., Höhn M, Wagner E; Mol Pharm. 2016 Jul 5; 13(7):2332-45, doi: 10.1021/acs.molpharmaceut. 6b00102.

Targeted siRNA delivery using a lipo-oligoaminoamide nanocore with an influenza peptide and transferrin shell; Zhang W, **Müller K,** Kessel E, Reinhard S, He D, Klein PM, Höhn M, Rödl W, Kempter S, Wagner E; Adv Healthc Mater. 2016 Jun; 5(12):1493-504, doi: 10.1002/adhm.201600057.

Combinatorial optimization of sequence-defined oligo(ethanamino)amides for folate receptor-targeted pDNA and siRNA delivery; He D, **Müller K,** Krhac Levacic A, Kos P, Lächelt U, Wagner E; Bioconjug Chem. 2016 Mar 16; 27(3):647-59, doi: 10.1021/acs. bioconjchem.5b00649.

Multifunctional polymer-capped mesoporous silica nanoparticles for pH-responsive targeted drug delivery; Niedermayer S, Weiss V, Herrmann A, Schmidt A, Datz S, **Müller K,** Wagner E, Bein T, Bräuchle C; Nanoscale. 2015 May 7; 7(17):7953-64, doi: 10.1039/c4nr07245f.

Twin disulfides as oppurtunity for improving stability and transfection efficiency of oligoaminoethane polyplexes; Klein PM, **Müller K,** Gutmann C, Kos P, Krhac Levacic A, Edinger D, Höhn M, Leroux JC, Gauthier MA, Wagner E; J Control Release. 2015 May 10; 205:109-19, doi: 10.1016/j.jconrel.2014.12.035.

Synthetic polyglutamylation of dual functional MTX ligands for enhanced combined cytotoxicity of poly(I:C) nanoplexes; Lächelt U, Wittmann V, **Müller K**, Edinger D, Kos P, Höhn M, Wagner E; Mol Pharm. 2014 Aug 4;11(8):2631-9, doi: 10.1021/mp500017u.

Native chemical ligation for conversion of sequence-defined oligomers into targeted pDNA and siRNA carriers; Zhang CY, Kos P, **Müller K,** Schrimpf W, Troiber C, Lächelt U, Scholz C, Lamb DC, Wagner E; J Control Release. 2014 Apr 28;180:42-50, doi: 10.1016/j.jconrel.2014.02.015.

6.3.2 Review

RNAi-based Nano-oncologicals: Delivery and clinical Applications; **Müller K,** Wagner E; In Nano-Oncologicals: New targeting and delivery approaches, Controlled release society and Springer; Part of the series Advances in Delivery Science and Technology. 2014 Sep 06; 245-268.

6.3.3 Meeting abstracts and poster presentations

A new platform for siRNA delivery: core-shell mesoporous silica nanoparticles with multifunctional polymer caps, Möller K, **Müller K**, Engelke H, Bräuchle C, Wagner E, Bein T; 14th European Symposium on Controlled Drug Delivery, Egmond aan Zee, the Netherlands, April 2016

miR-200c: function and delivery; **Müller K**, Klein PM, Kopp F, Roidl A, Wagner E; SFB 1032 meeting, München, Germany , January 2016

Conquer the barriers: optimization of sequence defined multifunctional nanocarriers for folate receptor targeted pDNA and siRNA delivery; He D, **Müller K**, Krhac Levacic A, Kos P, Lee DJ, Wagner E; 1st LMU-ChAN (China Academic Network) Scientific Forum, Munich, Germany, November 2015

microRNA-200c and molecular nanoagents; Heissig P, Schrimpf W, **Müller K**, Lamb D, Wagner E, SFB 1032 meeting, Altötting, Germany, February 2015

Cargo-specific optimization of sequence defined non-viral nucleic acid carriers for folate receptor targeted pDNA or siRNA delivery; He D, **Müller K**, Kos P, Lee DJ, Lächelt U, Wagner E; XIX. Annual Meeting of German Society for Gene Therapy, Ulm, Germany, March 2014

Native chemical ligation for conversion of sequence-defined oligomers of different topologies into targeted pDNA and siRNA carriers; Kos P, **Müller K**, Zhang CY, Troiber C, Lächelt U, Scholz C, Wagner E; Young Ideas in Nanoscience, NIM Workshop, Munich, Germany, November 2013

Targeted sequence-defined oligomers of different topologies for pDNA and siRNA delivery synthesized via native chemical ligation; Kos P, **Müller K**, Zhang CY, Troiber C, Lächelt U, Scholz C, Wagner E; Nanosciences: Great Adventures on Small Scales, CeNS Workshop, Venice, Italy, September 2013

Molecular nanoagents utilizing the intracellular microRNA machinery for switching functions in cells; Heissig P, **Müller K**, Wagner E; SFB 1032 retreat, February 2013

6.3.4 Oral presentation

Molecular nanoagents for anti-metastatic miR200c overexpression and detection, SFB 1032 retreat, Frauenchiemsee, Germany, February 2014

6.4 Copyright

7 References

1. Krol J, Loedige I, Filipowicz W. The widespread regulation of microRNA biogenesis, function and decay. Nature Reviews Genetics 2010; 11(9):597-610.
2. Treiber T, Treiber N, Meister G. Regulation of microRNA biogenesis and function. Thrombosis and Haemostasis 2012; 107(4):605-10.
3. Ma JB, Ye K, Patel DJ. Structural basis for overhang-specific small interfering RNA recognition by the PAZ domain. Nature 2004; 429(6989):318-22.
4. Meister G, Tuschl T. Mechanisms of gene silencing by double-stranded RNA. Nature 2004; 431(7006):343-9.
5. Kim DH, Rossi JJ. Strategies for silencing human disease using RNA interference. Nature Reviews Genetics 2007; 8(3):173-84.
6. Bartel DP. MicroRNAs: target recognition and regulatory functions. Cell 2009; 136(2):215-33.
7. Khvorova A, Reynolds A, Jayasena SD. Functional siRNAs and miRNAs exhibit strand bias. Cell 2003; 115(2):209-16.
8. Lim LP, Lau NC, Garrett-Engele P, Grimson A, Schelter JM, Castle J, Bartel DP, Linsley PS, Johnson JM. Microarray analysis shows that some microRNAs downregulate large numbers of target mRNAs. Nature 2005; 433(7027):769-73.
9. Yates LA, Norbury CJ, Gilbert RJ. The long and short of microRNA. Cell 2013; 153(3):516-9.
10. Kim VN. MicroRNA biogenesis: coordinated cropping and dicing. Nature Reviews Molecular Cell Biology 2005; 6(5):376-85.
11. Bartel DP. MicroRNAs: genomics, biogenesis, mechanism, and function. Cell 2004; 116(2):281-97.
12. Guzman-Villanueva D, El-Sherbiny IM, Herrera-Ruiz D, Vlassov AV, Smyth HD. Formulation approaches to short interfering RNA and MicroRNA: challenges and implications. Journal of Pharmaceutical Sciences 2012; 101(11):4046-66.
13. Müller K, Wagner E. RNAi-based Nano-Oncologicals – Delivery and Clinical Applications. In: Alonso MJ, Garcia-Fuentes M, editors. Nano-Oncologicals: New Targeting and Delivery Approaches: Controlled Release Society and Springer; 2014; 245-68.
14. Elbashir SM, Harborth J, Lendeckel W, Yalcin A, Weber K, Tuschl T. Duplexes of 21-nucleotide RNAs mediate RNA interference in cultured mammalian cells. Nature 2001; 411(6836):494-8.
15. Kim HJ, Kim A, Miyata K, Kataoka K. Recent progress in development of siRNA delivery vehicles for cancer therapy. Advanced Drug Delivery Reviews 2016; 104:61-77.
16. Hatakeyama H, Wu SY, Mangala LS, Lopez-Berestein G, Sood AK. Assessment of In Vivo siRNA Delivery in Cancer Mouse Models. Methods in Molecular Biology 2016; 1402:189-97.
17. Wu SY, Lopez-Berestein G, Calin GA, Sood AK. RNAi therapies: drugging the undruggable. Science Translational Medicine 2014; 6(240):240ps7.
18. Edinger D, Kläger R, Troiber C, Dohmen C, Wagner E. Gene Silencing and Antitumoral Effects of Eg5 or Ran siRNA Oligoaminoamide Polyplexes. Drug Delivery and Translational Research 2013; 4(1):84-95.
19. Bartlett DW, Davis ME. Insights into the kinetics of siRNA-mediated gene silencing from live-cell and live-animal bioluminescent imaging. Nucleic Acids Research 2006; 34(1):322-33.
20. Zimmermann TS, Lee AC, Akinc A, et al. RNAi-mediated gene silencing in non-human primates. Nature 2006; 441(7089):111-4.
21. Haussecker D. The Business of RNAi Therapeutics in 2012. Molecular Therapy-Nucleic Acids 2012; 1:e8.

22. Haussecker D, Kay MA. RNA interference. Drugging RNAi. Science 2015; 347(6226):1069-70.
23. Davis ME. The first targeted delivery of siRNA in humans via a self-assembling, cyclodextrin polymer-based nanoparticle: from concept to clinic. Molecular Pharmaceutics 2009; 6(3):659-68.
24. Davis ME, Zuckerman JE, Choi CH, Seligson D, Tolcher A, Alabi CA, Yen Y, Heidel JD, Ribas A. Evidence of RNAi in humans from systemically administered siRNA via targeted nanoparticles. Nature 2010; 464 1067-70.
25. Zuckerman JE, Davis ME. Clinical experiences with systemically administered siRNA-based therapeutics in cancer. Nature Reviews Drug Discovery 2015; 14(12):843-56.
26. Santel A, Aleku M, Keil O, et al. A novel siRNA-lipoplex technology for RNA interference in the mouse vascular endothelium. Gene Therapy 2006; 13(16):1222-34.
27. Aleku M, Schulz P, Keil O, et al. Atu027, a liposomal small interfering RNA formulation targeting protein kinase N3, inhibits cancer progression. Cancer Research 2008; 68(23):9788-98.
28. Schultheis B, Strumberg D, Santel A, et al. First-in-human phase I study of the liposomal RNA interference therapeutic Atu027 in patients with advanced solid tumors. Journal of Clinical Oncology 2014; 32(36):4141-8.
29. Schultheis B. SD, Kuhlmann J., Wolf M., Link K., Seufferlein, T., Kaufmann J., Gebhardt F., Bruyniks N., Pelzer U. A phase Ib/IIa study of combination therapy with gemcitabine and Atu027 in patients with locally advanced or metastatic pancreatic adenocarcinoma. Journal of Clinical Oncology 2016; 34:385.
30. Tabernero J, Shapiro GI, LoRusso PM, et al. First-in-humans trial of an RNA interference therapeutic targeting VEGF and KSP in cancer patients with liver involvement. Cancer Discovery 2013; 3(4):406-17.
31. Bouchie A. First microRNA mimic enters clinic. Nature Biotechnology 2013; 31(7):577.
32. Trang P, Wiggins JF, Daige CL, Cho C, Omotola M, Brown D, Weidhaas JB, Bader AG, Slack FJ. Systemic delivery of tumor suppressor microRNA mimics using a neutral lipid emulsion inhibits lung tumors in mice. Molecular Therapy 2011; 19(6):1116-22.
33. Beg M.S. BA, Sachdev J., Ejadi S., Borad M., Kang Y., Lim H., Kim T., Bader A., Stoudemire J., Smith S., Kim S., Hong D. Abstract C43: Safety, tolerability, and clinical activity of MRX34, the first-in-class liposomal miR-34 mimic, in patients with advanced solid tumors. Molecular Cancer Therapeutics 2015; 14(12).
34. Beg M.S. BM, Sachdev J., Hong D.S., Smith S., Bader A., Stoudemire J., Kim S., Brenner A. Abstract CT327: Multicenter phase I study of MRX34, a first-in-class microRNA miR-34 mimic liposomal injection. Cancer Research 2014; 74(19 Suppl).
35. Yazbeck DR, Min KL, Damha MJ. Molecular requirements for degradation of a modified sense RNA strand by Escherichia coli ribonuclease H1. Nucleic Acids Research 2002; 30(14):3015-25.
36. Kanasty RL, Whitehead KA, Vegas AJ, Anderson DG. Action and reaction: the biological response to siRNA and its delivery vehicles. Molecular Therapy 2012; 20(3):513-24.
37. Soutschek J, Akinc A, Bramlage B, et al. Therapeutic silencing of an endogenous gene by systemic administration of modified siRNAs. Nature 2004; 432(7014):173-8.
38. Jackson AL, Burchard J, Schelter J, Chau BN, Cleary M, Lim L, Linsley PS. Widespread siRNA "off-target" transcript silencing mediated by seed region sequence complementarity. RNA 2006; 12(7):1179-87.
39. Birmingham A, Anderson EM, Reynolds A, et al. 3' UTR seed matches, but not overall identity, are associated with RNAi off-targets. Nature Methods 2006; 3(3):199-204.

40. Pecot CV, Calin GA, Coleman RL, Lopez-Berestein G, Sood AK. RNA interference in the clinic: challenges and future directions. Nature Reviews Cancer 2011; 11(1):59-67.
41. Medzhitov R, Janeway CA, Jr. Decoding the patterns of self and nonself by the innate immune system. Science 2002; 296(5566):298-300.
42. Rettig GR, Behlke MA. Progress toward in vivo use of siRNAs-II. Molecular Therapy 2012; 20(3):483-512.
43. Seth RB, Sun L, Chen ZJ. Antiviral innate immunity pathways. Cell Research 2006; 16(2):141-7.
44. Hornung V, Guenthner-Biller M, Bourquin C, et al. Sequence-specific potent induction of IFN-alpha by short interfering RNA in plasmacytoid dendritic cells through TLR7. Nature Medicine 2005; 11(3):263-70.
45. Kota J, Chivukula RR, O'Donnell KA, et al. Therapeutic microRNA delivery suppresses tumorigenesis in a murine liver cancer model. Cell 2009; 137(6):1005-17.
46. Rana TM. Illuminating the silence: understanding the structure and function of small RNAs. Nature Reviews Molecular Cell Biology 2007; 8(1):23-36.
47. Ku SH, Jo SD, Lee YK, Kim K, Kim SH. Chemical and structural modifications of RNAi therapeutics. Advanced Drug Delivery Reviews 2016; 104:16-28.
48. Behlke MA. Progress towards in vivo use of siRNAs. Molecular Therapy 2006; 13(4):644-70.
49. Judge AD, Sood V, Shaw JR, Fang D, McClintock K, MacLachlan I. Sequence-dependent stimulation of the mammalian innate immune response by synthetic siRNA. Nature Biotechnology 2005; 23(4):457-62.
50. Bumcrot D, Manoharan M, Koteliansky V, Sah DW. RNAi therapeutics: a potential new class of pharmaceutical drugs. Nature Chemical Biology 2006; 2(12):711-9.
51. Elmen J, Thonberg H, Ljungberg K, et al. Locked nucleic acid (LNA) mediated improvements in siRNA stability and functionality. Nucleic Acids Research 2005; 33(1):439-47.
52. Obad S, dos Santos CO, Petri A, et al. Silencing of microRNA families by seed-targeting tiny LNAs. Nature Genetics 2011; 43(4):371-8.
53. Wolfrum C, Shi S, Jayaprakash KN, et al. Mechanisms and optimization of in vivo delivery of lipophilic siRNAs. Nature Biotechnology 2007; 25(10):1149-57.
54. Oberhauser B, Wagner E. Effective incorporation of 2'-O-methyl-oligoribonucleotides into liposomes and enhanced cell association through modification with thiocholesterol. Nucleic Acids Research 1992; 20(3):533-8.
55. Krutzfeldt J, Rajewsky N, Braich R, Rajeev KG, Tuschl T, Manoharan M, Stoffel M. Silencing of microRNAs in vivo with 'antagomirs'. Nature 2005; 438(7068):685-9.
56. Plank C, Oberhauser B, Mechtler K, Koch C, Wagner E. The influence of endosome-disruptive peptides on gene transfer using synthetic virus-like gene transfer systems. The Journal of Biological Chemistry 1994; 269(17):12918-24.
57. Dohmen C, Edinger D, Frohlich T, et al. Nanosized multifunctional polyplexes for receptor-mediated siRNA delivery. ACS Nano 2012; 6(6):5198-208.
58. Gallas A, Alexander C, Davies MC, Puri S, Allen S. Chemistry and formulations for siRNA therapeutics. Chemical Society Reviews 2013:7983-97.
59. Zamecnik J, Vargova L, Homola A, Kodet R, Sykova E. Extracellular matrix glycoproteins and diffusion barriers in human astrocytic tumours. Neuropathology and Applied Neurobiology 2004; 30(4):338-50.
60. Shim MS, Kwon YJ. Efficient and targeted delivery of siRNA in vivo. The FEBS Journal 2010; 277(23):4814-27.
61. Wagner E. Biomaterials in RNAi therapeutics: quo vadis? Biomaterials Science 2013; (8):804-9.
62. Lächelt U, Wagner E. Nucleic Acid Therapeutics Using Polyplexes: A Journey of 50 Years (and Beyond). Chemical Reviews 2015; 115(19):11043-78.

63. Hartmann L, Krause E, Antonietti M, Borner HG. Solid-phase supported polymer synthesis of sequence-defined, multifunctional poly(amidoamines). Biomacromolecules 2006; 7(4):1239-44.
64. Schaffert D, Badgujar N, Wagner E. Novel Fmoc-polyamino acids for solid-phase synthesis of defined polyamidoamines. Organic Letters 2011; 13(7):1586-9.
65. Schaffert D, Troiber C, Salcher EE, et al. Solid-phase synthesis of sequence-defined T-, i-, and U-shape polymers for pDNA and siRNA delivery. Angewandte Chemie 2011; 50(38):8986-9.
66. Salcher EE, Kos P, Frohlich T, Badgujar N, Scheible M, Wagner E. Sequence-defined four-arm oligo(ethanamino)amides for pDNA and siRNA delivery: Impact of building blocks on efficacy. Journal of Controlled Release 2012; 164(3):380-6.
67. He D, Müller K, Krhac Levacic A, Kos P, Lachelt U, Wagner E. Combinatorial Optimization of Sequence-Defined Oligo(ethanamino)amides for Folate Receptor-Targeted pDNA and siRNA Delivery. Bioconjugate Chemistry 2016; 27(3):647–59.
68. Lee DJ, Kessel E, Edinger D, et al. Dual antitumoral potency of EG5 siRNA nanoplexes armed with cytotoxic bifunctional glutamyl-methotrexate targeting ligand. Biomaterials 2016; 77:98-110.
69. Beckert L, Kostka L, Kessel E, Krhac Levacic A, Kostkova H, Etrych T, Lachelt U, Wagner E. Acid-labile pHPMA modification of four-arm oligoaminoamide pDNA polyplexes balances shielding and gene transfer activity in vitro and in vivo. European Journal of Pharmaceutics and Biopharmaceutics 2016; 105:85-96.
70. Kos P, Lachelt U, Herrmann A, et al. Histidine-rich stabilized polyplexes for cMet-directed tumor-targeted gene transfer. Nanoscale 2015; 7(12):5350-62.
71. Kwok A, Hart SL. Comparative structural and functional studies of nanoparticle formulations for DNA and siRNA delivery. Nanomedicine 2011; 7(2):210-9.
72. Scholz C, Wagner E. Therapeutic plasmid DNA versus siRNA delivery: common and different tasks for synthetic carriers. Journal of Controlled Release 2012; 161(2):554-65.
73. Troiber C, Edinger D, Kos P, Schreiner L, Klager R, Herrmann A, Wagner E. Stabilizing effect of tyrosine trimers on pDNA and siRNA polyplexes. Biomaterials 2013; 34(5):1624-33.
74. Troiber C, Kasper JC, Milani S, et al. Comparison of four different particle sizing methods for siRNA polyplex characterization. European Journal of Pharmaceutics and Biopharmaceutics 2012; 84(2):255-64.
75. Fröhlich T, Edinger D, Kläger R, et al. Structure-activity relationships of siRNA carriers based on sequence-defined oligo (ethane amino) amides. Journal of Controlled Release 2012; 160(3):532-41.
76. Bloomfield VA. DNA condensation by multivalent cations. Biopolymers 1997; 44(3):269-82.
77. Baker A, Saltik M, Lehrmann H, Killisch I, Mautner V, Lamm G, Christofori G, Cotten M. Polyethylenimine (PEI) is a simple, inexpensive and effective reagent for condensing and linking plasmid DNA to adenovirus for gene delivery. Gene Therapy 1997; 4(8):773-82.
78. Lächelt U, Kos P, Mickler FM, Herrmann A, Salcher EE, Rodl W, Badgujar N, Brauchle C, Wagner E. Fine-tuning of proton sponges by precise diaminoethanes and histidines in pDNA polyplexes. Nanomedicine 2014; 10(1):35-44.
79. Rejman J, Oberle V, Zuhorn IS, Hoekstra D. Size-dependent internalization of particles via the pathways of clathrin- and caveolae-mediated endocytosis. The Biochemical journal 2004; 377(Pt 1):159-69.
80. Rejman J, Bragonzi A, Conese M. Role of clathrin- and caveolae-mediated endocytosis in gene transfer mediated by lipo- and polyplexes. Molecular Therapy 2005; 12(3):468-74.

81. Yuan F, Dellian M, Fukumura D, Leunig M, Berk DA, Torchilin VP, Jain RK. Vascular permeability in a human tumor xenograft: molecular size dependence and cutoff size. Cancer Research 1995; 55(17):3752-6.
82. Fang J, Nakamura H, Maeda H. The EPR effect: Unique features of tumor blood vessels for drug delivery, factors involved, and limitations and augmentation of the effect. Advanced Drug Delivery Reviews 2011; 63(3):136-51.
83. Ogris M, Steinlein P, Carotta S, Brunner S, Wagner E. DNA/polyethylenimine transfection particles: influence of ligands, polymer size, and PEGylation on internalization and gene expression. AAPS PharmSci 2001; 3(3):E21.
84. Wagner E, Cotten M, Foisner R, Birnstiel ML. Transferrin-polycation-DNA complexes: the effect of polycations on the structure of the complex and DNA delivery to cells. Proceedings of the National Academy of Sciences of the United States of America 1991; 88(10):4255-9.
85. Hanahan D, Weinberg RA. The hallmarks of cancer. Cell 2000; 100(1):57-70.
86. Martin I, Dohmen C, Mas-Moruno C, et al. Solid-phase-assisted synthesis of targeting peptide-PEG-oligo(ethane amino)amides for receptor-mediated gene delivery. Organic & Biomolecular Chemistry 2012; 10(16):3258-68.
87. Weitman SD, Lark RH, Coney LR, Fort DW, Frasca V, Zurawski VR, Jr., Kamen BA. Distribution of the folate receptor GP38 in normal and malignant cell lines and tissues. Cancer Research 1992; 52(12):3396-401.
88. Ross JF, Chaudhuri PK, Ratnam M. Differential regulation of folate receptor isoforms in normal and malignant tissues in vivo and in established cell lines. Physiologic and clinical implications. Cancer 1994; 73(9):2432-43.
89. Sudimack J, Lee RJ. Targeted drug delivery via the folate receptor. Advanced Drug Delivery Reviews 2000; 41(2):147-62.
90. Wang X, Shen F, Freisheim JH, Gentry LE, Ratnam M. Differential stereospecificities and affinities of folate receptor isoforms for folate compounds and antifolates. Biochemical Pharmacology 1992; 44(9):1898-901.
91. Antony AC. Folate receptors. Annual Review of Nutrition 1996; 16:501-21.
92. Matherly LH, Hou Z, Deng Y. Human reduced folate carrier: translation of basic biology to cancer etiology and therapy. Cancer Metastasis Reviews 2007; 26(1):111-28.
93. Zhao R, Min SH, Wang Y, Campanella E, Low PS, Goldman ID. A role for the proton-coupled folate transporter (PCFT-SLC46A1) in folate receptor-mediated endocytosis. The Journal of Biological Chemistry 2009; 284(7):4267-74.
94. Xia W, Low PS. Folate-targeted therapies for cancer. Journal of Medicinal Chemistry 2010; 53(19):6811-24.
95. Yang J, Chen H, Vlahov IR, Cheng JX, Low PS. Evaluation of disulfide reduction during receptor-mediated endocytosis by using FRET imaging. Proceedings of the National Academy of Sciences of the United States of America 2006; 103(37):13872-7.
96. Lu Y, Low PS. Folate-mediated delivery of macromolecular anticancer therapeutic agents. Advanced Drug Delivery Reviews 2002; 54(5):675-93.
97. Leamon CP, Pastan I, Low PS. Cytotoxicity of folate-Pseudomonas exotoxin conjugates toward tumor cells. Contribution of translocation domain. The Journal of Biological Chemistry 1993; 268(33):24847-54.
98. Yang T, Li B, Qi S, et al. Co-delivery of doxorubicin and Bmi1 siRNA by folate receptor targeted liposomes exhibits enhanced anti-tumor effects in vitro and in vivo. Theranostics 2014; 4(11):1096-111.
99. Lee ES, Na K, Bae YH. Polymeric micelle for tumor pH and folate-mediated targeting. Journal of Controlled Release 2003; 91(1-2):103-13.
100. Gottschalk S, Cristiano RJ, Smith LC, Woo SL. Folate receptor mediated DNA delivery into tumor cells: potosomal disruption results in enhanced gene expression. Gene Therapy 1994; 1(3):185-91.

101. Hofland HE, Masson C, Iginla S, Osetinsky I, Reddy JA, Leamon CP, Scherman D, Bessodes M, Wils P. Folate-targeted gene transfer in vivo. Molecular Therapy 2002; 5(6):739-44.
102. Lee DJ, He D, Kessel E, Padari K, Kempter S, Lachelt U, Radler JO, Pooga M, Wagner E. Tumoral gene silencing by receptor-targeted combinatorial siRNA polyplexes. Journal of Controlled Release 2016:doi: 10.1016/j.jconrel.2016.06.011.
103. Liu L, Zheng M, Librizzi D, Renette T, Merkel OM, Kissel T. Efficient and Tumor Targeted siRNA Delivery by Polyethylenimine-graft-polycaprolactone-block-poly(ethylene glycol)-folate (PEI-PCL-PEG-Fol). Molecular Pharmaceutics 2016; 13(1):134-43.
104. Mickler FM, Mockl L, Ruthardt N, Ogris M, Wagner E, Brauchle C. Tuning nanoparticle uptake: live-cell imaging reveals two distinct endocytosis mechanisms mediated by natural and artificial EGFR targeting ligand. Nano letters 2012; 12(7):3417-23.
105. Blessing T, Kursa M, Holzhauser R, Kircheis R, Wagner E. Different strategies for formation of pegylated EGF-conjugated PEI/DNA complexes for targeted gene delivery. Bioconjugate Chemistry 2001; 12(4):529-37.
106. de Bruin K, Ruthardt N, von Gersdorff K, Bausinger R, Wagner E, Ogris M, Brauchle C. Cellular dynamics of EGF receptor-targeted synthetic viruses. Molecular Therapy 2007; 15(7):1297-305.
107. Yarden Y. The EGFR family and its ligands in human cancer. signalling mechanisms and therapeutic opportunities. European Journal of Cancer 2001; 37 Suppl 4:S3-8.
108. Nicholson RI, Gee JM, Harper ME. EGFR and cancer prognosis. European Journal of Cancer 2001; 37 Suppl 4:S9-15.
109. Hynes NE, Lane HA. ERBB receptors and cancer: the complexity of targeted inhibitors. Nature Reviews Cancer 2005; 5(5):341-54.
110. Chong CR, Janne PA. The quest to overcome resistance to EGFR-targeted therapies in cancer. Nature Medicine 2013; 19(11):1389-400.
111. Ciardiello F, Tortora G. EGFR antagonists in cancer treatment. The New England journal of medicine 2008; 358(11):1160-74.
112. Li Z, Zhao R, Wu X, Sun Y, Yao M, Li J, Xu Y, Gu J. Identification and characterization of a novel peptide ligand of epidermal growth factor receptor for targeted delivery of therapeutics. FASEB journal : official publication of the Federation of American Societies for Experimental Biology 2005; 19(14):1978-85.
113. Schafer A, Pahnke A, Schaffert D, et al. Disconnecting the yin and yang relation of epidermal growth factor receptor (EGFR)-mediated delivery: a fully synthetic, EGFR-targeted gene transfer system avoiding receptor activation. Human Gene Therapy 2011; 22(12):1463-73.
114. Abourbeh G, Shir A, Mishani E, Ogris M, Rodl W, Wagner E, Levitzki A. PolyIC GE11 polyplex inhibits EGFR-overexpressing tumors. IUBMB Life 2012; 64(4):324-30.
115. Wagner E. Strategies to improve DNA polyplexes for in vivo gene transfer: will "artificial viruses" be the answer? Pharmaceutical Research 2004; 21(1):8-14.
116. Meyer M, Philipp A, Oskuee R, Schmidt C, Wagner E. Breathing life into polycations: functionalization with pH-responsive endosomolytic peptides and polyethylene glycol enables siRNA delivery. Journal of the American Chemical Society 2008; 130(11):3272-3.
117. Whitehead KA, Langer R, Anderson DG. Knocking down barriers: advances in siRNA delivery. Nature Reviews Drug Discovery 2009; 8(2):129-38.
118. Lee M, Kim SW. Polyethylene glycol-conjugated copolymers for plasmid DNA delivery. Pharmaceutical Research 2005; 22(1):1-10.
119. Lee M, Kim SW. Polyethylene glycol-conjugated copolymers for plasmid DNA delivery. PharmRes 2005; 22(1):1-10.

120. Hatakeyama H, Akita H, Harashima H. A multifunctional envelope type nano device (MEND) for gene delivery to tumours based on the EPR effect: A strategy for overcoming the PEG dilemma. Advanced Drug Delivery Reviews 2010; 63(3):152-60.
121. Mishra S, Webster P, Davis ME. PEGylation significantly affects cellular uptake and intracellular trafficking of non-viral gene delivery particles. European Journal of Cell Biology 2004; 83(3):97-111.
122. Walker GF, Fella C, Pelisek J, Fahrmeir J, Boeckle S, Ogris M, Wagner E. Toward synthetic viruses: endosomal pH-triggered deshielding of targeted polyplexes greatly enhances gene transfer in vitro and in vivo. Molecular Therapy 2005; 11(3):418-25.
123. Maxfield FR, McGraw TE. Endocytic recycling. Nature Reviews Molecular Cell Biology 2004; 5(2):121-32.
124. Mellman I. The importance of being acid: the role of acidification in intracellular membrane traffic. The Journal of Experimental Biology 1992; 172:39-45.
125. Marshansky V. The V-ATPase a2-subunit as a putative endosomal pH-sensor. Biochemical Society Transactions 2007; 35(Pt 5):1092-9.
126. Behr JP. The proton sponge: A trick to enter cells the viruses did not exploit. Chimia 1997; 51(1-2):34-6.
127. Sonawane ND, Szoka FC, Jr., Verkman AS. Chloride Accumulation and Swelling in Endosomes Enhances DNA Transfer by Polyamine-DNA Polyplexes. The Journal of Biological Chemistry 2003; 278(45):44826-31.
128. Kos P, Wagner E. Polymers for siRNA Delivery: Combining precision with multifunctionality. Chimica Oggi - Chemistry Today 2013; 31(2):6-10.
129. Meyer M, Dohmen C, Philipp A, Kiener D, Maiwald G, Scheu C, Ogris M, Wagner E. Synthesis and Biological Evaluation of a Bioresponsive and Endosomolytic siRNA-Polymer Conjugate. Molecular Pharmaceutics 2009; 6(3):752-62.
130. Kresge. Ordered mesoporous molecular sieves synthesized by a liquid-crystal template mechanism. Nature 1990; 359:710 - 2.
131. Argyo C. VW, Christoph Bräuchle, Thomas Bein. Multifunctional Mesoporous Silica Nanoparticles as a Universal Platform for Drug Delivery. Chemistry of Materials 2014; 26(1):435–51.
132. Slowing, II, Vivero-Escoto JL, Wu CW, Lin VS. Mesoporous silica nanoparticles as controlled release drug delivery and gene transfection carriers. Advanced Drug Delivery Reviews 2008; 60(11):1278-88.
133. Tang F, Li L, Chen D. Mesoporous silica nanoparticles: synthesis, biocompatibility and drug delivery. Advanced Materials 2012; 24(12):1504-34.
134. Vallet-Regi M. RA, del Real R.P., Pérez-Pariente J. A New Property of MCM-41: Drug Delivery System. Chemistry of Materials 2001; 13(2):308–11.
135. Moulari B, Pertuit D, Pellequer Y, Lamprecht A. The targeting of surface modified silica nanoparticles to inflamed tissue in experimental colitis. Biomaterials 2008; 29(34):4554-60.
136. Zhao Y, Trewyn BG, Slowing, II, Lin VS. Mesoporous silica nanoparticle-based double drug delivery system for glucose-responsive controlled release of insulin and cyclic AMP. Journal of the American Chemical Society 2009; 131(24):8398-400.
137. Lu J, Liong M, Li Z, Zink JI, Tamanoi F. Biocompatibility, biodistribution, and drug-delivery efficiency of mesoporous silica nanoparticles for cancer therapy in animals. Small 2010; 6(16):1794-805.
138. Xia T, Kovochich M, Liong M, Meng H, Kabehie S, George S, Zink JI, Nel AE. Polyethyleneimine coating enhances the cellular uptake of mesoporous silica nanoparticles and allows safe delivery of siRNA and DNA constructs. ACS Nano 2009; 3(10):3273-86.
139. Hom C, Lu J, Liong M, Luo H, Li Z, Zink JI, Tamanoi F. Mesoporous silica nanoparticles facilitate delivery of siRNA to shutdown signaling pathways in mammalian cells. Small 2010; 6(11):1185-90.

140. Li X, Xie QR, Zhang J, Xia W, Gu H. The packaging of siRNA within the mesoporous structure of silica nanoparticles. Biomaterials 2011; 32(35):9546-56.
141. Ashley CE, Carnes EC, Epler KE, et al. Delivery of small interfering RNA by peptide-targeted mesoporous silica nanoparticle-supported lipid bilayers. ACS Nano 2012; 6(3):2174-88.
142. Chen AM, Zhang M, Wei D, Stueber D, Taratula O, Minko T, He H. Co-delivery of doxorubicin and Bcl-2 siRNA by mesoporous silica nanoparticles enhances the efficacy of chemotherapy in multidrug-resistant cancer cells. Small 2009; 5(23):2673-7.
143. Meng H, Mai WX, Zhang H, et al. Codelivery of an optimal drug/siRNA combination using mesoporous silica nanoparticles to overcome drug resistance in breast cancer in vitro and in vivo. ACS Nano 2013; 7(2):994-1005.
144. Klein PM, Müller K, Gutmann C, et al. Twin disulfides as opportunity for improving stability and transfection efficiency of oligoaminoethane polyplexes. Journal of Controlled Release 2015; 205:109-19.
145. Zhang CY, Kos P, Müller K, Schrimpf W, Troiber C, Lachelt U, Scholz C, Lamb DC, Wagner E. Native chemical ligation for conversion of sequence-defined oligomers into targeted pDNA and siRNA carriers. Journal of Controlled Release 2014; 180:42-50.
146. Müller K, Kessel E, Klein PM, Höhn M, Wagner E. Post-PEGylation of siRNA Lipo-oligoamino Amide Polyplexes Using Tetra-glutamylated Folic Acid as Ligand for Receptor-Targeted Delivery. Molecular Pharmaceutics 2016; 13(7):2332-45.
147. Müller K, Klein PM, Heissig P, Roidl A, Wagner E. EGF receptor targeted lipo-oligocation polyplexes for antitumoral siRNA and miRNA delivery. Nanotechnology 2016; 27(46):464001.
148. Möller K, Müller K, Engelke H, Brauchle C, Wagner E, Bein T. Highly efficient siRNA delivery from core-shell mesoporous silica nanoparticles with multifunctional polymer caps. Nanoscale 2016; 8(7):4007-19.
149. Schaffert D, Kiss M, Rodl W, Shir A, Levitzki A, Ogris M, Wagner E. Poly(I:C)-mediated tumor growth suppression in EGF-receptor overexpressing tumors using EGF-polyethylene glycol-linear polyethylenimine as carrier. Pharmaceutical Research 2011; 28(4):731-41.
150. Fröhlich T, Edinger D, Klager R, et al. Structure-activity relationships of siRNA carriers based on sequence-defined oligo (ethane amino) amides. Journal of Controlled Release 2012; 160(3):532-41.
151. Wu C, Leroux JC, Gauthier MA. Twin disulfides for orthogonal disulfide pairing and the directed folding of multicyclic peptides. Nature Chemistry 2012; 4(12):1044-9.
152. Dawson PE, Muir TW, Clark-Lewis I, Kent SB. Synthesis of proteins by native chemical ligation. Science 1994; 266(5186):776-9.
153. Byun E, Kim J, Kang SM, Lee H, Bang D, Lee H. Surface PEGylation via native chemical ligation. Bioconjugate Chemistry 2011; 22(1):4-8.
154. Dawson PE, Kent SB. Synthesis of native proteins by chemical ligation. Annual Review of Biochemistry 2000; 69:923-60.
155. Blanco-Canosa JB, Dawson PE. An efficient Fmoc-SPPS approach for the generation of thioester peptide precursors for use in native chemical ligation. Angewandte Chemie 2008; 47(36):6851-5.
156. Ogris M, Walker G, Blessing T, Kircheis R, Wolschek M, Wagner E. Tumor-targeted gene therapy: strategies for the preparation of ligand-polyethylene glycol-polyethylenimine/DNA complexes. Journal of Controlled Release 2003; 91(1-2):173-81.
157. Fella C, Walker GF, Ogris M, Wagner E. Amine-reactive pyridylhydrazone-based PEG reagents for pH-reversible PEI polyplex shielding. European Journal of Pharmaceutical Sciences 2008; 34(4-5):309-20.
158. Ogris M, Brunner S, Schuller S, Kircheis R, Wagner E. PEGylated DNA/transferrin-PEI complexes: reduced interaction with blood components, extended circulation in blood and potential for systemic gene delivery. Gene Therapy 1999; 6(4):595-605.

159. El Fadili A, Kundig C, Ouellette M. Characterization of the folylpolyglutamate synthetase gene and polyglutamylation of folates in the protozoan parasite Leishmania. Molecular and Biochemical Parasitology 2002; 124(1-2):63-71.
160. Chabner BA, Roberts TG, Jr. Timeline: Chemotherapy and the war on cancer. Nature Reviews Cancer 2005; 5(1):65-72.
161. Lächelt U, Wittmann V, Müller K, Edinger D, Kos P, Hohn M, Wagner E. Synthetic polyglutamylation of dual-functional MTX ligands for enhanced combined cytotoxicity of poly(I:C) nanoplexes. Molecular Pharmaceutics 2014; 11(8):2631-9.
162. Knorr V, Russ V, Allmendinger L, Ogris M, Wagner E. Acetal linked oligoethylenimines for use as pH-sensitive gene carriers. Bioconjugate Chemistry 2008; 19(8):1625-34.
163. Barz M, Canal F, Koynov K, Zentel R, Vicent MJ. Synthesis and in vitro evaluation of defined HPMA folate conjugates: influence of aggregation on folate receptor (FR) mediated cellular uptake. Biomacromolecules 2010; 11(9):2274-82.
164. Mie G. Beiträge zur Optik trüber Medien, speziell kolloidaler Metallösungen. Annalen der Physik 1908; 25(3):377-445.
165. Cochrane DR, Howe EN, Spoelstra NS, Richer JK. Loss of miR-200c: A Marker of Aggressiveness and Chemoresistance in Female Reproductive Cancers. Journal of Clinical Oncology 2010:821717.
166. Comijn J, Berx G, Vermassen P, Verschueren K, van Grunsven L, Bruyneel E, Mareel M, Huylebroeck D, van Roy F. The two-handed E box binding zinc finger protein SIP1 downregulates E-cadherin and induces invasion. Molecular Cell 2001; 7(6):1267-78.
167. Korpal M, Kang Y. The emerging role of miR-200 family of microRNAs in epithelial-mesenchymal transition and cancer metastasis. RNA Biology 2008; 5(3):115-9.
168. Howe EN, Cochrane DR, Richer JK. Targets of miR-200c mediate suppression of cell motility and anoikis resistance. Breast Cancer Research 2011; 13(2):R45.
169. Wellner U, Schubert J, Burk UC, et al. The EMT-activator ZEB1 promotes tumorigenicity by repressing stemness-inhibiting microRNAs. Nature Cell Biology 2009; 11(12):1487-95.
170. Kopp F, Oak PS, Wagner E, Roidl A. miR-200c sensitizes breast cancer cells to doxorubicin treatment by decreasing TrkB and Bmi1 expression. PLoS One 2012; 7(11):e50469.
171. Kopp F, Wagner E, Roidl A. The proto-oncogene KRAS is targeted by miR-200c. Oncotarget 2014; 5(1):185-95.
172. Xie Y, Wehrkamp CJ, Li J, Wang Y, Wang Y, Mott JL, Oupicky D. Delivery of miR-200c Mimic with Poly(amido amine) CXCR4 Antagonists for Combined Inhibition of Cholangiocarcinoma Cell Invasiveness. Molecular Pharmaceutics 2016; 13(3):1073-80.
173. Cortez MA, Valdecanas D, Zhang X, et al. Therapeutic delivery of miR-200c enhances radiosensitivity in lung cancer. Molecular Therapy 2014; 22(8):1494-503.
174. Cittelly DM, Dimitrova I, Howe EN, et al. Restoration of miR-200c to ovarian cancer reduces tumor burden and increases sensitivity to paclitaxel. Molecular Cancer Therapeutics 2012; 11(12):2556-65.
175. Hurteau GJ, Carlson JA, Spivack SD, Brock GJ. Overexpression of the microRNA hsa-miR-200c leads to reduced expression of transcription factor 8 and increased expression of E-cadherin. Cancer Research 2007; 67(17):7972-6.
176. Korpal M, Lee ES, Hu G, Kang Y. The miR-200 family inhibits epithelial-mesenchymal transition and cancer cell migration by direct targeting of E-cadherin transcriptional repressors ZEB1 and ZEB2. The Journal of Biological Chemistry 2008; 283(22):14910-4.
177. Kiaris H, Spandidos D. Mutations of ras genes in human tumors (review). International Journal of Oncology 1995; 7(3):413-21.
178. Shimono Y, Zabala M, Cho RW, et al. Downregulation of miRNA-200c links breast cancer stem cells with normal stem cells. Cell 2009; 138(3):592-603.

179. Leskela S, Leandro-Garcia LJ, Mendiola M, et al. The miR-200 family controls beta-tubulin III expression and is associated with paclitaxel-based treatment response and progression-free survival in ovarian cancer patients. Endocrine-Related Cancer 2011; 18(1):85-95.
180. Lee JW, Park YA, Choi JJ, et al. The expression of the miRNA-200 family in endometrial endometrioid carcinoma. Gynecologic Oncology 2011; 120(1):56-62.
181. Vallejo DM, Caparros E, Dominguez M. Targeting Notch signalling by the conserved miR-8/200 microRNA family in development and cancer cells. The EMBO Journal 2011; 30(4):756-69.
182. Liu L, Qiu M, Tan G, Liang Z, Qin Y, Chen L, Chen H, Liu J. miR-200c inhibits invasion, migration and proliferation of bladder cancer cells through down-regulation of BMI-1 and E2F3. Journal of Translational Medicine 2014; 12:305.
183. Blangy A, Lane HA, d'Herin P, Harper M, Kress M, Nigg EA. Phosphorylation by p34cdc2 regulates spindle association of human Eg5, a kinesin-related motor essential for bipolar spindle formation in vivo. Cell 1995; 83(7):1159-69.
184. Kapitein LC, Peterman EJ, Kwok BH, Kim JH, Kapoor TM, Schmidt CF. The bipolar mitotic kinesin Eg5 moves on both microtubules that it crosslinks. Nature 2005; 435(7038):114-8.
185. Kapoor TM, Mayer TU, Coughlin ML, Mitchison TJ. Probing spindle assembly mechanisms with monastrol, a small molecule inhibitor of the mitotic kinesin, Eg5. The Journal of Cell Biology 2000; 150(5):975-88.
186. DeBonis S, Skoufias DA, Lebeau L, Lopez R, Robin G, Margolis RL, Wade RH, Kozielski F. In vitro screening for inhibitors of the human mitotic kinesin Eg5 with antimitotic and antitumor activities. Molecular Cancer Therapeutics 2004; 3(9):1079-90.
187. Nakai R, Iida S, Takahashi T, et al. K858, a novel inhibitor of mitotic kinesin Eg5 and antitumor agent, induces cell death in cancer cells. Cancer Research 2009; 69(9):3901-9.
188. Yan Y, Sardana V, Xu B, et al. Inhibition of a mitotic motor protein: where, how, and conformational consequences. Journal of Molecular Biology 2004; 335(2):547-54.
189. Matsuda M, Yamamoto T, Matsumura A, Kaneda Y. Highly efficient eradication of intracranial glioblastoma using Eg5 siRNA combined with HVJ envelope. Gene Therapy 2009; 16(12):1465-76.
190. Edinger D, Klager R, Troiber C, Dohmen C, Wagner E. Gene silencing and antitumoral effects of Eg5 or Ran siRNA oligoaminoamide polyplexes. Drug Delivery and Translational Research 2014; 4(1):84-95.
191. Martin TM, Plautz SA, Pannier AK. Temporal endogenous gene expression profiles in response to polymer-mediated transfection and profile comparison to lipid-mediated transfection. The Journal of Gene Medicine 2015; 17(1-2):33-53.
192. Martin TM, Plautz SA, Pannier AK. Temporal endogenous gene expression profiles in response to lipid-mediated transfection. The Journal of Gene Medicine 2015; 17(1-2):14-32.
193. Shen J, Kim HC, Su H, et al. Cyclodextrin and polyethylenimine functionalized mesoporous silica nanoparticles for delivery of siRNA cancer therapeutics. Theranostics 2014; 4(5):487-97.
194. Wang M, Li X, Ma Y, Gu H. Endosomal escape kinetics of mesoporous silica-based system for efficient siRNA delivery. International Journal of Pharmaceutics 2013; 448(1):51-7.
195. Bhattarai SR, Muthuswamy E, Wani A, Brichacek M, Castaneda AL, Brock SL, Oupicky D. Enhanced gene and siRNA delivery by polycation-modified mesoporous silica nanoparticles loaded with chloroquine. Pharmaceutical Research 2010; 27(12):2556-68.
196. Ashley CE, Carnes EC, Phillips GK, et al. The targeted delivery of multicomponent cargos to cancer cells by nanoporous particle-supported lipid bilayers. Nature Materials 2011; 10(5):389-97.

197. Na HK, Kim MH, Park K, Ryoo SR, Lee KE, Jeon H, Ryoo R, Hyeon C, Min DH. Efficient functional delivery of siRNA using mesoporous silica nanoparticles with ultralarge pores. Small 2012; 8(11):1752-61.
198. Zhang W, Müller K, Kessel E, et al. Targeted siRNA Delivery Using a Lipo-Oligoaminoamide Nanocore with an Influenza Peptide and Transferrin Shell. Advanced Healthcare Materials 2016; 5(12):1493-504.
199. Merkel OM, Librizzi D, Pfestroff A, Schurrat T, Buyens K, Sanders NN, De Smedt SC, Behe M, Kissel T. Stability of siRNA polyplexes from poly(ethylenimine) and poly(ethylenimine)-g-poly(ethylene glycol) under in vivo conditions: effects on pharmacokinetics and biodistribution measured by Fluorescence Fluctuation Spectroscopy and Single Photon Emission Computed Tomography (SPECT) imaging. Journal of Controlled Release 2009; 138(2):148-59.
200. Ogris M, Steinlein P, Kursa M, Mechtler K, Kircheis R, Wagner E. The size of DNA/transferrin-PEI complexes is an important factor for gene expression in cultured cells. Gene Therapy 1998; 5(10):1425-33.
201. Antony AC. The biological chemistry of folate receptors. Blood 1992; 79(11):2807-20.
202. Low PS, Henne WA, Doorneweerd DD. Discovery and development of folic-acid-based receptor targeting for imaging and therapy of cancer and inflammatory diseases. Accounts of Chemical Research 2008; 41(1):120-9.
203. Thomas M, Kularatne SA, Qi L, Kleindl P, Leamon CP, Hansen MJ, Low PS. Ligand-targeted delivery of small interfering RNAs to malignant cells and tissues. Annals of the New York Academy of Sciences 2009; 1175:32-9.
204. Lee H, Lytton-Jean AK, Chen Y, et al. Molecularly self-assembled nucleic acid nanoparticles for targeted in vivo siRNA delivery. Nature Nanotechnology 2012; 7(6):389-93.
205. Willibald J, Harder J, Sparrer K, Conzelmann KK, Carell T. Click-modified anandamide siRNA enables delivery and gene silencing in neuronal and immune cells. Journal of the American Chemical Society 2012; 134(30):12330-3.
206. Dohmen C, Frohlich T, Lachelt U, Rohl I, Vornlocher HP, Hadwiger P, Wagner E. Defined Folate-PEG-siRNA Conjugates for Receptor-specific Gene Silencing. Molecular Therapy-Nucleic Acids 2012; 1:e7.
207. Lopes I, A CNO, M PS, J PNS, Goncalves O, Gomes AC, Real Oliveira ME. Monoolein-based nanocarriers for enhanced folate receptor-mediated RNA delivery to cancer cells. Journal of Liposome Research 2016; 26(3):199-210.
208. Nahire R, Hossain R, Patel R, et al. pH-triggered echogenicity and contents release from liposomes. Molecular Pharmaceutics 2014; 11(11):4059-68.
209. Ohyama A, Higashi T, Motoyama K, Arima H. In Vitro and In Vivo Tumor-Targeting siRNA Delivery Using Folate-PEG-appended Dendrimer (G4)/alpha-Cyclodextrin Conjugates. Bioconjugate Chemistry 2016; 27(3):521-32.
210. Novo L, Takeda KM, Petteta T, et al. Targeted decationized polyplexes for siRNA delivery. Molecular Pharmaceutics 2015; 12(1):150-61.
211. Choi HS, Liu W, Misra P, Tanaka E, Zimmer JP, Itty Ipe B, Bawendi MG, Frangioni JV. Renal clearance of quantum dots. Nature Biotechnology 2007; 25(10):1165-70.
212. Buyens K, Lucas B, Raemdonck K, Braeckmans K, Vercammen J, Hendrix J, Engelborghs Y, De Smedt SC, Sanders NN. A fast and sensitive method for measuring the integrity of siRNA-carrier complexes in full human serum. Journal of Controlled Release 2008; 126(1):67-76.
213. Shane B. Folylpolyglutamate synthesis and role in the regulation of one-carbon metabolism. Vitamins & Hormones 1989; 45:263-335.
214. Moran RG. Roles of folylpoly-gamma-glutamate synthetase in therapeutics with tetrahydrofolate antimetabolites: an overview. Seminars in Oncology 1999; 26(2 Suppl 6):24-32.

215. Mislick KA, Baldeschwieler JD. Evidence for the role of proteoglycans in cation-mediated gene transfer. Proceedings of the National Academy of Sciences of the United States of America 1996; 93(22):12349-54.
216. Ruponen M, Honkakoski P, Ronkko S, Pelkonen J, Tammi M, Urtti A. Extracellular and intracellular barriers in non-viral gene delivery. Journal of Controlled Release 2003; 93(2):213-7.
217. Kopatz I, Remy JS, Behr JP. A model for non-viral gene delivery: through syndecan adhesion molecules and powered by actin. The Journal of Gene Medicine 2004; 6(7):769-76.
218. Zelphati O, Uyechi LS, Barron LG, Szoka FC, Jr. Effect of serum components on the physico-chemical properties of cationic lipid/oligonucleotide complexes and on their interactions with cells. Biochimica et Biophysica Acta 1998; 1390(2):119-33.
219. Wagner E. Effects of membrane-active agents in gene delivery. Journal of Controlled Release 1998; 53(1-3):155-8.
220. Boeckle S, Fahrmeir J, Roedl W, Ogris M, Wagner E. Melittin analogs with high lytic activity at endosomal pH enhance transfection with purified targeted PEI polyplexes. Journal of Controlled Release 2006; 112(2):240-8.
221. Meyer M, Zintchenko A, Ogris M, Wagner E. A dimethylmaleic acid-melittin-polylysine conjugate with reduced toxicity, pH-triggered endosomolytic activity and enhanced gene transfer potential. The Journal of Gene Medicine 2007; 9(9):797-805.
222. Lorenzer C, Dirin M, Winkler AM, Baumann V, Winkler J. Going beyond the liver: progress and challenges of targeted delivery of siRNA therapeutics. Journal of Controlled Release 2015; 203:1-15.
223. McLean JW, Fox EA, Baluk P, Bolton PB, Haskell A, Pearlman R, Thurston G, Umemoto EY, McDonald DM. Organ-specific endothelial cell uptake of cationic liposome-DNA complexes in mice. American Journal of Physiology 1997; 273(1 Pt 2):H387-404.
224. Chen Y, Zhu X, Zhang X, Liu B, Huang L. Nanoparticles modified with tumor-targeting scFv deliver siRNA and miRNA for cancer therapy. Molecular Therapy 2010; 18(9):1650-6.
225. Kos P, Lachelt U, He D, Nie Y, Gu Z, Wagner E. Dual-targeted polyplexes based on sequence-defined peptide-PEG-oligoamino amides. Journal of Pharmaceutical Sciences 2015; 104(2):464-75.
226. Hatakeyama H, Akita H, Harashima H. The polyethyleneglycol dilemma: advantage and disadvantage of PEGylation of liposomes for systemic genes and nucleic acids delivery to tumors. Biological and Pharmaceutical Bulletin 2013; 36(6):892-9.
227. Wojcik EJ, Buckley RS, Richard J, Liu L, Huckaba TM, Kim S. Kinesin-5: cross-bridging mechanism to targeted clinical therapy. Gene 2013; 531(2):133-49.
228. Kops GJ, Weaver BA, Cleveland DW. On the road to cancer: aneuploidy and the mitotic checkpoint. Nature Reviews Cancer 2005; 5(10):773-85.
229. Mayer TU, Kapoor TM, Haggarty SJ, King RW, Schreiber SL, Mitchison TJ. Small molecule inhibitor of mitotic spindle bipolarity identified in a phenotype-based screen. Science 1999; 286(5441):971-4.
230. Carol H, Lock R, Houghton PJ, et al. Initial testing (stage 1) of the kinesin spindle protein inhibitor ispinesib by the pediatric preclinical testing program. Pediatric Blood & Cancer 2009; 53(7):1255-63.
231. Li Z, Barnes JC, Bosoy A, Stoddart JF, Zink JI. Mesoporous silica nanoparticles in biomedical applications. Chemical Society Reviews 2012; 41(7):2590-605.
232. Li X, Chen Y, Wang M, Ma Y, Xia W, Gu H. A mesoporous silica nanoparticle--PEI--fusogenic peptide system for siRNA delivery in cancer therapy. Biomaterials 2013; 34(4):1391-401.
233. Gao F, Botella P, Corma A, Blesa J, Dong L. Monodispersed mesoporous silica nanoparticles with very large pores for enhanced adsorption and release of DNA. The Journal of Physical Chemistry B 2009; 113(6):1796-804.

234. Hartono SB, Yu M, Gu W, Yang J, Strounina E, Wang X, Qiao S, Yu C. Synthesis of multi-functional large pore mesoporous silica nanoparticles as gene carriers. Nanotechnology 2014; 25(5):055701.
235. Hartono SB, Gu W, Kleitz F, Liu J, He L, Middelberg AP, Yu C, Lu GQ, Qiao SZ. Poly-L-lysine functionalized large pore cubic mesostructured silica nanoparticles as biocompatible carriers for gene delivery. ACS Nano 2012; 6(3):2104-17.

8 Acknowledgements

Over the past four years, many people contributed to this thesis. At this point, I would like to thank these people for their help and support.

First of all, I would like to thank my supervisor Prof. Dr. Ernst Wagner for giving me the opportunity to do my thesis in his group. I am very grateful for his guidance, scientific support, beneficial advice and his encouragement to develop own ideas and to grow with the demands.

Thanks to Philipp K., Dongsheng and Canyang for the good collaborations and the synthesis of many oligomers. In this regard, special thanks to Philipp K. for the continuous supply of oligomers and reagents for my projects. I would like to thank Philipp H. for his contribution to the stable cell line and for being a helpful and assistant seat-neighbour. Furthermore, I would like to thank Eva for carrying out the *in vivo* experiments. I want to thank Dr. Karin Möller for the close and productive collaboration on mesoporous silica nanoparticles. Special thanks to Ruth for constant support and help in all aspects of lab and life.

Many thanks to Wolfgang for solving every technical and computer problem also by remote diagnosis on phone. Thanks to Miriam for her contribution to the microscopy experiments and to Ursula and Anna for keeping the lab running.

I would like to thank the former group members Petra, Daniel and Flo for showing me all the techniques and work processes at the beginning of my PhD. Thanks to Claudia, who became a dear colleague and friend.

My gratitude goes to Dr. Martina Rüffer for showing me the beauty of the world of plants and for the organization of Christmas parties, summer hiking trips, “Weißwurstfrühstück” and lab courses. I would like to thank Dr. Andreas Roidl and his group for their help in terms of miR-200c assays. Special thanks to Uli for his great advice and for always having an open door. I want to thank the whole Wagner group for the nice working atmosphere and my master and bachelor students for their contribution.

Furthermore, I want to thank my friends and my brother Jonas for distraction and for their company during the last years.

I would like to thank Flo for being at my side for many years, for supporting me and for always believing in me. Finally, I owe my deepest gratitude to my parents, who have always been there for me, supported me and gave me the best advices for every problem and in any difficult situation.